Title
ROLE OF NCX1 IN EPICARDIAL CALCIUM DYNAMICS AND ELECTRICAL SIGNALING

Author
Petrosky, Azade Dominique

Publication Date
2013

Peer reviewed|Thesis/dissertation

ROLE OF NCX1 IN EPICARDIAL CALCIUM DYNAMICS AND ELECTRICAL SIGNALING

By:

Azadé Dominiqué Petrosky

B.S. (University of California, Merced) 2008

DISSERTATION

Submitted in satisfaction of the requirements for the degree of

DOCTORATE OF PHILOSOPHY
in

BIOLOGICAL ENGINEERING AND SMALL-SCALE TECHNOLOGIES

with an emphasis in

CARDIAC ELECTROPHYSIOLOGY

in the

OFFICE OF GRADUATE STUDIES

of the

UNIVERSITY OF CALIFORNIA, MERCED

Committee Advised:

Dr. Wei-Chun Chin, Chair
Dr. Ariel L. Escobar, Advisor
Dr. Linda Hirst
Dr. Nestor Oviedo

2013

The dissertation of Azadé Dominiqué Petrosky is approved by, and is accepted in the quality and form for publication on microfilm and electronically:

_____
Dr. Wei-Chun Chin, Chair

_____
Dr. Ariel L. Escobar, Advisor

_____
Dr. Linda Hirst

_____
Dr. Nestor Oviedo

DEDICATION

I am dedicating this dissertation thesis to my mother, Maryam Petrosky. If it weren't for your love, support and tremendous effort, I wouldn't be where I am today. None of this was possible without your guidance …Thank you.

TABLE OF CONTENTS

LIST OF FIGURES

LIST OF TABLES

ACKNOWLEDGEMENTS

The studies performed in this dissertation were primarily funded by NIH R01-HL084487 and NIH grant R44GM093521. Addition funding includes the University of California, Merced Graduate Student Research Summer Fellowship and Graduate Division USAP Fellowship Award.

I would also like to acknowledge the following collaborators:

Dr. Kenneth Philipson at the department of physiology in University of California, Los Angeles School of Medicine for providing the transgenic cardiac-specific sodium-calcium exchanger knock-out mice.

Dr. Bijorn Knollmann at Vanderbilt University Medical Center, Nashville, Tennessee

Dr. Alicia Mattiazzi at Facultad de Cs. Me´dicas, Centro de Investigaciones Cardiovasculares, UNLP, Conicet, La Plata, Argentina

I would like to Thank:

Dr. Dmytro Kornyeyev for providing a portion of intra-SR Ca^{2+} recordings.

Mariana Argenziano for providing real-time data and analysis of NCX1 KO hearts.

Dr. Marcela Ferreiro and Yuriana Aguilar for help and guidance.

Azadé Dominiqué Petrosky
apetrosky2@ucmerced.edu or azade.petrosky@gmail.com
(985) 807-5096 cell

Education:

University of California, Merced,
Bachelor of Science, Emphasis in Human Biology 2008
University of California, Merced,
Doctorate in Biological Engineering and Small-scale Technologies, 2013
Emphasis in Cardiac Electrophysiology

Experience:

Teaching Assistant, *University of California, Merced*
School of Engineering

- Physiology for Engineers (Lab/Discussion): Spring 2012-13
  Prepare additional lectures, assign reading of additional research articles to assist in-group discussions, and provide clear explanations of mechanisms taught in the course. Guided students in applications of tools used in conducting research. Assist in evaluation of assignments and grades during the course.

School of Natural Sciences

- General Chemistry (Discussion): Fall 2011
  Prepare lectures, provided detailed explanations on concepts covered in class and applied to real-life situations, assisted students on worksheets and homework assignments. Graded all assignments.
- Introduction to Molecular Biology (Lab): Summer 2010
  Set-up labs, taught students foundation to understanding concepts from lab and how to apply them to lectures, designed quizzes and prepared final exam. Graded all assignments.

Certified Training: 2008-present

- CITI Program Training.
- Animal Skills Training.
- Laboratory Safety Training.

Clubs/Organizations: *University of California, Merced*

Biophysical Society 2008 - present
American Heart Association 2008 - present
Women in Science & Engineering (WiSE) 2010 - 2012
Flying Samaritans, *Modesto Chapter* 2007 - 2009

Conferences/Presentations:

- Biophysical Society Meeting Philadelphia, PA Feb2013
  Petrosky, Azade D., Rafael Mejia-Alvarez, and Ariel L. Escobar. *Impact of SR Ca^{2+} Release on the Cardiac Action Potential Repolarization during Postnatal Development.* Biophysical Journal, vol. 104:290. DOI: 10.1016/j.bpj.2012.11.1621
- American Heart Association, Los Angeles, CA Nov2012
  Scientific Sessions

- Biophysical Society Meeting San Diego, CA Feb2012
  Petrosky, Azade D.; Zepeda, Bernardo; Petrosky, Alexander B.; Kornyeyev, Dmytro; Contreras, Paola; Valdivia, Hector H.; Escobar, Ariel L. *Relationship between Ca^{2+} Alternans and T-wave Alternans: Role of Calsequestrin and Sorcin.* Biophysical Journal, vol. 102, issue 3, pp. 553a DOI:10.1016/j.bpj.2011.11.3015
- Biophysical Society Meeting Baltimore, MD Mar2011
  Korneyeyev, Dmytro; **Petrosky, Azade D.**; Escobar, Ariel L. *Mechanisms Regulating the Organellar Ca^{2+} Dynamics in Intact Hearts during Ischemia-Reperfusion.* Biophysical Journal, vol. 100, issue 3, pp. 292a-292a. DOI: 10.1016/j.bpj.2010.12.1798
- Ceres High School, Ceres, CA Jan2011
  AP Biotechnology class presentation; *Cardiophysiology: Studying heart failure using laser optics on intact mouse hearts*
- Biophysical Society Meeting San Francisco, CA Feb2010
  Ferreiro, Marcela; **Petrosky, Azade D.**; Korneyeyev, Dmytro; Escobar, Ariel L. *Do Mouse Epicardial Action Potentials Present Phase 2?.* Biophysical Journal, vol. 98, issue 3, pp. 532a-532a. DOI: 10.1016/j.bpj.2009.12.2886
- UC System-wide Engineering Symposium Merced, CA Jun2009
  Petrosky AD, Kornyeyev D, and Escobar AL. *Inhibition of the Sodium/Calcium Exchanger by Lithium in Intact Mouse Hearts Modifies Cardiac Alternans*
- Biophysical Society Meeting Boston, MA Feb2009
  Kornyeyev D., **Petrosky A.D.**, Knollmann B., and Escobar A.L., *Effect of Extracellular Ca^{2+} On Intracellular Ca^{2+} dynamics in Intact Hearts of Wild Type and Calsequestrin KO Mice.* Biophysical Journal, vol. 96, issue 3, pp. 516a-516a. DOI: 10.1016/j.bpj.2008.12.2658
- American Heart Association, Davis, CA Aug2008
  Young Investigators

Publications:

- Petrosky, A.D., Kornyeyev D., and Escobar A.L. (2013) **Genesis of calcium alternans. Effect of sarcoplasmic reticulum calcium load.** In preparation.
- Petrosky, A.D., Philipson K.D., and Escobar A.L. (2013) **NCX1 Modifies Epicardial Intracellular Ca^{2+} dynamics and Membrane Potential in Intact Na^{+}-Ca^{2+} Exchanger Knockout Mouse Hearts.** In preparation.
- Kornyeyev D., Petrosky A.D., Zepeda B, Ferreiro M, Knollmann B., and Escobar A.L., (2012) **Calsequestrin 2 deletion shortens the refractoriness of Ca^{2+} release and reduces rate-dependent Ca^{2+}-alternans in intact mouse hearts,** J Mol Cell Cardiol 52 (1): 21-31. doi:10.1016/j.yjmcc.2011.09.020
- Ferreiro M., Petrosky A.D. Escobar A.L. (2011). **Intracellular Ca^{2+} Release underlies the Development of Phase 2 in Mouse Ventricular Action Potentials.** Am J Physio. doi: 10.1152/ajpheart.00524.2011
- Valverde C.A., Kornyeyev D., Ferreiro M., Petrosky A.D., Mattiazzi A., Escobar A.L. (2010). **Transient Ca^{2+} depletion of the sarcoplasmic reticulum at the onset of reperfusion.** Cardiovascular Research 85: 671-680. doi: 10.1093/cvr/cvp371

Funding & Awards: *University of California, Merced*

- Graduate Student Research Summer Fellowship May2012
- Graduate Research Council Travel Grant Feb2012
- Outstanding Graduate Student Award in BEST (Biological Engineering and Small-scale Technologies) May2010
- Graduate Division USAP Fellowship Award Jan2010

ABSTRACT:

ROLE OF NCX1 IN EPICARDIAL CALCIUM DYNAMICS AND ELECTRICAL SIGNALING

Azadé Dominiqué Petrosky

Doctorate of Philosophy in Biological Engineering and Small-scale Technologies, with an emphasis in Cardiac Electrophysiology at the University of California, Merced, 2013

The Na/Ca^{2+} exchanger (NCX1) plays an important role in defining cardiac function by regulating the contractility and excitability of the heart. The aim of my research was to study the effect of impairing NCX1 with various LiCl concentrations (Na^+ replaced by Li^+), known NCX blockers KBR-7943 and SEA0400 in wild-type intact mouse hearts. In addition to this, cardiac-specific NCX1 KO mice were used to further evaluate intracellular Ca^{2+} dynamics and the electrical properties of the heart. We hypothesized that impairment of the exchanger would lead to an increase of Ca^{2+} in the cytosol and consequently an accumulation of Ca^{2+}in the sarcoplasmic reticulum (SR). This accumulation will result in a larger release of $Ca^{2+}$from the SR. In addition to this, NCX1 impairment will lead to a change in the membrane potential during the repolarization phase of epicardial action potentials. Experiments performed in this dissertation were by the use of a modified version of the pulsed local-field fluorescent microscopy (PLFFM), where hearts were loaded with Ca^{2+} sensitive fluorescent dyes (rhod-2, AM and mag-fluo-4, AM) or the potentiometric dye (DI-8ANEPPS). Microelectrode impalement for epicardial action potential recordings were also used in this dissertation for simultaneous recordings of intracellular Ca^{2+} dynamics and left ventricular transmural electrocardiographic recordings. To conclude, impairment of the NCX1 alters intracellular Ca^{2+} dynamics and changes the electrical properties of the heart.

Graduate Advisor: Dr. Ariel L. Escobar, Advisor
Committee Chair: Dr. Wei-Chun Chin, Chair

LIST OF ABBREVIATIONS:

Symbol	Definition
Ca^{2+}	Calcium
Na^{+}	Sodium
K^{+}	Potassium
Li^{+}	Lithium
Cl^{-}	Chloride
RyR2	Ryanodine Receptor type 2
SERCA, SERCA2a	Sarco-Endoplasmic Reticulum Ca^{2+} -ATPase
NCX	Sodium-Calcium Exchanger
NCX1	Na^{+}-Ca^{2+} Exchanger type 1
CSQ2	Calsequestrin type 2
PLB	Phospholamban
PM	Plasma membrane
SR	Sarcoplasmic Reticulum
T-tubule	Transverse tubule
TMS	Transmembrane-segment
GIG	Glycine Isoleucine Glycine
CICR	Calcium Induced Calcium Release
ECC	Excitation-Contraction Coupling
AP	Action Potential
APD	Action Potential Duration
APD_{50}	Action Potential Duration at 50% Repolarization
APD_{70}	Action Potential Duration at 70% Repolarization
APD_{90}	Action Potential Duration at 90% Repolarization
ECG	Electrocardiogram
PLFFM	Pulsed Local Field Fluorescence Microscopy
β-AR	Beta-adrenergic receptors
LTCC	L-type Ca^{2+}-channels
Ca-Alt	Ca^{2+} alternans
AP-Alt	Action potential alternans
TW-Alt	T-wave alternans
cAMP	cyclic-adenosine monophosphate
ATP	adenosine triphosphate
Epi	Epicardium
Endo	Endocardium
CPVT	Catecholaminergic polymorphic ventricular tachycardia
I_{Ca}	Calcium Current
I_{TO}, K_{ITO}	Potassium transient outward current
PKA	Protein Kinase A
CAMKII	Ca^{2+}/calmodulin-dependent protein kinases II
EAD	Early after-depolarization
DAD	Delayed after-depolarization
SA	Sinoatrial
AV	atrioventricular

NHE	Na^+/H^+ exchanger
CBD1 and CBD2	Ca^{2+}-binding domain
Ry	Ryanodine
Tg	Thapsigargin
RT	Room temperature
KO	Knock-Out Mouse
WT	Wild Type Mouse

PREFACE:

The heart is the central organ of the cardiovascular system. It is responsible for pumping deoxygenated blood to the lungs and oxygenated blood to the rest of our body. This mechanical hydraulic function is achieved by a two-stroke pump that is electrically and metabolically controlled (Opie 2004). In order to activate this mechanical function, there must be a dramatic increase in free Ca^{2+} concentration within the cytoplasm of specialized heart cells (cardiomyocytes). These changes in intracellular free Ca^{2+} occur in response to a change in the membrane potential of cardiomyocytes. Figure i, illustrates a simplified scheme of a ventricular cardiac myocyte. This scheme emphasizes the morphological arrangement of the plasma membrane (PM), the transverse tubular (T-tubule) system, and the junctional sarcoplasmic reticulum (SR) where the contractility related changes in free Ca^{2+} concentration occurs in cardiomyocytes.

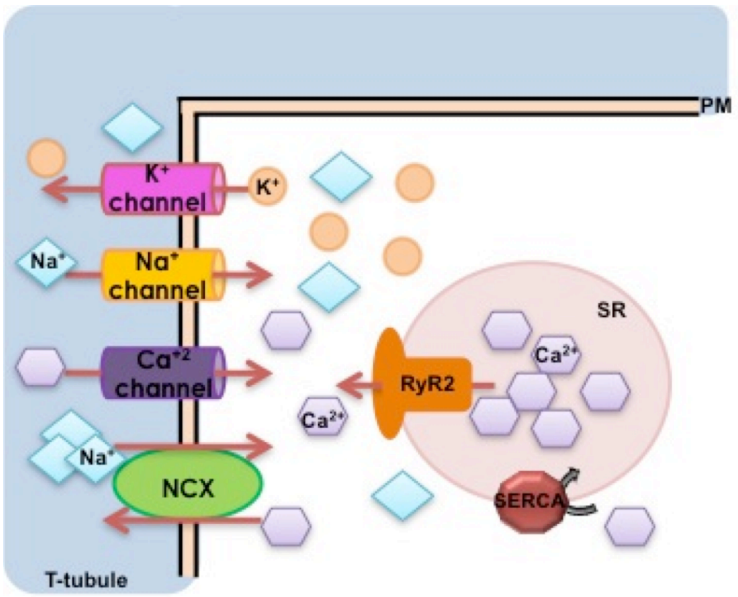

Figure i. Ca^{2+} influx through the Ca^{2+}-channel (LTCC), induces Ca^{2+} release from the SR via RyR2 (i.e. CICR). Ca^{2+} is extruded out of the cell through the Na^{+}-Ca^{2+} exchanger (NCX).

When an electrical stimulus elicits the depolarization of the PM and T-tube, it activates the opening of voltage-sensitive Ca^{2+}-channels (in T-tubule; Figure i). A small Ca^{2+} influx through these Ca^{2+}-channels triggers the opening of specialized intracellular Ca^{2+}-release channels, the ryanodine receptor (RyR2), located in the terminal cistern of the SR (Figure i). Once RyR2s open, a large amount of intracellular Ca^{2+} rushes out of the SR into the cytosol; a process named Ca^{2+}-Induced-Ca^{2+}-Release (CICR) (Fabiato and Fabiato 1975). Changes in cytosolic free Ca^{2+} will activate a Ca^{2+}-mediated transporter in the PM and T-tubules, the Na^{+}-Ca^{2+} exchanger (NCX1). NCX1 is an electrogenic transporter that exchanges three Na^{+} for one Ca^{2+}, which drives an influx of monovalent cations in order to extrude excess cytosolic Ca^{2+} in order to maintain the intracellular Ca^{2+} homeostasis. The electrogenicity of this transporter can produce a transient change

in the membrane potential and thereby modify the repolarization phase of cardiac action potentials (AP). Changes in the repolarization of ventricular APs, more specifically the outermost layer (epicardial APs), can trigger fatal cardiac arrhythmias.

Cardiac arrhythmias are produced by beat-to-beat fluctuations in the electrical activity between different regions within the heart. These electrical fluctuations can be mediated by Ca^{2+} released from the SR (Rosenbaum, Jackson et al. 1994). Therefore, it is crucial to identify the specific properties that underlie the relationship between Ca^{2+} dynamics and AP repolarization at the organ level. The relationship between Ca^{2+} dynamics and the electrical activity have been extensively studied; however most of these studies were performed in isolated cardiomyocytes at low non-physiological temperatures. Isolation of the cardiomyocytes causes loss of the complex metabolic, electrical, mechanical and regulatory environment that is normally necessary for proper physiological function. Thus, in order to gain a more comprehensive understanding of the basic mechanisms that underlie ventricular arrhythmias, experiments must be conducted in an intact whole-heart under near physiological conditions. A novel technique, the pulsed local-field fluorescence microscopy (PLFFM) (Mejia-Alvarez, Manno et al. 2003) provides access to whole-heart simultaneous recordings of intracellular Ca^{2+} dynamics and the electrical properties of cardiomyocytes found at the epicardial layer of Langendorff-perfused mouse hearts, under near true physiological conditions.

In particular, this dissertation focuses on the role of NCX1 in epicardial Ca^{2+} dynamics and electrical signaling in intact mouse hearts. Preliminary data led to the following central ***hypothesis:*** **NCX1 impairment will lead to an increase in the cytosolic Ca^{2+} and consequently an accumulation of Ca^{2+} in the SR. As a result of this accumulation, a larger Ca^{2+}-release produced from the SR will activate NCX1, modifying the action potential repolarization**.

To further expand previous findings and investigate the role of NCX1 in the genesis of electrocardiographic (ECG) signals, a modified version of the PLFFM , was used. The PLFFM not only records Ca^{2+} in the cytosol and inside the SR, but also provides ability to simultaneously record the membrane potential, via microelectrodes, and ECG of an intact mouse heart. This set of integrated techniques has allowed us to study sub-cellular events at an organ level in a near true physiological environment (see Chapter 2 for methodology). In the chapters that follow (Chapters 3-6), this hypothesis is divided to test a specific sub-hypothesis.

Chapter 3: ***Intracellular Calcium Dynamics***

In this chapter we will explore ***the hypothesis that the impairment of NCX1 modifies cytosolic Ca^{2+} dynamics.*** To evaluate this hypothesis the following mechanisms were tested: *(I)* during diastole NCX1 will be impaired by replacing Na^+ with Li^+ (a non-translocable ion), producing changes in the resting diastolic Ca^{2+}; *(II)* these changes will reduce NCX1 activation and induce a diminution in the transmembrane Ca^{2+} gradient; and *(III)* the decreased extrusion by the NCX1 will augment the amplitude of Ca^{2+} transients during systole. These experiments were performed using the PLFFM to measure the cytosolic Ca^{2+} by means of Ca^{2+} dye fluorescence (rhod-2, AM).

In addition, we will evaluate the intra-organellar Ca^{2+} dynamics by direct measurement of SR Ca^{2+} dynamics from the intracellular compartment to test ***the hypothesis that the impairment of NCX1 modifies intra-SR Ca^{2+} dynamics.*** Specifically we will evaluate the role of NCX1 in the subcellular Ca^{2+} dynamics, by studying the effect of Li-induced cytosolic Ca^{2+} increases in relation to the intra-SR Ca^{2+}

dynamics. The mechanisms tested when 70 mM Na-Li Tyrode was used to impair NCX1 are as follows: *(I)* the sarcoplasmic/endoplasmic reticulum Ca^{2+} ATPase (SERCA2a) will pump more Ca^{2+} into the SR, at elevated diastolic Ca^{2+} concentrations, thereby *(II)* increasing the SR Ca^{2+} content. *(III)* Higher intra-SR free Ca^{2+} will promote a larger Ca^{2+}-release, which would increase the amplitude of Ca^{2+} transients. These experiments were performed using the PLFFM to measure the intra-SR Ca^{2+} with a low affinity fluorescent Ca^{2+} indicator (mag-fluo4, AM) located inside the SR.

Chapter 4: ***Electrical Signaling***

Data represented in Chapter 4 specifically evaluates the electrogenicity of the sarcolemma protein NCX1 by means of membrane potential measurements. Hence, we propose to assess ***the hypothesis that the impairment of NCX1 modifies the epicardial AP repolarization. This was*** evaluated by studying the effect of the Ca^{2+} released from the SR on the repolarization of epicardial APs. Thus, *(I)* impairment of NCX1 augments intracellular Ca^{2+} release, whereas, the AP will repolarize faster because the electrogenicity imposed by the exchanger will be lost. This further implies that *(II)* impairing intracellular Ca^{2+} release may also decrease the activation of NCX1 as promoting a faster AP repolarization. Changes in the membrane potential were recorded either by using a potentiometric dye (Di-8-ANEPPS), via the PLFFM, or glass microelectrode impalement.

Chapter 5: ***Kinetic properties of APs in NCX1 transgenic Mouse Model***

The use of a NCX1 KO transgenic mouse, designed via Cre/lox technology, is extensively studied in Chapter 5 to further ***test the hypothesis that NCX1 regulates the repolarization of mouse ventricular APs.*** We evaluated the morphology of epicardial APs in cardiac-specific NCX1 KO mice under various experimental conditions. Specifically, we evaluated *(I)* the effect of SR Ca^{2+} release on AP repolarization in animals were NCX1 has been ablated and *(II)* we examined the competition between K^+ efflux through the plasma membrane as a competitive/compensatory mechanism to the influx of Na^+ via NCX1. These experiments were performed by epicardial microelectrode impalement for changes in the membrane potential.

Chapter 6: ***Intracellular Ca^{2+} dynamics and Electrocardiographic properties of NCX1 transgenic Mouse Model***

In this chapter we address ***the hypothesis that the impairment of NCX1 modifies Ca^{2+} signaling and generate a substrate for electrocardiographic changes.*** *(I)* Intracellular Ca^{2+} dynamics was then evaluated and compared to NCX WT mice. Finally, we evaluated *(II)* if these cellular physiological events were transduced to changes in the electrocardiographic properties of the heart. These experiments were performed in various combinations of simultaneous recordings using the PLFFM to measure the cytosolic Ca^{2+} (rhod-2, AM) and Ag-AgCl pellets for transmural ECG recordings of the left ventricle.

All in all, results presented in this dissertation will not only enhance our knowledge of ventricular arrhythmias, but will also provide a link between intracellular Ca^{2+} signaling and excitability at the whole-organ level under experimental and physiological conditions.

CHAPTER 1 *: Background and Significance*

1.1 History of whole-heart studies

The study of an organ such as the heart has been a long-standing scientific problem. Every heartbeat is solely responsible for pumping oxygenated blood to all of our organs, integrating the animal anatomy as a whole. Its primary role is to provide a constant supply of nutrients to the body, thus if it fails, so would every organ in the body. Although the heart is not entirely independent, it does have the molecular machinery to continue beating on its own as long as the appropriate perfusate is provided. It is therefore an organ that can survive without a host.

Whole-heart studies began in the 1800s with frog hearts. The anatomical structure of an amphibian heart differs from that of a mammalian heart (Figure 1.1). Amphibian hearts have only three chambers; two atria and one ventricle (Figure 1.1 A). Mammalian hearts, on the other hand have four chambers; two atria and two ventricles (Figure 1.1 B). Elias Cyon at the Carl Ludwig Institute of Physiology (1866) developed a perfusion method to study whole frog hearts (Cyon 1866). Perfusion of these hearts were through the vena cava, into the ventricle (Cyon 1866; Langendorff 1898). Cyon's perfusion technique was efficient for amphibian hearts because their anatomical and physiological attributes allow the ventricular tissue to absorb ions through the endocardium. In 1895, Oscar Langendorff hypothesized that mammalian hearts received their nutrients through the coronary arteries and not through diffusion mechanisms via the endocardium like amphibians that have no coronary vasculature (Langendorff 1898; Zimmer 1998). In order to test this hypothesis, Langendorff created a device where solution flowed through the aorta; perfusing the coronary arteries and not the ventricles (retro-grade perfusion). Although there are anatomical differences between these species, cardiac function appeared to remain somewhat similar. For instance, Cyon studied the temperature effects on the heart's function by measuring the heart rate and circulatory pressure as well as the need of an adequate supply of oxygen (Cyon 1866; Zimmer 1998). Langendorff took this knowledge and methodology a step further and applied it to the mammalian heart (Figure 1.2) (Langendorff 1898). The apparatus shown in Figure 1.2 allowed Langendorff to document changes observed in the whole heart

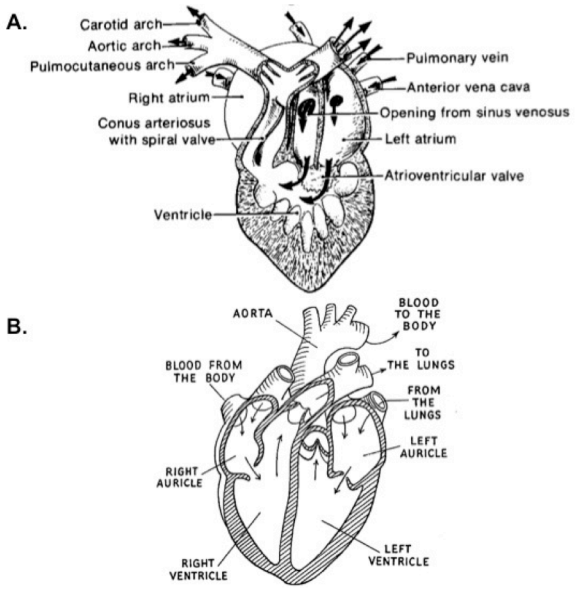

Figure 1.1 Anatomical structure of Frog heart (A)* and Mammalian heart (B). Acquired from online source**

*(A) http://www.arthursclipart.org/frogs/frogs/page_02.htm
**(B) http://suupedupscience.blogspot.com/2011/08/you-wear-your-heart-on-your-sleeve-mr.html

under extreme temperature change (low of 6°C and the high of 49°C) that reflected variation in the coronary circulation (Langendorff 1898). The coronary system became the underlying key to understanding mammalian heart conditions. In fact it was Langendorff who first administered muscarinic agonists to induce heart failure and that high concentrations of potassium chloride leads to cardiac arrest (Langendorff 1898) (i.e. how lethal injections are done).

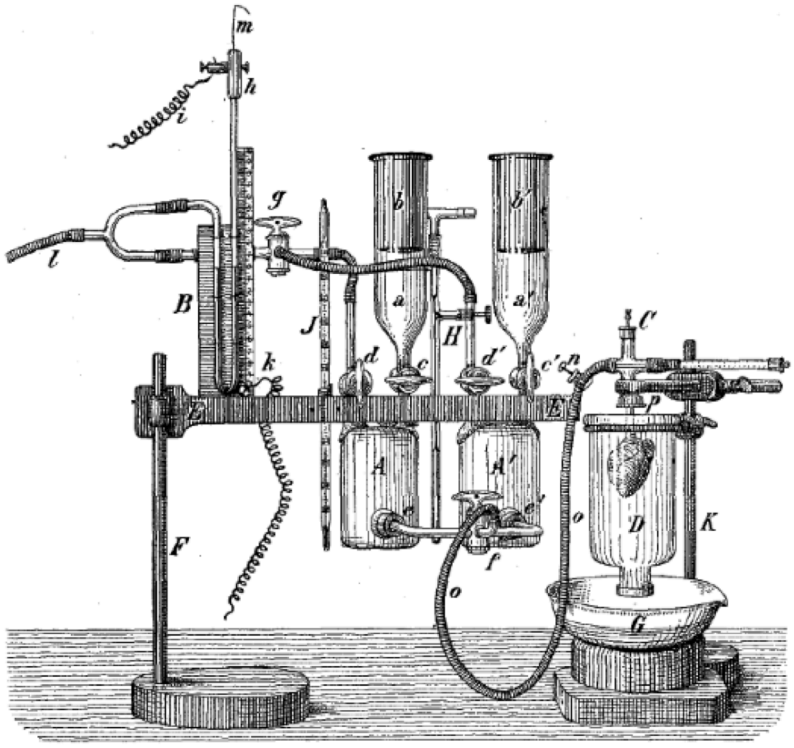

Figure 1.2 Langendorff apparatus that shows a rabbit heart in a glass beaker (D) that is being retro-graded perfused through the aorta. The two cylinders shown to the left (b,a,b',a',A,A') are where the blood is stored at equal pressure for constant flow into the heart. A valve is shown at f to control turning off and on flow. A thermometer is located at J and C to insure temperature of perfusate before entering the heart (Langendorff 1898).

At that time it was common to perfuse hearts with rabbit blood. However, this provided some complications; not only because of the species difference, but also because of the clotting that would occur overtime. To avoid these clots, the blood was then diluted into a serum. Eventually, a saline medium that contained albumin, and tromethamine along with glucose was made as a substitute perfusate known as Krebs-Henseleit solution (Döring 1990). Today scientists use different perfusion solutions that contain sodium (Na^+), calcium (Ca^{2+}), potassium (K^+), magnesium, glucose, and a neutral buffer to regulate the pH. Most commonly used solutions are a Ringer solution, developed in the late 1880s (Ringer 1883), or a modified Ringer solution for mammals termed Tyrode. Depending on the species and technique, the concentrations of the composed ions slightly varied. Nevertheless, Ca^{2+} was required in the perfusate in order

for contraction to occur in the heart (Ringer 1883). Modifications of the Langendorff perfusion technique have changed over the years to answer specific features of cardiac function.

The mechanical function of the heart became more defined by measurements of not only flow rate, but also changes in the vasoactive properties of the arteries as drugs were released in addition to neuronal regulation. Katz modified the perfusion technique so that he could control the flow rate in which the coronary arteries are perfused. This improvement allowed him to measure in great detail the rate in which drugs reached a specific area in the heart and their vascular response of the heart (Skrzypiec-Spring, Grotthus et al. 2007). Neuronal innervation plays an extremely significant role in the mechanical function of the heart. Many scientists studied the vasomotor nerves of the coronary vessels via Langendorff perfusion under numerous experimental conditions, one of which includes the arterial distending plasticity that lead to the foundation of myogenic auto-regulation (Bayliss 1902). This discovery by Bayliss (1902) initiated the study of circulation properties in other organs (Skrzypiec-Spring, Grotthus et al. 2007).

In the early 1900s Starling monitored the stroke volume of the heart to pump blood and its correlation to the end-diastolic volume. The contractile forces required for the cardiac muscle to pump efficiently led physiologists further into understanding the underlying molecular mechanisms that control these contractile forces (Skrzypiec-Spring, Grotthus et al. 2007). The continued use of the Langendorff perfusion as a working heart was later modified for rodents by Morgan and Neely (1967) to study the effects of drug administration, by bubbling oxygen and carbon dioxide in solution that bathed the intact heart (Neely, Lieberme.H et al. 1967). At this point, scientist would use this method to isolate heart cells (cardiomyocytes; non-specific species) and analyze them on a subcellular level.

Whole-heart preparation is an ideal way to study physiological events of cardiomyocytes in comparison to single-cell recordings. Although insightful to the basic scientific understand of how channels and organelles function, single-cell measurements present limitations when we want to analyze these functions on a more integrative context. Nonetheless, single-cell recordings provide a significant foundation for understanding cardiac function at a molecular level. Multiple factors are to be considered when comparing data from single-cell and whole-heart experiments; one being temperature differences. Experiments conducted on single cells are commonly recorded at room temperature (RT; ~23°C), although some are recorded at 37°C it is difficult to maintain the cells at higher temperatures once isolated. Temperature has been shown in early Langendorff experiments, to be particularly important for proper cardiac function (Langendorff 1898). More recently it has be determined that certain proteins retain a temperature dependency to function at full capacity. Thus by reducing the rate of activation of temperature-dependent proteins limits the ability to fully understand functional attributes of the heart under physiological and pathophysiological conditions.

The use of rodent hearts, specifically mouse, is especially appetizing to cardio-physiologists for studying cardiac function. Mouse cardiac tissue is anatomically and physiologically similar to larger mammalian cardiac tissue, but not identical. For instance, the innate structure of mouse heart cells (cardiomyocytes) is structured specifically to maintain a fast heart rate. Thus, mouse cardiac tissue contains a vast amount of transverse tubules (t-tubes) for maximum ion exchange that is required for efficient heart function. Whereas larger animals (i.e. guinea pigs, canine, sheep, etc. (Brette and Orchard 2003; Brette and Orchard 2007)) have a slower heart rate, require less t-tubular systems. Hence in mice, exchange of extracellular ion concentrations can

present immediate results. On the other hand, certain drugs require the opening of channels to take affect; therefore binding affinities are reflected in the heart rate corresponding to the flow rate. Nevertheless, the use of mouse hearts provides numerous transgenic possibilities, thus exemplifying one of the greatest advantages.

***1.2** Cardiomyocytes and Excitation-Contraction Coupling (ECC)*

Ventricular cardiac myocytes are very large (100 µm long, 25 µm wide and 10 µm high) striated cells (Huxley and Taylor 1958; Bers 2002). These cells are electrically and metabolically connected through gap junctions at a structure called intercalated disks. Although these are huge cells, the essential working unit of the cell is concentrated in a very small structure (1.8 µm) called sarcomere (see Figure 1.3)[*]. Within the sarcomere are the contractile proteins (myofibrils) where myocardial contraction occurs. These sarcomeres are periodically distributed along the cell with transverse invaginations of the plasma membrane called t-tubules. Alongside the t-tubules are intracellular Ca^{2+}-reservoirs (the SR) for myocardial contraction.

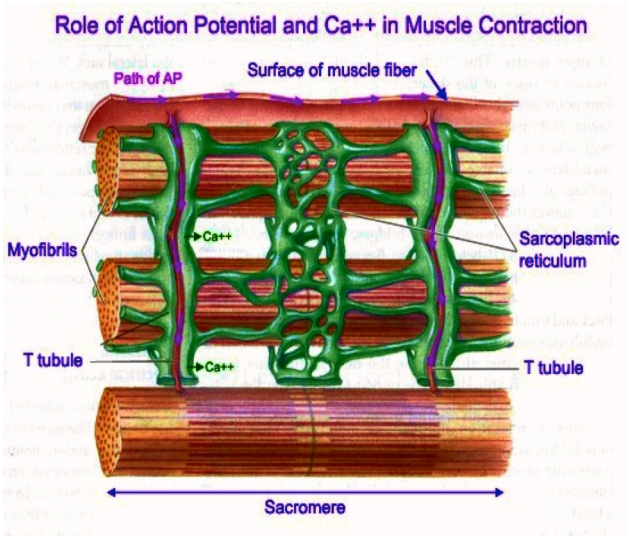

Figure 1.3 Cartoon of cardiomyocyte tubular system and action potential pathway. Acquired from online source*

Excitation-contraction coupling (ECC) is the conversion of an electrical stimulus (action potential) into a mechanical response (contraction of myocyte filaments). The electrical signal travels across the plasma membrane and down the t-tubules inducing a local-propagated action potential (AP). A typical epicardial AP portrays a spike and dome behavior, described in several phases (Figure 1.4). Phase 0 of a typical AP starts with the opening of sodium channels ($Na^{+}_{v1.5}$). As these channels open, a rush of Na^{+} ions through this channel from the extracellular side, into the cell (Na^{+}-influx) will depolarize the plasma membrane ("spike") (Huxley and Taylor 1958; Bers 2002). Changes in the membrane potential drive the opening of specialized potassium channels ($K_{V4.3}$, ITO), which rapidly repolarize the membrane during Phase 1 (Huxley and Taylor 1958; Bers 2002). In addition to the K^{+} transient outward current (via K_{ITO}-channels), the depolarization of the membrane by Na^{+}-channels will also drive the opening of voltage-sensitive Ca^{2+}-channels (L-Type) (Huxley and Taylor 1958; Bers 2002). As Ca^{2+} enters the cell through these L-Type Ca^{2+}-channels (LTCC), it triggers the release of intracellular Ca^{2+} from the sarcoplasmic reticulum (SR) through specialized SR-Ca^{2+} channels termed Ryanodine receptors (RyR2) (Huxley and Taylor 1958; Fabiato and Fabiato 1975; Fabiato 1983; Fabiato 1992; Bers 2002). This trigger mechanism occurs

*http://www.colorado.edu/intphys/Class/IPHY3730/image/figure9-2.jpg

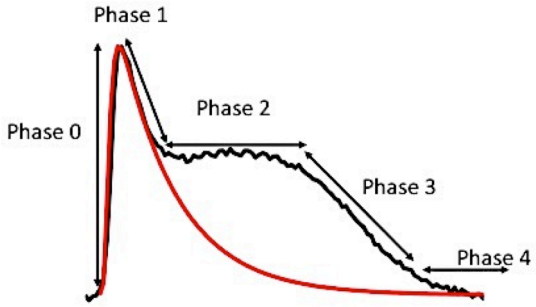

Figure 1.4 Mouse epicardial action potential recording, representing a "spike" and "dome" behavior with defined phases. (acquired using Di-8-ANEPPS, 4 Hz, 37ºC)

at the same time in the AP as Phase 2 ("dome") in myocytes (Bers 2002). In 1975, Alex Fabiato revealed this phenomenon and termed the triggering of SR-Ca^{2+} release, Calcium-Induced-Calcium-Release (CICR) (Fabiato and Fabiato 1975; Fabiato 1983). His studies suggested a positive feedback system that activated CICR and a negative feedback system to terminate the release process (Fabiato and Fabiato 1975; Fabiato 1983). The positive feedback would be the opening of the LTCC to trigger SR-Ca^{2+} release and once the cytosolic Ca^{2+} levels rose, there was a negative feedback mechanism that inactivated the Ca^{2+} release from the SR (Fabiato 1983; Fabiato 1992). Since Phase 2 of a ventricular AP is characterized as the late-depolarized phase, where Ca^{2+} released from the SR will bind to myofilaments for myocardial contraction, the duration of Phase 2 is longer and thus slower than skeletal APs. Once myocardial contraction had occurred, cardiomyocytes would be in a relaxation phase, priming for the next contraction. Fabiato proposed that during this relaxation phase, a re-uptake of Ca^{2+} into the SR would occur (Fabiato 1983). It was later determined that the reuptake of cytosolic Ca^{2+} was through a Sarco-Endoplasmic Reticulum Ca^{2+}-ATPase (SERCA; SERCA2a). After the late-depolarization phase (Phase 2) of the ventricular APs, is the late-repolarization phase (Phase 3). Membrane repolarization occurs when K^+-channels (K_v and K_{ir}) open to reestablish the resting membrane potential (Phases 3 and 4), however other ion transport mechanisms also participate during these phases to regulate intracellular dynamics (Huxley and Taylor 1958; Bers 2002).

The mechanical response of ECC, as the result of CICR, is the contraction of the cardiomyocytes (Figure 1.5). As Ca^{2+} is released from the SR, some of the ions will bind to a protein complex called troponin C (Bers 2008). This protein complex is found on top of actin filaments of cardiomyocytes (Bers 2002; Brette and Orchard 2003; Brette and Orchard 2007; Bers 2008) (Figure 1.5, bottom right). Once Ca^{2+} is bound, the complex shifts to reveal a binding site in which the motor proteins, myosin, can attach (Bers 2002; Brette and Orchard 2003; Brette and Orchard 2007; Bers 2008). As they attach, the myosin heads "walk" across the filament, contracting the muscle fiber (Figure 1.5, bottom right in red). Ca^{2+} is released from the myosin complex in preparation for the next cycle. After contraction, relaxation occurs lowering cytosolic Ca^{2+} concentration by sequestering Ca^{2+} into the SR via the SERCA2a (Bers 2008). Some of this Ca^{2+} is also extruded out of the cell via the Na^+-Ca^{2+} exchanger (NCX1). Figure 1.5 shows a simplified version of CICR during cardiac ECC. Since Ca^{2+} is a second messenger, the CICR phenomenon is a critical aspect in understanding the regulation and deregulation of cardiac ECC.

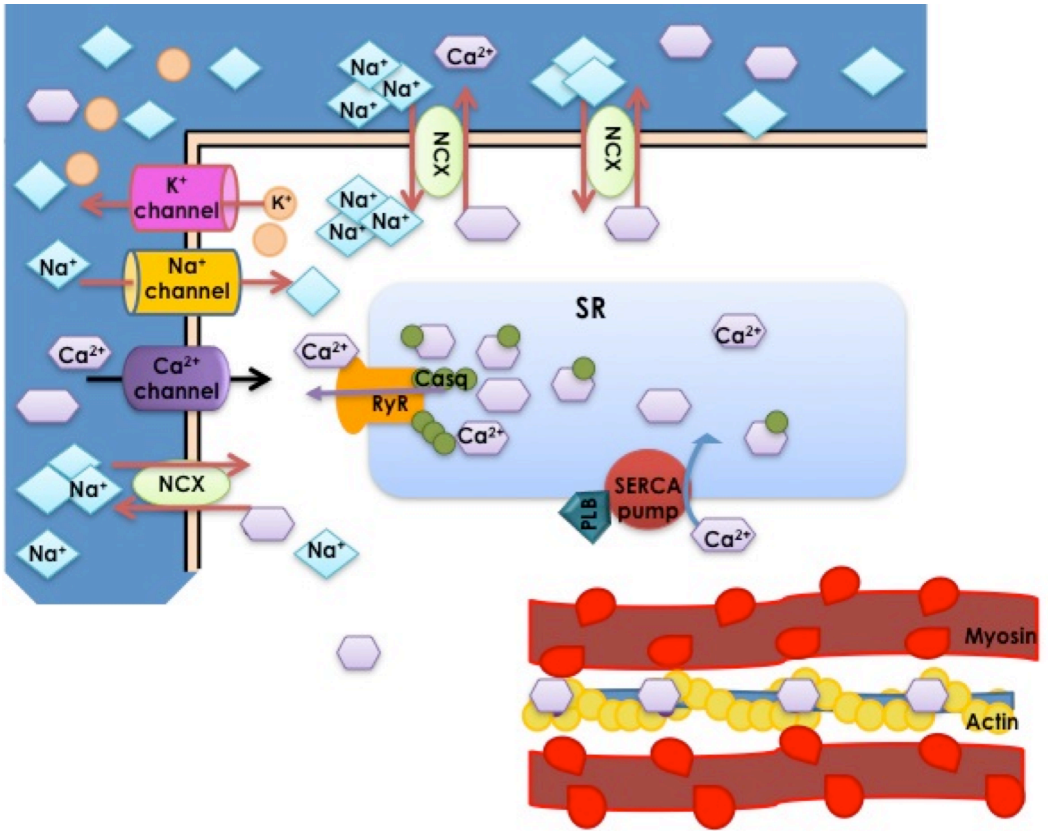

Figure 1.5 A simplified cartoon representation of ECC and CICR. Electrical signal propagates across the plasma membrane and down the T-tubular system activating Na^+-channels (yellow). Changes in the membrane potential activate Ca^{2+}-channels (purple). Ca^{2+} through the Ca^{2+}-channel will activate the release of intra-SR Ca^{2+} through the RyR (orange). Ca^{2+} expelled into the cytosol will either be extruded by NCX (light green) in exchange for 3 Na^+ ions or Ca^{2+} will bind to troponin C on the actin filaments (bottom right, yellow). Ca^{2+} bound to troponin C will shift the myofilament complex so that myosin heads can attach and myocardial contraction occurs. After contraction, Ca^{2+} is pumped back into the SR through the SERCA pump (dark red). Notate: Ca^{2+} in the SR is buffered by calsequestrin (CSQ) and phospholamban (PLB) is an inhibitor of the SERCA.

***1.3** History of the Cardiac-Specific Sodium-Calcium Exchanger (NCX1)*

The idea that there was a protein that exchanged intracellular Ca^{2+} for extracellular Na^{+} was a revolutionary concept that has led scientists to an extraordinary advancement in the mechanisms of Ca^{2+} transport across the membrane. The discovery of what we know today as the cardiac-specific sodium-calcium exchanger (NCX1) was first established in 1968, from experiments conducted on guinea-pig, sheep and calf hearts, as a sarcolemma protein able to translocate two different cations (Reuter and Seitz 1968). Prior to 1968, experiments conducted on frog hearts (de Burgh Daly and Clark 1921; Luttgau and Niedergerke 1958; Niedergerke 1963; Niedergerke 1963; Niederge.R and Orkand 1966; Niederge.R and Orkand 1966), dog hearts (Langer 1964), and squid axons (Hodgkin and Keynes 1957) provided insight into the mechanism of the exchanger, however the relationship between extracellular Na^{+} and intracellular Ca^{2+} was not clearly identified. For instance, the correlation between these ions first reigned importance in 1958 when it was observed that a reduction in extracellular Na^{+} (replaced by Li^{+}) had induced an increase in intracellular Ca^{2+} (Luttgau and Niedergerke 1958). The proposed mechanism was that Ca^{2+} would enter the cell via a carrier mechanism retained a 1:2 ratio for a binding site with extracellular Na^{+} (Luttgau and Niedergerke 1958; Niedergerke 1963; Niedergerke 1963). In other words, the entry of Ca^{2+} was readily accessible when the extracellular Na^{+} concentration was reduced. However, in the late 1960's the mechanism that involved the competition between extracellular Na^{+} and Ca^{2+} was dismissed when Reuter and Seitz (1968) applied a previously proposed theory of an ion transport mechanism(Ussing 1947) to the Ca^{2+} extrusion rate that occurred in Na^{+}-free Tyrode. In this study, data acquired also suggested a temperature dependence of the protein to translocate external Ca^{2+} or Na^{+} into the cell (Reuter and Seitz 1968). Although there was no evidence of ATP-hydrolysis, activation of this protein was predicted to have a higher affinity for Ca^{2+} on the intracellular side of the membrane and not the extracellular side (Reuter and Seitz 1968). All in all, Reuter et al. acknowledged that this electro-neutral exchange mechanism was in fact a crucial transport mechanism responsible for the reduction of cytosolic Ca^{2+} during ECC in mammalian hearts (Reuter and Seitz 1968). During this time period, another group of scientists working with squid axons published evidence of an electrochemical gradient across the sarcolemma that provided a driving force for a protein that exchanged Na^{+} for Ca^{2+} (Baker, Blaustein et al. 1969). The use of an electrochemical gradient as a driving force is notated as a secondary active transport mechanism, verses a primary active transporter were the hydrolysis of ATP is the driving force. This was determined by Baker et al. (1969) by the application of a cardiac glycoside (ouabain) to block the primary active transporter, Na^{+}/K^{+} pump, and collected measurements of Na^{+} efflux as external NaCl was replaced with low concentrations of LiCl. Ca^{2+} influx was also notated to increase after the application of the cardiac glycoside and even more so after the external NaCl was replaced with LiCl (Baker, Blaustein et al. 1969). These events linked a plausible correlation between extracellular Na^{+} and intracellular Ca^{2+}, as well as introduced the idea of the bi-directionality of the Na^{+}-Ca^{2+} exchanger (NCX) as intracellular concentrations changed. The evidence provided by the Baker et al (1969) further supported the findings of other scientists working to identify the role of NCX.

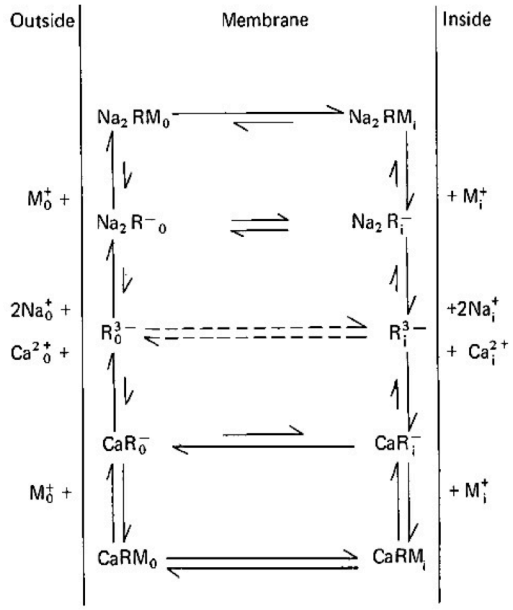

Figure 1.6 Diagram of the Ca^{2+}-cation counter-transport carrier mechanism. Outside (left) is the extracellular side of the membrane and inside is the intracellular side of the membrane (right). NCX is notated as "R_o^{3-}" for extracellular and "R_i^{3-}" for intracellular of the free carrier. The monovalent binding sites of this carrier are indicated by "M^+" and the divalent binding sites are indicated by either 2 Na^+ or 1 Ca^{2+}. Arrows illustrate favored (long) and unflavored (short) directionality of ion transport. (Blaustein, Russell et al. 1974)

The coupling counter transport ratio of 2 [Na^+] : 1 [Ca^{2+}] was challenged in 1974 when Blaustein et al. observed the inter-relationship between Na^+ and Ca^{2+} fluxes (Blaustein, Russell et al. 1974). They determined a coupling ratio of the exchanger to be 3 [Na^+] : 1 [Ca^{2+}] due to a cationic influx, thereby disqualifying an electro-neutral exchange. However, proposed mechanisms of this protein to exchange 1 [Ca^{2+}] : 1 [Ca^{2+}] remained as a trait of the protein (Blaustein and Lederer 1999). In this study, the activation of the exchanger was speculated to require congruent binding on both the extracellular and intracellular sides of the plasma membrane. Figure 1.6 illustrates their proposed mechanism of the sodium-calcium exchanger (NCX) across the plasma membrane (Blaustein, Russell et al. 1974). The NCX protein was described as a counter-transport carrier ("R^{3-}"), having two possible binding sites on both sides of the membrane. One binding site is able to bind 2 Na^+ or 1 Ca^{2+}, whereas the other binding site can only bind a monovalent ion ("M^+"; Li^+ or Na^+). Once these ions bind on the intracellular and extracellular sides of the membrane, they are transported across the membrane; as indicated by the long arrows in Figure 1.6. The preferred mode of the exchanger was anticipated for the extrusion of intracellular Ca^{2+}, thus a cationic influx via 3 Na^+ was produced (Blaustein, Russell et al. 1974). Binding properties for activation of the exchanger to extrude Ca^{2+} required the intracellular binding of Ca^{2+}; one of which is not translocated. On the other hand, extracellular binding sites were able to bind either

Na^+ or Ca^{2+} for active transport. These results were consistent with the findings of Ca^{2+}-Ca^{2+} and Na^+-Ca^{2+} exchange (Blaustein and Lederer 1999). The driving force of the exchanger became more evident, however the energy source required for transport of these ions across the plasma membrane was yet clearly defined. The electrogenic property of this protein was theorized to be voltage-sensitive, thereby providing sufficient energy to extrude Ca^{2+} (Blaustein, Russell et al. 1974; Blaustein and Russell 1975; Mullins and Brinley 1975). Although many of these experiments were conducted in squid axons, they provided a foundation for further inquiry in the function and key importance of the NCX1 ("NCX isofom1").

Prior to 1989, experimental techniques were somewhat inadequate for measuring direct effects of NCX on the membrane potential. Current through NCX is relatively small in comparison to the current carried through ionic channels, due to the counter-ion transport mechanism. The most ideal way of measuring the exchanger activity was to use a whole-cell voltage-clamp technique. However this technique imposed some technical limitations in gaining direct access to the intracellular side of the plasma membrane, which limited recordings of this protein's regulatory mechanisms. Nevertheless, the coupling ratio of NCX was verified to be 3:1 when operating in either mode of operation; forward-mode (3 Na^+ in: 1 Ca^{2+} out) or reverse-mode (1 Ca^{2+} in: 3 Na^+ out) (Reeves and Hale 1984; Kimura, Miyamae et al. 1987; Bridge, Smolley et al. 1990). In 1989 the transport field was revolutionized by the development of a "giant patch-clamp" technique. The giant-excised-membrane-patch technique mimicked the standard patch-clamp technique via access to the intracellular membrane, with the resolution of whole-cell recordings (Hilgemann 1995). The larger surface area and low leak current allowed for recordings of multiple exchangers, thus a large enough current could be detected (Hilgemann 1989). Scientists were now able to obtain data on the intracellular regulation and deregulation of NCX in addition to insight into its electrogenicity (Hilgemann 1989; Hilgemann 1990; Hilgemann and Collins 1990; Hilgemann, Nicoll et al. 1991).

At this time the scientific community operated under the understanding that NCX1 is synergically coupled with L-type Ca^{2+}-channels in the t-tubules; Ca^{2+} influx through the L-type Ca^{2+}-channels is removed by the exchanger (Bridge, Smolley et al. 1990; Leblanc and Hume 1990; Sham, Cleemann et al. 1992; Philipson and Nicoll 2000; Bers 2008). Being that NCX1 is the main extruder of cytosolic Ca^{2+}, it therefore must participate in the maintenance of intracellular Ca^{2+} homeostasis. Consequently, the extrusion of Ca^{2+} by NCX1 produces a bi-directional cationic transport across the membrane of 3 Na^+ per Ca^{2+} ion. The transport of Ca^{2+} out of the cell is against the Ca^{2+} gradient (2 mM extracellular from 100 nM intracellular) and therefore dependent on the extracellular Na^+ electrochemical gradient (i.e. a secondary active transporter) (Hilgemann 1990). Primary active transporters, although these are ATP-dependent, also drive a bi-directional cationic transport that are sensitive to changes in the membrane potential and therefore it is safe to assume that NCX1 must also be sensitive to changes in the membrane potential. In the early 90s the voltage-sensitive properties of the exchanger became more apparent as the molecular structure for translocation of Ca^{2+} and Na^+ was further investigated (Nicoll, Longoni et al. 1990; Hilgemann, Nicoll et al. 1991). Advancements in technology during this era focused on molecular cloning and mutagenesis for transgenic expression in mice. For instance, intracellular sensitivity was determined by giant-patch clamp current measurements of native, cloned and mutated cytoplasmic intracellular loop of NCX1 proteins (Matsuoka, Nicoll et al. 1993).

In 2004 NCX1 was categorized under the solute carrier-8 (SLC8) superfamily due to its Ca^{2+}-Na^{+} antiporter characteristics (Cai and Lytton 2004). Within this counter-transporter family are two other isoforms, NCX2 and NCX3. NCX2 is found in primarily in the brain, whereas NCX3 is more commonly found in both the brain and skeletal muscle (Nicoll, Longoni et al. 1990; Blaustein and Lederer 1999; Philipson and Nicoll 2000; Quednau, Nicoll et al. 2004; Lytton 2007). NCX1 on the other hand is particularly special because it has been found in all tissue types with high expression in the heart, kidneys and the brain (Nicoll, Longoni et al. 1990; Blaustein and Lederer 1999; Philipson and Nicoll 2000; Quednau, Nicoll et al. 2004; Lytton 2007). Within these tissue types, NCX1 sensitivity and regulation varies due to alternative splicing within a specific region of the intracellular loop (Philipson and Nicoll 2000).

It is known thus far that the cardiac-specific Na^{+}-Ca^{2+} exchanger (NCX1) is a nine transmembrane-segmented (TMS) protein with a large intracellular loop (Figure 1.7) (Philipson and Nicoll 2000). The first five TMS consists of the amino-terminus (N-terminal) domain of NCX1 (Figure 1.7, left). Within this domain, TMS 2-3 retain a highly conserved alpha-repeat (α-1) that has been implicated as a region for ion binding/transporting (Figure 1.7, shaded region). On the cytosolic side of TMS 5 is a 20-amino acid endogenous exchange inhibitory peptide region (XIP), thought to be the site for Na^{+}-dependent inactivation. Following this region is the cytoplasmic loop, which connects the N-terminal domain to the carboxyl-terminus (C-terminus) domain (Figure 1.7, between TMS 5-6). There are several regulatory sites located on and around the intracellular loop of NCX1; which include a Na^{+}-dependent inactivation site (shares site with XIP), two Ca^{2+}-binding domains (CBD1 and CBD2), a phosphorylation site, and a region where alternative splicing can occur for tissue-specific NCX1 variation (Figure 1.7, bottom). The C-terminus domain of NCX1 consists of the four remaining TMS with another α-repeat (α-2) located on the cytosolic side between TMS 7 and 8 (Figure 1.7, shaded region). The α-2 domain is of particular interest due to the GIG sequence located within the membrane as the conductive segment of NCX1 (Philipson and Nicoll 2000). In addition, the α-2 domains reentry loop has shown to alter the Na^{+} and Ca^{2+} affinities when mutated (Matsuoka, Nicoll et al. 1993). Moreover, the cytosolic side of the α-2 domain was found to be the binding-site for the pharmaceutical NCX1 reverse-mode inhibitor, KB-R7943 (Iwamoto, Kita et al. 2001).

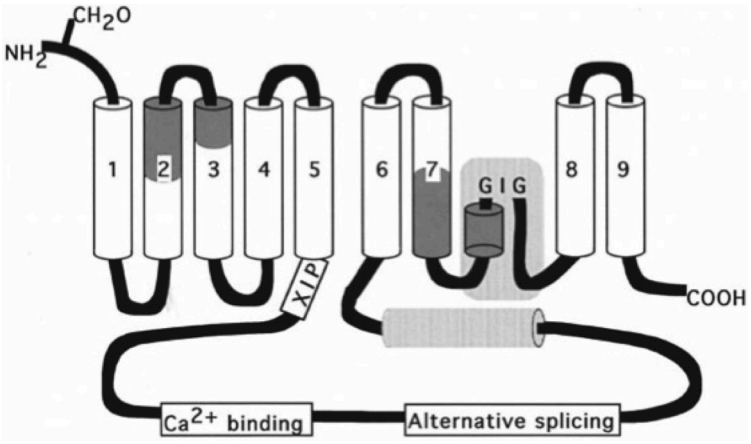

Figure 1.7 Model of NCX representing the Ca^{2+}-binding site, XIP (Na^{+}-inactivation) site and the conductive segment (GIG sequence) within the transmembrane protein. (Philipson and Nicoll 2000)

The GIG sequence suggests that activation of the exchanger can also be initiated by changes in the membrane potential, thus a voltage-sensitive electrogenic trait. Further suggesting the exchanger's ability to catalyze the extrusion of Ca^{2+} (forward-mode) or reverse the exchange process by extruding excess Na^{+} (reverse-mode), in order to re-establish Ca^{2+} homeostasis (Philipson and Nicoll 2000). It is still up for debate which mode is key in excitation-contraction coupling (Sipido, Maes et al. 1997; Litwin, Li et al. 1998; Hobai and O'Rourke 2000; Matsumoto, Miura et al. 2003).

Intracellular activation of NCX1 to extrude cytosolic Ca^{2+} against its concentration gradient (2 mM extracellular, 100 nM intracellular resting) starts with Ca^{2+}-binding to the CBD1 and CBD2 domains. When intracellular Ca^{2+} levels increase, Ca^{2+} ions will bind to the CBD1 and CBD2 domains. An increase in cytosolic Ca^{2+} is also shown to relieve the Na^{+}-inactivation site (XIP; Figure 1.7), thereby activating the forward-mode of operation. The translocation site for Na^{+} and Ca^{2+} is thought to be within highly conserved α-repeat segments (Hilge 2012; Khananshvili 2013; Ottolia and Philipson 2013). Unfortunately very little is known about the exact translocation site and the residues responsible for identifying Na^{+} and/or Ca^{2+} ions for exchange (Ottolia and Philipson 2013). Nevertheless, the binding sites and translocations sites differ for both Na^{+} and Ca^{2+}. Due to the Na^{+}-driven electrochemical gradient, the NCX1 will exchange 3 Na^{+} in and 1 Ca^{2+} out of the cell. As intracellular Na^{+} levels increase, Na^{+} will bind to the XIP region to inactivate the forward-mode operation of NCX1. Activation of reverse-mode exchange of NCX1 is speculated to depend on rapid rises in intracellular Na^{+} or as a result of disruption of intracellular Ca^{2+}-homeostasis where Ca^{2+}-entry via NCX1 is needed along with LTCC opening to trigger CICR from the SR (Figure 1.8).

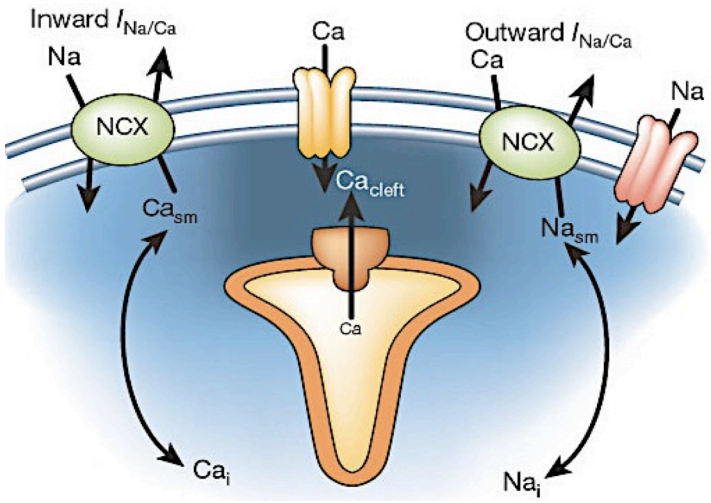

Figure 1.8 Cartoon representation of NCX functioning in forward-mode (left) and the reverse-mode (right). (acquired from Bers, 2002)

Modification of NCX1 has been shown to either increase or decrease heart function, depending on the type of modification to the protein and/or the technique used in obtaining the data (Barry 2000; Pogwizd 2000; Armoundas, Hobai et al. 2003). It is, however established that a drug called Digitalis is used to treat patients with a decrease in heart contractility, to increase the contractility of their weakened heart (Altamirano, Li et al. 2006). Digitoxin (or experimentally used ouabain) is derived from the leaves of a foxglove plant. This drug specifically binds to the Na^{+}/K^{+}-pump (an ATPase), inhibiting

the extrusion of intracellular Na^+. As a consequence there is an increase in the cytosolic [Na^+], thereby activating NCX1 in the reverse-mode to trigger CICR from the SR (Altamirano, Li et al. 2006) (Figure 1.8, right). After all, it only takes a small influx of Ca^{2+} to trigger the opening of RyR2 channel. On the other hand, increases in cytosolic Na^+ can also occur as a consequence of acidosis. Acidosis is most commonly found during ischemia-reperfusion. An over activity of the Na^+/H^+-exchanger (NHE); exchanging H^+_{out} and Na^+_{in} will create an increase in intracellular [Na^+], hence triggering NCX1 to function in the reverse-mode, creating an influx of Ca^{2+} (Kusuoka, Porterfield et al. 1987; Bolli and Marban 1999; Vittone, Mundina-Weilenmann et al. 2002; Said, Becerra et al. 2008). Local increases in cytosolic [Ca^{2+}] will trigger Ca^{2+}-release from the SR (i.e. CICR) in addition to activating other pathways that will open more $Ca_{v1.2}$-channels (i.e. LTCC) and increases activity of SERCA2a to restore Ca^{2+}-reservoir. This increase in CICR activity will increase the mechanical response of the cardiomyocyte filaments, thereby increasing the heart contractility. However, under these circumstances there will be a decrease in the heart function due to the increase in cytosolic Ca^{2+} levels can desensitize RyR2 (via cytosolic regulation), and the increases in SERCA2a activity will enhance intra-SR Ca^{2+} content. These elevations in myoplasmic Ca^{2+} levels and lack of Ca^{2+}-homeostasis can lead to ventricular fibrillation and myocardial stunning (Kornyeyev, Petrosky et al. 2011).

1.4 *Cardiac Sympathetic Regulation*

CICR is a complex mechanism that involves several intracellular pathways. One particular pathway of great interest is the βeta-adrenergic (β-adrenergic) stimulatory pathway. β-adrenergic receptors (β-AR) are located in the plasma membrane of cardiomyocytes and are responsible for a cascade of events that regulates CICR (Mazzanti and DeFelice 1990; Fan, Shuba et al. 1996; Barman, Choisy et al. 2011). Activation of the β-adrenergic pathway is modulated by sympathetic neurons under the autonomic nervous system and by the release of catecholamines by the adrenal medulla. In response to the sympathetic "fight and flight" response, neurons located at the base of the heart will release neurotransmitters, epinephrine or norepinephrine. These neurotransmitters will bind to β-AR in pacemaker cells (SA node) to speed up the heart rate (Pogwizd, Schlotthauer et al. 2001; Lakatta 2004; Bers 2008). In the ventricles, β-ARs are activated to increase myocardial contractility (Lakatta 2004). Experimentally the perfusion of a β-agonist, like isoproterenol, is widely used to activate this pathway in cardiomyocytes (Mazzanti and DeFelice 1990; Fan, Shuba et al. 1996; Barman, Choisy et al. 2011). Once isoproterenol is bound to the β-AR (Figure 1.9), the intracellular coupled G-protein (G_s) will activate adenylyl-cyclase to convert an adenosine triphosphate (ATP) to cyclic-adenosine monophosphate (cAMP). This is will trigger a downstream pathway carried out by protein kinase A (PKA). PKA is involved in several intracellular regulatory pathways, specifically in response to β-adrenergic stimulation PKA will facilitate L-type Ca^{2+}-channels (LTCC) to open and will phosphorylate phospholamban (PLB). Phosphorylation of PLB will relieve the SERCA2a pump, so that cytosolic Ca^{2+} can be pumped faster into the SR and Ca^{2+} stores are fully replenished for the next release (Figure 1.9). Under normocardic conditions, activation of this pathway can reduce the appearance of Ca^{2+}-alternans by facilitating a larger trigger (via LTCCs) for SR Ca^{2+} release through the RyR2 and a faster Ca^{2+} reuptake (via SERCA2a). On the other hand, clinically β-blockers are used as a treatment option for patients with atrial fibrillation, ventricular tachycardia, and/or heart failure.

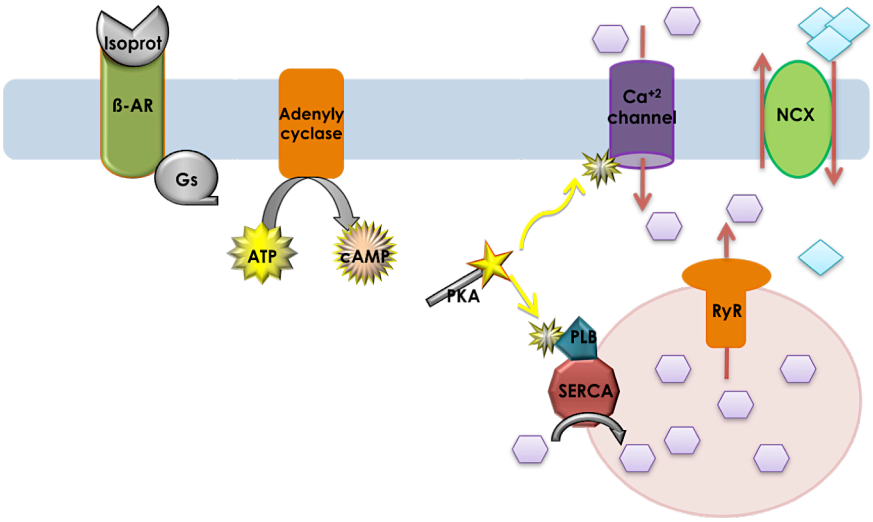

Figure 1.9 Cartoon representation of the β-adrenergic stimulatory pathway. Light blue triangles are Na^+ ions and light purple hexagons represent Ca^{2+} ions.

1.5 Cardiac Arrhythmogenesis

One of the most common forms of electric cardiac dysfunction is atrial fibrillation. Although this cardiac arrhythmia is not always lethal, it can generate thrombotic effects that can lead to a substantial morbidity and mortality in patients presenting this dysfunction. Atrial fibrillation imposes a chaotic behavior in the firing of electrical impulses in the atriums. If these impulses are able to conduct to the ventricles in this chaotic behavior, ventricular tachycardia can present itself.

Ventricular tachycardia occurs when uncontrolled extra-systolic electrical impulses are initiated in the ventricles. These spontaneous electrical impulses will produce changes in the heart rate, resulting in disturbances of the electrical behavior and metabolic regulation of the heart. Polymorphic ventricular tachycardia is found in various medical conditions such as, torsade de pointes, long Q-T syndrome, and patients suffering from catecholaminergic polymorphic ventricular tachycardia (CPVT); all of which share abnormal characteristics in the T-wave formation in electrocardiogram (ECG) recordings (Pham, Quan et al. 2003).

Initiation of the cardiac cycle begins in very specialized excitable cells within the right atrium; sinoatrial nodal cells (SA node) and atrioventricular nodal cells (AV node). These cells control the automaticity of the heart and are characterized as pacemaker cells (Bers and Bridge 1989; Bogdanov, Vinogradova et al. 2001; Schram, Pourrier et al. 2002; Sasse, Zhang et al. 2007). Electrical impulses, initiated by the SA node, are relayed to the ventricles through the AV node. Propagation through the AV node provides a delay in the electrical signal allowing the chambers to efficiently fill with blood during diastole (relaxation phase) (Bers and Bridge 1989; Schram, Pourrier et al. 2002; Sasse, Zhang et al. 2007). Systole (contraction phase) occurs after the signal has travelled down the AV bundle (“bundle of His”) towards the apex and spans across the right and left ventricles in an upward motion. AP propagation of the ventricles begins

with cardiomyocytes located on the inner surface of the ventricles; endocardial myocytes of the endocardium (Figure 1.10, lower panel). Conduction of the electrical signal radiates in an outward direction, through the mid-myocardium arriving at the epicardium. Duration and morphology of endocardial APs differ from that of any other cardiomyocytes, including those found in the epicardium (Zygmunt, Goodrow et al. 2000; Bers 2002; Brette and Orchard 2003; Brette and Orchard 2007; Xu, Chen et al. 2011). Differences are defined by a gradient in the molecular properties of myocytes laying different layers within the ventricular free wall. Subsequently, this electrical behavior is reflected in the morphology of ECG recordings (Figure 1.10).

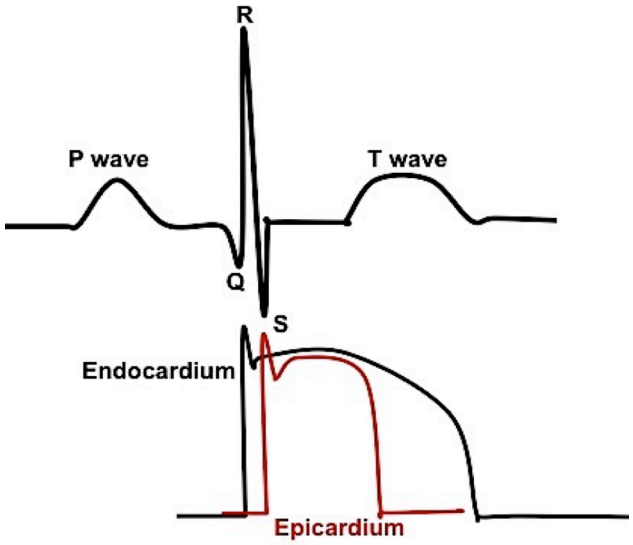

Figure 1.10 Top panel: Basic ECG drawing showing a P-wave, QRS, and positive T-wave. Bottom panel: AP traces of the ventricular electrical activity from the endocardium (black trace) to epicardium (red trace) and its correlation to the QRS and T-wave formation.

As the electrical signal travels its path (as mentioned above), changes in the membrane potential for each region of the cardiac cycle is translated and recorded with the aid of an electrocardiogram (ECG). Human ECGs (Figure 1.10, top panel) have a distinctive “P-wave”, “QRS” and “T-wave”. Depolarization of the atrium is represented by the “P-wave”. In addition, the ECG morphology changes as the endocardium becomes depolarize producing a Q-R segment (negative to positive spike) and the R-S segment as the epicardium depolarizes (peak to negative spike back to baseline). On the other hand, the collective difference between repolarization of these regions will produce a large (positive) wave, called the T-wave. Needless to say, changes in the repolarization of either membrane can produce alternations in the amplitude of T-waves (TW-Alt). Diversifications in T-wave morphology are often found in ECG recordings of patients suffering with myocardial infarction (Laurita, Katra et al. 2003; Wilson and Rosenbaum 2007; Rosenbaum 2008; Cutler, Jeyaraj et al. 2011) (Verrier, Kumar et al. 2009). One example of this is the inversion of the T-wave, where the endocardium repolarizes before the epicardium (Figure 1.11 B). This is often represented in ischemic hearts or those having an infarction. TW-Alts can be a predictor of to sudden cardiac death (SCD) (Pham, Quan et al. 2003). Lack of a definite marker for SCD is an ongoing problem for clinicians to effectively diagnose patients that may be at risk (Pham, Quan et al. 2003)

(Verrier, Kumar et al. 2009). Nevertheless, the occurrences of these T-wave alternans (TW-Alt) are extensively studied in various species to understand the basic mechanisms that attribute to this unique beat-to-beat behavior.

Beat-to-beat alternations in the duration of APs are termed “AP-alternans” (AP-Alt). These beat-to-beat alternations can be formed in response to a disruption in the electrical signal, thus elicit an arrhythmogenic behavior of the heart (Figure 1.11). Elicitation of AP-Alts are still unclear, although several studies have proposed Ca^{2+} instability within the cardiomyocytes are a major cause of cardiac alternans (Chudin, Goldhaber et al. 1999; Choi and Salama 2000; Carmeliet 2004; Wan, Laurita et al. 2005; Clusin 2008). Because intracellular Ca^{2+}-handling is a complex system, irregularities to this system can potentially produce beat-to-beat changes in the amplitude of SR-Ca^{2+} release.

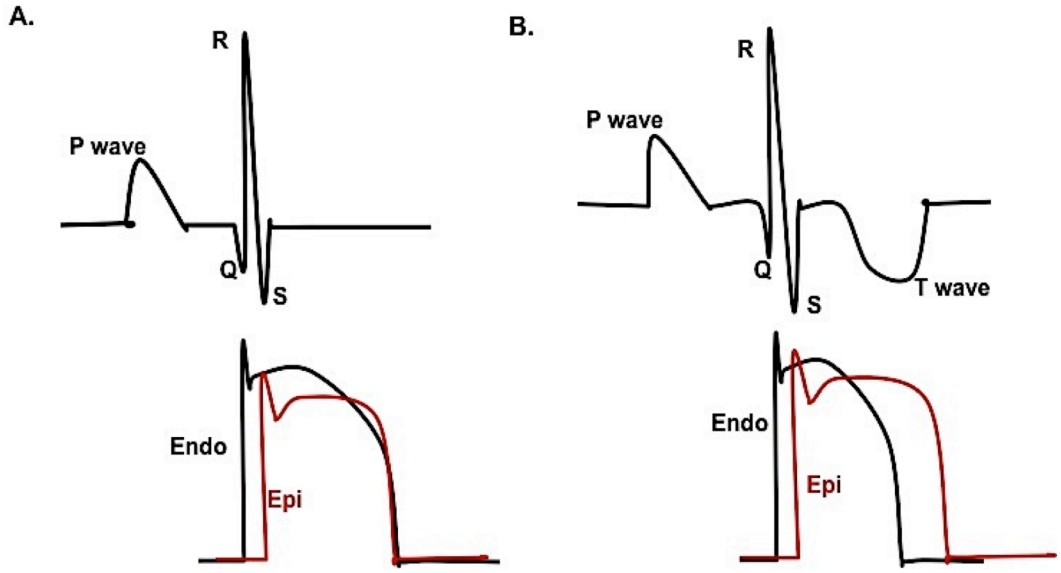

Figure 1.11 Basic ECG and AP electrical activity if the AP repolarization were to differ. No T-wave will be represented in the ECG when both the endocardium (Endo) and the epicardium (Epi) layers repolarize at the same time (A). Inversion of the T-wave will appear if the endo layer repolarizes first (B).

Ca^{2+} alternans (Ca-Alt) are recorded as changes in the amplitude of Ca^{2+} transients. Mechanisms proposed of origin of these release patterns are related to the SR’s ability to store and release Ca^{2+}, on the other hand these contributions are not solely responsible for Ca^{2+}-homeostasis of the heart. Other mechanisms include the extrusion of Ca^{2+}, via NCX1. Nevertheless, the amount of depletion from intracellular Ca^{2+} stores is considered to be a key aspect controlling the magnitude of Ca^{2+} release (Terentyev, Viatchenko-Karpinski et al. 2002). Further suggesting, strong releases of Ca^{2+} from the SR can become difficult for ATP hydrolysis of the SERCA2a pump in order to efficiently replenish the Ca^{2+} stores before having to release again. Lack of proper replenishment is enhanced at higher heart rates, resulting in fractional releases (Valverde, Kornyeyev et al. ; Xie, Sato et al. 2008; Kornyeyev, Petrosky et al. 2011). Suggesting multiple factors can be involved in the enhancement of Ca^{2+} release, thus having the potential to induce or augment Ca-Alt. On the other hand, elevations in SR-Ca^{2+} can also increase the likelihood of local spontaneous Ca^{2+} releases, termed Ca^{2+}-

sparks. Multiple Ca^{2+}-sparks would eventually lead to Ca^{2+} release in a wave-like formation. Ca^{2+}-waves could then trigger arrhythmogenic propagation to neighboring cells if the Ca^{2+}-release from the SR is sufficient to depolarize the membrane. This depolarization can occur during the repolarizing phase of the AP leading to delayed after-depolarization (DAD) (Spencer and Sham 2003) (Diaz, O'Neill et al. 2004).

As previously described, cardiac APs possess specific "phases" that contribute to their unique "spike and dome" morphology (see Figure 1.4). Within each phase are different channels, receptors and proteins that maintain the hearts function. Nonetheless, changes in the membrane potential can elicit abnormal depolarization during the late-repolarizing phase of cardiac APs (Harris, Mills et al. 2005) (Figure 1.11, bottom traces). Cardiac APs display a functional property called a refractory period, where the initiation of the next full AP depending on the time it takes for the Na^{+} channels to recover from it inactivated state (Figure 1.12). During the "relative refractory period" AP's can occur, but not to full capacity (Figure 1.12; "S2").

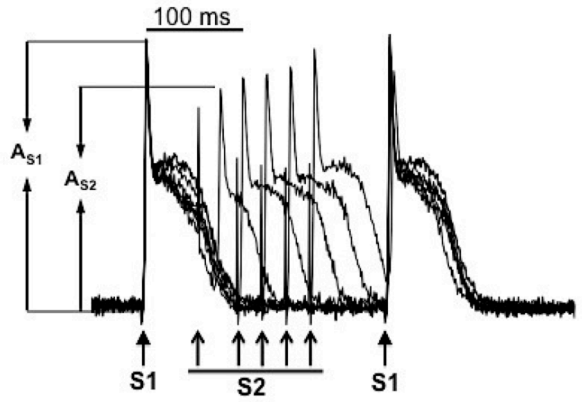

Figure 1.12 Epicardial AP recorded during restitution protocol. Arrows indicate normal stimulus (S1) and the extra-systolic pulse (S2). A_{S1} and A_{S2} indicate the amplitude of the first AP and the elicited AP, respectively (acquired at 4 Hz, 37°C, using Di-8-ANEPPS).

During the repolarization phase the APs can display some abortive and spontaneous APs, termed "early after-depolarization (EAD) (Harris, Mills et al. 2005). EADs have been suggested to be directly related to the intracellular Ca^{2+}-dynamics that occur in phase 2 & phase 3 (Harris, Mills et al. 2005) (Xie, Sato et al. 2008). Specifically, the extension of the plateau phase (phase 2) that occurs during a long Q-T interval in the ECG in combination with an increased heart rate, will lead to the manifestation of EADs (Shimizu and Antzelevitch 1999).

In addition to EADs, spontaneous AP can occur when the membrane potential has been fully repolarized. These spontaneous electrical events are called delayed after-depolarizations (DADs) (Nemec, Kim et al. 2010) (Harris, Mills et al. 2005). DADs differ from EADs in that the extra AP will occur in between normal pacing durations, thus a "delay" in depolarization of the membrane produced in late phase 3 or phase 4 of APs (Nemec, Kim et al. 2010) (Harris, Mills et al. 2005). Due to the location of DADs, it is suggested that spontaneous Ca^{2+}-release mechanisms resulting in an increase in cytosolic Ca^{2+} levels are responsible for their occurrence (Shimizu and Antzelevitch 1999; Volders, Vos et al. 2000; Spencer and Sham 2003; Harris, Mills et al. 2005; Verrier, Kumar et al. 2009; Nemec, Kim et al. 2010) (Ter Keurs and Boyden 2007). Moreover, there are multiple factors and secondary pathways that can promote or are activated as a result of increases in intracellular $[Ca^{2+}]$ that can also contribute to the prolongation of the AP plateau phase. For instance, the Ca^{2+}/calmodulin-dependent protein kinases II (CaMKII) pathway is activated in response to increases in intracellular Ca^{2+}. Recent studies have shown an increase in CaMKII can result in the slowing of Na^{+}-

channel inactivation (Wagner, Dybkova et al. 2006; Ashpole, Herren et al. 2012) and therefore prolong the relative refractory period.

Although many pathways are speculated and currently researched, this dissertation will focus on the mechanisms surrounding the sarcolemma NCX1. NCX1 is an electrogenic transporter that exchanges 3 Na^+ by 1 Ca^{2+}. The electrogenicity of this transporter can produce a change in the membrane potential that introduces a feedback that can modify the repolarization of cardiac APs. Changes in the AP repolarization are especially important at the epicardial layer of the ventricles because they can trigger fatal cardiac arrhythmias. Therefore, these mechanisms are ideal for targeting NCX1's role in the genesis of arrhythmias and development of anti-arrhythmogenic drugs.

SIGNIFICANCE:

The heart is a complex organ where different biophysical and biochemical events are orchestrated together in order to define the physiological function of the system. Assessing hypothesis in a model system have allowed biomedical scientist to define the function of the system from the molecule to the organ. The hierarchized organization of the information permitted in the last century to understand the molecular basis of disease and to develop pharmacological strategies to improve the public health in an unprecedented way. For instance, in the 1890s when Langendorff derived a perfusion system for mammalian hearts because of discrepancies in the anatomy of frog hearts and their ability to absorb Ca^{2+} from the environment verses coronary arteries. Today we not only implement this technique for research, but this system is also used clinically for heart and lung transplantation; as well as, opened the doors to cardiac gene therapy (Katz, Swain et al. 2010).

Over the years, the evaluation of molecular hypotheses at the systemic level has been challenged by the absence of experimental technique to measure critical subcellular parameters. As new techniques are developed and more knowledge is acquired about how molecular mechanisms are applied in a functioning organ, the more precise pharmacological targets can be developed.

According to the American Heart Association 13% of all natural deaths in the USA is categorized as sudden cardiac deaths (~300,000 per year) (Zipes, Camm et al. 2006). Unfortunately these deaths are categorized solely on the fact that the individual would die approximately 1 hour after cardiac symptoms appear; thus a broad diagnosis and limited ability to predict prior to event. On the other hand, some cardiac arrhythmias that can lead to SCD are evaluated by ECG screening. Ventricular tachycardia, for example, has been shown to present TW-Alt in the ECG recordings and often result in SCD (Rosenbaum, Jackson et al. 1994; Pham, Quan et al. 2003; Rosenbaum 2008). The appearance of TW-Alts can be induced by an increased heart rate, however if this increase in heart rate was modulated by the sympathetic nervous system TW-Alts will not present itself in healthy individuals (Laurita, Katra et al. 2003). On the other hand, individuals with genetic abnormalities or a cardiac disease, that could eventually lead to heart failure, can onset arrhythmias when the heart rate is increased. Thus why it is crucial to understand all aspects of the fundamental mechanisms involved in Ca^{2+} regulation in the heart. The more we know, the more we will be able to create and better advance the medical field. After all, it's the small advancements in science that one-day would compile into plausible solutions.

The main significance of this dissertation has been to evaluate the role of NCX1 as a key protein that defines contractility and excitability in the heart. It has been established that NCX1 plays a significant role in intracellular Ca^{2+} dynamics regulation. Taking into account that Ca^{2+} is a second messenger; very small changes in intracellular [Ca^{2+}] can disturb the homeostasis of the cell. Seeing that NCX1 is embedded within the t-tubules and co-localized with Ca^{2+}-channels, it is responsible for the immediate extrusion of excess cytosolic Ca^{2+} whereas the Ca^{2+} re-sequestered by SERCA2a would occur later (in the relaxation phase). Following this train of thought, modification to the activity of NCX1 would therefore limit the access for normal regulation of intracellular Ca^{2+} levels as the cell prepares for myocardial contraction. Therefore deviation in intracellular Ca^{2+} levels would not only affect multiple downstream pathways that normally regulate various feedback loops for myocardial contractility but also pathways that can perpetuate a chemical response that is able to modify the electrical activity of the cell. The relationship between intracellular Ca^{2+} dynamics and electrical excitability is a key factor that correlates metabolic, mechanical and electrical function in the heart. Furthermore, addressing the pathway that links the function of an intracellular organelle (SR) with the membrane potential is essential for developing pharmacological strategies to deal with different type of ventricular arrhythmias during stress (e.g. CPVT), ischemia (infarction) and heart failure.

CHAPTER 2 *: Materials and Methods*

2.1 *Animal Models*

Mouse has been use as the animal model throughout this dissertation. Three different types of mouse strains were used to investigate the role of the NCX protein in the function of the heart during the cardiac cycle. Hearts obtained from C57BL-6 mice were used to investigate the basic bioelectrical properties and Ca^{2+} signaling when the transport of Na^{+} and Ca^{2+} through the exchanger has been pharmacologically challenged (Chapters 3 and 4). Additionally, in order to definitively rule out the role of the NCX1 we used transgenic animals* in which a conditional KO of NCX1 was induced (Chapters 5 and 6).

Cardiac-specific NCX1 knockout mice and wild-type NCX1 Flox mice, derived from Cre/loxP technology(Kos 2004), between 4-9 weeks of age were used in experiments conducted in Chapters 5 and 6. Breeding of these particular transgenic mice was difficult due to the significant role of NCX1 in the excitability, chronotropism and contractility of the heart. Female KO's were unable to breed due to the stress on their hearts during breeding and delivery. Generation of NCX KO mice with 80-90% ablation efficiency highly depends on the content of a tyrosine recombinase enzyme, the Cre recombinase, under the cardiac-specific MLC2v promoter that confer ventricular specificity. To increase this efficiency, a separate Cre hemizygous mouse line was developed by backcrossing a NCX KO with a wild-type mouse that contains a non-flanked NCX protein on the loxP site. Thereby generating three transgenic mouse lines; NCX Flox (WT), NCX Cre, and NCX Cre/Flox (KO) (Figure 2.1).

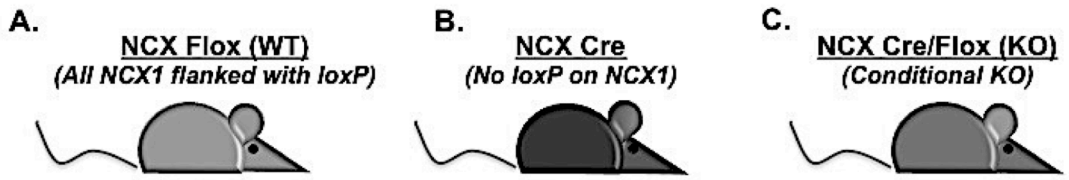

Figure 2.1 Transgenic mouse lines generated from Cre/loxP technology for cardiac-specific NCX1 knockout breeding. NCX Flox (WT) mice (A) have all of the NCX1 exon 11 flanked with loxP (amino acids 722-813), NCX Cre mice (B) have only the hemizygous Cre recombinase expressed under the cardiac specific MLC2v promoter, NCX Cre/Flox (KO) mice (C) express all exon 11 sites flanked with loxP for excision by expressed Cre recombinase.

Ear samples were collected and genotyped using polymerase chain reaction (PCR) to verify, prior to further breeding and use of mice for experimentation. Ear samples were digested at 95°C in 100 µl [25 mM] NaOH, [0.2 mM] EDTA for 1 hr. Once digested, 100 µl of [29.2 mM] Tris-HCl is added and the samples were vortex and centrifuged to separate the tissue and hair from the solution containing DNA. During this time a master-mix was made composing of: [25 mM] MgCl2, GoTag Buffer 5x (Promega M500A), dNTP mix (U151A) ([10 mM] stock, 50x), GoTaq Hot Start Polymerase (stock 5 µ/µl), nuclease-free H2O, along with the following primers:

* NCX1 mice were generously provided by Dr. Kenneth D. Philipson.

G2-F (20 µM),
5'-AGGCATTCCAAAGGATGAGTGAAG-3'

G2-R (20 µM),
5'-ATCCCAGTGGAGTTTGCTACCAGA-3' (flanks the loxP site upstream of exon 11)

F4-F (20 µM),
5'-CCAGGGGAGAGGTATTTATTGTTC-3' (binds ventricular myosin light chain-2 promoter)

F4-R (20 µM),
5'-ACGGACAGAAGCATTTTCCAGGT-3' (to bind the Cre coding sequences).

The master-mix (in aliquots of 29 µl) was distributed into 200 µl PCR tubes; 1 µl of solution containing DNA was added to the mastermix, vortexed and placed in an Eppendorff thermocycler PCR machine (Mastercycler epgradient S, Eppendorff, Germany). This PCR reaction was completed under duplex PCR conditions, where the cycles were as follows: denature at 95°C x 3 min; amplify for 35 cycles at 95°C x 30 sec, 56.5°C x 30 sec, 72°C x 30 sec; with the final extension at 72°C x 7 min. The PCR products were run on an agarose gel (1.5%) containing Ethidium Bromide (6%; EthBr). An aliquot of 6 µl of each sample was loaded into a 15 well chamber, using a 100 bp ladder. Electrophoresis (PowerPac Basic, BioRad, Hercules, CA) was performed at 70 V for 1 hr. The mice that correlate to the NCX Flox and NCX KO genotype were used in experimentation or breeding.

Unfortunately, this genotype expression is limited to just the presence of the appropriate sequence to KO the expression levels of the NCX1 protein in the heart. These particular mice are conditional in the fact that there is a variation in the content of the NCX protein. Therefore, real-time PCR (rtPCR) analysis was done after hearts were used in experiments to measure the efficiency of the Cre enzyme to degrade the exon11 region of NCX1 in the ventricular tissue. According to previously published data using these transgenic mice, there was a KO efficiency of 90% (Henderson, Goldhaber et al. 2004). While conducting experiments presented in Chapters 5 and 6, some KO hearts presented similar wild-type AP kinetic features during recordings that suggested a 40-60% ablation (see Figure 5.4 in Chapter 5 for rtPCR). All mice and hearts used were prepared as described below (see section 2.2), with the exception that some hearts were preserved (-80°C) for further rtPCR analysis.

Real-time PCR experiments were specifically designed to identify the expression levels of messenger RNA (mRNA) for a specified protein. Extraction of mRNA from the ventricular tissue of conditional KO mouse hearts were obtained from preserved hearts collected after some experiments conducted in Chapters 5 and 6. These hearts were cut into small pieces and placed in TRIzol (Invitrogen) to facilitate RNA extraction, according to the manufactures instructions. A master-mix was prepared using the following: random primers (Biodymanics) and RevertAid M-MuLV Reverse Transcriptase (Fermentas), for reverse transcription; and Fast Start Universal Sybr Green Master Rox (Roche); NCX primers used above were also used to determine the same portion of the NCX protein sequence. Using the real-time PCR system (StepOnePlus, Applied Biosystems, Carlsbad, CA), rtPCR samples were loaded using the following cycles: 50°C for 2 min, denaturation at 95°C for 10 min, again at 95°C for 20 sec, followed by 60°C for 1 min (annealing), and finally at 72°C for 20 sec. In order to obtain control

experiments Glyceraldehyde 3-phosphate dehydrogenase (GAPDH) mRNA expression was also processed alongside these NCX mRNA samples for normalization. Data presented in Chapter 5 **(**Figure 5.4**)** were obtained and analyzed by Mariana Argenziano using Pfaffl method (Pfaffl 2001) and were included in this dissertation with her authorization. All mice and hearts used were prepared as described below (see section 2.2), with the exception that some hearts were preserved (-80°C) for further rtPCR analysis.

***2.2** Whole-Heart Preparations*

All functional experiments presented in this thesis were performed in hearts obtained from young mice (4-12 weeks old). Mice having a C57BL/6 background and conditional KOs transgenic animals (see section 2.1) were used as an experimental model. Mice were injected with Na-Heparin (15,000 USP units per Kg; USP stands for United States Pharmacopeia) approximately 20 minutes before euthanasia in order to avoid clotting. All mice were sacrificed using a cervical dislocation protocol to avoid any anesthetic effect on the heart electrical function. This protocol was approved by the Institutional Animal Care and Use Committee of the University of California (Merced, CA). Following animal thoracotomy, the heart and thymus were quickly removed. The isolated heart was gently placed in a horizontal chamber where the aorta was cannulated on to a Langendorff-perfusion apparatus driven by gravity (Figure 2.2). The

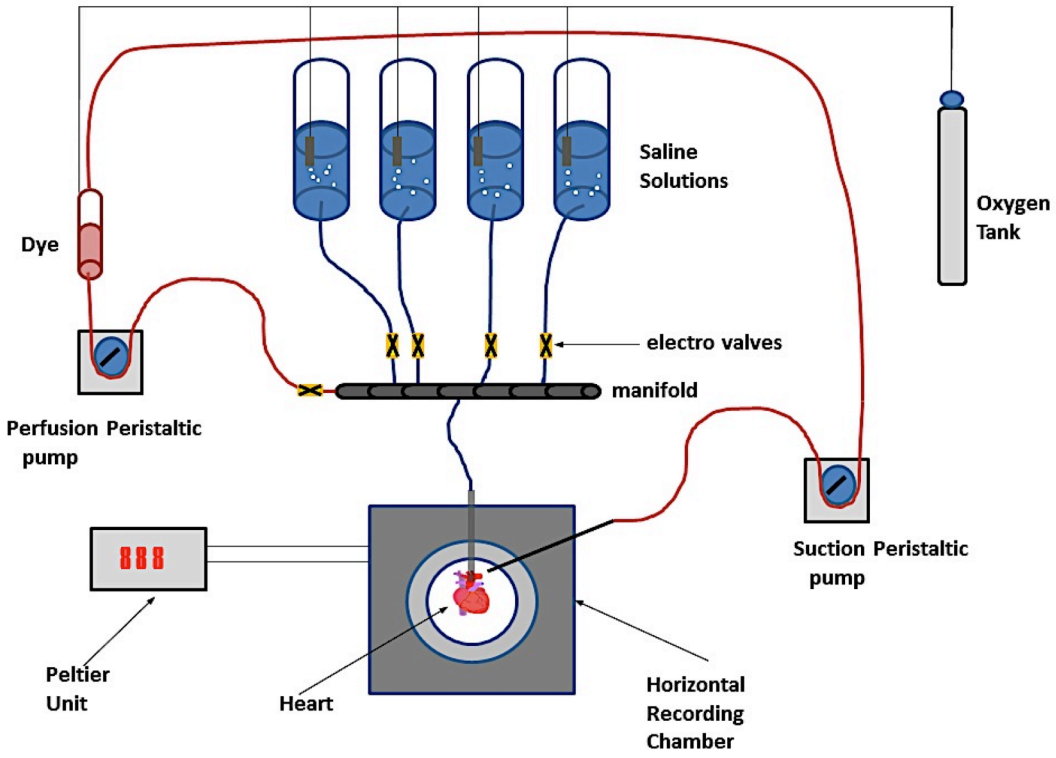

Figure 2.2 Langerdorff perfusion system used for optical electrophysiological recordings (image provided by A.L Escobar).

heart was constantly perfused with normal Tyrode solution (Table 1) at room temperature in order to remove the blood from the ventricles and the coronary circulation. The hearts were stabilized for 10 minutes before any experimental recording procedure took place.

Compound	Molecular Weight (g/M)	Concentration (mM)	Weight for 1L (g)
NaCl	58.44	140	8.1816
KCl	74.55	5.4	0.4025
$CaCl_2$	147.02	2	0.2940
$MgCl_2$	203.3	1	0.2033
$NaPO_4H_2$	138	0.33	0.0455
HEPES	238.31	10	2.3831
Glucose	180.16	10	1.8016

Table 4. Normal Tyrode solution at pH 7.4.

Most of the experimental data presented in this dissertation were obtained at 37°C. Recordings at different temperatures will be specifically indicated. There were several benefits of using a horizontal perfusion system. One benefit is the reduction of motion artifacts from the contracting heart and its interaction with the recording optical fiber surface. Another benefit is that this experimental approach allows the heart to be submerged in thermostabilized recording solution. This approach allowed us to increase the environmental temperature to 37°C without damaging the organ. The temperature of the solution outside the heart was controlled with a Peltier unit positioned at the bottom of the recording chamber (see Figure 2.2). The right atrium was removed and pacemaker cells of the sinoatrial and atrioventricular nodes were electrically ablated with the aid of an ophthalmic bipolar pencil (Mentor Ophthalmics, Santa Barbara, CA) to gain external control of the heart rate. During the experiments, each heart was continuously paced at 4 Hz through a silver bipolar electrode placed at the apex of the heart. The stimulus electrodes were wired to an electrical stimulator ISOSTIM A320 (World Precision Instruments, Sarasota, FL) controlled by a PC. All solutions were equilibrated with 100% oxygen.

Compound	Molecular Weight (g/M)	Concentration (mM)	Weight for 1L (g)
LiCl	42.39	140	5.9346
KCl	74.55	5.4	0.4025
$CaCl_2$	147.02	2	0.2940
$MgCl_2$	203.3	1	0.2033
$NaPO_4H_2$	138	0.33	0.0455
HEPES	238.31	10	2.3831
Glucose	180.16	10	1.8016

Table 3. Lithium Tyrode solution at pH 7.4

Experiments in which Na^+ was replaced by Li^+ were carried out by equimolarly replacing NaCl by LiCl. Tyrode–Li solution composition is presented in Table 2. For Lithium replacement experiments, distributions of Na-Li tyrode solutions are as follows: 25% replacement (105 mM NaCl, 35 mM LiCl); 50% replacement (70 mM NaCl, 70 mM LiCl) and 75% replacement (35 mM NaCl, 105 mM LiCl). All solutions are equilibrated

with 100% O_2. All reagents and drugs used were purchased from Sigma-Aldrich Chemical Company (St Louise, MI), unless specified.

2.3 *Ca^{2+} and potentiometric dye loading*

All hearts were stabilized at 23°C (room temperature) prior to perfusion with fluorescent dyes. The Ca^{2+} indicator rhod-2 AM (Invitrogen, Carlsbad, CA) was dissolved in 45 µl Dimethyl sulfoxide (DMSO) with 2.5% of the triblock copolymer surfactant Pluronic and added to 1 ml normal Tyrode solution. The dye was perfused with the aid of two peristaltic pumps (Masterflex, USA) and oxygenated in a close chamber to avoid bubbling of the solution with the gas (Figure 2.1). This maneuver prevents the evaporation of DMSO and the precipitation of the dye. Rhod-2 AM (Invitrogen, Carlsbad, CA), a rhodamine based dye that binds Ca^{2+} through a high affinity BAPTA binding site, was used to measure cytosolic Ca^{2+} transients. This particular dye is an ester and carries positive charges, thus once it is inside the cell it will be hydrolyzed by an endogenous esterase. The hydrolysis of the ester and the fact the rhodamines are highly charges, prevents the extrusion of the dye out of the cell (Du, MacGowan et al. 2001). The binding of Ca^{2+} to the dye induces a dramatic change in the quantum yield of the indicator (100 times). Upon excitation with a green laser beam (532 nm), the dye will emit a fluorescent signal having an emission spectrum between 560 and 630 nm that will be measured using the Pulsed Local-Field Fluorescence Microscopy (PLFFM; see section 2.4 below) and recorded with an acquisition program written in LabVIEW (National Instruments, Austin, Tx) (Figure 2.3). All recordings were done at 37°C (body temperature) and the hearts were externally paced at 4 Hz, unless specified.

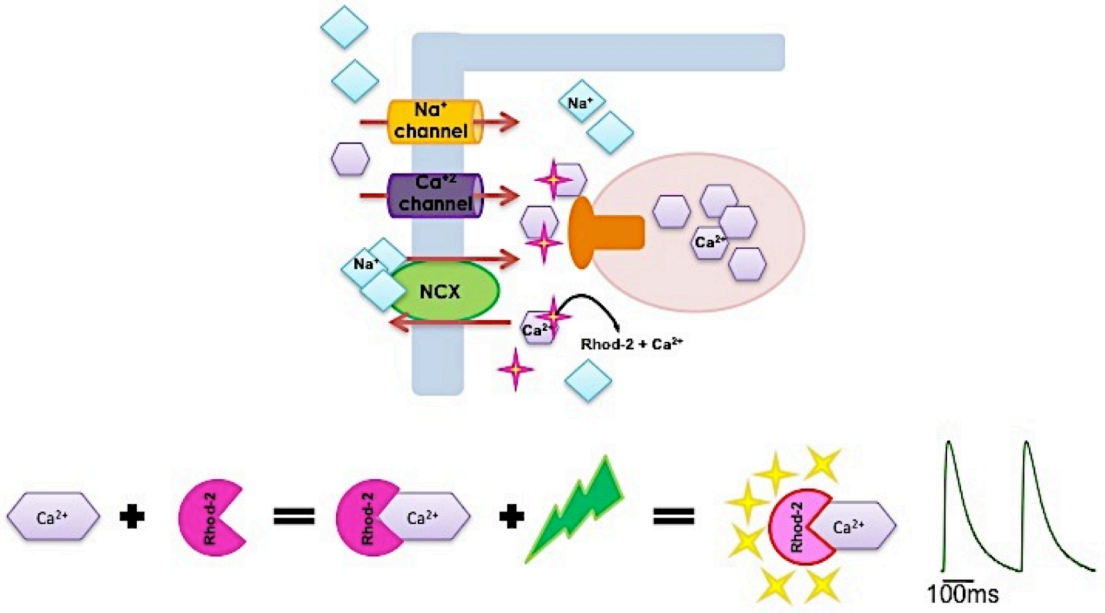

Figure 2.3 Cartoon illustration of rhod-2 fluorescence and excitation translated to cytosolic Ca^{2+}-transients.

Mag-fluo-4 AM (Invitrogen, Carlsbad, CA) was used to measure changes in the intra-SR Ca^{2+} concentration. The dye was dissolved in 45 µl DMSO with 2.5% Pluronic and added to 1 ml normal Tyrode solution. Perfusion with dye was performed in a similar way as for rhod-2 AM and started after the spontaneous heart rate became regular (within 10 min after cannulation). After 1 hour of perfusion at room temperature (21–23°C), the solution was switched to normal Tyrode solution and the temperature was increased to 37°C within 10 min. The temperature increase activates a multidrug resistance protein (MDRP), an adenosine binding cassette molecular pump present in the plasma membrane of the cardiac ventricular myocyte and that participates in a low energy shock adaptive response in cells when are loaded with an exogenous drug (Oehlke, Beyermann et al. 1997). As mag-fluo-4 is a weakly charged dye (Shmigol, Eisner et al. 2001), it can be efficiently extruded out of the cell but not from the SR where MDRP are not present. This differential extrusion induced the washing out of mag-fluo-4 from the cytosol, allowing us to measure intra-SR Ca^{2+} signals. In most cases, a downward fluorescence signal reflecting depletion of the SR was apparent even before the heart was warmed up, although some minor upward (cytosolic) component was still present. This upward component completely disappeared within 10–20 min after the temperature reached 37°C. After mag-fluo-4 was removed from the cytosol, a sufficient amount of dye remained inside the SR to generate detectable signals for at least 2 hr. Upon excitation with a blue laser beam (473 nm), the dye will emit a fluorescent signal having an emission spectrum between 510 and 560 nm that will be measured using the PLFFM and an acquisition program written in LabVIEW (National Instruments, Austin, Tx) (Figure 2.4).

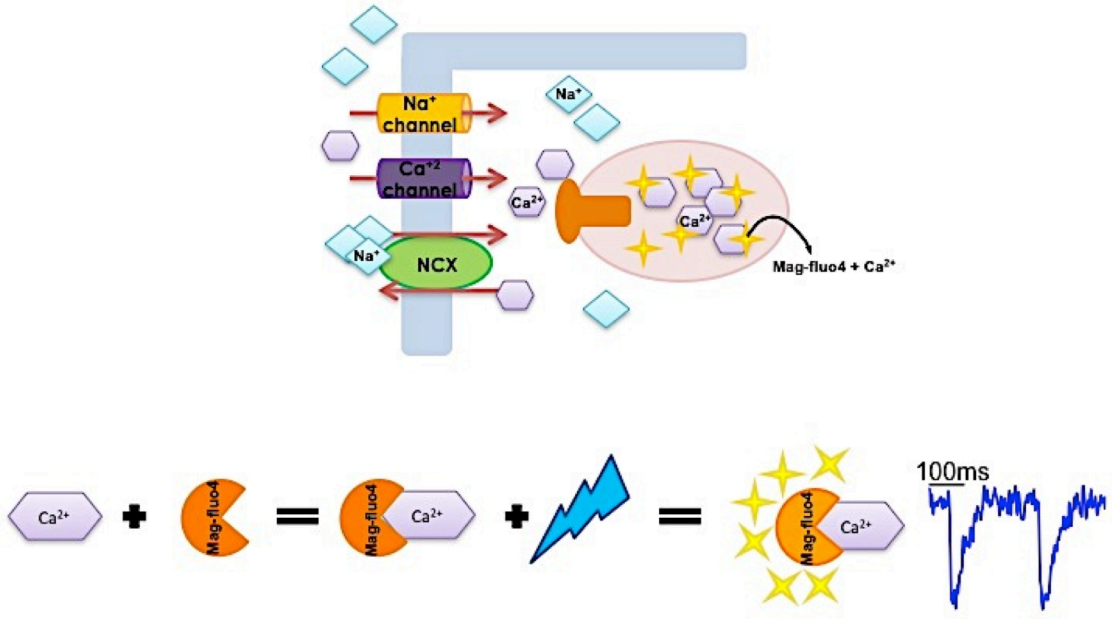

Figure 2.4 Cartoon illustration of mag-fluo4 fluorescence and excitation translated to intra-SR Ca^{2+}-transients.

Changes in the membrane potential were measured using the potentiometric fluorescent dye, Di-8-ANEPPS. This dye was chosen because it is a hydrophobic molecule that stays in the lipid bilayer, staining both the plasma membrane and t-tubules. The fast kinetic and high dynamic rage of Di-8-ANEPPS allows the measurement of APs (DiFranco, Capote et al. 2005). Di-8-ANEPPS is prepared similarly as other dyes used in this proposal, with the exception of being diluted in 10 mL normal tyrode solution (instead of 1 mL). When excited with the light from a green laser beam at 532 nm, the emission spectrum between 590 nm and 700 nm will have a shift to lower wavelengths the membrane potential becomes more positive. This will induce a reduction of the number of photons measured at 630 nm. Finally, once Di-8-ANEPPS is excited on the epicardial layer of the left ventricle and there is a stimulus prompting the initiation of an AP, a decrease in the fluorescent signal is produced as the membrane depolarizes that resembles phase 0 (Figure 2.5). The recorded morphology of the AP clearly shows a prominent plateau phase. Epicardial APs were recorded as an average of several neighboring myocytes due to diameter of fiber. These recorded signals were inverted for better comparison of the contribution of phase 2 (*shown in black*, Figure 2.5). All hearts were recorded at 4 Hz and 37°C, unless specified.

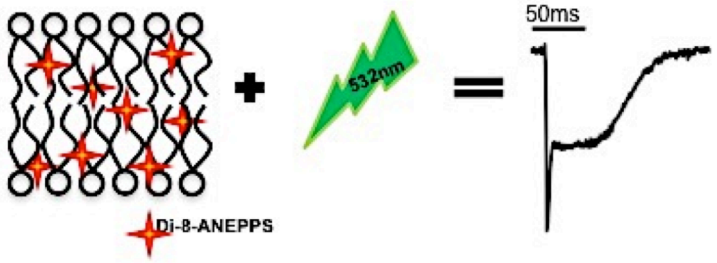

Figure 2.5 Cartoon illustration of DI-8-ANEPPS fluorescence and excitation translated into inverted action potential traces.

2.4 *Pulsed-Local Field Fluorescence Microscopy*

Several electrophysiological techniques (i.e. patch-clamp, voltage-clamp, etc.) are usually used to study the function of cardiomyocytes. However in most of these experimental approaches the cells are isolated and therefore conducted at the single cell level. One concern when studying cardiac function under these conditions is that ventricular myocytes are electrically and metabolically coupled through intercellular communication pathways molecularly defined by different types of gap junction proteins called connexins. Additionally, the myocytes laying the free wall of the ventricle display strong molecular and functional differences for different anatomical areas. For example, the morphology of AP differs tremendously between epicardium and endocardium. Moreover, the kinetics of APs are much faster in the apex of the ventricle than in the base. During an enzymatic isolation cells are randomly mixed, this precludes the evaluation of the functional transmural properties of the electrical activity. In the isolated cell approach these important intrinsic properties are removed, therefore creating a gap in knowledge between the basic mechanisms of these cells and how they can create arrhythmias that can lead to sudden cardiac death (SCD). Over the years, advancements in fiber optics based techniques led to the development of a Langendorff-apparatus based experimental approach called the Pulsed-Local Field Fluorescence Microscopy (PLFFM)(Mejia-Alvarez, Manno et al. 2003). The PLFFM is an integrative technique that takes advantage of high numerical aperture multimode optical fibers as

an imaging optical element and solid state silicon avalanche photodiodes to record the fluorescence signal emitted from fluorophores loaded in the heart. This dramatically enhances the ability to record subcellular variables (i.e. intracellular Ca^{2+}, membrane potential, etc) under a more physiological environment. Modifications and advancements have been made since Mejia-Alvarez et al first introduced it to the scientific world in 2003. Moreover, the PLFFM is a useful tool in filling some gaps of knowledge that lingers between subcellular events occurring at a single-cell level and the collection of these events occurring at the whole heart level. A schematic representation of the PLFFM is shown in Figure 2.6.

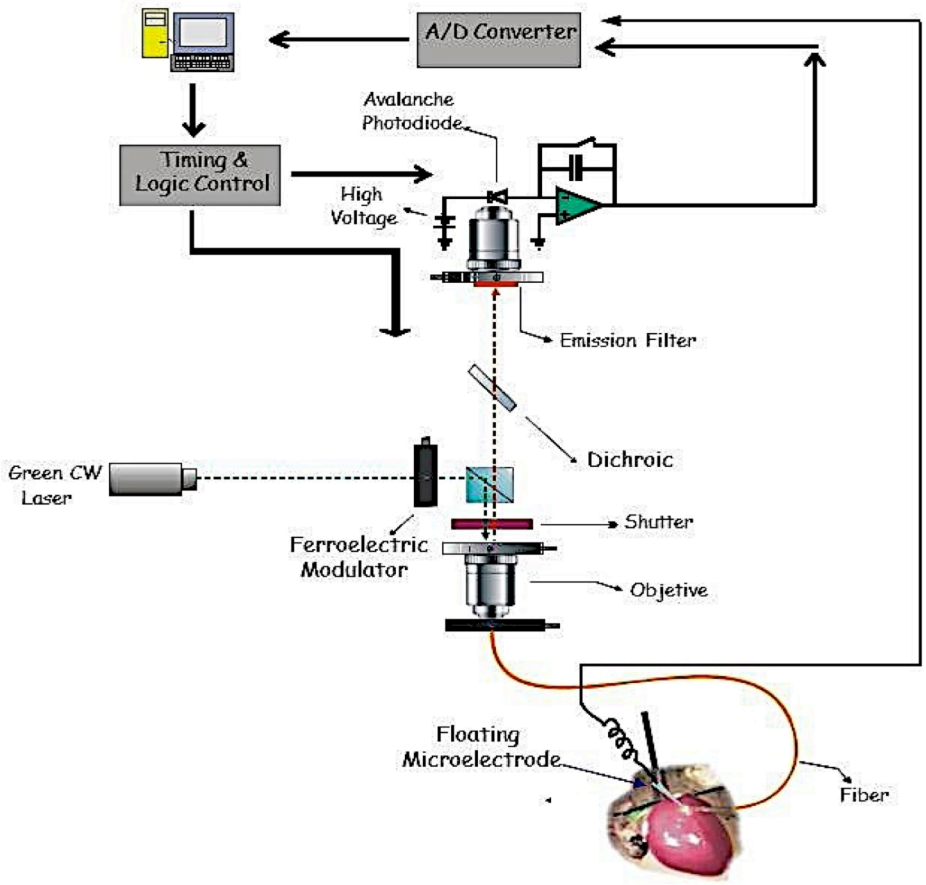

Figure 2.6 Schematic representation of the PLFFM (image provided by A.L. Escobar).

One of salient advantages of the PLFFM is the high spatio-temporal resolution of fluorescent measurements. The use of solid-state YAG lasers; either MGL-50B-1 CW Ng-YAG laser (Enlight Technologies, Branchburg, NJ), for the excitation of rhodamine-based dyes (rhod-2) with a green light (532 nm), or MBL-10-3 CW Ng-YAG laser (Enlight Technologies), for the excitation of a fluorescein-based dye (mag-fluo4) with a blue light (473 nm), were used as an illuminating source. These lasers have a continuous wave, thus a ferroelectric modulator (50075 Oriel optical shutters, Newport, Stratford, CT) was

placed in front of the beam to pulsate the light. Dichroic mirrors are aligned so that the excitation light pulses from the laser are reflected and focused by an aspheric lens (X40, numerical aperture: 0.45) into a small multimode optical fiber on one end. The other end of the optical fiber was gently placed on the tissue (Figure 2.7). This effectively allowed synchronous movement of the end of the fiber together with the heart surface. Such procedures considerably attenuated the motion artifacts generated by the beating hearts. Recently published data from our lab has shown that, the myosin II inhibitor BBS can be used to immobilize the heart(Valverde, Kornyeyev et al.), without affecting intracellular Ca^{2+} handing or the membrane potential(Allingham, Smith et al. 2005; Dou, Arlock et al. 2007; Fedorov, Lozinsky et al. 2007; Farman, Tachampa et al. 2008). The use of this drug ([7-10 μM]) minimizes tissue damage from beating heart at the fiber-surface interaction during recordings at higher temperatures. Fiber size can vary depending on depth of measurements (Note: fiber diameter used in this dissertation is either 200 μm or 400 μm; measuring approximately 40-100 epicardial cells, respectively). Light focused on the epicardial layer of the heart will excite the perfused fluorophores, at 532 nm or 473 nm depending on the dye.

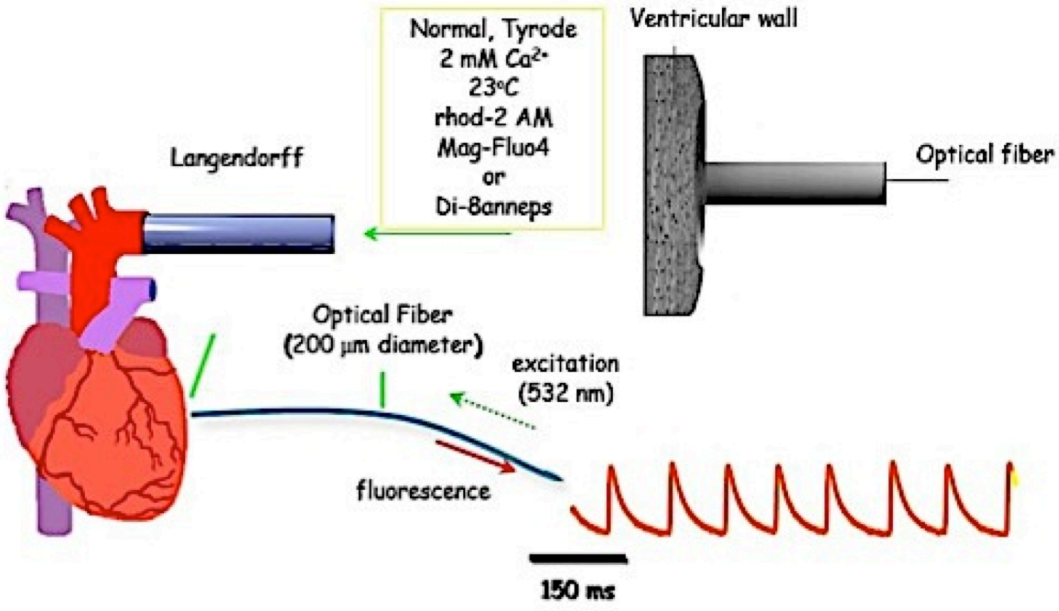

Figure 2.7 Cartoon representation of optical fiber position on Langendorff perfused mouse heart after perfusion fluorescent indicator. Arrows indicate direction of excitation and emission to produce Ca^{2+}-transients (red traces) when perfused with a rhod-2 at 23°C (image provided by A.L. Escobar).

Emitted light from the epicardial tissue is then carried back through the same fiber, where the beam will be split at the dichroic mirror. The excitation wavelengths will be reflected whereas the emitted light from the heart will pass and transmitted through a barrier filter (a long-pass filter allowing longer wavelengths to propagate through; i.e. 590 for rhod-2 and 520 nm for mag-fluo-4). An avalanche photodiode, connected to an integrating current-to-voltage converter controlled by a digital signal processor (DSP 320, Texas Instruments) acts as the main photodetection unit. Briefly, the dye emits photons that were focused onto a headstage unit biased by a high voltage pack of 9 volts batteries. This converts emitted light into an electrical signal that is converted from

analog to digital inside the DSP to be finally acquired into a PC by a control program written in LabVIEW (National Instruments, Austin, Tx) (Figure 2.6). Fluorescence signals were digitized at a sampling frequency of 5 MHz and filtered to a bandwidth of 500 kHz.

2.5 *Electrophysiological Recordings*

Epicardial APs were simultaneously recorded with electrocardiographic recordings in electrophysiological experiments. These AP recordings were obtained using glass microelectrodes pulled from borosilicate glass capillaries (Kwik-Fill, WPI, Sarasotra, FL) using a computarized horizontal Flaming/Brown puller (P-97, Sutter Instruments, Novato, CA). The glass microlectrodes were backfilled with a solution of 3 M KCl (10–20 MΩ resistance) and kept in the same solution overnight. The microelectrodes were connected with a holder to a high input impedance differential amplifier (World Precision Instruments-Duo 773 Electrometer). An Ag-AgCl pellet (2.0mm; E206, Warner Instruments, Hamden, CT) was used as reference electrode and was positioned in the recording chamber close to the ventricular epicardial area. A second Ag-AgCl pellet was used to actively ground the bath of the recording chamber (Figure 2.8 A). This differential configuration allowed us to minimize the interference produced by the capacitive coupling of the line 60 Hz spurious signals. The electrical signals were filtered to a bandwidth of 500 kHz, digitally sampled at a frequency of 5 MHz, and then digitally resampled to 2 kHz (Figure 2.6). In order to impale epicardial myocytes, microelectrodes were micropositioned with the aid of a mechanical micromanipulators (M325, WPI, Sarasotra, FL). The quality of the impalement was evaluated by measuring of the resting membrane potential of the epicardial ventricular myocytes. Cells that had a negative membrane potential, more negative than -60 mV, were used for the AP recordings.

The difference between the endocardial (inside the heart) and the epicardial electrical activity was assesed by evaluating the extracellular potentials generated during a normal cardiac cycle. Transmural electrocardiographic signals in a mouse heart present a complex time course that cannot be evaluated with clinical-grade AC coupled electrocardiogram amplifiers. Thus, electrocardiographic (ECG) recordings were performed using homemade DC coupled instrumentation amplifiers. Ag-AgCl pellet junction potentials were dynamically controlled at the input of the differential amplifier in order to prevent the saturation of the recording apparatus. Because the ECG is the transmural electrical activity across the ventricular walls, Ag-AgCl micro-pellets (0.8mm; E255A, In Vivo Metric, Healdsburg, CA) were used to obtain the propagation of the electrical activity from the endocardium to the epicardium. One Ag-AgCl micro-pellet (was gently placed outside the epicardial layer of the left ventricle and another was inserted through the mitral valve of the left ventricle (Figure 2.8B). A third pellet was placed in the bathing solution as a ground. Hearts were paced using acupuncture needles that gently pierced the apex connected to the stimulus isolation unit described previously. The pacing of the hearts was controlled as previously indicated (see section 2.4). Figure 2.8 illustrates these recordings separately, however these were simultaneously recorded and sometimes included a fiber optic to record Ca^{2+} transients. The acquisition system was controlled by a PC running a custom-designed G-based software program (LabVIEW; National Instruments).

The use of these multiple parameter recordings by this modified version of the innovative PLFFM can provide a powerful understanding into the gateway of subcellular mechanisms that underlie ventricular tachycardia and SCD. Thus, it was used to study the role of the NCX and its relationship between intracellular calcium dynamics and the electrical properties of epicardial cardiac myocytes in a beating whole mouse heart at various physiological conditions.

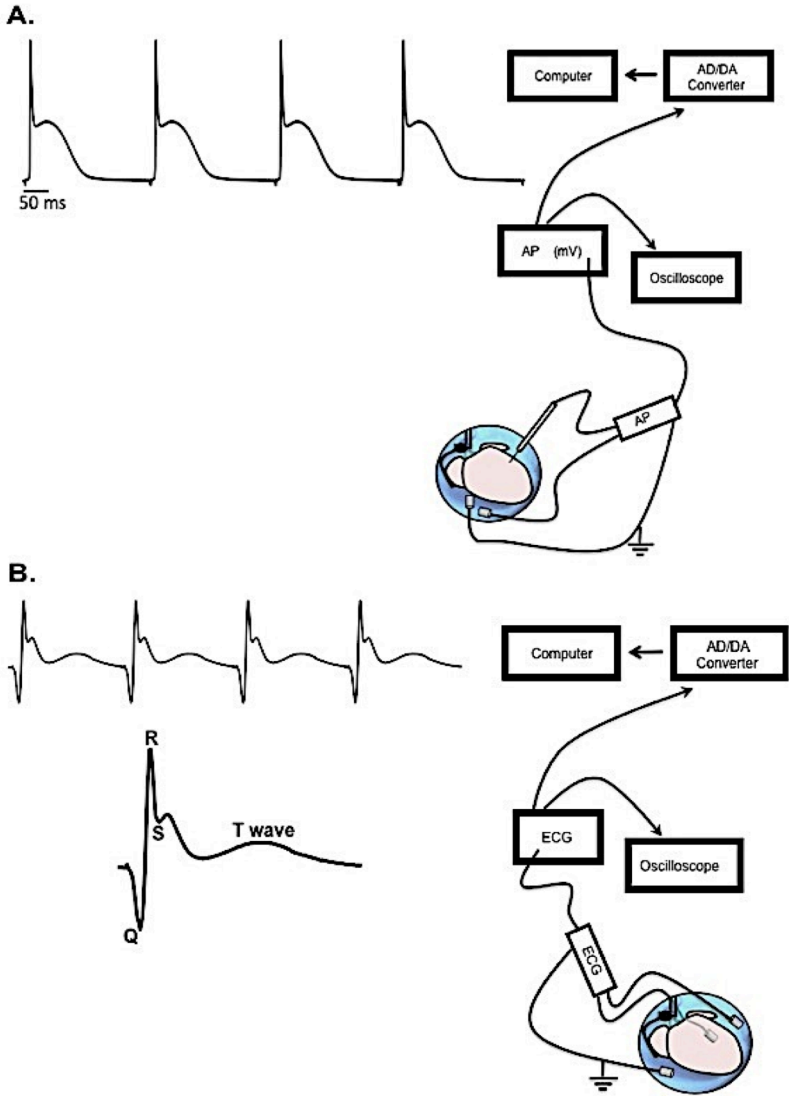

Figure 2.8 Schematic illustration of simultaneous recordings of microelectrode impalement (A) and electrocardiographic recordings (B) recorded using a modified version of the PLFFM.

2.6 Methods of Analysis

Ca^{2+} transients:

Multiple parameters of the Ca^{2+} transients such as the time to peak, amplitude, decay time from 10 to 90 % of the recovery were measured with the aid of a homemade analysis program developed in the LabVIEW environment. Typically, 20 traces from every recording spot were obtained for every experimental condition. Data was exported to a commercial graphical software (Origin 8, Microcal, USA) in order to be graphed.

Evaluation of the recovery of Ca^{2+} release during extra-systolic stimulation was achieved by performing restitution experiments. These experiments defined the refractoriness of Ca^{2+} release under different experimental conditions. In a typical restitution protocol (Figure 2.9), were obtained by applying an additional stimulation pulse (S2) at different times (described as S1–S2 coupling intervals) with respect to the regular pacing pulses (S1). By changing the time interval between electrical stimulations (S1–S2), we were able to analyze the kinetics of the recovery of different variables such as Ca^{2+}-transients and AP triggering. Restitution curves were obtained by applying an extra-systolic pulse (S2), in increments of 25 ms and then 10 ms as the S2 pulse approaches the first Ca^{2+} transient (S1), with respect to the regular pacing pulses at 4 Hz Restitution curves were built using data from several independent experiments (hearts) and presented as a semilog plot to better illustrate the exponential nature of the recovery process. Fractional recovery ratios (A_{S2}/A_{S1}) were calculated from the peak amplitudes of the S2 (extra-systolic) and S1 (initial pulse) stimulations (Figure 2.9).

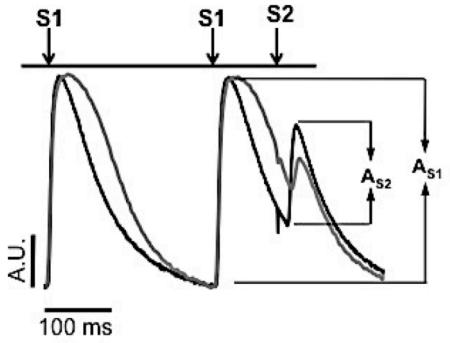

Figure 2.9 Ca^{2+}-transients recorded during restitution. Arrows indicate normal stimulus (S1) and the extra-systolic pulse (S2) for control (black) and 50% Na-Li perfused (grey) heart. (acquired at 4 Hz, 37°C, using rhod-2)

In addition, we also performed experiments where we explored the heart rate dependency of several physiological variables. In this experiments the heart rate was increased by external stimulation applied either by stimulus plates in tyrode bath placed on both sides of the ventricles, or two teflonated silver electrodes are gently placed on the apex of the ventricles. Frequency was increased gradually in 0.5 Hz increments (in LabVIEW) until reaching desired frequency prior to recording. Changes in amplitudes of alternans are all calculated using the ratio (Amax-Amin)/Amax (Figure 2.10).

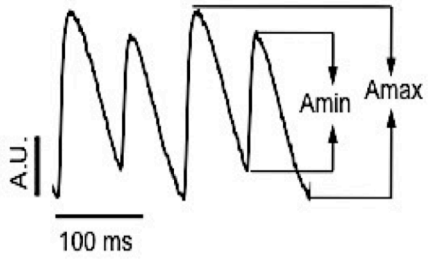

Figure 2.10 Ca^{2+}-transients representing Ca-Alt. Amax is the maximum amplitude of release and Amin is the corresponding smaller amplitude of release. Acquired at 14 Hz, 37°C, using rhod-2.

Action potentials:

Different parameters of APs were measured using the same analysis platform described already for Ca^{2+} transients. The duration of the AP at the 50 % or the 90 % of the recovery was used a regular way to evaluate the repolarization of the AP. However, the repolarization of the mouse ventricular AP has a complex waveform so the contribution of phase 2 to the AP was evaluated. This method for evaluating the contribution of phase 2 to the AP provided us with a parameter that has less scattering than the usual report of AP durations (APDs) at different levels of repolarization. An integration-subtraction procedure was utilized to measure the contribution of phase 2 to the total area under the AP. First, phases 0 and 1 (ph_{01}) of the AP were fitted with an exponential function of the form:

Equation 1

$$ph_{01} = V_m + V_{amp} \cdot \left(1 - e^{-\frac{t-t_1}{\tau_{on}}}\right) \cdot e^{-\frac{t-t_1}{\tau_{off}}}$$

Where V_m is the resting membrane potential, V_{amp} is the amplitude of the AP, t_{on} is the time constant for phase 0, t_{off} is the time constant for phase 1 and t_1 is the delay time for the electrical stimulus. Second, the area under this function was calculated using a numerical integration procedure ($A1$). Third the area under the whole AP was calculated by numerically integrating the AP trace (A_{total}). Finally the contribution of the phase 2 (A2) to the total AP was calculated using the following expression:

Equation 2

$$A_2 = \frac{A_{total} - A_1}{A_{total}}$$

AP recordings calculating the contribution of phase 2 is determined by the ratio, A2/A1, where A1 is the area under phases 0 & 1 and A2 is the area of phase 2 (Figure 2.11).

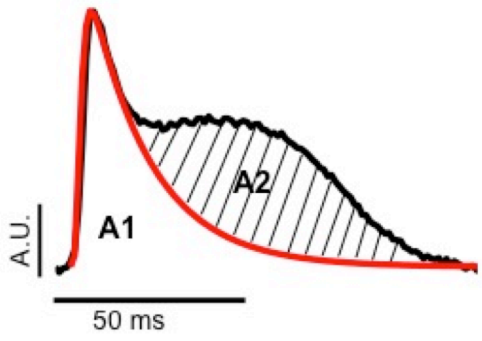

Figure 2.11 Contribution of phase 2 calculation ratio, A2/A1, where A1 is the area under phases 0 & 1 and A2 is the area of phase 2 (acquired using DI-8-ANEPPS)

2.7 *Statistical analysis*

Data are expressed as means ± SE; *N* indicates the number of independent experiments. The total number of animals used in this study was 81 (25 in Chapter 3, 27 in Chapter 4, and 29 in Chapters 5-6). Statistical significance was considered to be significant if the value of p was ≤ 0.05.

CHAPTER 3 *: Intracellular Ca^{2+} Dynamics*

Cytosolic Ca^{2+} Dynamics

Ca^{2+} is the key second messenger that regulates all the aspects of the cardiac function. This section of the dissertation focuses on the regulation of inotropism (ion dependent contractility) and the impact of intracellular Ca^{2+} dynamics on the cardiac excitability (i.e. electrical excitability). In order to evaluate its inotropic role, intracellular Ca^{2+} dynamics was evaluated by recording Ca^{2+} dependent fluorescent signals in the cytosolic compartment of epicardial ventricular cardiomyocytes. To start, we emphasized within this region to gain a better understanding of the relationship between NCX1 activity and cytosolic Ca^{2+} dynamics during diastole and systole. Specifically, ***test the hypothesis that the impairment of NCX1 modifies cytosolic Ca^{2+} dynamics.*** Impairment of NCX1 was accomplished by replacing Na^{+} with Li^{+} (a non-translocable monovalent cation) in the extracellular solution. Experiments were performed using the PLFFM to measure the cytosolic Ca^{2+} by means of Ca^{2+} dye fluorescence (rhod-2).

***3.1** Does the impairment of NCX1 produce an increase in the diastolic free Ca^{2+}?*

NCX1 is a secondary active transporter with an intracellular Ca^{2+} binding site. Once Ca^{2+} is bound, NCX1 is activated in the forward-mode, initiating the translocation of 3 Na^{+} from the extracellular side in exchange for 1 cytosolic Ca^{2+}. Activation of NCX1 normally occurs when a large amount of Ca^{2+} is released from the SR into the cytosol. Since NCX1 plays a prominent role in Ca^{2+} homeostasis, its ability to extrude cytosolic Ca^{2+} is crucial.

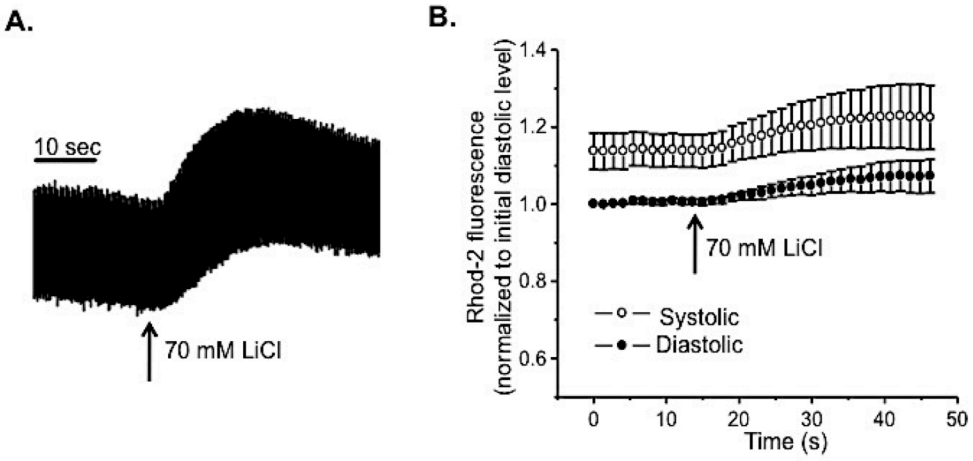

Figure 3.1 Effect of 70 mM LiCl on Ca^{2+} transients measured at a pacing rate of 4 Hz and 37°C. Changes in the fluorescent signal from the cytosol (fluorescent dye rhod-2, AM). As a result of perfusion with Tyrode solution with 50% of Na^{+} was replaced with Li^{+} (A). Recordings of Ca^{2+} transients during application of 70 mM LiCl (the vertical arrow indicates the onset of perfusion with Tyrode containing LiCl) shows an increase in the systolic (peak) and diastolic (resting) levels of the Ca^{2+} transients (B). Changes in fluorescence was corrected for dye bleaching and normalized to initial level prior to application of LiCl. The data in panel B represent the average means ± SE (N=5).

Unfortunately, known pharmacological antagonists of this transporter also interact with other membrane proteins involved in the CICR process. On the other hand, it is well known that Li^+ cannot be transported through the NCX1. Interestingly, Li^+ can permeate just as well as Na^+ through the voltage-dependent Na^+-channel allowing a normal upstroke of an AP. Thus, the equimolar replacement of Na^+ by Li^+ in the external Tyrode solution can serve as a way to evaluate the fractional contribution of the NCX1 exchanger. When replacing 50% Na^+ for Li^+ (70 mM) to impair the transport of the sarcolemma Na^+-Ca^{2+} exchanger (NCX1), there were increases in the rhod-2 fluorescence (Figure 3.1, A). Clearly, the equimolar replacement of Na^+ by Li^+ not only increased the resting fluorescence (diastolic Ca^{2+} concentration) but also promotes an increase in the amplitude of the fluorescence Ca^{2+} transients (systolic Ca^{2+}). These increases are represented as the resting Ca^{2+} diastolic and systolic levels in the cytosolic compartment (Figure 3.1, B).

In order to evaluate if the impairment of the NCX1 produced the increase in the diastolic Ca^{2+} concentration (Figure 3.1), experiments at different extracellular Li^+ concentration were performed (equimolar replacement). Increases in the molar ratio replacement of Na^+ for Li^+ in different hearts clearly resulted in an augmentation of the resting diastolic Ca^{2+} levels (Figure 3.2; p-value < 0.01). Changes in the resting diastolic levels were determined by measuring changes in the fluorescent signal produced as rhod-2 binds to free Ca^{2+} in the cytosol.

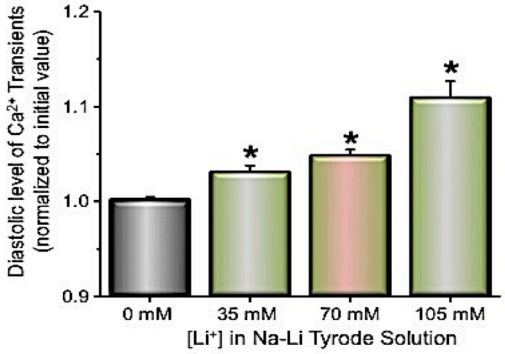

Figure 3.2 Comparison of the diastolic levels of rhod-2 fluorescence in the presence of different concentrations of LiCl. Changes in fluorescence was corrected for bleaching and normalized to initial level prior to application of LiCl. The data represent means ± SE (N=4-5) * p < 0.05 when compared to their own control.

Augmentation in diastolic (resting) levels of rhod-2 fluorescence illustrated in Figure 3.1 shows an increase of Ca^{2+} in the cytosolic compartment, as NCX1 was impaired with Tyrode solution containing 70 mM Na-Li. This increase in the diastolic Ca^{2+} concentration could be associated with changes in Ca^{2+} fluxes across the plasma membrane or due to alterations of fluxes across the membrane of intracellular organelles. Along these lines, the most likely organelle involved in myocyte intracellular Ca^{2+} dynamics is the SR. To further evaluate if the increase in diastolic Ca^{2+} levels are produced from Ca^{2+} release from the SR, we pharmacologically blocked the key Ca^{2+} transport proteins located in the SR membrane. Specifically, Ryanodine (Ry) and Thapsigargin (Tg) were used to block the Ca^{2+}-release (RyR2) and re-uptake (SERCA2a) mechanisms from the SR. Figure 3.3 shows that even in an experimental condition in which Ca^{2+} transport across the SR membrane was heavily compromised,

by the application of 10 µM of the alkaloide Ryanodine (Ry) and 2 µM of sesquiterpene lactone Thapsigargin (Tg), an equimolar replacement of Na^+ by Li^+ was able to induce an increase in the diastolic Ca^{2+} level (p-value < 0.01). This indicates that the Li^+ replacement is responsible for the increases in the diastolic Ca^{2+} concentration by impairment of the Ca^{2+} transport across the plasma membrane and not by promoting Ca^{2+} release from the SR.

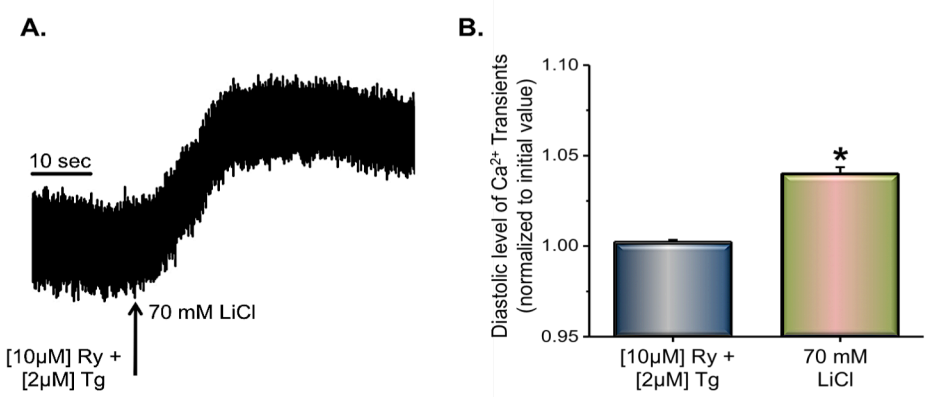

Figure 3.3 Effect of 70 mM LiCl on cytosolic Ca^{2+} transients after perfusion of [10 µM] Ry + [2 µM] Tg, measured at 4 Hz and 37°C. Changes in the fluorescence signal (fluorescent dye rhod-2, AM) as a result of perfusion with Tyrode solution containing 70 mM LiCl is indicated by the vertical arrow (left) Changes in the resting cytosolic Ca^{2+} transient levels after locking the RyR2 in a subconductive state and inhibiting SERCA2a from replenishing Ca^{2+}, measured before and after application of 70 mM LiCl (right). The data represent means ± SE (N=5) * p < 0.05 .

3.2 Does the impairment of NCX1 produce a change in cytosolic Ca^{2+} transients?

NCX1 impairment not only produced a significant increase in the diastolic levels (p-value < 0.01), but also produced an increase in the systolic Ca^{2+} level (Figure 3.1). Systolic Ca^{2+} levels represent the systole (contraction) phase of the cardiac cycle. During this phase, the rate of release and reuptake of cytosolic Ca^{2+} is primarily accomplished through SR membrane proteins RyR2 and SERCA2a, which define the amplitude and the kinetics of Ca^{2+} transients. On the other hand, NCX1 can also contribute to shape

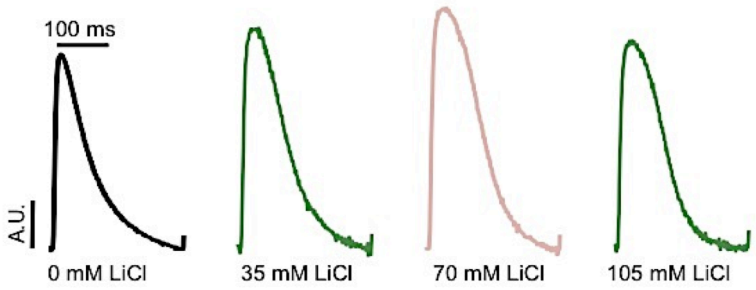

Figure 3.4 Typical Ca^{2+} transients recorded in the presence of different concentrations of LiCl, measured in intact mouse hearts with fluorescent dye rhod-2 AM at 4 Hz and 37°C.

Ca^{2+} transients because it is a major Ca^{2+} extruding mechanism. In order to evaluate how NCX1 regulates the systolic Ca^{2+} dynamics, cytosolic Ca^{2+} transients were recorded in each heart when perfused with normal Tyrode (control, 0 mM LiCl) followed by perfusion with 25%, 50%, or 75% Na-Li Tyrode (35 mM LiCl, 70 mM LiCl, 105 mM LiCl; respectively; Figure 3.4).

As Ca^{2+} is released from the SR and the extrusion of cytosolic Ca^{2+} was impaired by various [Li^{+}] in the extracellular solution, the amplitude of release is increased (Figure 3.5, A; p-value < 0.01). However, when 75% of Na^{+} was replaced by Li^{+} there was a decrease in the amplitude compared to the previously used Na-Li Tyrode solutions. This increase is still larger than the control, however not significant (Figure 3.5, A; p-value < 0.01).

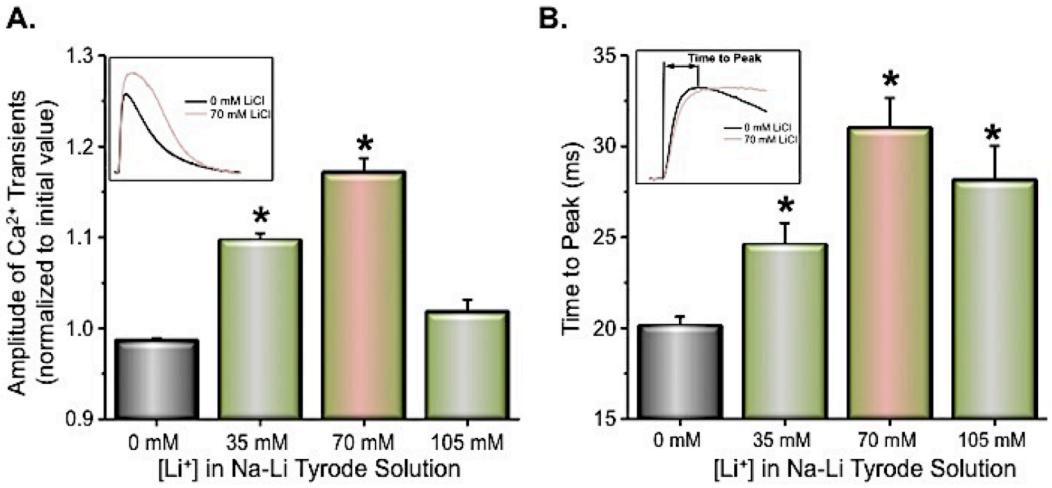

Figure 3.5 Changes in cytosolic Ca^{2+} transient amplitude in the presence of [35 mM] LiCl, [70 mM] LiCl, and [105 mM] LiCl replaced-Tyrode solutions (A). The amplitude of the Ca^{2+} transients were calculated using the ratio Amax/Ai, where Amax is the amplitude of the Ca^{2+} release and Ai is the initial amplitude of release of the first transient, respectively (A-insert). Kinetics of the cytosolic Ca^{2+} transient release (time to peak) in the presence of different concentrations of LiCl (B). Measurements of time to peak were calculated from the time of initial release to maximum release as represented in the diagram within panel B. Data represent means ± SE (N=4-5) * p < 0.05 when compared to their own control.

The increase in amplitude of the intracellular Ca^{2+} transients in presence of Li^{+} could be due to a decreased extrusion (Ca^{2+} efflux) from the myoplasm or by a secondary phenomenon prompted by the increase in diastolic Ca^{2+} on the RyR2 mediated Ca^{2+} release. If the mechanism responsible for this increase is related to the cytosolic regulation of the RyR2, we would expect to see changes in the kinetics of the Ca^{2+} transients. The time to maximum amplitude (time to peak) of Ca^{2+} transients somehow reflects the duration of the mean population of RyR2 that were open. To address this idea, we evaluated the time to peak of the Ca^{2+} transients a different extracellular Li^{+} concentration. Data illustrated in Figure 3.5 B demonstrates that there was a significant increase in the time to peak when Na^{+} was replaced by various [Li^{+}] (p-value < 0.01). This supports that the increases in the amplitude of Ca^{2+} transients are

not only related with a decrease in the rate of Ca^{2+} extrusion by the NCX1 but by a regulatory effect of diastolic Ca^{2+} on the release machinery as well.

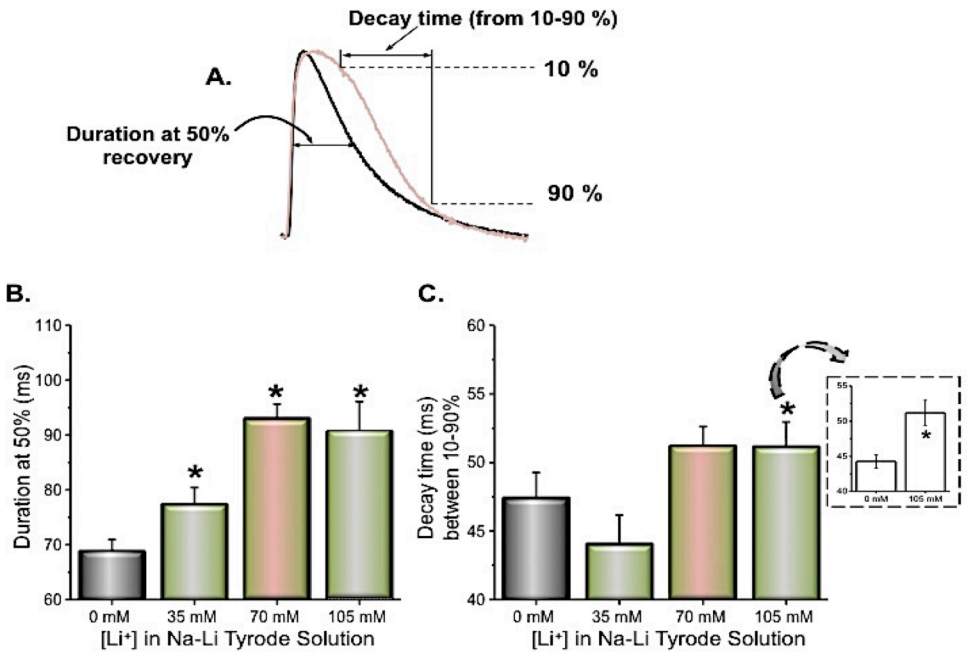

Figure 3.6 Effect of LiCl on the kinetics of cytosolic Ca^{2+} transients measured with rhod-2 AM at 4 Hz and 37°C. Cytosolic Ca^{2+} transients recorded in the absence (black) and in the presence (pink) of 70 mM LiCl (A). The curves were normalized to peak amplitude. Panels B &C represent the duration at 50% recovery & the decay time between 90 & 10% (divided by 2.2). The data in panels B & C represent means ± SE (N=4-5) * p < 0.05 when compared to their own control.

The superposition of Ca^{2+} transients before and after the Li^{+} treatment reveals that there are other apparent kinetic differences in these Ca^{2+} transients (Figure 3.6A). As extracellular Na^{+} is replaced with Li^{+} and the cytosolic Ca^{2+} starts to accumulate, there is not only an increase in Ca^{2+}-release from the SR (Figure 3.5, A), but also a prolongation for the time to maximum amplitude (time to peak) (Figure 3.5, B). As these increases occur, there is a change the morphology of the Ca^{2+} transients which significantly modify the duration to reach 50% recovery (Figure 3.6, B; 35 mM p-value < 0.05; 70 mM p-value < 0.01; 105 mM p-value < 0.01). The increase in the duration at the 50% of the Ca^{2+} transient is consistent with the idea that the NCX1 is a crucial mechanism involved in the relaxation of AP induced Ca^{2+} transients. Paradoxically, the changes in the decay time are steeper when perfused with 35 mM LiCl and prolonged with higher concentrations of Na-Li Tyrode (Figure 3.6, C). Perfusion with 105 mM LiCl produced a significant difference in the decline time of the Ca^{2+} transients when compared to its own control (Figure 3.6, C insert: 0 mM LiCl avg 44.26±0.94 ms vs. 105 mM LiCl avg 51.178±1.78 ms; p-value < 0.01). These conflicting results between concentrations can be attributed to the fact that not only does the duration of the Ca^{2+} transient change, but also there is a morphological change in the Ca^{2+} transients in the presence of Li^{+}. One possibility is that at higher diastolic Ca^{2+} concentrations, there is an initial increase in the SERCA2a activity that was not present under normal ionic

conditions (0 mM LiCl avg 47.45 ± 1.81 ms vs. 35 mM LiCl avg 44.09 ± 2.04 ms; p-value 0.23). Indeed, SERCA2a has two cytoplasmic Ca^{2+} binding sites that can accelerate the pump turnover when diastolic Ca^{2+} is increased.

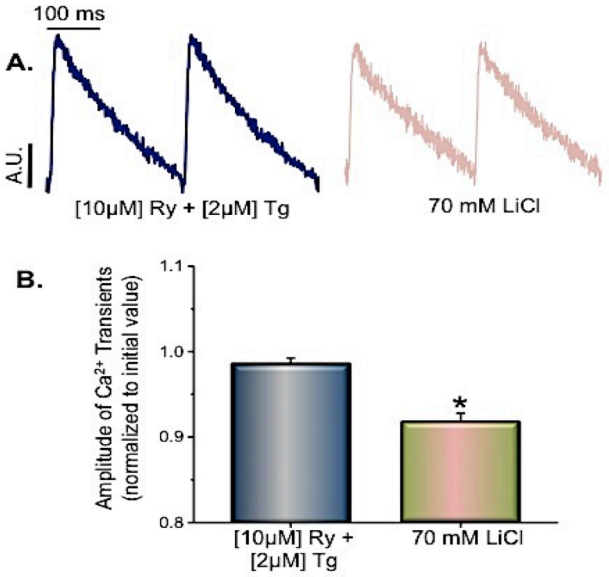

Figure 3.7 Typical cytosolic Ca^{2+} transients after perfusion of [10 μM] Ry + [2 μM] Tg (navy blue) and shortly after perfusion of 70 mM LiCl (pink), measured at 4 Hz and 37°C (A). The amplitude of the Ca^{2+} transients were measured before and after application of 70 mM LiCl (B). Calculated using the ratio Amax/Ai, where Amax is the amplitude of the Ca^{2+} release and Ai is the initial amplitude of release of the first transient, respectively. The data in panel B represent means ± SE (N=5) * p < 0.05.

The fact that NCX1 impairment induced both an increase in the amplitude and the time to peak of the Ca^{2+} transient supports the idea that changes in the diastolic Ca^{2+} levels were responsible for an increase in Ca^{2+} release through the RyR2 (Ca^{2+} transient amplitude). Two competing but not excluding hypotheses underlying the role of diastolic Ca^{2+} regulating the SR-Ca^{2+} release are the following. First, at high diastolic Ca^{2+} concentration it will be easier for Ca^{2+} influx through the LTCC, during an AP, to further increase the open probability of the RyR2. Secondly, an increase in diastolic Ca^{2+} will increase the SERCA2a activity. A higher turnover of this SR Ca^{2+} pump would increase the Ca^{2+} content in the lumen of the SR. As the luminal Ca^{2+} increases, both the Ca^{2+} driving force and the opening time of RyR2 would be longer leading to the release of Ca^{2+} from the SR to be larger. To test these ideas, experiments were performed to evaluate the time course of Ca^{2+} transients under conditions where the SERCA2a pump was blocked with Tg and the RyR2 channel was inhibited with Ry (Figure 3.7A, navy blue trace). Impairment of NCX1 by Li^{+} and its contribution to the augmentation of cytosolic Ca^{2+} transients, were further evaluated under these conditions. Measurements of the maximum amplitude of the Ca^{2+} transients pre-treated with [10 μM] Ry and [2 μM] Tg were evaluated just before and after Li-perfusion. Once SR Ca^{2+} is depleted, residual cytosolic Ca^{2+} transients were generated by a Ca^{2+} influx through the plasma membrane (Figure 3.7A). Under this experimental condition, the perfusion with Na-Li Tyrode did not induce an increase, but a significant decrease in the Ca^{2+} transient amplitude (Figure 3.7B; p-value < 0.01). These results further support the idea that increases in Ca^{2+}

transient amplitude induced by Li^+ perfusion, to impair NCX1, is due to an accumulation of Ca^{2+} inside the SR and not due to additional Ca^{2+} through the LTCC. However, a clean experimental way to test if there was an accumulation of luminal Ca^{2+} that induced the increase in Ca^{2+} transient amplitude in presence of Li^+ is by measuring the free Ca^{2+} within the SR.

Sarcoplasmic Reticulum Ca^{2+} Dynamics

Evaluating the free Ca^{2+} dynamics in an intracellular organelle is experimentally demanding. For example, to discriminate between different functional and physical subcellular compartments could be a challenge if genetically targeted indicators are unable to be used. In our experimental model, the intact heart, the only proven methodology is to load Ca^{2+} dyes within these cells through the retro-coronary perfusion with the acetyl methyl ester ("AM") form of the indicators. As described in the methods section (see section 2.3, Chapter 2), these dyes are very lipophilic and can be easily transported across cellular membranes. Indeed, when a cell is loaded with this methodology, every compartment of the cell will be loaded to some extent. For instance, when cells are loaded with the acetyl methyl ester form of a high affinity Ca^{2+} indicator such as rhod-2 (AM), both the cytosol and the SR will be loaded with the dye. However, as the free Ca^{2+} concentration in the SR is in the order of 1 mM and the estherized form of the dye has an affinity of 1 μM, all the molecules of the dye within this compartment will be saturated with Ca^{2+}. This will preclude the dye to report any changes of free Ca^{2+} concentration in the SR. Saturation of rhod-2 within the SR, implies that the only way to measure the free Ca^{2+} in a compartment where there is a higher free Ca^{2+} content (~2 mM), is a low affinity dye. The use of a low affinity dye is difficult to evaluate small changes in free Ca^{2+} concentration produced in the cytosol; however it will be in an optimal rage to measure Ca^{2+} with in the SR.

Direct recordings of SR Ca^{2+} were accomplished by the means of a low affinity fluorescent Ca^{2+} indicator located inside the SR (Mag-fluo4). Briefly, Mag-Fluo4 will be extruded from the cytosol through an ABC transporter (MDRP) at 37°C. As MDRP is not present in the SR membrane, Mag-Fluo-4 will stay in the SR and will report Ca^{2+} changes within this organelle (for loading procedure see Chapter 2). A blue laser (473 nM; via PLFFM) must excite the cellular volume where there are proteins that spectrally absorbed and emit in the same spectral band of this particular dye. This added to the fact the SR volume is only 1 to 2 % of the cellular volume; results in more noisy measurements than those obtained with rhod-2 for cytosolic Ca^{2+} measurements.

To ***test the hypothesis that the impairment of NCX1 modifies intra-SR Ca^{2+} dynamics,*** experiments were designed to study the effects of Li^+-induced increases in cytosolic Ca^{2+} on the intra-SR Ca^{2+} dynamics.

***3.3** Does impairment of NCX1 increase the diastolic SR Ca^{2+}?*

The NCX1 is the major extruder of Ca^{2+} out of cardiomyocytes, however is it not the only "buffering" mechanism. When Ca^{2+} is released from the sarcoplasmic reticulum (SR), it will diffuse to various locations in the cell. One of these locations is the myoplasm where Ca^{2+}-binding to troponin c initiates muscle contraction. Since Ca^{2+} is a second messenger, there are many pathways in which Ca^{2+}-released from the SR is involved. Regardless of the path Ca^{2+} takes, once it has accomplished its goal it will

either be extruded by NCX1 or re-sequestered into the SR through a Ca^{2+}-ATPase (SERCA2a). SERCA2a is a Ca^{2+}-pump that uses ATP hydrolysis to pump Ca^{2+} against its concentration gradient into the SR, where is it stored awaiting the activation of RyR2 to release Ca^{2+} during the CICR phenomena (Huxley and Taylor 1958; Fabiato and Fabiato 1975; Fabiato 1983; Fabiato 1992; Bers 2002)' (Bers 2008). Interestingly, SERCA2a is also regulated by cytosolic Ca^{2+}, in which it can increase its turnover rate when free Ca^{2+} concentration increases in the cytosol. Therefore, as Li^{+} impairs NCX1 and cytosolic free Ca^{2+} increases, the transport rate of SERCA2a is anticipated to increase. As a result there will be an increase in free Ca^{2+} levels within the SR. Activation of Ca^{2+} release from the SR is known to be regulated cytosolically and luminally (Valverde, Kornyeyev et al. ; Zhang, Kelley et al. 1997; Bers 2002; Terentyev, Viatchenko-Karpinski et al. 2002; Qin, Porta et al. 2005). Thus, an increase in cytosolic Ca^{2+} could not only increase the open probability of the RyR2 channel and increase the driving force for Ca^{2+} release. Furthermore, it has been shown that the open probability of RyR2 channels increases as luminal Ca^{2+} increases (Gyorke and Terentyev 2008).

In order to test if these assumptions are correct, hearts were loaded with Mag-fluo-4 (see Chapter 2, section 2.3). At 37°C, SR Ca^{2+} was measured in long recordings before and after perfusion of 50% Na-Li Tyrode. Data presented in Figure 3.8 illustrates the Ca^{2+} levels within the SR. As Na-Li Tyrode was perfused (indicated by the arrow), there was a drastic increase in fluorescence (mag-fluo-4), which suggests an augmentation of free Ca^{2+} within the SR as the sarcolemma NCX1 was impaired (p-value < 0.01). Changes in intra-SR free Ca^{2+} fluorescence parallels the changes in resting cytosolic Ca^{2+} levels in Figure 3.1, before and after treatment with 50% Na-Li Tyrode solutions. This corroborates the idea that impairment of NCX1 would induce an increase in SR Ca^{2+} load, by an increase in SERCA2a activity. If this holds true, then these increases in free Ca^{2+} with in the SR is expected to also correspond with the increase in amplitude of Ca^{2+}-released from the SR into the cytosol (Figure 3.4).

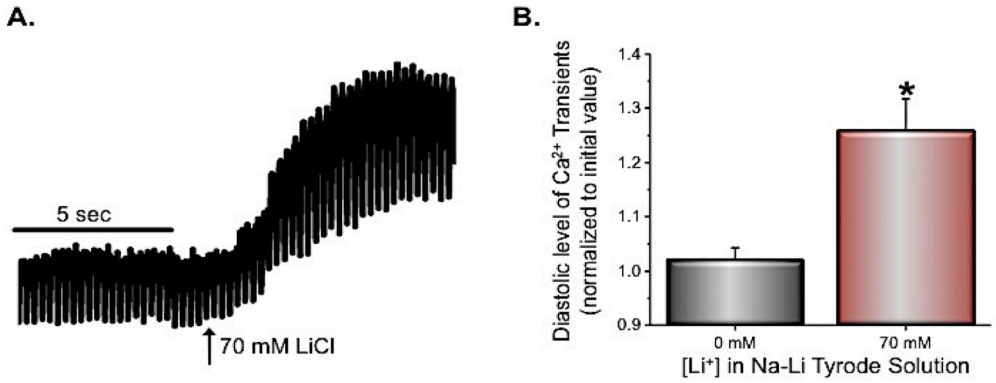

Figure 3.8 Effect of 70 mM LiCl on intra-SR Ca^{2+} transients recorded at 4 Hz and 37°C. Changes in the fluorescence signal from the SR (fluorescent dye mag-fluo-4, AM) before and after the onset of 70 mM LiCl (A). Resting fluorescence indicates the intra-SR Ca^{2+} diastolic level before and after application of 70 mM LiCl (B). Changes in the diastolic level was calculated by normalizing initial diastolic values prior to the onset of 70 mM LiCl Tyrode (B). The data in panel B represent means ± SE (N=6) * p < 0.05.

3.4 *Does the impairment of NCX1 increase the amplitude and alter the kinetics of Ca^{2+} transients released from the SR?*

As previously described (Chapter 1, sec 1.2), the unique physicochemical and morphological arrangement of the SR allows a large amount of Ca^{2+} to be stored due to the presence of low affinity-high capacity Ca^{2+} binding proteins (buffering proteins; i.e. calsequestrin) (Gyorke and Carnes 2008) (Gyorke and Terentyev 2008) (Terentyev, Viatchenko-Karpinski et al. 2002; Szentesi, Pignier et al. 2004; Qin, Porta et al. 2005; Knollmann, Chopra et al. 2006; Kornyeyev, Petrosky et al. 2011). As a result, the SR is readily available to release the free Ca^{2+} ions once the RyR2 is opened during CICR under normal physiological conditions. However, when NCX1 is impaired, there is an accumulation of free luminal Ca^{2+} (Figure 3.8). Conveniently, the RyR2 is luminally regulated (Zoghbi, Copello et al. 2004) thus making it easier for cytosolic Ca^{2+} to activate the channel to open. As Ca^{2+} is released, the free Ca^{2+} inside the SR will decrease. Therefore, the fluorescent signal will illustrate a sharp decrease, which will represent Ca^{2+} leaving the SR ("max amplitude"; nadir) (Kornyeyev, Reyes et al. 2010). Ca^{2+} transients recorded with Mag-fluo4, as the extracellular Tyrode solution is changed from normal Tyrode (0 mM LiCl) to a 50% Na-Li Tyrode (70 mM LiCl) are shown in Figure 3.9. Changes in the SR Ca^{2+}-release amplitude show a significant increase after 70 mM Na-Li treatment (Figure 3.9, B; (p-value < 0.01), which corresponds to the fluorescent changes observed in the cytosolic Ca^{2+}- release (via rhod-2, Figure 3.4). However, the rate to max amplitude (time to peak) appears to increase although not significantly possibly due to large margin in error collected from a low fluorescent signal in transient recordings (Figure 3.9, C 0 mM LiCl avg 16.83±1.13 ms vs. 70 mM LiCl avg 20.35±2.14 ms; p-value 0.18).

In coordination with the accumulation of cytosolic free [Ca^{2+}] during NCX1 impairment is the increase in intra-SR free [Ca^{2+}]. This could be a result of multiple mechanisms involved in the regulation of Ca^{2+}-homeostasis of cardiomyocytes. For instance, the efficiency of SERCA2a to reuptake Ca^{2+}, the SR being a Ca^{2+}-reservoir prepping for the release of free Ca^{2+} ions, and the cytosolic and luminal regulation of the RyR2 are all key mechanisms in defining the refractoriness of Ca^{2+}-released. Hence, the rate of Ca^{2+} depletion and replenishment within the SR were analyzed (Figure 3.10B,C). The relationship between intracellular Ca^{2+}-dynamics and NCX1 can be evaluated by measuring the time course of SR Ca^{2+}-release (time to peak; Figure 3.9A,C), the rate to half replenishment of SR Ca^{2+}-stores (50% recovery) and the rate of re-uptake (decay between 10-90 %) prior to the initiation of the next full cycle before and after Li-perfusion (Figure 3.10A).

As Li^{+} impairs the extrusion of Ca^{2+} (via NCX1) and intracellular Ca^{2+} concentration was accumulated, the kinetics of intra-SR Ca^{2+} replenishment was not significantly modified (Figure 3.10 B, p-value 0.29; C, p-value 0.29). Luminal regulation primes the RyR2 channels to spew large amounts of Ca^{2} into the cytosolic region. This luminal regulation of the RyR2 will not only increase the probability of RyR2 to be open by cytosolic Ca^{2+} but it will attempt to stabilize the channels in an open state that will finally lead to an increase in the time to peak of the cytosolic Ca^{2+} transients (Figure 3.5 B). Normally, a decrease in the rate of replenishment would suggest a decrease in the rate of reuptake by the SERCA2a however this was not significantly reduced with perfusion of 70 mM Na-Li Tyrode (Figure 3.10 C). On the other hand the data presented in Figure 3.10 suggests a tendency for a reduction, which is consistent with the idea of some luminal inhibition of SERCA2a by Ca^{2+}.

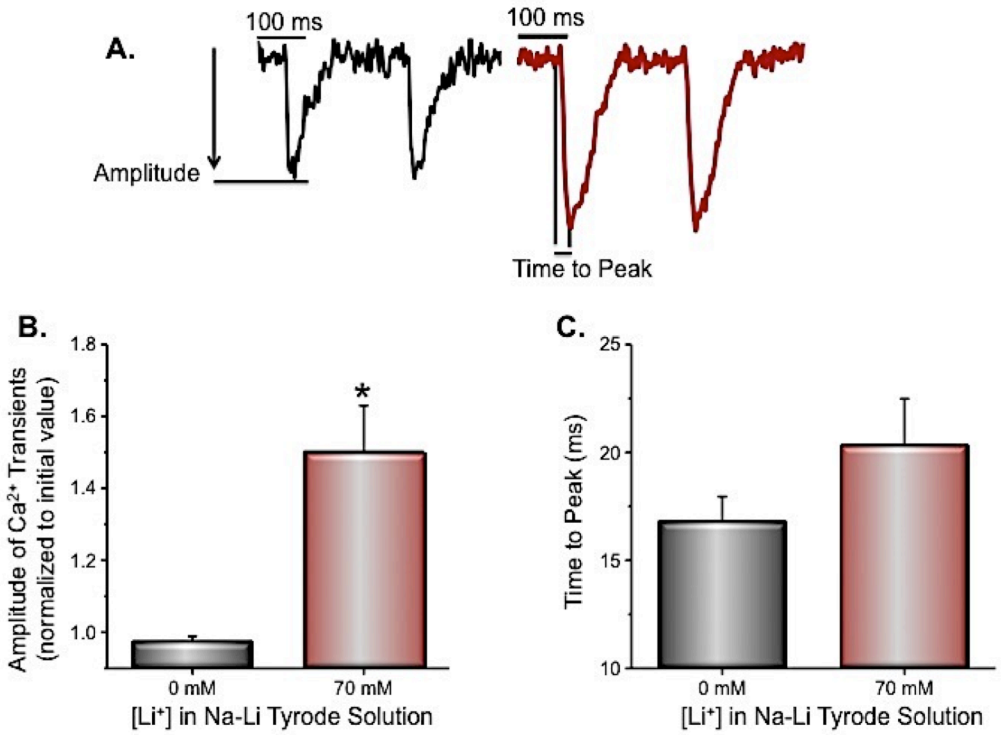

Figure 3.9 Effect of 70 mM LiCl on intra-SR Ca^{2+} transients recorded at 4 Hz and 37°C. Typical Ca^{2+} transient traces (averaged) measured with fluorescent dye mag-fluo-4 AM before (left) and after (right) application of 70 mM LiCl Tyrode (A). A decrease in the fluorescent signal is a representative of Ca^{2+} leaving the sarcoplasmic reticulum. An increase in the intra-SR Ca^{2+} transient amplitude before and after application of 70 mM LiCl is represented in panel B. Time to maximum amplitude is represented as time to peak in panel C. Maximum amplitude of Ca^{2+} transient release was determined by measuring the change in fluorescence from the baseline to the maximum decrease in fluorescence. Amplitudes were calculated using the ratio Amax/Ai, where Amax is the maximum decrease in fluorescent amplitude and Ai is the initial amplitude of release of the first set of averaged transients, respectively. The data in panel B and C represent means ± SE (N=6) * $p < 0.05$.

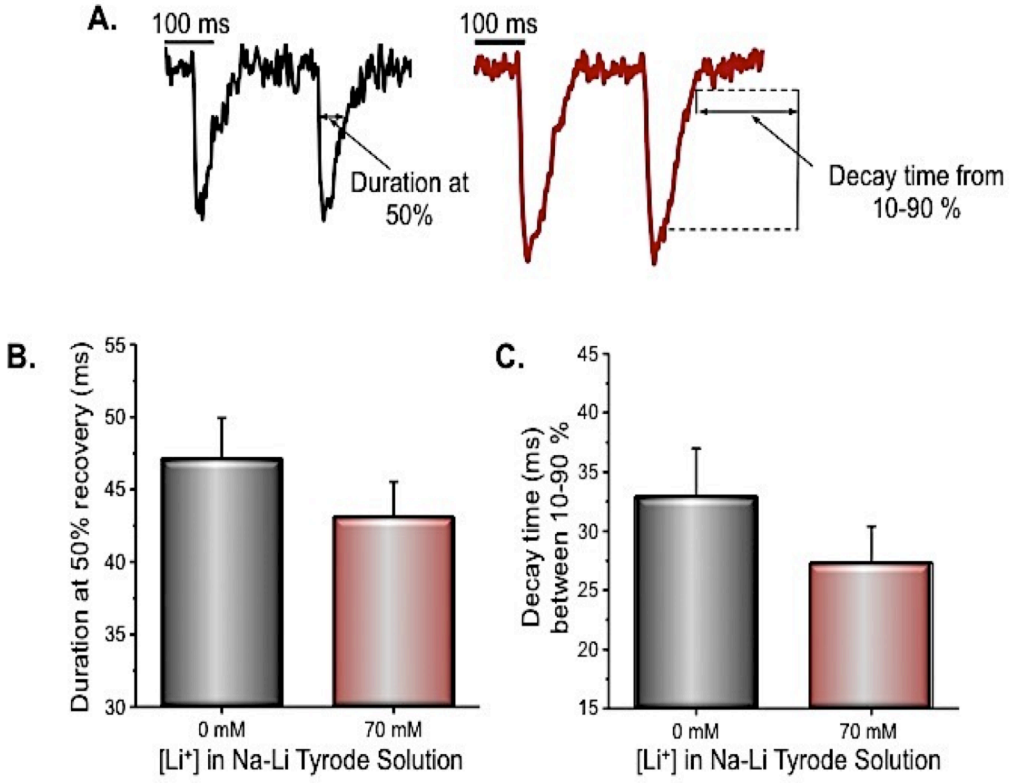

Figure 3.10 Effect of 70 mM LiCl on the kinetics of intra-SR Ca^{2+} transients measured with mag-fluo-4 AM at 4 Hz and 37°C. Intra-SR Ca^{2+} transients recorded in the absence (left) and in the presence (right) of 70 mM LiCl (A). The curves were normalized to peak amplitude. Panels B &C represent the duration at 50% decay & the decay time between 90 & 10% (divided by 2.2). The data in panels B & C represent means ± SE (N=6).

All in all, the data presented in this section demonstrates that the inotropic consequences of impairing the NCX1 are directly related to an increase in the SR Ca^{2+} load that finally will promote an increase of the Ca^{2+} release from this organelle. These differences in the magnitude and the kinetics of Ca^{2+} release will impose tight constrains to the effect of the heart rate on the cardiac cycle. Next we will test these constraints when the heart rate is increased.

Heart Rate Dependency of Intracellular Ca^{2+} Dynamics

The heart is the organ in charge of pumping blood through both the pulmonary and the systemic circulatory system. As a pump, the heart is responsible for delivering nutrients to every tissue in the body as well as washing out the waste produce by the cell's metabolism. Under different physiological demands, the metabolic needs of different tissues change. The way the body adapts to this situation is by changing the cardiac output. The cardiac output is directly proportional to the heart rate, so under normal circumstances the heart will need to change its heart rate in order to maintain the homeostasis of the body. Interestingly, during tachycardia the increase in the heart rate will challenge the time for the heart to initiate the next cardiac cycle. We already demonstrated that impairing the NCX1 activity would modify the rate of release of Ca^{2+} transients. Thus, we speculate that changes in the NCX1 transport capacity will change the way the heart responds to different heart rates.

***3.5** Does the impairment of NCX1 modify the frequency dependency of intracellular Ca^{2+} dynamics?*

Mice are mammals that function at significantly higher heart rates than other mammals. At rest, the typical heart rate for a mouse is 600 beats per minute (10 Hz). However, when the heart is removed from the animal and it is attached to a Langendorff perfusion system the resting heart rate of the organ is significantly slower (4 to 6 Hz). This bradycardic heart rate is mostly defined by the fact that when a heart is removed from the body it loses all the sympathetic drive that is in charge of maintaining the normal 10 Hz heart rate. Experiments presented in this section were designed to evaluate the role of the NCX1 under normal and tachycardic heart rates.

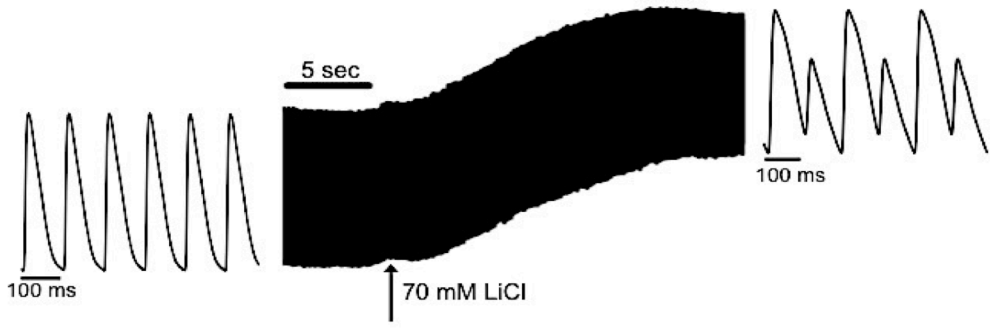

Figure 3.11 Induction of Ca-Alt during treatment with Tyrode solution containing 70 mM LiCl, at 10 Hz and 37°C using rhod-2 AM. Typical cytosolic Ca^{2+} transients at normal mouse heart rate (10Hz) recorded before (left) and during treatment of 50% of Na^{+} replaced with Li^{+}. Vertical arrow indicates onset of Li-treatment.

Figure 3.11 shows a typical experiment in which the NCX1 was challenged during a normocardic condition. It was very interesting to notice that this maneuver induced a biphasic behavior named Ca^{2+} alternans (Ca-Alt). Cytoplasmic Ca-Alt is an abnormality in Ca^{2+} handling characterized by alternating large and small amplitudes of Ca^{2+} transients. Signs of cardiac dysfunction have been correlated to the appearance of alternans (Schouten and Terkeurs 1985). Data presented in Figure 3.12 not only shows

a significant increase in Ca^{2+} amplitude of release (A, p-value < 0.01), but also the induction of Ca-Alt as perfusion of 70 mM LiCl Tyrode was applied (B, p-value < 0.01). At this heart rate, the time between transients is limited; thus when NCX1 extrusion rate is reduced there is an apparent Ca^{2+} overload; an increase in resting diastolic levels leading to increase in SR-Ca^{2+} release (Figure 3.11, Figure 3.12A). This suggests that a slower re-uptake from the SR, leading to less free Ca^{2+} ions in the SR resulting in alterations in Ca^{2+} transient amplitudes.

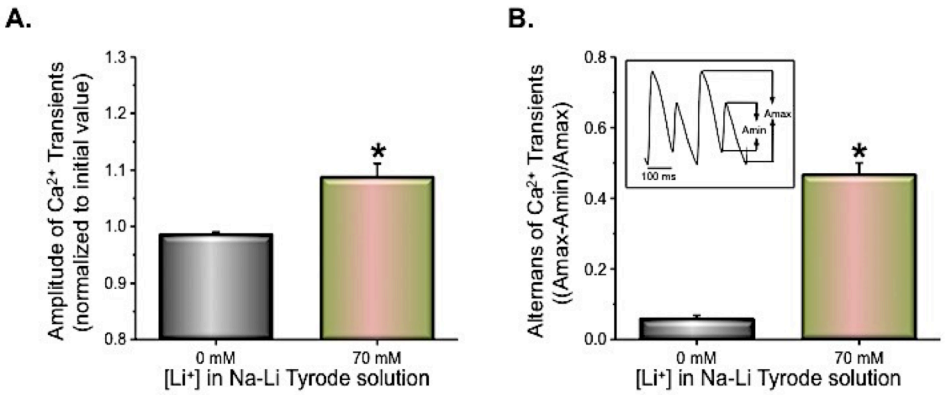

Figure 3.12 Induction of Ca-Alt during treatment with Tyrode solution containing 70 mM LiCl. The recordings were conducted at 10 Hz and 37°C using rhod-2 AM. Corresponding changes in the amplitude of Ca^{2+} transients at normal heart rate before and after the onset of 70 mM LiCl Tyrode (A). Statistical data reflecting these changes in the amplitude of Ca-Alt (B). As represented in the insert,, the induction of Ca-Alt was determined by measuring the maximum amplitude of Ca^{2+} release (Amax) and the corresponding smaller release (Amin). The data represents means ± SE (N=4) * p < 0.05.

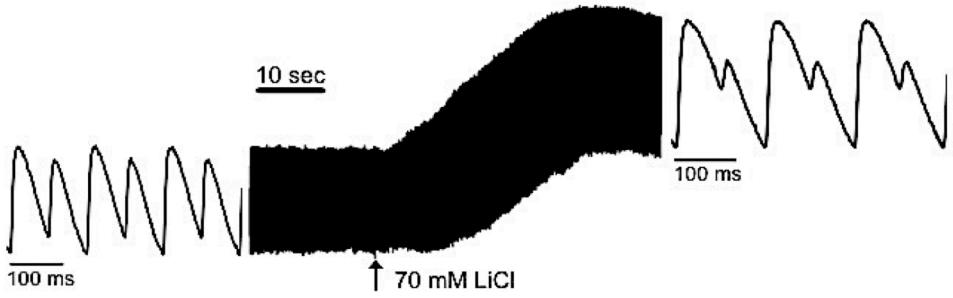

Figure 3.13 Augmentation of Ca-Alt as a result of treatment with Li-replacement Tyrode solutions. These recordings were conducted at a heart rate of 14 Hz where there are clear alterations in Ca^{2+}-release represented in a 70:30 ratio, at 37°C using rhod-2 AM. Typical recordings of Ca^{2+} transients before (left) and after the application of 70 mM LiCl Tyrode (right).

To gauge if NCX1 will further augment the Ca^{2+}-release from the SR during tachycardia, hearts were paced at 14 Hz where prominent Ca-Alt are observed (Figure 3.13). Ca^{2+}-transients that produced alternans in a 70:30 ratio (large peak to small peak, shown in Figure 3.13, left) were recorded before and after treatment with various Na-Li Tyrode solutions. Data collected in Figure 3.14 further supports the idea that during tachycardia, NCX1 impairment can contribute to Ca^{2+} -overload in the SR, thereby augmenting Ca-Alt (Figure 3.14 p-value < 0.01).

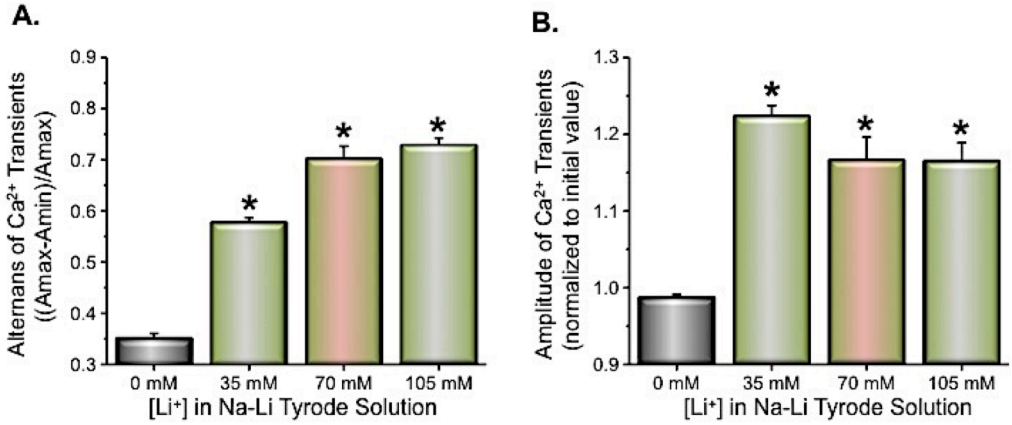

Figure 3.14 Augmentation of Ca-Alt was determined by measuring the maximum amplitude of Ca^{2+} release (Amax) and the corresponding smaller release (Amin) (A). Changes in the amplitude of Ca^{2+} transients at 14 Hz before and after the onset of different LiCl Tyrode concentration (B). Data represents means ± SE (N=4-6) * p < 0.05 when compared to their own controls.

As has been already shown, NCX1 impairment can induce Ca-Alt in normocardic and tachycardic hearts but not in bradycardic ones. This indicates that the refractoriness of Ca^{2+} release from the SR must be dramatically modified during a SR Ca^{2+} overload induced by NCX1 impairment. The refractoriness of Ca^{2+} release is an indication of how much Ca^{2+} can be released from the SR during an extra-systolic stimulation.

In order to further assess the effect of NCX1 activity during extra-systolic events, the refractoriness of Ca^{2+} release from the SR is measured using a double-pulse protocol (restitution). Restitution curves are designed to evaluate SR Ca^{2+}-kinetics, specifically the ability for the SR to reload and generate a second release. Illustrated in Figure 3.15A are superimposed normalized Ca^{2+}-transients during restitution for normal (control) and 50% LiCl replacement Tyrode solutions. Changes in the rate of recovery by the second pulse prior to and after different Na-Li Tyrode solutions provide valuable information on the time-dependency of SR Ca^{2+} recycling as NCX1 is impaired (Figure 3.15, B). A reduction in Ca^{2+} amplitude of the second pulse becomes smaller as $[Li^+]$ increases (Figure 3.15A). The slowing of the Ca^{2+} refractoriness as $[Li^+]$ increases provides supporting evidence that NCX1 plays an important role in Ca^{2+}-homeostasis (Figure 3.15B). The lack to release a sufficient amount of Ca^{2+} when an extra-systolic pulse is introduce suggests that NCX1 may also participate in the genesis of epicardial Ca-Alt. Data collected thus far supports the hypothesis that the impairment of NCX1 not only modifies cytosolic Ca^{2+} dynamics but also as a consequence modifies the intra SR Ca^{2+} dynamics. Moreover, this data supports the idea that intra SR Ca^{2+} dynamics has a strong impact in setting the refractoriness of cardiac contractility.

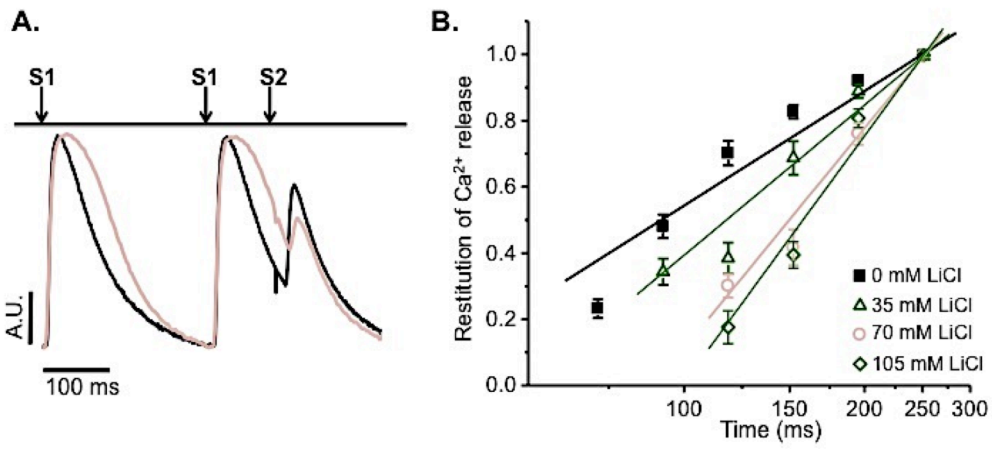

Figure 3.15 Effect of Li-treatment on the restitution of Ca^{2+} in intact hearts at 4 Hz and 37°C. Representative normalized traces recorded using a double-pulse protocol to assess the restitution of Ca^{2+} release in the absence (black traces) and in the presence (pink traces) of 70 mM LiCl (A). The levels of rhod-2 fluorescence were normalized to the amplitude of the first peak and the normalized traces were superimposed. Semilogarithmic plots of the restitution of Ca^{2+} release obtained at different concentrations of LiCl in Tyrode (B). The data in panel B represent means ± SE (N=4-5).

Finally, the data presented in this chapter demonstrated that NCX1 defines several aspects of Ca^{2+} homeostasis during the cardiac cycle. From the changes in the diastolic and systolic properties of Ca^{2+} levels in the cytosol, to the modulation of Ca^{2+} in the SR, and to the rate dependency of physiological phenomena.

CHAPTER 4 *: Electrical Signaling*

Epicardial Action Potential

In the previous chapter, we established the effects of impairing NCX1 with Li^+ on intracellular Ca^{2+} dynamics. Chapter 4 is focused on the implications of NCX1 impairment on the electrogenicity regulated by this sarcolemma protein in terms of the membrane potential. Specifically, experiments were designed to test the ***hypothesis that the impairment of NCX1 modifies the AP repolarization.*** Changes in the membrane potential were recorded either by using a potentiometric dye (Di-8-ANEPPS) via the PLFFM or glass microelectrode impalement (see Figure 2.5 and 2.8A, respectively). Di-8-ANEPPS is a lipophilic, residing in the plasma membrane and the membrane of t-tubular system. Once an electrical stimulus is introduced to pace the heart, changes in the membrane potential will produce a shift in both the absorption and the emission spectrum of this dye (Montana, Farkas et al. 1989)**.** When illuminated by a light source (green laser, 532 nm), emission of fluorescence represents a change in the membrane potential along the plasma membrane and down the t-tubules (see Methods, Figure 2.5). Recently, we published data where we compared the use of Di-8-ANEPPS to microelectrode impalement for measurements of epicardial APs (Ferreiro, Petrosky et al. 2012). In this paper, either a 1000 µm or a 200 µm-optical fiber was used (via Di-8-ANEPPS) and a microelectrode, recorded within the same region of the heart, to measure changes in the membrane from a single cell laying on the epicardial layer of an intact mouse heart. Because these cells are electrically and metabolically coupled, electrical recordings of the membrane potential generated a collective membrane potential of the surrounding cells. For instance, when APs from hearts perfused with Di-8-ANEPPs were compared to simultaneous microelectrode impalement, the optical fiber with a larger diameter generated a slower phase 0 than recordings from the microelectrode (Ferreiro, Petrosky et al. 2012). However when compared to the 200 µm-optical fiber, kinetics of the upstroke and plateau phase of the epicardial AP was nearly identical (Ferreiro, Petrosky et al. 2012). This is thought to be due to the larger diameter of the optical fiber that would allow for more fluorescence to be collected from cardiomyocytes in deeper regions of the ventricular wall, whereas a microelectrode would only record one cell lying at the epicardial layer. Although these cells are electrically coupled, they were paced and responded in an isopotential way within a fraction of the space constant of the tissue (1 mm). Therefore the slower upstroke, from a larger diameter optical fiber, would indicate the time for the dye to be detected as the AP propagates through the ventricular wall and not along the epicardial layer. Within this chapter, a 400 µm-optical fiber was used to measure changes in the membrane potential when hearts were loaded with Di-8-ANEPPS. Experiments conducted with a microelectrode (see Figure 4.6 - 4.7) were conducted simultaneously with some previously presented Ca^{2+} experiments (see Figure 3.3 - 3.7).

4.1 *Does NCX1 modify the epicardial AP morphology?*

Cardiac AP morphology is not only unique in different species, but can also differ in different regions of the heart. Mouse atrial cardiomyocytes have short AP durations and lack a prominent dome. In fact, their purpose is to pump blood into the ventricles through a low resistant hydrodynamic pathway (mitral and tricuspid valves). Whereas their ventricular myocytes, display APs that are much longer and have a more prominent

spike and dome behavior which allows sufficient time for contraction of the ventricles in order to pump blood against afterload to either the lungs or the rest of the body. Ventricular cardiomyocytes also exhibit variations in their AP morphology throughout the ventricular walls. The inner most cells, endocardial myocytes, display APs with a slower phase 1 repolarization, an extended late-depolarization, and a slower late-repolarization phase. Endocardial myocytes are the first to depolarize in the ventricular wall and the last to repolarize. On the other hand epicardial myocytes, located on the outermost layer of the heart, present APs with a sharp repolarization during phase 1 (apparent "notch"), a dome-like late-depolarization, and a faster late-repolarization phase. These particular cells are the last to depolarize and the first to repolarize, therefore are considered crucial in the genesis of ventricular arrhythmias. In addition to these morphological differences through the ventricular wall, APs on the epicardium exhibit differences in morphology in the apex and basal region of the heart due to the electrical propagation pathway for syngeneic contraction (for more details see Chapter 1, sec 1.5;). Experiments conducted in this chapter were recorded from the mid-left ventricle.

Initiation of an AP starts when there is an influx of Na^+ through voltage dependent Na^+-channels, which will depolarize the membrane and produce a sharp upstroke (phase 0). In the epicardial region of mouse hearts, there is a large amount of K^+-channels called Kv 4.3 that are responsible for the very fast and transient outward K current (I_{to}). This current is activated during the early repolarization phase, which present a "notch" characteristic (phase 1). In most mammals at this point, the time course of the AP produce changes in the membrane potential that activate the voltage-dependent LTCC to open. An influx of Ca^{2+} through these channels would then activate the RyR2, in the SR membrane, to open for additional Ca^{2+} release (i.e. CICR). Some of the expelled Ca^{2+} is then extruded from the cell by NCX1; 1 Ca^{2+} out : 3 Na^+ in. These events occur in the late-depolarization phase (phase 2) during the repolarization time course of the membrane.

NCX1 is characterized for it electrogenic behavior. This electrogenicity is driven by the protein ionic transport stoichiometry. Therefore NCX1 is capable to either produce a Na^+ influx as it extruded Ca^{2+} (forward-mode) or a Na^+ efflux, to extrude excess Na^+ from the cytosolic region (reverse-mode). In terms of its role to extrude excess Ca^{2+} that accumulated in the cytosol after Ca^{2+} release from the SR, the forward-mode would be favored. To test if a decrease in the cationic influx through NCX1 would alter the late-depolarization phase, hearts were loaded with Di-8-ANEPPS and epicardial APs were recorded. APs recorded when NCX1 was impaired, via perfusion of Na-Li Tyrode (various equimolar concentrations) as done for experiments conducted with rhod-2 for Ca^{2+} (Figure 3.4); Figure 4.1 shows typical AP traces under these conditions.

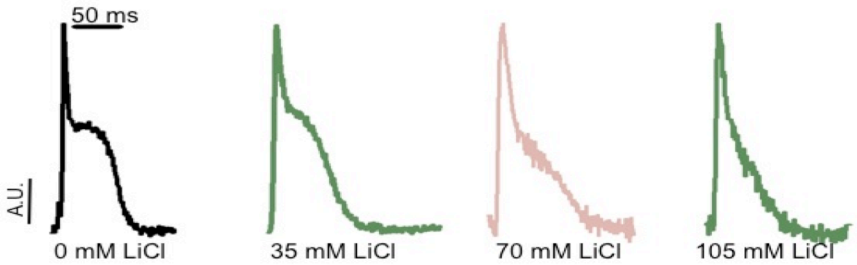

Figure 4.1 Effect of Li-treatment on the contribution of phase 2 of epicardial APs in intact hearts at 4 Hz and 37°C. Typical AP recordings measured optically using potentiometric dye Di-8-ANEPPS, recorded in the presence of different Na-Li Tyrode.

The morphology of the AP late-depolarization phase (phase 2) and late repolarization phases (phase 3) is drastically altered as the extracellular molar ratio of Li^+ to Na^+ increased (Figure 4.1). At this epicardial APs late phases intracellular Ca^{2+} dynamics plays a key role. Thus, we decided to evaluate the contribution of phase 2 as Li^+ impaired NCX1 (Figure 4.2B). Changes in Di-8-ANEPPS fluorescence were recorded at the different Na-Li concentrations and compared to their own controls. The ratio A2/A1 was used to determine the contribution of phase 2 of individual epicardial APs (Figure 4.2A; see also Figure 2.11), as the extracellular solution was replaced with equimolar Li^+ to Na^+. For instance when [Li^+] was increased, the contribution of phase 2 was significantly reduced (Figure 4.2B, 70 mM and 105 mM p-value < 0.01;). This decrease in contribution coincides with the idea that a reduction in the exchange rate would result in a decreased cationic influx, thereby leading to a faster repolarization. In other words, the inability of the NCX1 to translocate 1 Ca^{2+} out for 3 Na^+ would reduce the inflow of positive charges across the membrane that normally will define the long depolarization phase (phase 2), thus eliminating the plateau phase of the epicardial AP.

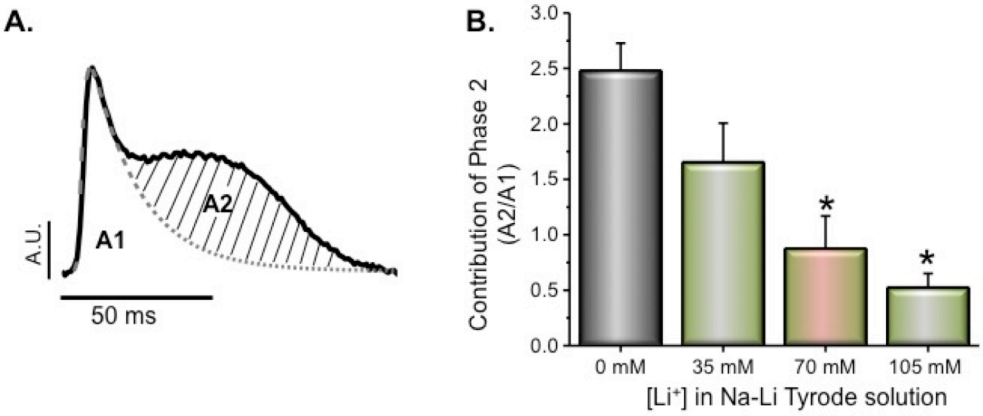

Figure 4.2 Contribution of phase 2 is determined by calculating the ratio, A2/A1, where A1 is the area under phases 0 & 1 and A2 is the area of phase 2 (B). Changes in the contribution of phase 2 of APs were determined by the ratio A2/A1 in the presence of normal Tyrode (0 mM LiCl), [35 mM], [70 mM], and [105 mM] LiCl replaced-Tyrode solutions, respectively (C). The data in panel C represent means ± SE (N=5) * p < 0.05 when compared to their own controls.

In addition to the apparent role of NCX1 in the late-depolarization phase of an epicardial AP (Figure 4.2B), NCX1 is assumed to play a major role in the late-repolarization phase (phase 3). To test if impairment of NCX1 would further alter the late-repolarization phase, measurements of the AP duration (APD) at 50% repolarization (APD_{50}) were calculated in epicardial APs perfused with various Na-Li Tyrode solutions (Figure 4.3A). Within Figure 4.3-B (insert) is an illustration of how epicaridal APs recorded with Di-8-ANEPPS were measured to determine APD_{50} and the normalize dV/dt. At APD_{50}, the duration of APs increased as Na-Li Tyrodes were applied (Figure 4.3A). Although there was a significant decline in the contribution of phase 2, impairment of NCX1 in phase 3 of the epicardial AP could result in a slower repolarization. On the other hand, this prolonged duration could also be correlated to the previously observed increase at 50% recovery in cytosolic Ca^{2+} transients recorded with the same extracellular Na-Li Tyrode concentrations (refer Figure 3.6B).

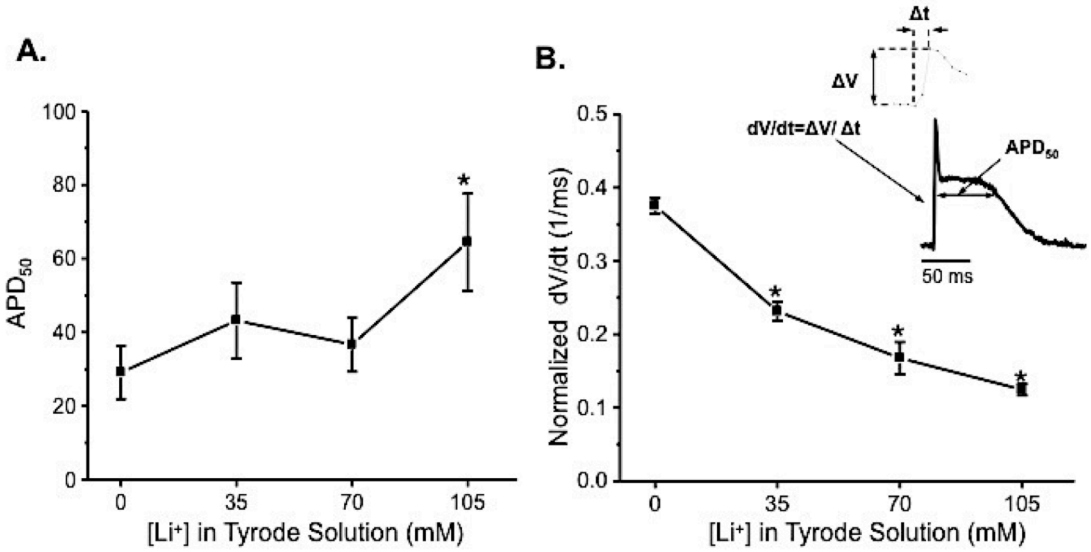

Figure 4.3 Effect of Li-perfusion on AP depolarization at 4 Hz and 37°C. AP duration of the late depolarization is calculated at 50% repolarization with different [Li^+] (A). The maximum rate of phase 0 depolarization (dV/dt) of the AP with different [Li^+] (B). Data is represented as means ± SE (N=5) * p < 0.05 when compared to their control.

Interestingly, measurements of phase 0 were also decreased in the rate of initial depolarization (phase 0) as extracellular Li^+ increased (Figure 4.3 B; p-value < 0.01). This reduction in speed during the first upstroke in the AP when 75 % extracellular Na^+ was replaced by Li^+ corresponds with the increase in the APD_{50} (Figure 4.3 A, 105mM p-value < 0.05). This attribute could be due to a decrease in NCX1 (during phase 3) and the inability of Na^+/K^+-ATPase to pump Li^+ out of the cell as the cytosolic [Li^+] : [Na^+] increased. However when 50% Na-Li Tyrode was perfused, APD_{50} had a tendency to decrease in comparison to other extracellular Li^+ concentrations, although not significant. This implies that increases in the cytosolic Li^+ concentrations would not necessarily alter phase 0. Another possibility is that changes in APD_{50} could be a simple measurement error since these results were obtained by measuring decreases in fluorescence. Phase 0 is extremely rapid; therefore if the perfusion of Li^+ increased this phase faster than the fluorescence could be detected, there would be a morphological change in the spike-dome ratio. A decrease in the spike-to-dome ratio would alter the measurements obtained at APD_{50} on APs perfused with Na-Li Tyrode. The difficulties in calibrating Di-8-ANEPPS signals as membrane potential values is one of the limitations of potentiometric dyes. Moreover, the use of Di-8-ANEPPS verses the use of microelectrode impalement is the ability to measure from the t-tubule system in addition to the collective measurement of the PM (Ferreiro, Petrosky et al. 2012). One way to test if the membrane potential is further depolarized due to the accumulation of Li^+ in the cytosol (Li^+ entry via Na^+-channels) is to use pharmacological blockers specific for NCX1.

The use of pharmacological blockers to test the function of a protein is a common experimental approach. However, drugs used for blocking NCX1 lack specificity when compared to other drugs used for other channels and pumps. Here, the use of known

NCX blockers KB-R7943 and SEA0400 were used at low concentrations to effectively block NCX1 (Satoh, Ginsburg et al. 2000; Bonazzola, Egido et al. 2002; Shinada, Hirayama et al. 2005; Tanaka, Namekata et al. 2005). The lack in specificity relates to the fact that these pharmacological blockers are considered “dirty” in that they tend to inhibit or block other channels (Hobai and O'Rourke 2000; Satoh, Ginsburg et al. 2000; Iwamoto, Kita et al. 2004; Matsuda, Koyama et al. 2005). APs recorded on the epicardial layer of different mouse hearts, using Di-8-ANEPPS, are shown in Figure 4.4. Upon perfusion of either drug, there is a significant reduction in phase 2 when compared to their control (Figure 4.4B, KBR p-value < 0.05; SEA p-value < 0.01). However, unlike the use of Na-Li Tyrode to impair NCX1 both NCX1 blockers produced a significant decrease in APD_{50} (Figure 4.4 C, KBR p-value < 0.05; SEA p-value < 0.01).

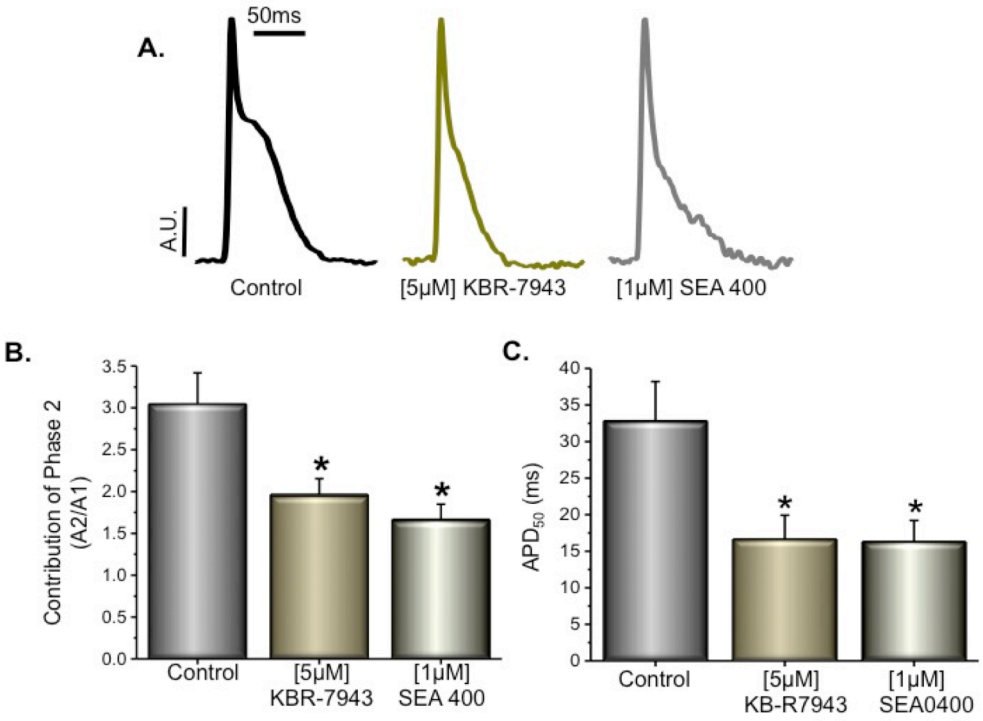

Figure 4.4 Effect of NCX blockers, KB-R7943 & SEA0400, on phase 2 of APs measured at 4 Hz and 37°C. Typical AP recordings measured optically using potentiometric dye Di-8-ANEPPS, before and after application of either [5 μM] KB-R7943 (gold traces) or [1 μM] SEA0400 (silver traces) (A). Contribution of phase 2 of APs before and after the presence of NCX blockers (B). Representation of APD50 dependence on the NCX blocker KB-R7943 and SEA0400 at 4 Hz and 37°C (C). Calculations for data in panel B were determined by the ratio A2/A1. The data in panels B and C represent means ± SE (N=5 & 10) * p < 0.05 when compared to their own controls.

To ensure minimal contamination of the drugs on the LTCC, cytosolic Ca^{2+}-transients were recorded in separate hearts (Figure 4.5, A-B). Rhod-2 recordings of cytosolic Ca^{2+}-transients in Figure 4.5 C show no significant changes in the Ca^{2+}-release amplitude when hearts were perfused with KB-R7943 (p-value 0.79; N=3). KB-R7943 is known for blocking the reverse-mode of NCX and have been reported to impair Ca^{2+}-channels; including RyR1 in skeletal muscle (Barrientos, Bose et al. 2009). In cardiac myocytes, LTCC, delayed rectifier and inward rectifier K^{+}-channels are also shown to be

impaired by KB-R7943 when blocking the reverse-mode of NCX1 (Tanaka, Nishimaru et al. 2002; Tanaka, Namekata et al. 2005). Perfusion with SEA0400, on the other hand clearly shows a significant increase in the amplitude of Ca^{2+}-transients (p-value < 0.01; N=5). SEA0400 has been shown to block the forward-mode of the exchanger more specifically than any other NCX blocker with little contamination to other channels involved in cardiac ECC (Tanaka, Namekata et al. 2005). The clear trend in Ca^{2+}-transient amplitude correlates with rhod-2 recordings obtained in hearts perfused with Na-Li Tyrode (Figure 3.5, A-B). Intra-SR Ca^{2+} recordings also exhibited a slight increase in amplitude of Ca^{2+} released from the SR (results not shown). Data presented here largely provides supporting evidence that Na^{+} translocated through NCX1 is the major contributor of phase 2 and is not an experimental artifact generated by to high cytosolic $[Li^{+}]$.

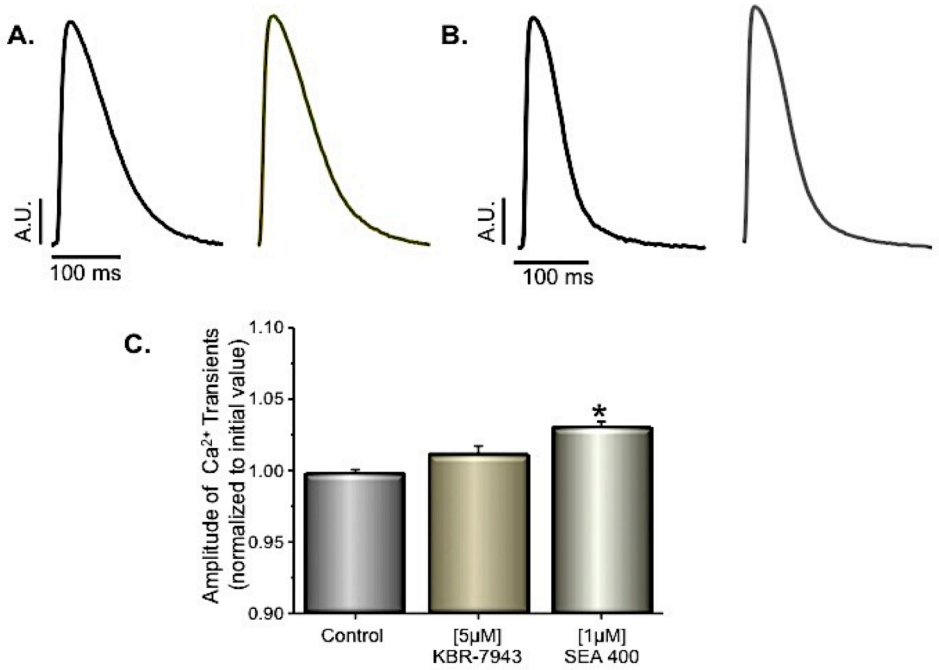

Figure 4.5 Effect of NCX blockers, KB-R7943 (A) and SEA0400 (B), on Ca^{2+} transients measured at 4 Hz and 37°C. Typical Ca^{2+} transients before (black traces) and after application of [5 μM] KB-R7943 (gold traces) and in separate hearts, [1 μM] SEA0400 (silver traces). The amplitude of the Ca^{2+} transients was calculated using the ratio Amax/Ai, where Amax is the amplitude of the Ca^{2+} release and Ai is the initial amplitude of release of the first transient, respectively (C). The amplitude was corrected for bleaching and normalized to initial level prior to application of drugs. The data in panel C represent means ± SE (N=3 & 5) * p < 0.05 when compared to their own controls.

As mentioned earlier in this section, one possibility for the prolongation in APD_{50} in Na-Li perfused hearts is the change in duration of cytosolic Ca^{2+} transient measured at 50% recovery (Figure 3.6 B). As previously illustrated in Chapter 3, impairment of NCX1 with 70 mM Na-Li Tyrode produced a morphological change in the cytosolic Ca^{2+} transients (Figure 3.5 A; trace insert). These changes in the Ca^{2+} transient morphology were evaluated by measuring the kinetics of the rhod-2 fluorescence, as Ca^{2+} was released and re-uptaken by the SR (Figure 3.6). As Ca^{2+} was released from the SR,

there was an increase in the time to maximum amplitude of the transient when perfused with 70 mM Na-Li Tyrode (Figure 3.5 B). The fact that the time to achieve peak amplitude was longer resulted in a longer duration for cytosolic Ca^{2+} to reach 50% recovery (Figure 3.5 A & 3.6 B, respectively). These prolongations in Ca^{2+} recovery are expected to be responsible of the changes in APD, however at APD_{50} when 70 mM Li^{+} was applied, there were no significant changes compared to control conditions (Figure 4.3 A, p-value 0.48). These results suggest that perhaps the Ca^{2+} released from the SR could contribute to the changes in the repolarization phase of epicardial APs.

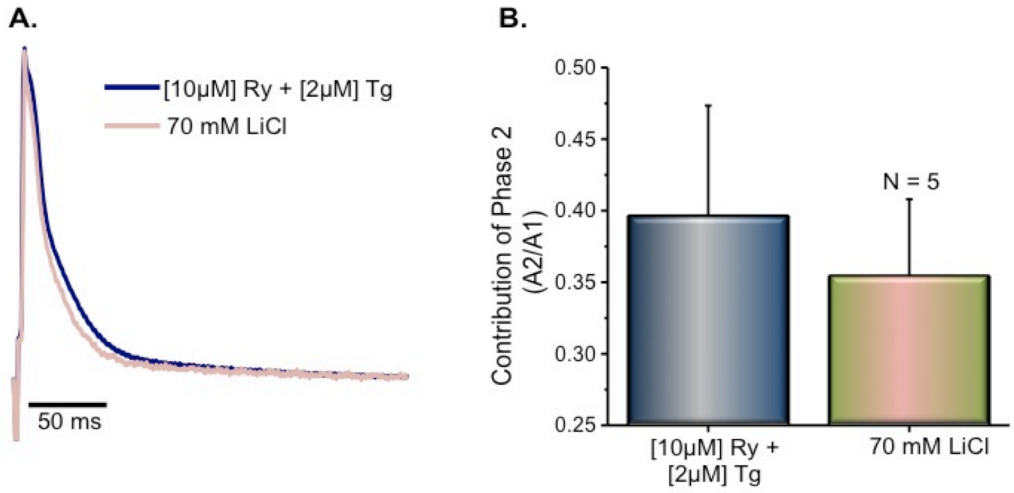

Figure 4.6 Effect of Li-treatment on the morphology of APs recorded with glass microelectrodes in intact hearts pre-treated with [10 μM] Ry + [2 μM] Tg, at 4 Hz and 37°C. Typical microelectrode recordings of epicardial APs, pre-treated with Ry+Tg before (navy blue trace) and after (pink trace) application of 70 mM LiCl Tyrode (A). Changes in the contribution of phase 2 of APs before and after the presence of 70 mM LiCl (B). Calculations were determined by the ratio A2/A1. The data in panel B represent means ± SE (N=5).

In order to test if SR-Ca^{2+} release would alter the contribution of phase 2, microelectrode recordings of the membrane potential were evaluated when Ca^{2+} released from SR was impaired by blocking the RyR2 with 10 μM of the alkaloid Ryanodine (Ry) and blocking the SERCA2a pump with 2 μM of Thapsigargin (Tg). This pharmacological treatment of Ry+Tg was applied prior to perfusion with 70 mM Na-Li Tyrode (Figure 4.6 A). Once SR-Ca^{2+} release was eliminated (via 10 μM Ry + 2 μM Tg), there was a decrease in the morphology of phase 2 (Figure 4.6 A, navy blue trace). Under these conditions changes in the repolarization is expected to occur because of two reasons. First the lack of Ca^{2+} release from the SR can modify the AP repolarization by damping the Ca^{2+} dependent inactivation of the LTCC. However, this possibility is not very likely because a decrease in SR Ca^{2+} release would produce a reduction in the Ca^{2+} dependent inactivation of the LTCCs. Thus, LTCC will be open for a longer period of time which should produce an increase in phase 2 and not a decrease in phase 2 as experimentally observe when SR Ca^{2+} is blocked (Figure 4.7C). Secondly, the lack of Ca^{2+} release would reduce the activation of NCX1, resulting in a reduced cationic influx that would normally further depolarize the membrane during phase 2. Intriguingly,

impairment of NCX1 by Li^+ alone produced similar results in the membrane potential (Figure 4.1), even though there was an increase in the diastolic Ca^{2+} levels (Figure 3.2).

Experiments shown in *Figure 4.6* were designed to evaluate if the Li^+ effect on phase 2 was mediated by SR Ca^{2+} release. Figure 4.6 shows the microelectrode recording of an epicardial AP before (navy blue line) and after treatment of 50% Na-Li Tyrode solution (pink line). Although the Ca^{2+} release from the SR was eliminated, impairment of NCX1 with Li^+ did not significantly alter the contribution of phase 2 (p-value 0.67), in spite of increases in the diastolic Ca^{2+} levels (Figure 3.7). The fact that Li-perfusion in Ry+Tg pre-treated hearts, did not further modify the membrane potential further supports the hypothesis that a decrease in the turnover rate of NCX1 is responsible for the changes observed in the late-depolarization phase of mouse ventricular epicardial APs and not changes in the Ca^{2+} released from the SR.

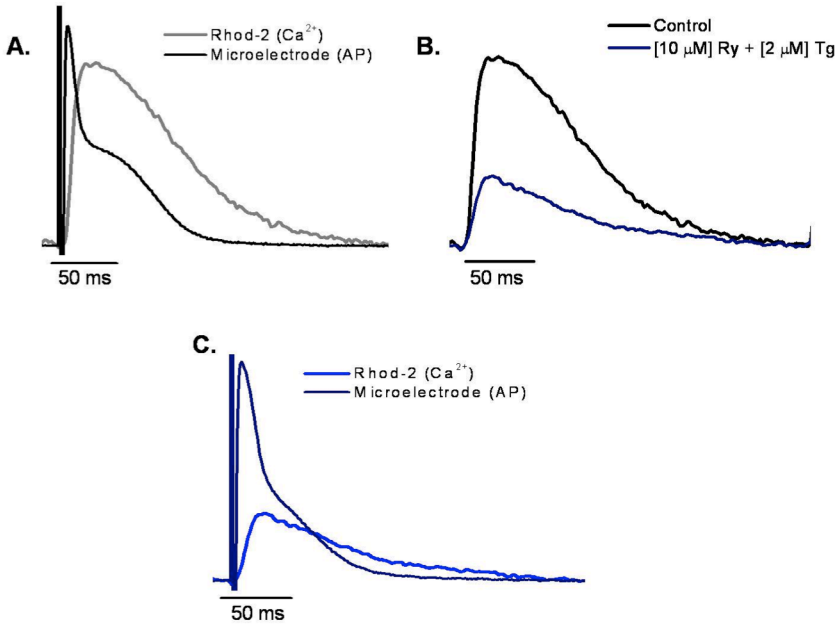

Figure 4.7 Typical superimposed traces of simultaneous recordings of Ca^{2+} (using rhod-2, 200 µm-fiber) and epicardial AP (using microelectrode impalement) at 4 Hz, 37°C. Superimposed traces under control conditions (A). Ca^{2+} transients before (black trace) and after (blue trace) pharmacological treatment of [10 µM] Ry + [2 µM] Tg (B). Superimposed simultaneous recordings of microelectrode impalement and rhod-2 recordings after application of Ry + Tg (C).

Although the current opinion on the role of LTCCs on the repolarization of the AP is that the Ca^{2+} current itself is the main responsible for this long depolarizing effect during phase 2, it is possible that the Ca^{2+} released from the SR play a key role in the genesis of the AP's phase 2. This encouraged us to perform experiments where APs and Ca^{2+} transients were recorded simultaneously microelectrodes and rhod-2 (Figure 4.7A; also see Figure 3.3 & 3.7 using a 200 µm-optical fiber). Once Ry and Tg reduced the amplitude of the cytosolic Ca^{2+} transients (Figure 4.7B), microelectrode impalement within the same region was recorded (Figure 4.7C). Ry and Tg. Fig. 4.7C illustrates the effect of 10 µM Ry and 2 µM Tg on APs and Ca^{2+} transients measured on the left ventricle epicardial layer. It is observed a dramatic and significant decrease in the

amplitude of the Ca^{2+} transients, even though Ry does not have a direct effect on the dihydropyridine receptor. Tg is a potent inhibitor of the SERCA2a pump, a Ca^{2+}–ATPase that is the Ca^{2+} active transporter in the SR, and when used in combination with Ry, it completely eliminates the SR Ca^{2+} release(Kornyeyev, Reyes et al. 2010). A statistical analysis of the contribution of phase 2 to the repolarization of the AP, the application of Ry+Tg also produced a significant reduction (34 ±3 %) in the phase 2 contribution to the optical and electrically recorded AP's (data not shown; n=5 animals; $p<0.01$).

***4.2** Does NCX1 modify the excitability of the heart?*

Kinetic changes in phase 0 of epicardial APs in Figure 4.3 (A) brought to light a decrease in the rate of upstroke when NCX1 was impaired with Li^{+}. The combination of this and a decrease in the plateau phase is anticipated to prompt a faster repolarization when 70 mM LiCl is applied. In other words a faster repolarization will drive the membrane potential to the resting potential sooner, thereby could promote the initiation of an early AP when an extra-systolic pulse is applied. To evaluate this idea, restitution curves were generated to evaluate the fast upstroke (phase 0) of the AP and its refractory period as the exchanger was impaired with 70 mM Na-Li Tyrode (Figure 4.8, A). Naturally, the AP restitution measurements are much faster than Ca^{2+} recordings due to the time to peak of phase 0 in APs occur rapidly (opening of Na^{+}-channels) and the release of Ca^{2+} is a more complex process that occurs later. Nevertheless, when comparing the restitution of Ca^{2+} and amplitude of the AP in hearts treated with Na-Li Tyrode, both experiments exhibited a slower restitution when NCX1's turnover was reduced (Figure 4.8, B). Having a slower AP-restitution implies that the initiation of an early AP is not prompted although there is a faster repolarization. On the other hand, these results somewhat correlate with the decrease in dV/dt of phase 0 seen in Figure 4.3, B.

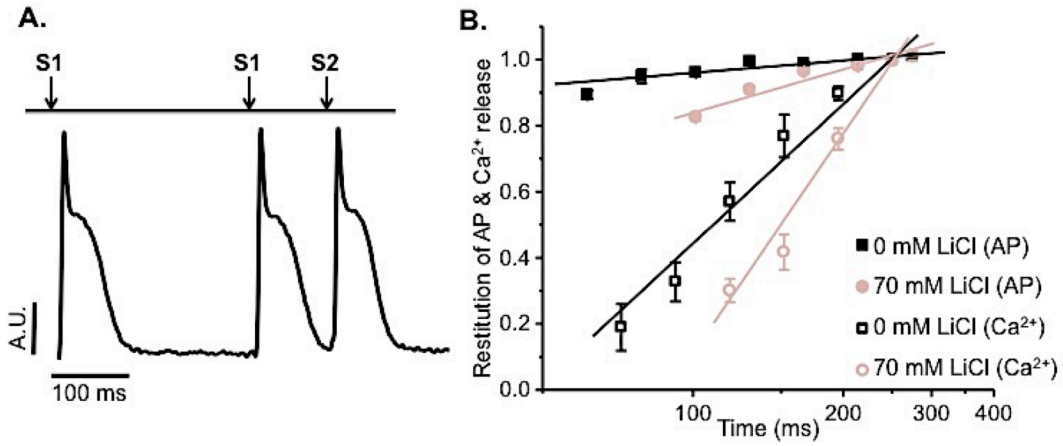

Figure 4.8 Effect of Li-treatment on the restitution of Ca^{2+} and AP in intact hearts at 4 Hz and 37°C. Typical recordings of AP measured optically using potentiometric dye Di-8-ANEPPS during double-pulsed experiments (A). Semilogarithmic plots of the restitution of the peak of AP (filled symbols) and Ca^{2+} release (open symbols) obtained in the absence (squares) and in the presence (circles) of 70 mM LiCl in Tyrode (B; N= 5 & 4, respectively).

These results support the idea that NCX1 plays a significant role in the duration of phase 2 by introducing the cationic influx of Na^+ as it extrudes Ca^{2+}-released from the SR. When there is a reduction in the cationic influx of Na^+ through the electrogenic protein (NCX1), there is an apparent reduction in the epicardial AP repolarization (phase 2). This is expected because of the high efficiency rate of the exchanger to extrude Ca^{2+} from the intracellular side of ventricular cardiomyocytes. Furthermore, Ca^{2+}-release from the SR is also responsible for the depolarization of the membrane during phase 2 (Figure 4.6 and 4.7). As previously shown in Chapter 3, as NCX1 is impaired, there is an increase in free [Ca^{2+}] resulting in a slower refractory period (Figure 3.15). This slower recovery during Li-perfusion was exemplified at higher frequencies that led to Ca-Alt (Figure 3.11 and 3.13).

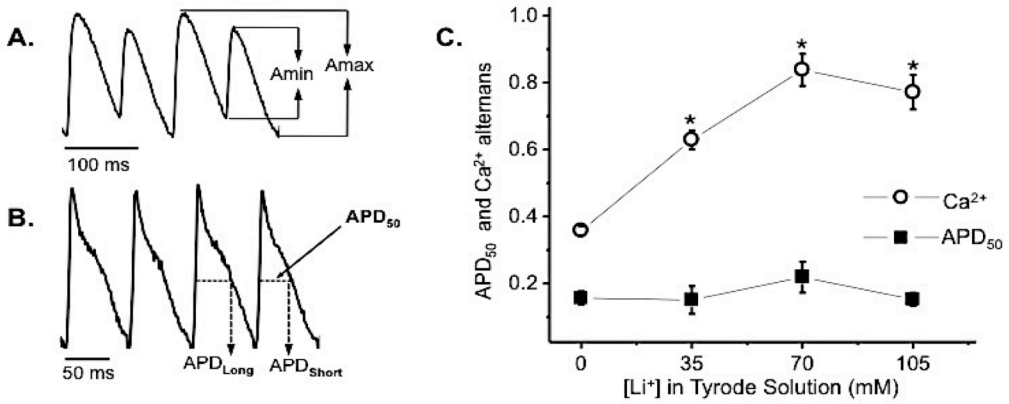

Figure 4.9 Effect of different concentrations of LiCl on Ca-Alt and AP-Alt (at APD50). Experiments were conducted at 37°C and 14 Hz, using rhod-2 AM for Ca^{2+} and Di-8-ANEPPS for AP in different hearts. Trace example of the calculation for Ca-Alt (A) and AP-Alt at APD50 (B). Averaged values of Ca-Alt and AP-Alt at 50% repolarization with different [Li^+] (C). Data represents means ± SE (N=4-6, respectively) * $p < 0.05$ when compared to their own controls.

Under tachycardic conditions (14 Hz), changes in the membrane potential were recorded before and after perfusion with different Na-Li Tyrode (Figure 4.9 C). In order to retain consistency in calculations, AP-Alts were determined in a similar way as Ca-Alt by using the ratio (Amax-Amin)/(Amax) (Figure 4.9 A). However, determination of AP-Alts were calculated at APD_{50} of the "long" AP to the "short" AP (i.e. "Amax" and "Amin", respectively, Figure 4.9 B) thereby providing the ratio Long-Short/(Long). When compared to Ca-Alt previously recorded (Figure 4.9 C; see also Figure 3.14 A), impairment of the translocation of Ca^{2+} via NCX1 produced changes in the intracellular Ca^{2+} dynamics prior to changes in the membrane potential of the epicardium at higher heart rates (14 Hz). This is expected to occur because small changes in intracellular [Ca^{2+}] are expected to induce significant changes in the Ca^{2+} handling and homeostasis of the cell (p-value < 0.01); whereas AP recordings of NCX1 impairment would only illustrate the reduced electrogenic properties of the membrane. Nevertheless, disruption in the intracellular Ca^{2+} dynamics, can lead to changes in the electrical activity of the cell.

Finally, data presented in this chapter demonstrate that NCX is not only involved in regulating the intracellular Ca^{2+} dynamics during the cardiac cycle but also modifies the electrical excitability. The NCX1 related changes in electrical excitability are mostly mediated by changes in the duration of the AP.

CHAPTER 5 *: Kinetic properties of APs in NCX1 transgenic Mouse Model*

NCX1 Conditional Knock-Out

Transgenic mouse models are frequently used in biomedical research to provide useful information about the role of specific proteins in the function of cells and organs. Chapter 5 continues to assess the hypothesis that NCX1 regulates the repolarization of mouse ventricular APs, by means of a cardiac-specific NCX1 KO transgenic mouse model. Utilizing some of the knowledge gained in the previous chapters in addition to data previously published with these cardiac-specific NCX KO mice; experiments were designed to further establish the role of NCX1 in epicardial Ca^{2+} dynamics and electrical signaling at the whole heart level. In doing so, various combinations of simultaneous PLFFM and microelectrode recordings were used to measure epicardial intracellular Ca^{2+} dynamics and membrane potential. In addition, Ag-AgCl pellets were used to record transmural ECG of mouse left ventricle.

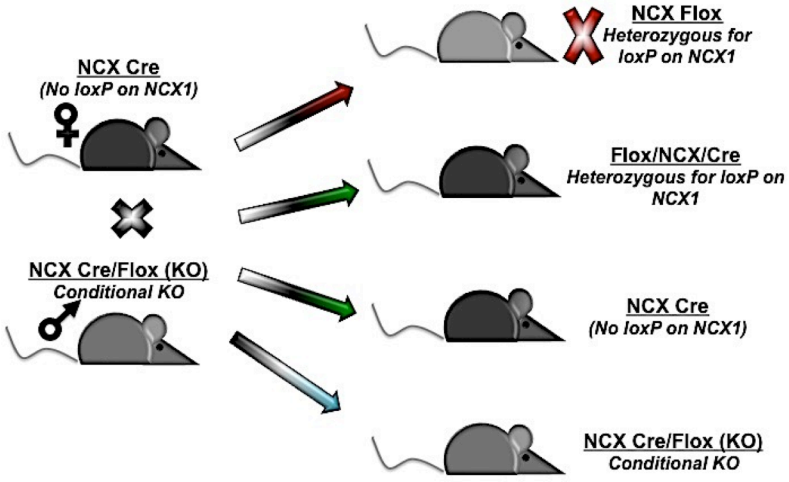

Figure 5.1 Breeding for generation of conditional tissue specific knockout mice with higher Cre content. Litters that produced a NCX Flox heterozygous (red arrow) will be euthanized, Flox/NCX/Cre or NCX Cre (green arrows) will be used for breeding. NCX Cre/Flox (blue arrow) are used for either breeding (male only) or for experimentation.

As previously mentioned in Chapter 2 (section 2.1), breeding of these NCX KO mice were difficult first to implement and then to preserve the KO efficiency without diminishing the animal lifespan. All NCX1 related mice were breed between 5-8 weeks of age in addition to crossbred with heterozygous littermates. For instance, NCX Cre females were crossed with a NCX KO male, to generate four possible offspring (Figure 5.1; Note: males KO were used due to additional stress on female KOs for offspring delivery). Mice produced with some of their NCX1 protein flanked for the loxP site (Flox heterozygous), either have no Cre expression ("NCX Flox Het"; euthanized) or express the Cre enzyme ("Flox/NCX/Cre"). In addition, these litters can generate more NCX Cre and conditional NCX KO mice (Figure 5.1), which are used for either breeding or experimentation, respectively. The generations of these heterozygous mice (Flox/NCX/Cre) were purely used for breeding either with a NCX KO littermate or mate with mice generated from the NCX Cre line to produce NCX KO mice with a higher Cre

enzyme content. Some of these NCX KO males were set aside to breed with the NCX Cre hemizygous mouse lineage again or with another "Flox/NCX/Cre" mouse, reintegrating the Cre enzyme. Male NCX KO mice generated were finally bred with a female NCX Flox, to produce only NCX KO and NCX Flox mice (Figure 5.2). NCX Flox mice produced from NCX KO litters were initially used as wild-type controls, however when compared to data collected from the NCX Flox lineage some of their littermates also indicated a small percentage of Cre present (data not shown).

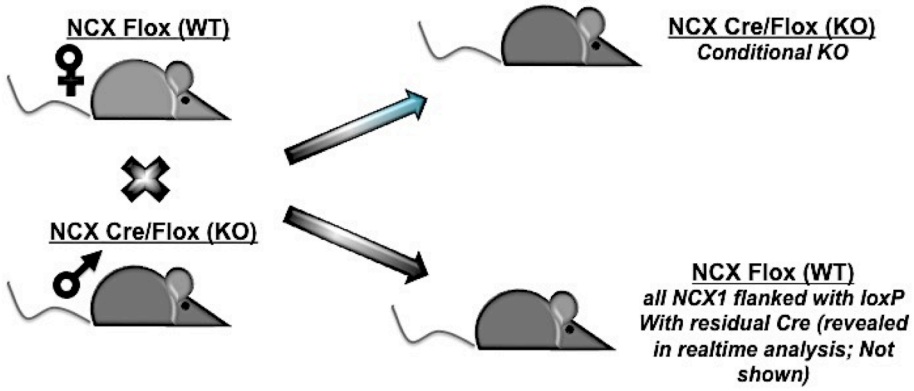

Figure 5.2 Breeding for generation of conditional tissue specific knockout mice. Litters that produced a NCX Flox (black arrow) were used for WT control experiments and NCX Cre/Flox were used as KO mice (blue arrow) for either breeding (male only) or for experimentation.

Determination of NCX1 genotypes was accomplished by ear samples that were processed and run in a DNA electrophoresis gel (see Chapter 2 Methods, sec 2.1). A picture of the gel was acquired using UV transmission to illuminate the fluorescence tag on the DNA sequence associated with the NCX genotype (Figure 5.3). In the gel each column is the PCR product of one mouse. Bands produced for the NCX Flox mice show only the Flox alleles at 526bp; NCX Cre mice show the alleles for both NCX protein at 366bp and Cre expression at 233bp; NCX KO mice will produce bands only at 526bp (Flox) and 233bp (Cre); Flox/NCX/Cre mice will produce all three bands when genotyped (Figure 5.3). The mice corresponding to the NCX Flox and NCX KO genotypes were used in experimentation or breeding.

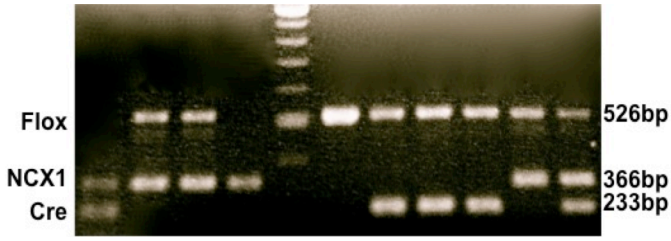

Figure 5.3 DNA electrophoresis gel from ear samples of NCX1 mice.

Unfortunately, PCR analysis to determine genotypic expression is limited to just the presence of the appropriate sequence to KO the NCX1 protein. These particular mice are conditional in the fact that there is a variation in the content of the NCX1 protein. Therefore, real-time PCR (rtPCR) analysis was done with tissue samples obtained from hearts previously used in optical and electrophysiological experiments to

measure the efficiency of the Cre enzyme to degrade the Exon11 region of NCX1 (Figure 5.4). Transcription levels are indicated as percentage retention of the functional NCX1 protein when normalized to NCX Flox hearts.

Interestingly, according to previously published data using these transgenic mice, there was a KO efficiency of 90% (approximately 10% retained expression) (Henderson, Goldhaber et al. 2004). While conducting experiments in this chapter, it was observed that some KO hearts presented similar WT AP kinetic features during recordings that later was revealed to have an approximate 40-60% ablation (Figure 5.4; KO2 & KO3). Data presented in Figure 5.4 was processed and analyzed by Mariana Argenziano using Pfaffl method (Pfaffl 2001).

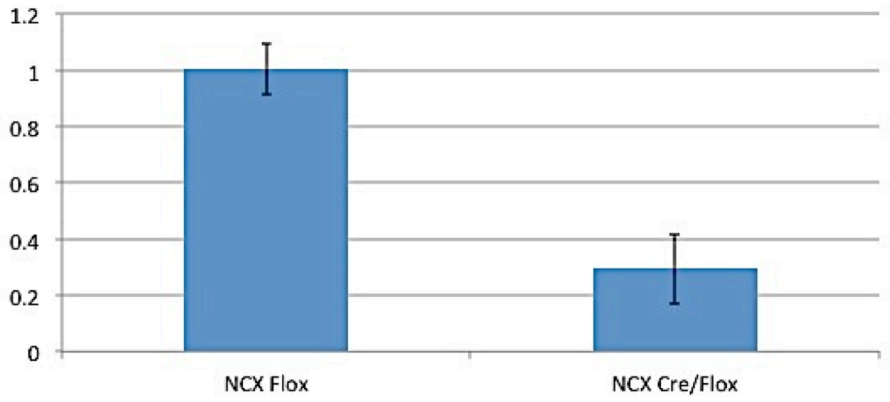

	Expression	% of Expression	Sex	DOB	Cage	Genotype
KO 1	0.18957618	19.0	Female	9/20/2010	6.2	Cre/Flox
KO 2	0.68991722	69.0	Male	9/20/2010	5.3	Cre/Flox
KO 3	0.46824482	46.8	Male	6/12/2012	77.2	Cre/Flox
KO 4	0.0805689	8.1	Male	9/20/2010	5.2	Cre/Flox
KO 5	0.04055704	4.1	Male	8/13/2012	87.3	Cre/Flox

Figure 5.4 Real-time PCR analysis of NCX mRNA expression from NCX KO hearts. Acquired from Mariana Argenziano.

Epicardial Action Potentials

Previous studies conducted on ventricular myocytes enzymatically isolated from adult NCX1 KO mice (80% of the protein is missing) (Henderson, Goldhaber et al. 2004), have shown a shortening of the AP duration at 90 % of repolarization compared to WT mice (Pott, Philipson et al. 2005; Pott, Ren et al. 2007). These authors proposed that this change in the duration of the AP was due to the lack of a forward-mode of a NCX1 current when Ca^{2+} was extruded from the cells (Pott, Philipson et al. 2005; Pott, Ren et al. 2007). However, these experiments were conducted in isolated cells at room temperature; an experimental condition in which AP phase 2 is mostly absent. These

previous experimental results and the results presented in Chapter 4 drove us to postulate that the NCX1 was a crucial protein involve in the regulation of AP repolarization. Thus, we propose to test the hypothesis that NCX1 regulates the repolarization of mouse ventricular epicardial APs, by use of conditional NCX1 KO hearts and compared to NCX Flox hearts at the whole heart level.

***5.1** Does the lack of cardiac-specific NCX1 modify the epicardial AP morphology?*

As we already have shown the repolarization morphology of an epicardial AP depends of several physiological parameters as the temperature, intracellular Ca^{2+} release from SR, the resting membrane potential and the heart rate(Ferreiro, Petrosky et al. 2012). Specifically, temperature has a dramatic effect on the AP repolarization due to the intrinsic temperature dependency of the Ca^{2+} release process and the temperature dependency of the plasma membrane conductance. This led us to speculate that at room temperature the difference in the AP repolarization between both the NCX1 KO and the NCX Flox mice will be smaller than at 37°C. Indeed, we were able to confirm this thermodynamic prediction. At 23°C (room temperature, Figure 5.5 A), AP recordings show a small phase 2 in both NCX Flox (WT) and KO mouse hearts. Once the temperature was increased to 37°C (body temperature, Figure 5.5 B), a prominent dome appears in WT epicardial APs due to the high temperature dependency of Ca^{2+} release (Q10~2.6 (Petrosky, Mejia-Alvarez et al. 2013)) and NCX1 (Q10~3.9 (Bersohn, Vemuri et al. 1991)).

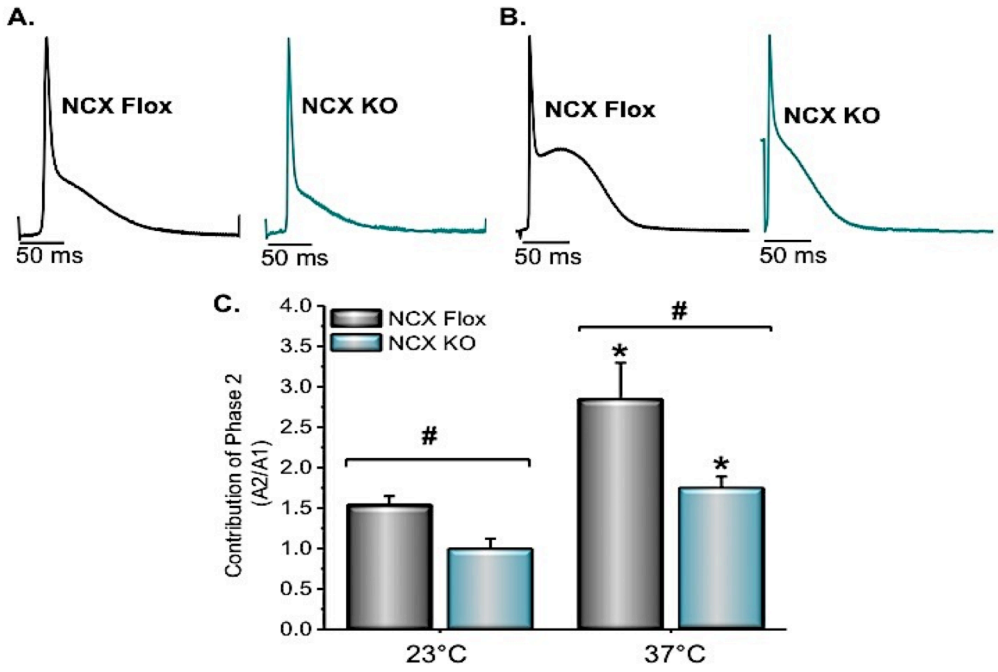

Figure 5.5 Microelectrode recordings of left ventricular epicardial APs in whole intact NCX Flox (WT) and NCX KO mouse hearts at RT (23°C, A) and body temperature (37°C, B). Changes in the contribution of phase 2 of both genotypes determined by the ratio A2/A1 is presented in bar graph (C). The data in bar graph represent means ± SE (N=5, per genotype) * $p < 0.05$ when compared to their own controls; # $p < 0.05$ when comparing genotypes.

Although at lower temperatures the morphology of the APs in both genotypes are similar, at 37°C there is a substantial difference in the morphology of the ventricular epicardial AP between NCX Flox and KO mice. This is best represented in the bar graph of Figure 5.5 C, comparing the contribution of phase 2 at both temperatures. NCX KO hearts are significantly different with a p-value < 0.01 at 23°C compared to NCX Flox hearts, whereas at 37°C there is a p-value < 0.05 for these hearts. NCX KO APs lack the dome-like characteristics, however present a p-value < 0.01 when compared to the APs recorded at 23°C.

Data presented in chapter 4 show that the impairment of NCX1 with Li^+ induce a reduction in the contribution of phase 2 of epicardial APs (Figure 4.1). Since these transgenic mice have significantly less NCX1 protein and present little to the contribution of phase2 at 37°C, we decided to test if perfusion of 50% Na-Li Tyrode (70 mM LiCl) would alter the late-depolarization phase (Figure 5.6).

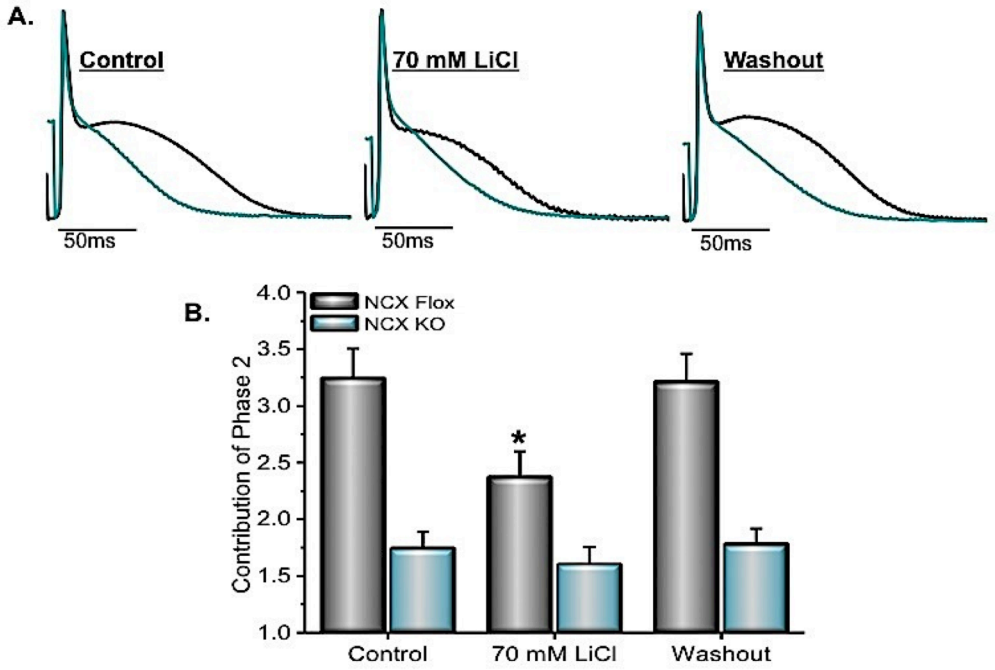

Figure 5.6 Effect of Li-treatment on the contribution of phase 2 of the AP in intact hearts at 4 Hz and 37°C. Typical AP recordings of NCX Flox (black lines) and NCX KO (light blue lines) measured via microelectrode impalement (A), recorded prior to and after presence of 70 mM LiCl (left to right, respectively). Changes in the contribution of phase 2 of APs were determined by the ratio A2/A1 in the presence of normal Tyrode (control), [70 mM] Na-Li replaced Tyrode, and washout (via normal Tyrode), respectively (B). The data in bar graph represent means ± SE (N=4-5, per genotype) * p < 0.05 when compared to their own controls.

Under control conditions, normal Tyrode solutions were perfused through the heart and microelectrode recordings of the left ventricular epicardial APs were obtained (Figure 5.6 top left). Shortly thereafter, brief application of 70 mM equimolar replacement of extracellular Na^+ for Li^+ Tyrode was performed (Figure 5.6 top middle). After a brief Li^+ exposure time (5 min), the Li^+ in the extracellular perfusate was washed with normal Tyrode, (Figure 5.6 top right). Calculations of the contribution of phase 2 of both genotypes clearly show that NCX Flox (WT) hearts are solely affected by Li^+ impairment

(p-value < 0.05). Data presented in Figure 5.6 C further supports the idea that NCX1 has a key role in the late-depolarizing phase of epicardial APs. Moreover, as Li^+ is washed-out of the heart, and the impairment of exchangers was relieved, there was an increase in the dome-like characteristics in the repolarization of the AP. This increase during the reperfusion is likely to be related to an increase in exchanger activity removing cytosolic Ca^{2+} in WT hearts, reestablishing intracellular Ca^{2+}-homeostasis.

We have already demonstrated that SR-Ca^{2+} release has a profound effect on AP repolarization (Ferreiro, Petrosky et al. 2012). Nevertheless, direct experimental evidence that this kinetic process is mediated by the crosstalk between the NCX1 and RyR2 mediated Ca^{2+} release was not available. Consequently, we propose to address if SR-Ca^{2+} release is modified in the late-depolarization phase of APs in NCX KO mice.

In a ventricular myocyte, an AP depolarization will increase the open probability of the LTCC leading to an influx of Ca^{2+} that finally will activate Ca^{2+} released from the SR. Interestingly in the earlier chapters we established that the late-depolarizing phase is produced by the activation of NCX1 that promotes a monovalent cationic influx as it extrudes excess cytosolic Ca^{2+}. Impairment of the exchanger or a reduction in the release of Ca^{2+} from intracellular Ca^{2+}-stores lessens the activation of NCX1, thereby decreasing phase 2 (Figure 4.7).

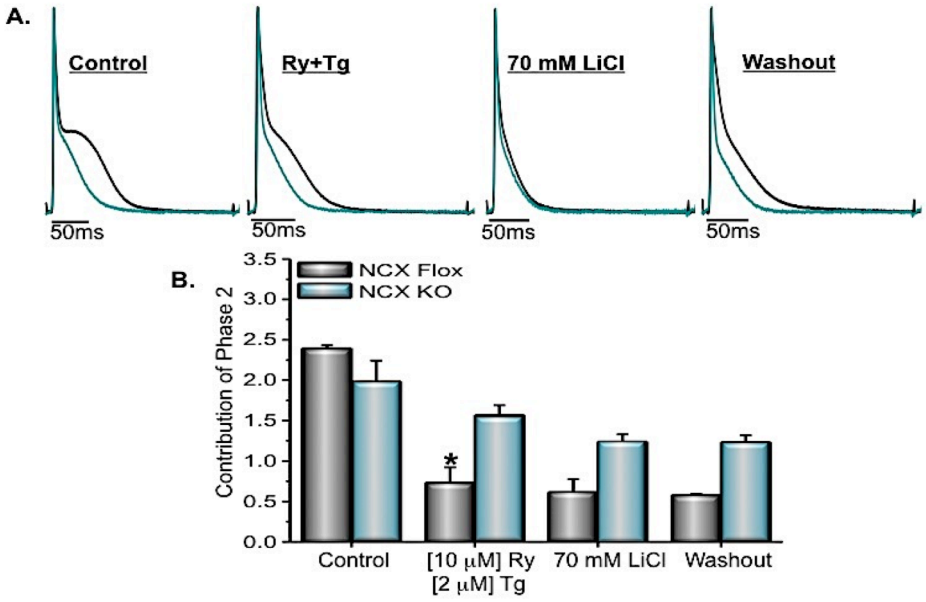

Figure 5.7 Effect of Li-treatment on the morphology of epicardial APs recorded in intact hearts treated with [10 μM] Ry + [2 μM] Tg at 4 Hz and 37°C. Typical microelectrode recordings of NCX Flox (black traces) and NCX KO (light blue traces) epicardial APs (A). Contribution of phase 2 was determined by calculating A2/A1 of APs from both genotypes before and after pharmacological treatment and Li-perfusion (B). The data in bar graph represent means ± SE (N=2-3, per genotype) * p < 0.05 when compared to their own controls.

In addition, Figure 4.6 in Chapter 4 showed that in WT mice depletion of the SR by means of Ryanodine (Ry) and Thapsigargin (Tg) induced a significant decrease in phase 2. Moreover, under this experimental condition, the perfusion of the hearts with 50% Na-Li Tyrode was not able to further attenuate phase 2 contribution. Thus, it is

expected that depletion of the SR, in NCX KO mouse hearts would not further alter the late-depolarizing phase of epicardial APs once perfused with 70 mM Na-Li Tyrode. Data is presented in Figure 5.7 support this idea. Hearts from both genotypes were paced at 4 Hz and stabilized at 37°C prior to treatment with [10 μM] Ry + [2 μM] Tg. A significant reduction of phase 2 was observed in NCX Flox but not in NCX KO animal. Furthermore a subsequent Li-application and washout of Li^+ from extracellular solution has no significant effect on NCX KO animals (Figure 5.7, A). As anticipated, only NCX Flox APs show an additional decrease in phase 2 when Ry+Tg is perfused in the heart (p-value < 0.05; Figure 5.7, B). Upon Li^+ impairment, both genotypes decreased in contribution, although not significant (p-value 0.68 NCX Flox, p-value 0.09 NCX KO; Figure 5.7, B).

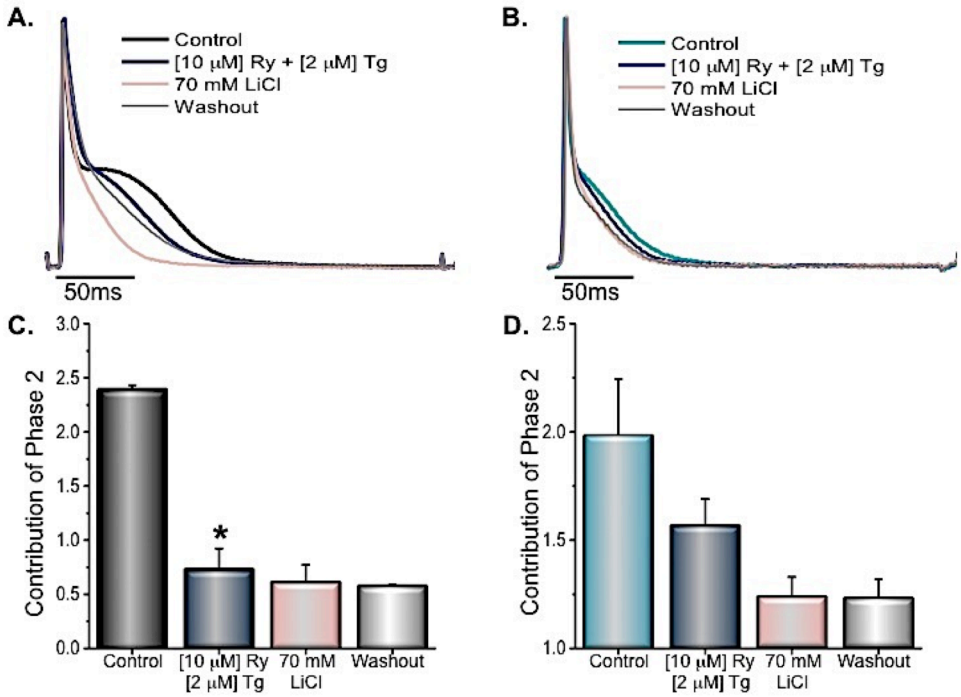

Figure 5.8 Effect of Li-treatment on the morphology of epicardial APs recorded in intact NCX Flox hearts (A) and NCX KO hearts (B) treated with [10 μM] Ry + [2 μM] Tg, at 4 Hz and 37°C. Typical microelectrode recordings of NCX Flox (black trace) and NCX KO (light blue trace) epicardial APs; treated with Ry and Tg, before (navy blue trace), application of 70 mM LiCl Tyrode (pink trace), and washout of Li^+ with normal Tyrode (grey traces). Contribution of phase 2 was determined by ratio A2/A1 for each genotype (C NCX Flox and D NCX KO). Bar graph represent means ± SE (N=2-3, respectively) * p < 0.05 when compared to their own controls.

Complementary results on the Li^+ treatment after CICR elimination are presented in Figure 5.8. This set of experiments illustrates each genotype during the application of Ry+Tg, Li-treatment, and the washout of extracellular Li^+ from the cytosol. Surprisingly NCX KO mice present a further decrease in the contribution of phase 2 during Li-perfusion (Ry+Tg avg 1.57±0.12; LiCl avg 1.241±0.09), although not significant (p-value 0.09; Figure 5.8, B).

5.2. *Does K^+ conductance play a role in defining the AP repolarization?*

AP morphology results presented in this thesis have been primarily focused on intracellular Ca^{2+}-dynamics and its relationship with the NCX1. However, various K^+-channels are active after the initial depolarization (phase 0) to repolarize the membrane potential; priming the membrane for the initiation of the next AP. Starting at phase 1, fast outward-transient K^+-channels (K_{ITO}) open and portray a sharp decline and a prominent "notch" characteristic that is unique to mouse epicardial APs. Next, is the activation of slower K^+-channels called delayed-rectifiers that open during phases 2 and 3. Also postulated to occur during phase 3 are inward-rectifying K^+-channels (Kir) that remain open until the membrane returns to its resting equilibrium potential (phase 4).

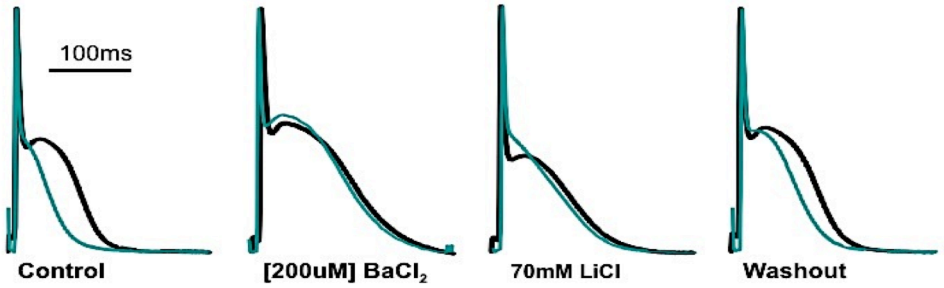

Figure 5.9 Effect of Li-treatment on the morphology of epicardial APs recorded in intact hearts treated with [200 µM] $BaCl_2$, at 4 Hz and 37°C. Typical microelectrode recordings of NCX Flox (black lines) and NCX KO (grey lines) epicardial APs, prior to (control, far left), during Ba-treatment (mid-left), perfusion with 70 mMLiCl (mid-right), and washout of Li-impairment (far right).

Since the magnitude of the membrane potential during phase 2 will be a balance between the efflux of K^+ through K^+ Channels and an influx of Na^+ through the NCX, we conducted experiments to test if the inward-rectifying K^+-channels also modify phase 2 in NCX KO mouse hearts. In order to block the efflux of K^+ from the cytosol, NCX Flox and KO hearts are perfused with normal Tyrode (Figure 5.9, far left) followed by normal Tyrode containing [200 µM] $BaCl_2$ (Figure 5.9, mid-left). Barium (Ba^{2+}) is a commonly used ion to block inward rectifying K^+-channels (Mazzanti and DeFelice 1990). It is ionically similar to Ca^{2+}, thus it is able to permeate through Ca^{2+}-channels (Mazzanti and DeFelice 1990; Pott, Yip et al. 2007). However, the low Ba^{2+} concentration [200 µM] used in the experiments in comparison with the [2 mM] Ca^{2+} in the normal Tyrode solution eliminates the likelihood of competing adverse effects. Interestingly, Ba^{2+} has a dramatic effect on action potential repolarization in both NCX Flox and NCX KO animals. These puzzling results can be interpreted based on the biophysical idea that in absence of a K^+ counter current even a small influx of Na^+ through the NCX1 that was not knocked down was able to induce a phase 2 in the AP repolarization. Alternatively, in conditions in which inward rectifying K^+ channels are block the input resistant of the myocyte will dramatically increase, allowing the influx of Ca^{2+} through LTCC to generate a late depolarization during the AP repolarization.

In order to discriminate between these two competitive hypotheses we decided to perform experiments to further impair the residual NCX1 activity in the NCX KO animals. Brief perfusion of 70 mM Na-Li Tyrode, impaired NCX1 and further decreased the dome-like characteristic in Ba^{2+} treated NCX KO mice. This experimental procedure not only induce a reduction in the Ba^{2+} treated NCX KO mice but in the NCX Flox animals as well (Figure 5.9, mid-right). This effect is partially recovered when both Li^{+} and Ba^{2+} were washed out (Figure 5.9, far right). This results favor the hypothesis that in absence of a K^{+} efflux through inward rectifying channels even a small forward mode Na^{+} current through the NCX1 is able to induce phase 2.

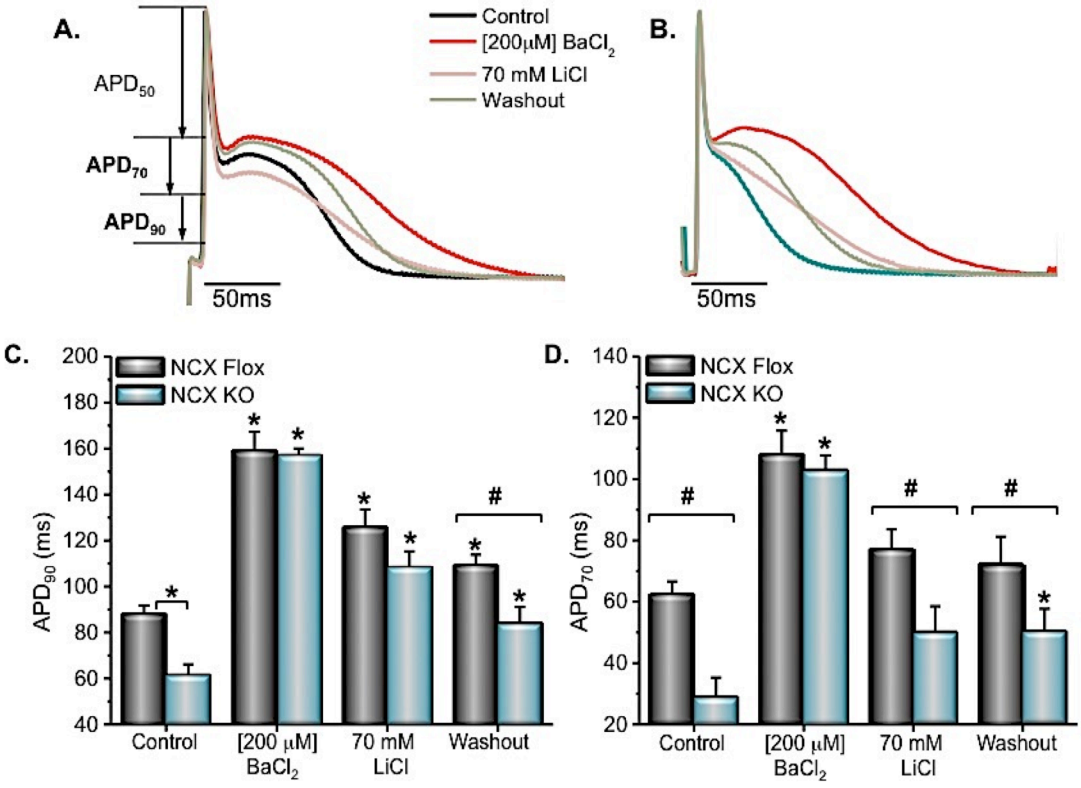

Figure 5.10 Effect of Li-treatment on the APD90 and APD70 of epicardial APs recorded in intact hearts treated with [200 μM] $BaCl_2$, at 4 Hz and 37°C. Superimposed AP recordings of NCX Flox (A) and NCX KO (B) as extracellular solution is changed. Bar graphs representing changes in the APD at 90% repolarization (C) and 70% repolarization (D) in both genotypes. Data in bar graph represent means ± SE (N=3, per genotype) * $p < 0.05$ when compared to their own controls; # $p < 0.05$ when comparing genotypes.

A detail quantification of the role of inward rectifying K^{+}-channel, as a counter-balance mechanism to the NCX1, to induce depolarization during AP repolarization is presented in Figure 5.10. Superimposed AP traces of NCX Flox (Figure 5.10, A) and KO (Figure 5.10, B) as extracellular solutions are exchanged, clearly show drastic changes in epicardial AP morphology. As Ba^{2+} blocks extrusion of K^{+} from the cytosol, the membrane potential remained depolarized longer. Elongation in AP duration (APD) and a more pronounced notch and dome characteristic of epicardial myocytes is produced in

both genotypes (red traces). Morphological changes were calculated in terms of APD at 90% repolarization (Figure 5.10, C). At APD_{90}, NCX Flox and KO hearts have similar kinetic changes, thus p-values for NCX KO hearts (p-value < 0.01) are drastically more significant than Flox hearts (p-value < 0.01). NCX KO mice have been shown to have an increase expression and activity of the outward-transient K^+-channel (K_{Ito}) (Pott, Henderson et al. 2007; Pott, Ren et al. 2007), which normally defines phase 1 and the notch of the AP. Up-regulation of these slow outward-transient K^+-channels can accelerate the extrusion of K^+ incidentally promoting an initial faster repolarization. APD at 90% repolarization remained elongated as the extracellular solution was changed in both genotypes (Figure 5.10, C). Interestingly, once perfused with Tyrode solution containing 70 mM Na-Li Tyrode to impair NCX1 (pink traces), there is a drastic decrease in the morphology of phase 2 and a shorter duration at APD_{70} (Figure 5.10, D) of the epicardial AP in WT hearts (p-value < 0.01). In NCX KO hearts, perfusion of Li^+ reduced the dome-like characteristic and more so the duration of the AP at 70% repolarization (p-value < 0.05 to Flox). Although not significantly different from its control (p-value 0.07; Figure 5.10, D), this reduction is assumed to be a combination of ~10% cells that retain the NCX1 protein (similar reduction as Figure 5.6), and the up-regulation of $K_{v4.2}$. Washout of Ba^{2+} and Li^+ from the hearts, once again produced an increase in phase 2 (grey traces). However this increase is thought to be a combination of an increase in exchanger activity removing cytosolic Ca^{2+} in WT hearts and the wash out of Ba^{2+}, allowing the extrusion of K^+ by K_{ir} to reestablish the resting membrane potential in KO hearts.

Experimental results presented in this chapter demonstrate at the molecular level that the activation of NCX1 has a dominant role in the genesis of AP phase 2. In addition, in animals where the NCX1 has been ablated, Ca^{2+} release from the SR cannot modify the repolarization of AP. Finally, the time course of AP phase 2 is a result of a competition between an efflux of K^+ through inward rectifying K^+ and an influx of Na^+ driven during the forward-mode activation of NCX1.

CHAPTER 6 *: Intracellular Ca^{2+} dynamics and Electrocardiographic properties of NCX1 transgenic Mouse Model*

Cytosolic Ca^{2+} dynamics

NCX1 is the main Ca^{2+} extrusion mechanism in ventricular myocyte. It is expected that the ablation of NCX1 will have a deep effect on all the intracellular Ca^{2+} mediated regulatory process. However, NCX1 KO mice have little compensation in the expression of the primary proteins involved in the CICR phenomena compared to their WT; yet the function of these proteins are somewhat altered (Henderson, Goldhaber et al. 2004). Philipson et al. published data that suggested an unknown compensatory mechanism that decreased the current through the LTCCs by 50% in these KO mice although the expression of LTCC remained normal (Henderson, Goldhaber et al. 2004). It is assumed that the reduction in current is carried out specifically to reduce the trigger of release from the SR in these mice or that Ca^{2+} released from the SR increased Ca^{2+} levels within the dyadic cleft that would lead early inactivation of LTCC (Henderson, Goldhaber et al. 2004; Pott, Philipson et al. 2005; Pott, Yip et al. 2007).

Experiments previously published using Nifedipine to block the influx of Ca^{2+} through the LTCCs have shown to decrease in Ca^{2+}-transient amplitude and consequently a decrease in phase 2 of epicardial APs (Ferreiro, Petrosky et al. 2012). Literature further supports the effect of Nifedipine on the Ca^{2+}-influx via the LTCCs, diminish phase 2 of APs (Bayer, Rodenkirchen et al. 1977; Bridge, Smolley et al. 1990; Lopez-Lopez, Shacklock et al. 1995; Litwin, Li et al. 1998). However, when there is no influx of Ca^{2+} through the LTCCs, then CICR would not occur at full capacity thus hinder activation of the exchanger to extrude cytosolic Ca^{2+}. Similar results are obtained when SR Ca^{2+} release and re-uptake is eliminated via Ry+Tg (Figure 4.7). Application of Ry+Tg in NCX KO hearts presented a similar decrease in phase 2 (Figure 5.8, B,D), however Ca^{2+} signals obtained during these recordings were diminished beyond analysis. This diminished fluorescent signal is not necessarily correlated to changes in Ca^{2+} current (I_{Ca}) but related to limitations in the fluorescent dye loading in an intact heart. On the other hand, Ca^{2+}-transients recorded with rhod-2 in NCX KO mouse hearts are expected to show a similar reduced signal as application of Nifedipine in WT hearts, but not similar to that of application of Ry+Tg.

***6.1** Does the lack of NCX1 produce a change in the cytosolic Ca^{2+} transients?*

To test if the cytosolic Ca^{2+} levels in NCX KO hearts differ from NCX Flox hearts, Ca^{2+} transients (recorded with rhod-2) were obtained simultaneously with previous AP recordings (recorded with microelectrode impalement; Figure 5.6) as the hearts were perfused with 70 mM Na-Li Tyrode to challenge NCX1 transport and consequently increase SR Ca^{2+} uptake. Changes in the fluorescent signal were normalized to the initial value to minimize beaching artifacts and avoid scattering in the reduced fluorescent signal obtained in NCX KO hearts prior to application of Na-Li Tyrode. NCX1 being the main extruder of cytosolic Ca^{2+} during CICR, has been shown to induce Ca^{2+}-overload when NCX1 is impaired with Li^{+} (Figure 3.1) therefore evaluation of the resting cytosolic Ca^{2+} fluorescent signal was acquired in both genotypes (Figure 6. 1).

If NCX1 is responsible for the previous increases in Ca^{2+} diastolic levels (Figure 3.1), then data collected from NCX KO hearts are expected reveal little change in the cytosolic Ca^{2+} diastolic and systolic levels. Changes in fluorescence of rhod-2 before Na-

Li Tyrode application, during application, and removal of Li^+ from the extracellular solution (washout), in NCX Flox and KO hearts were recorded (Table 3) and illustrated in Figure 6.1.

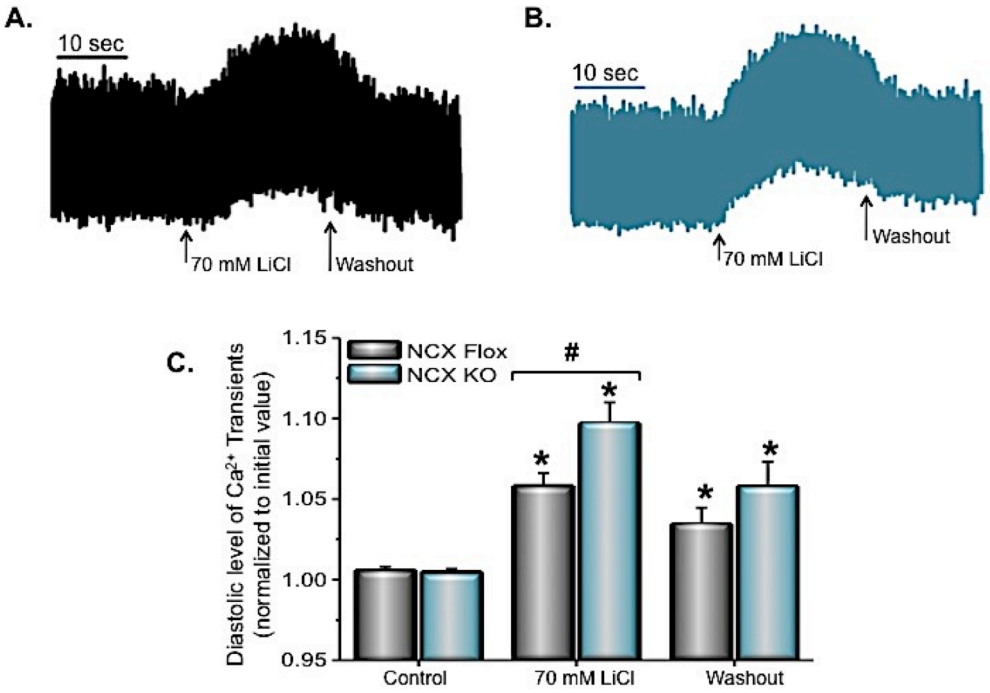

Figure 6.1 Effect of 70 mMLiCl on Ca^{2+} diastolic level of NCX Flox (A) and NCX KO (B) hearts measured at 4 Hz and 37°C. Vertical arrows indicate the onset of perfusion with 70 mM Na-Li Tyrode and later the onset of normal Tyrode solution to washout LiCl. Baseline recordings of Ca^{2+} transients are used to determine the resting diastolic levels (C). Changes in rhod-2 fluorescence were normalized to the initial level. The data represents means ± SE (N=5, per genotype) * p < 0.05 when compared to their own controls; # p < 0.05 when comparing genotypes.

Heart	Control	StErr	70 mM LiCl	StErr	Washout	StErr
Flox 1	1.0124	0.0036	1.1738	0.0112	1.0513	0.0078
Flox 2	1.0285	0.0058	1.1207	0.0063	1.1370	0.0027
Flox 3	0.9996	3.55E-4	1.0073	5.40E-4	1.0039	7.63E-4
Flox 4	0.9968	8.91E-4	1.0287	0.003	1.0167	0.0032
Flox 5	0.9953	0.0013	1.0121	0.0029	0.9678	0.006
KO 1	1.0001	9.50E-4	1.0216	0.0014	0.995	0.0028
KO 2	1.0007	6.15E-4	1.0143	0.0012	1.0223	9.84E-4
KO 3	0.9982	7.01E-4	1.0149	0.001	1.0156	7.33E-4
KO 4	1.0117	0.0069	1.1319	0.0027	1.0272	0.0093
KO 5	1.0122	0.0046	1.2927	0.0178	1.2296	0.0096

Table 3. Normalized diastolic levels of individual NCX Flox and NCX KO (littermates) hearts used in experiment before and after Li-treatment.

As anticipated, impairment of NCX1 by Li^+ produced an increase in Ca^{2+} diastolic levels in NCX Flox hearts (p-value < 0.01; Figure 6. 1,A). However NCX KO hearts also produced an increase in the resting diastolic levels that is more significant that NCX Flox hearts (p-value < 0.01; Figure 6.1, B). After evaluation of Table 3 of each heart, data presented in Figure 6.1C bar graph of both genotypes as extracellular solution is changed indicates several possibilities. One assumption is that some of the cells collectively measured (fiber size 200 µm, approximately 40 cells) at the epicardial layer of the whole heart may have some functional sarcolemma NCX present in KO hearts 4 and 5 and NCX Flox hearts 1 and 2 may retain meniscal amounts of Cre whereas Flox hearts 3 and 5 may retain slightly higher content of Cre that is still not detected in the DNA electrophoresis gel (see Figure 5.3). Microelectrode impalement recorded epicardial APs of these hearts presented phase 2 in NCX Flox and less contribution in NCX KO hearts. The other possibility is the lack of cardiac NCX already induces Ca^{2+} overload in the dyadic cleft during CICR thus further impairment of any residual NCX1 in the neighboring tissues would result in an augmentation of resting Ca^{2+} levels. Lastly, the NCX expression in the endothelial cells lying on the surface of the ventricular tissue additionally contributes to changes in the resting diastolic levels. Recently, our lab published data on rhod-2 fluorescence collected from IP3 induced release on the epicardial layer of whole hearts (Escobar, Perez et al. 2012). This paper concluded that a significant amount of resting fluorescence collected with rhod-2 fluorescence originates from the vascular endothelial cells, though the amplitude of release collected from Ca^{2+}-transients were in fact from the ventricular cells (Escobar, Perez et al. 2012). The fact that washout of Li^+ from the extracellular solution produced a substantial decrease in the resting diastolic levels in both genotypes, although more significant in NCX KO hearts (p-value < 0.01), brings to light the main experimental challenge to answer the question if the Li^+ increases of the NCX1 KO diastolic were the Li^+ response of endothelial cells and not from ventricular myocytes. Interestingly, endothelial cells are non-excitable cells. This means that endothelial cells, in contrast to ventricular myocytes, will not be able to respond to AP stimulation. Thus, the unexpected Li^+ dependent diastolic fluorescence results drove us to pursue a further evaluation of the amplitude of these cytosolic Ca^{2+}-transients (Figure 6.2).

Normalization of the Ca^{2+}-transient amplitude to the pre treatment conditions, allowed for discrete fractional changes in the release to be obtained. In contrast to what happen with diastolic fluorescence upon Li^+ application in the NCX1 KO animals, drastic changes in the resting cytosolic Ca^{2+} levels (Figure 6.1, B) were not observed in the amplitude of release in NCX KO hearts (Figure 6.2). Upon application of 70 mM LiCl, there was a significant increase in both genotypes however changes obtained in KO hearts appear to be significantly smaller than Flox hearts (p-value < 0.01). This is also true for when Li^+ was removed from the extracellular solution (p-value < 0.01). These results suggest that removal of Li^+ impairment from NCX1 in Flox hearts induced faster turnover rate, drastically reducing cytosolic Ca^{2+} and consequently lessening release of Ca^{2+} from the SR. Following this line of logic, NCX KO hearts lack majority of their NCX1, thus removal of Li^+ from the extracellular solution did not increase the rate of Ca^{2+}-extrusion from the cytosol. Thereby perfusion with 70 mM LiCl in NCX KO hearts, the amplitude of Ca^{2+} transients was not significantly different to washout Ca^{2+} amplitudes (p-value 0.35). Altogether, these results favors the idea that the Li^+ dependent increase in the diastolic florescence in NCX KO hearts were due to increases in resting Ca^{2+} levels of the endothelial cells and not from the ventricular myocytes. It is

important to notice that NCX1 ablation was specifically induced in ventricular myocytes and not in any other cellular structure in the animal.

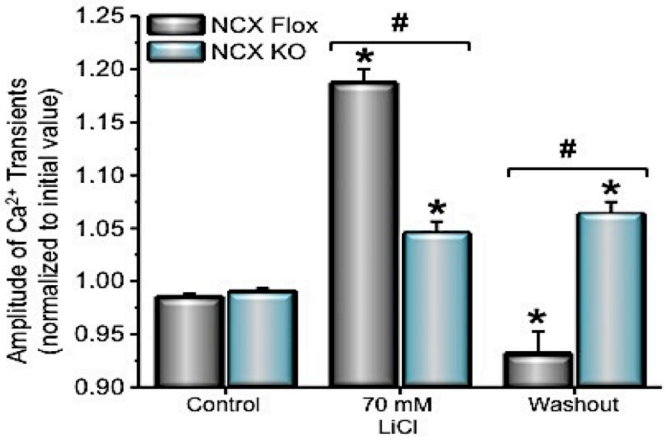

Figure 6.2 Comparison of the changes in maximum amplitude of rhod-2 fluorescence prior to, during perfusion of 70 mM Na-Li Tyrode, and washout of Li^+ from extracellular solution. Changes in fluorescence was corrected for bleaching and normalized to initial level prior to application of LiCl. Data in bar graph represent means ± SE (N=5, per genotype) * $p < 0.05$ when compared to their own controls; # $p < 0.05$ when comparing genotypes.

NCX1 mediated transport is the main Ca^{2+} extraction pathway during the cardiac cycle. We have previously shown that impairment of the exchanger will to induce Ca^{2+}-overload when this transporter is impaired with Li^+ (Figure 3.2). This impairment also reduced the contribution of phase 2 in wild-type hearts (Figure 4.1 & 4.2). Ca^{2+}-transients evaluated in this section were recorded within the same region as microelectrode impalement AP recordings of NCX Flox and NCX KO hearts presented in Figure 5.6. Thus, it is crucial to evaluate Ca^{2+}-transient kinetics under control conditions (normal Tyrode) in both NCX KO and NCX Flox hearts (Figure 6.3). Superimposed Ca^{2+}-transients from Flox (WT) and KO hearts are shown in Figure 6.3A where evaluation of their kinetics was determined.

The lack of the cardiac-specific NCX1 is expected to alter the kinetics of intracellular Ca^{2+} dynamics due to its crucial role in extruding Ca^{2+} from the myocytes (decay of Ca^{2+} transient). Previously published single-cell experiments tested SR Ca^{2+} content by application of caffeine pulses to deplete the SR in these conditional KO mice (Henderson, Goldhaber et al. 2004; Pott, Philipson et al. 2005). They determined that SR Ca^{2+} content was similar to that in WT ventricular myocytes, with significant differences in the reuptake (decay time) of the Ca^{2+} fluorescence between genotypes (Henderson, Goldhaber et al. 2004; Pott, Philipson et al. 2005). Concurrent NCX current (I_{NCX}) was measured to confirm lack of NCX1 in KO cells (Henderson, Goldhaber et al. 2004; Pott, Philipson et al. 2005). In fact this procedure of caffeine pulses became commonly used to determine which cells lacked NCX1 for comparison with isolated Flox cardiomyocytes (Henderson, Goldhaber et al. 2004; Pott, Philipson et al. 2005; Pott, Ren et al. 2007). In order to determine whether or not the kinetics of intracellular Ca^{2+} dynamics was altered due to the ablation process, cytosolic Ca^{2+} transient kinetics of both genotypes were measured. If cytosolic Ca^{2+} dynamics were altered, then there would be changes in NCX KO Ca^{2+} transient kinetics in terms of their time to peak (rate

to maximum amplitude), time to half-duration, and the decline time between 10-90% (Figure 6.3, A).

Interestingly, there were no significant changes in the Ca^{2+} transient kinetics of either genotype in the epicardial layer of cardiomyocytes (Figure 6.3, B,C,D). Although the fluorescent amplitude of Ca^{2+} transients appear to be less in NCX KO (Figure 6.1, B) and the time to this maximum release is longer (KO avg 24.7±0.98 vs. Flox avg 22.95±01.15 Figure 6.3, B), there are no significant differences in the Ca^{2+} transient rates under control conditions when compared to NCX Flox transient kinetics (Figure 6.3, B p-value 0.26; C p-value 0.14; D p-value 0.15). Fluorescent measurements at the whole-heart level imply that the SR-Ca^{2+} load does not appear to be significantly altered in NCX KO ventricular cardiomyocytes as seen in single-cell experiments.

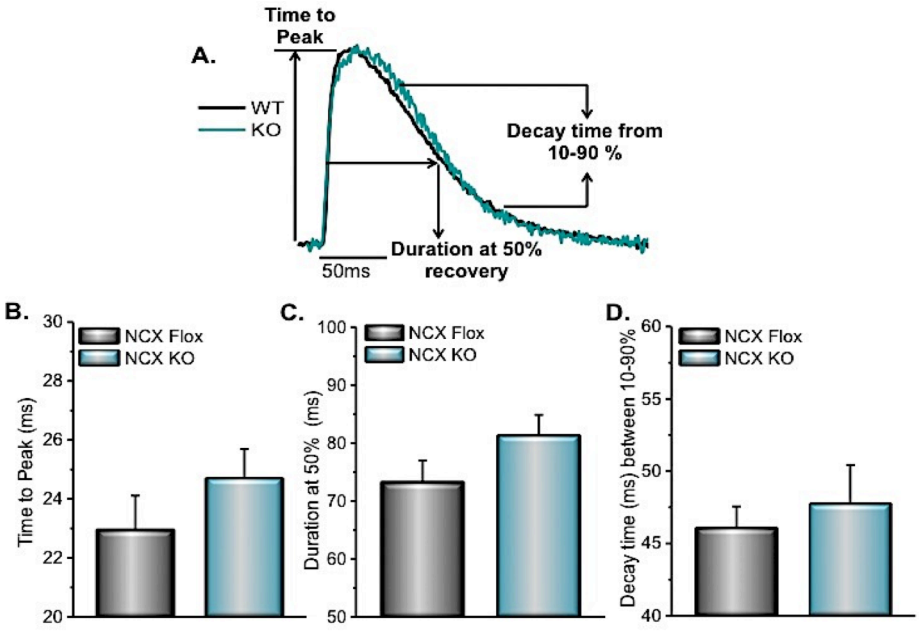

Figure 6.3 Cytosolic Ca^{2+} transient kinetics measured with rhod-2 AM at 4 Hz and 37°C. Superimposed transients of NCX Flox (black line) and NCX KO (light blue line) illustrate kinetics measurements. Time to maximum peak (A), duration at 50% recovery (C) & the decay time between 90 & 10% (divided by 2.2; D) of NCX Flox and NCX KO Ca^{2+}-transients are collected and compared. Data represents means ± SE (N= 4-5, respectively).

Heart Rate Dependency of Intracellular Ca^{2+} Dynamics

Data reported in the literature indicates that in single isolated cardiac myocytes the frequency dependency of Ca^{2+} transients of NCX KO mice, were similar to that found in NCX Flox (Henderson, Goldhaber et al. 2004). Unfortunately, enzymatically isolated ventricular myocytes present serious limitations when are challenged with frequency dependency protocols. Specifically, most of isolated cells studies were done low pacing frequencies (0.2 to 2 Hz) and at room temperature. Under physiological conditions the

mouse heart beats at 10 Hz and is thermally regulated at 37°C. Furthermore, under pathophysiological conditions the heart can experience heart rates higher than 10 Hz and temperatures higher than 37°C. These physiological constrains drove us to design experiments to assess the role of NCX1 in hearts functioning with physiological constrains.

6.2 Does the lack of cardiac specific NCX1 alter the frequency dependency of intracellular Ca^{2+} dynamics?

To assess whether or not Ca^{2+} release from the SR is challenged in NCX KO mice at normal heart rate we performed PLFFM experiments to evaluate the properties of Ca^{2+}-transients. Heart rate was increased to the normal heart rate of the mouse (10 Hz, 37°C). Additionally, the hearts were perfused with 50% LiCl Tyrode solution, to impair Ca^{2+} extrusion. As previously shown in Chapter 3 (Figure 3.8), impairment of NCX1 when the heart was paced at 10 Hz resulted in Ca^{2+} overload that led to insufficient re-uptake from the SERCA2a to induce Ca-Alt. NCX Flox and NCX KO hearts were exposed to a similar protocol. Ca^{2+} traces of both genotypes are represented in Figure 6.4.

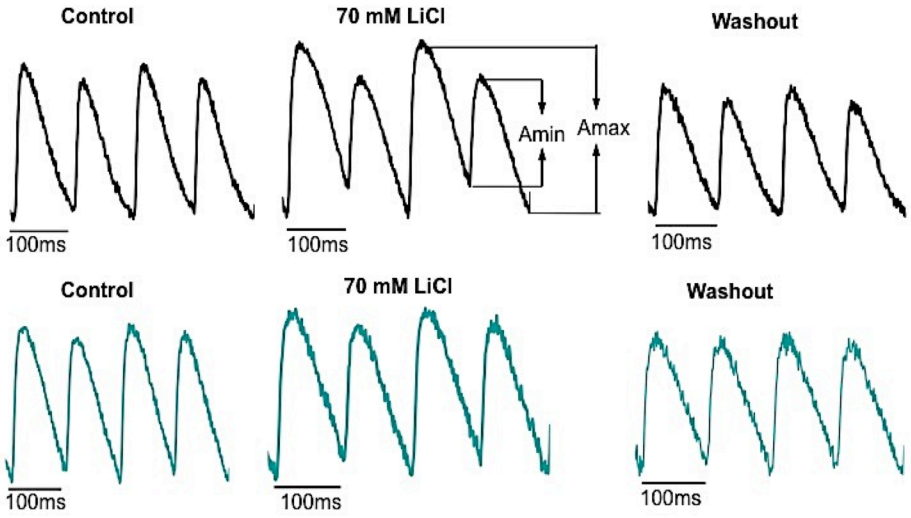

Figure 6.4 Typical cytosolic Ca^{2+} transients at normal mouse heart rate (10 Hz, 37°C, rhod-2) recorded in NCX Flox (top panel) and NCX KO (bottom panel) hearts. Transients illustrate perfusion of normal Tyrode (control, left), 70 mM Na-Li Tyrode (middle) and washout (via normal Tyrode; right). Arrows illustrate how the induction of Ca-Alt is determined by measuring the maximum amplitude of Ca^{2+} release and the corresponding smaller release (Amin).

Although at 10 Hz the hearts should display little to no Ca-Alt, NCX Flox hearts present small alterations on the epicardial layer of the mid-left ventricle. NCX Flox mice used in these experiments were littermates of the NCX KO mice, therefore some Cre activity maybe at play decreasing the total content of NCX1.

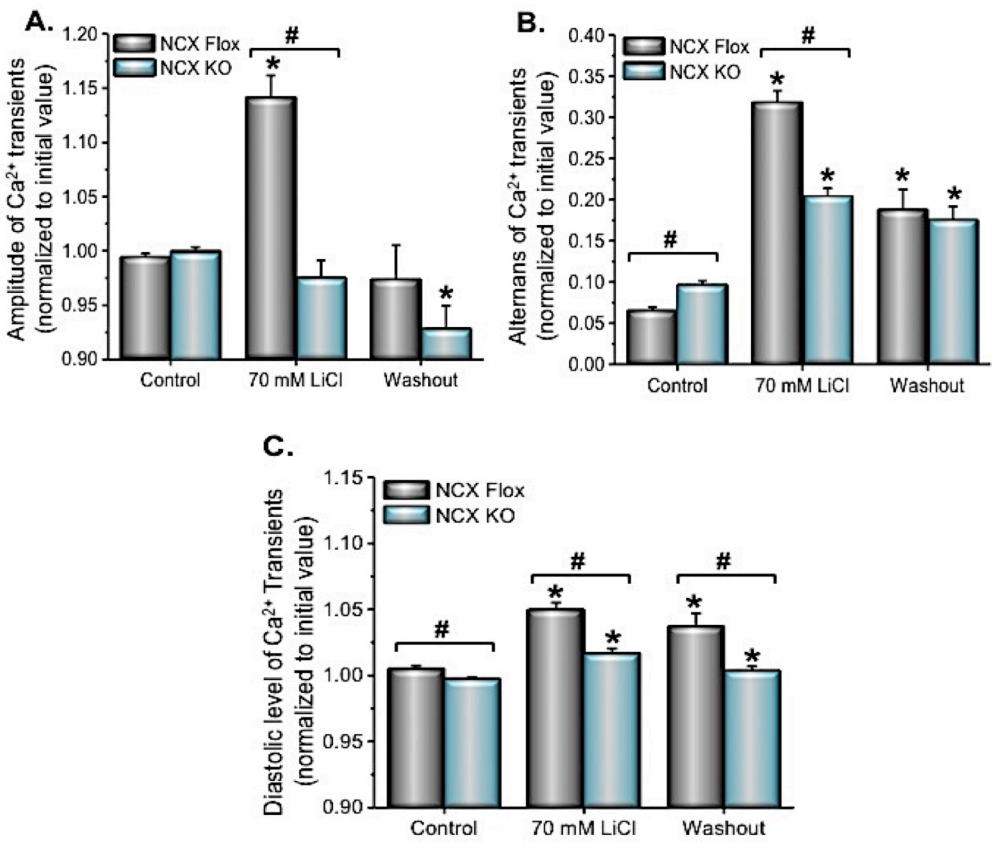

Figure 6.5 Effect of Li-treatment at 10 Hz and 37°C using rhod-2 AM in NCX Flox and NCX KO hearts. Corresponding changes in the Ca^{2+} transient amplitude (A), Ca^{2+} alternans as extracellular solution is replaced (B) and baseline recordings of Ca^{2+} transients to determine the resting diastolic levels (C). Comparison of the diastolic levels of rhod-2 fluorescence prior to, during perfusion of 70mM Na-Li Tyrode, and washout of Li^+ from extracellular solution. Changes in fluorescence was corrected for bleaching and normalized to initial level prior to application of LiCl. The data represent means ± SE (N= 4, per genotype) * p < 0.05 when compared to their own controls; # p < 0.05 when comparing genotypes.

As 70 mM Na-Li Tyrode was perfused, there was an observed augmentation of Ca-Alt in NCX Flox hearts (Figure 6.4, top panel). Attenuation of Ca-Alt occurred as Li^+ was washed from the extracellular solutions, relieving NCX1 impairment (Figure 6.4, top far right). Interestingly there were no visible changes in NCX KO Ca-Alt at 10 Hz as 50 % of Li^+ was replaced in the extracellular solutions (Figure 6.4, bottom mid-panel). Ca^{2+} transient amplitudes and Ca-Alt were also recorded as extracellular solution was exchanged in both genotypes (Figure 6.5 A, B). As Li^+ impairs NCX1, the clearance of cytosolic Ca^{2+} is limited by the hydrolysis of the ATP driven SERCA2a pump that replenishes Ca^{2+} stores. Insufficient transport activity of SERCA2a to replenish the SR Ca^{2+} could result in alterations in Ca^{2+} release when NCX1 is impaired (Figure 6.5B).

Data collected as NCX1 activity was challenged in both genotypes are represented in Figure 6.5.

As anticipated, Ca^{2+} transient amplitudes were increased in WT hearts (p-value < 0.01), whereas KO hearts presented a non-significant decrease in transient amplitude (p-value 0.15; Figure 6.5, A). As expected, the application of Li^{+} triggered Ca-Alt significantly higher in NCX Flox than in NCX KO mice (p-value < 0.05; Figure 6.5, B). A representation of how Ca-Alts were calculated is shown in Figure 6.4 (where Amax is the maximum amplitude, Amin is amplitude of the second smaller release). As Amin decrease there is an increase in the alternans, aside from the increase in Amax seen in WT hearts as Na-Li Tyrode was applied. The augmentation of Ca-Alt represented by a smaller concurrent release, supports the idea that there is an increase in the resting Ca^{2+} diastolic levels. This holds true for both genotypes with perfusion with Na-Li Tyrode, as shown in Figure 6.5 C. As 70 mM LiCl was perfused, cytosolic Ca^{2+} diastolic levels increased in both WT and KO hearts (Figure 6.5 C, p-value < 0.01). Although more prominent in WT epicardial myocytes, there is a significance difference of KO epicardial myocytes to control levels (p-value < 0.01). Ca^{2+}-overload in the dyadic cleft in NCX KO cardiomyocytes is already expected to occur without additional perfusion of Na-Li Tyrode, thus Ca-Alt are significant higher in NCX KO hearts than in NCX Flox hearts at 10 Hz (Figure 6.5 B p-value < 0.01).

Since Ca-Alts appeared at the normal heart rate under control conditions, experiments to test heart rate dependency of intracellular Ca^{2+} dynamics were conducted in NCX Flox mice that were not littermates of NCX KO mice to avoid presence of Cre activity in WT controls. Normally mice present a stereotypical frequency dependency behavior termed “negative-staircase” in intracellular Ca^{2+} as the heart rate increases (Figure 6.6, A). In short, there is a decrease in Ca^{2+} amplitude, thus producing less alternans at higher frequencies. Incidentally when the extrusion of cytosolic Ca^{2+} by the exchanger is either impaired or ablated, there are changes in the intracellular Ca^{2+} dynamics that attenuates the second release of Ca^{2+} from the SR (Figure 6.4-6.5B). RyR2 have complex regulatory mechanisms that contribute to the opening and closing of this channel. For instance, in Chapter 3 (Figure 3.4) when 105 mM Na-Li Tyrode was perfused in WT hearts, there was a decrease in the Ca^{2+} amplitude compared to 70 mM Na-Li Tyrode.

We indicated there that this could be related to cytosolic Ca^{2+}-regulation of the RyR2, increasing Ca^{2+} dependent inactivation due to excessive Ca^{2+}-levels present in the cytosol. However, in a recent paper from our Laboratory (Kornyeyev, Petrosky et al. 2011) we demonstrate that both the negative-staircase behavior and Ca-Alt were generated within the SR due to the Ca^{2+} dependent RyR2-CSQ2 interaction. The negative-staircase behavior and Ca-Alt can be observed in both genotypes in Figure 6.6A-B. These experiments were conducted in NCX Flox and NCX KO under control conditions, measuring the frequency dependency of intracellular Ca^{2+} handling. Presumably, NCX KO hearts present this negative-staircase similar as WT hearts (Figure 6.6 A-B). However, Ca-Alts appear much earlier in NCX KO hearts and begin to taper in alterations around the normal heart rate (10 Hz) (Figure 6.6 C). This is expected to occur earlier in these hearts because the lack of NCX1 prompts a higher Ca^{2+}-load due to the inability to extrude Ca^{2+} out of the cell; however only at 9 Hz were there significant differences in Ca-Alts between genotypes (Figure 6.6 C p-value < 0.05).

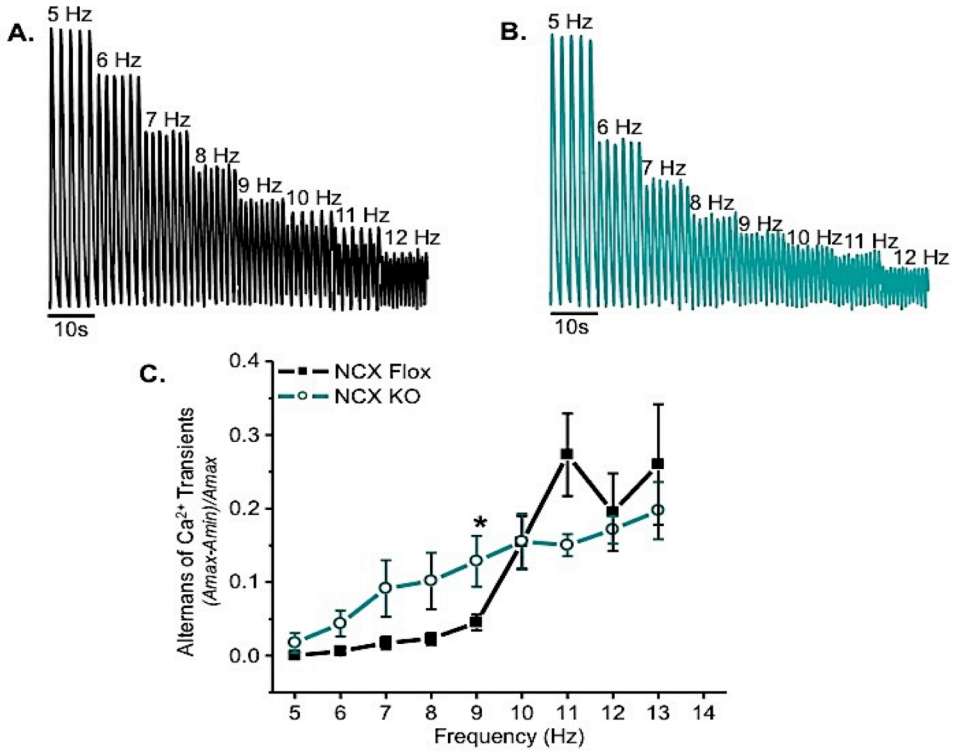

Figure 6.6 Heart rate dependency of Ca^{2+} transients (using rhod-2) on epicardial layer of the left ventricle of NCX Flox and NCX KO hearts, at 37°C. Ca^{2+} transients illustrating a negative staircase as the frequency was increased from 5 Hz to 12 Hz; NCX Flox (A) and NCX KO (B). Data collected in the lower graph (C) compares Ca-Alt in NCX Flox (filled symbols) and NCX KO (open symbols) hearts. Data represents means ± SE (N=5, respectively) * $p < 0.05$ when comparing genotypes.

Role of NCX1 in the Electrocardiographic Properties of a mouse heart

Until now I have shown that impairment of the basic Ca^{2+}-extrusion mechanism (NCX1) not only alters intracellular Ca^{2+}-dynamics (Chapter 3), but also modifies the repolarization of the membrane potential (Chapter 4). Chapter 5 focused on the use of a cardiac-specific NCX KO mouse to provide us with sufficient experimental data to supported the hypothesis that ***NCX1 regulates the repolarization of mouse epicardial ventricular APs***.

If these events occur at the epicardium, then it is expected that there will also be changes in the endocardial AP. In order to further evaluate the relationship between NCX1 and AP propagation from the endocardium to the epicardium, simultaneous recordings were conducted to measure the transmural electrical gradient (via ECG) of the left ventricle and AP microelectrode recordings from the epicardial layer of the left ventricle of both NCX Flox and NCX KO mouse hearts.

***6.3** Does the lack of cardiac-specific NCX1 alter the ECG properties of the heart?*

Figure 6.7 illustrates ECG recordings from the left ventricle of NCX Flox (black lines) and KO (light blue lines) hearts. Both genotypes retain distinctive Q-R-S waveforms. This Q-R-S complex is generated by the delay AP depolarization (phase 0) of the epicardium respect to the endocardium. Additionally, mouse AP display a small "J-wave" generated by the fast epicardial repolarization during phase 1. In NCX Flox hearts the appearance of a J-wave is more apparent when the stimulus is turned off and natural pacemaker activity controls the heart rate. A positive T-wave formation is the representation of the difference in the late-repolarization of the epicardial layer followed by the repolarization of the endocardial layer. Since NCX KO hearts present a dramatic reduction in phase 2 in the epicardium, T-wave formation appears to be mostly abolished at 5 Hz (Figure 6.7, right). The reduction in the T-wave could be associated with two factors. First, the AP not only repolarizes faster in the epicardium but in the endocardium as well. Second, the epicardium and endocardium AP must repolarize mostly at the same. To test if NCX KO hearts present a negative T-wave at higher heart rates, the frequency was gradually increased and observed (Figure 6.8).

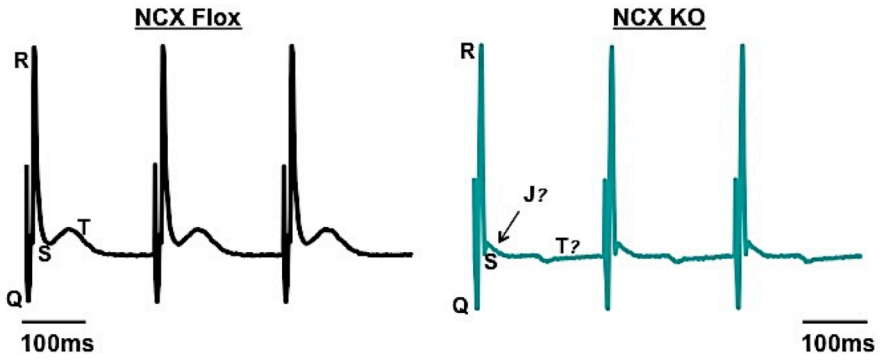

Figure 6.7 Typical ECG recordings of NCX Flox (left) and NCX KO (right) measured via Ag-AgCl pellet within left ventricle at 5 Hz and 37°C.

Interestingly, as the heart rates T-wave also disappeared in NCX KO hearts (Figure 6.8, light blue lines). Modifications in AP repolarization are expected alter T-wave morphology, thus as the heart rate increased the appearance of T-wave alternans (TW-Alt) occurred in NCX Flox hearts (Figure 6.8, black lines). On the other hand, the lack of NCX1 lessens the duration of the ventricular AP thereby eliminating the production of TW-Alt (Figure 6.8, blue lines).

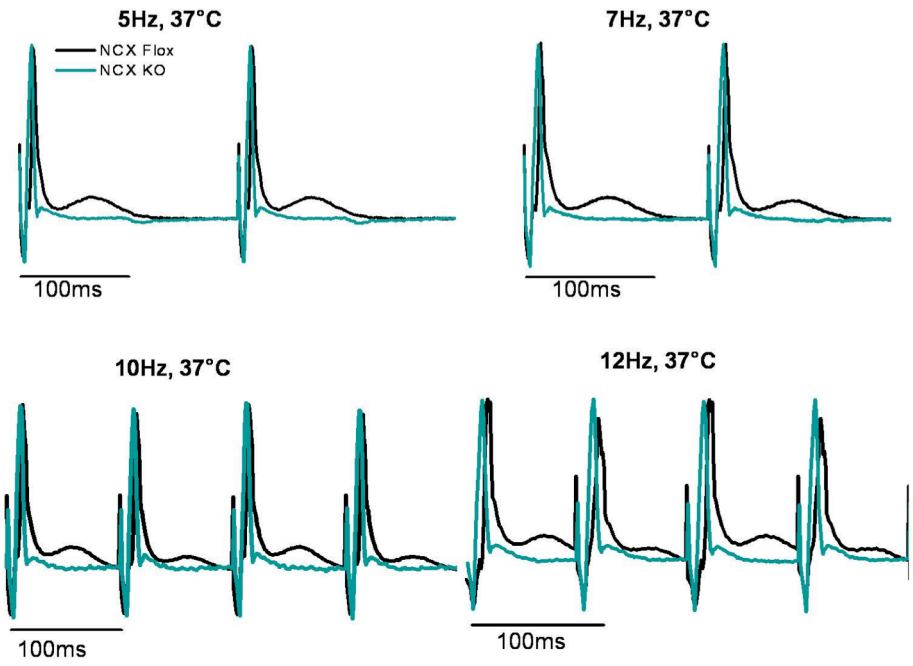

Figure 6.8 Heart rate dependency of T-wave formation of the electrocardiogram from NCX Flox (black lines) and NCX KO (light blue lines). ECG recordings were obtained via Ag-AgCl pellet inserted via mitral valve of the left ventricle as the frequency was increased from 5 Hz to 12 Hz, at 37°C. Typical trace examples are superimposed at 5 Hz (top left), 7 Hz (top right), 10 Hz (bottom left) and at 12 Hz (bottom right).

The frequency dependency of the heart has been well documented to modify intracellular Ca^{2+}-dynamics, APD, as well as altered T-wave formation in ECGs (Verrier, Kumar et al. 2009; Cutler, Jeyaraj et al. 2011). Unfortunately, the link between these events is not fully understood [48]. Nevertheless, the late-repolarization phase of ventricular APs is responsible for the production of the T-wave in ECG recordings. Hence, an increased heart rate would produce a shortening in the APD (Figure 6.9, A-B). Shorter durations in APs could lead to the genesis of AP-Alt. To test if the lack of NCX1 activity would modify AP-Alt, APD at 90% repolarization was measured for more reliable comparison to NCX KO mice (Figure 6.9, A). It is expected that since NCX KO hearts already present a shorter APD and a decreased phase 2, the appearance of AP-Alt would be less than that found in NCX Flox hearts. Measurements collected at APD90 present AP-Alts to be more prominent in NCX Flox mice (Figure 6.9, C). At 10 Hz, not significant small AP-Alts (p-value 0.29) appear in both genotypes. Once the frequency increased to 11 Hz, augmentation of AP-Alt prevailed in NCX Flox hearts, whereas AP-Alts in NCX KO hearts were significantly less (p-value < 0.01) than in NCX Flox. This was true as well for APs recorded at 12 Hz (p-value < 0.05). Unfortunately recordings at higher hearts rate were difficult to maintain, therefore AP-Alt recorded at 13 Hz was only collected from three hearts and considered not significant compared to NCX Flox hearts (p-value 0.13; N=3 per genotype). Data collected at 14 Hz (Flox, N = 2; KO N = 3) show

the trend that increases in the frequency would eventually lead to less AP-Alt in both genotypes, therefore not significant (p-value 0.24).

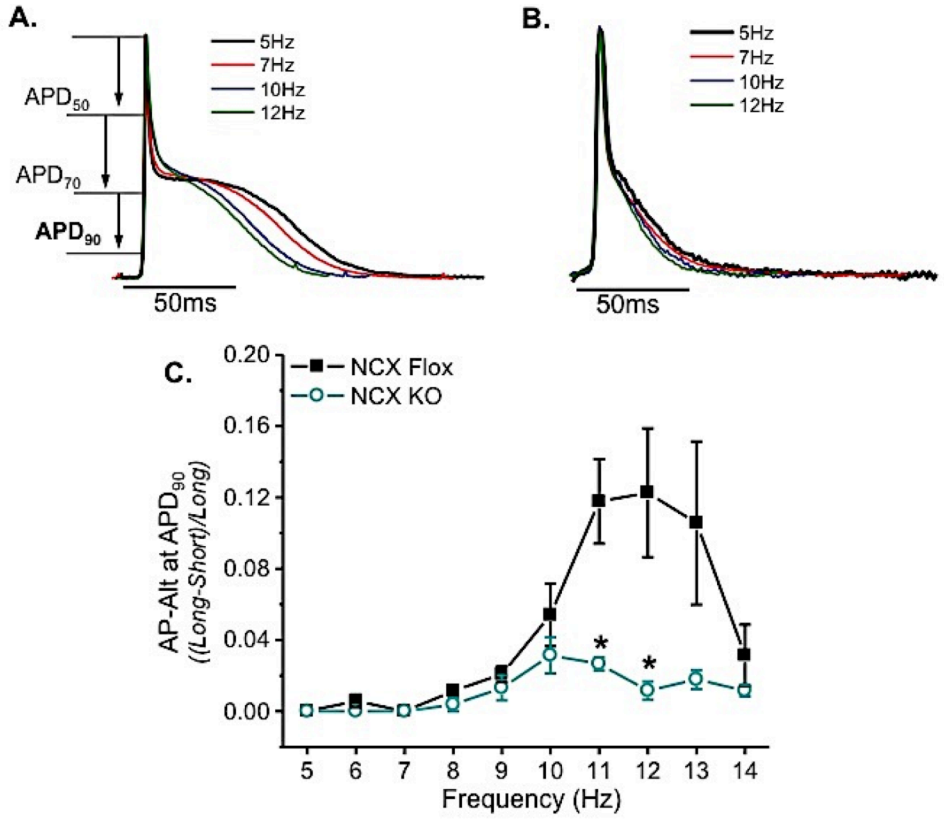

Figure 6.9 Heart rate dependency of AP on the epicardial layer of the left ventricular at 37°C via microelectrode impalement, in NCX Flox and NCX KO hearts. Superimposed AP traces as the frequency was increased from 5 Hz to 14 Hz; NCX Flox (A) and NCX KO (B). NCX Flox illustrates different AP duration measurements. APD 90 was used to represent the shortening of phase 2 as the heart rate was increased. AP alternans were plotted in respect to the frequency in the lower graph (C); NCX Flox (filled symbols) and NCX KO (open symbols). Data represents means ± SE (N=5, respectively) * p < 0.05 when comparing genotypes.

In mouse epicardial myocytes, we have shown that NCX1 is activated during the late-depolarization phase of an AP to extrude Ca^{2+}. Hence, the impairment of NCX1 produced an augmentation of cytosolic free [Ca^{2+}] (Figure 6.5 C), induced Ca-Alt at lower heart rates (Figures 6.6 C) and in NCX Flox hearts, an increase in the Ca^{2+}-transient amplitude (Figures 6.5 A). Altogether, these results indicate that activation of NCX1 may be involved in the genesis of arrhythmias. However, the ablation of NCX1 significantly reduced the likelihood of developing AP-Alt (Figures 6.9 C). On the other hand, the development of Ca-Alts occurred earlier in NCX KO hearts (at 10 Hz) and was less prominent than NCX Flox hearts when perfused with Na-Li Tyrode (Figure 6.5 B). The induction of Ca-Alts were seen under normal conditions as the frequency increased in both genotypes (Figure 6.6, C). It is clear that NCX KO hearts show beat-to-beat alterations in their cytosolic Ca^{2+} transients at lower frequencies than WT hearts (Figure

6.6, C). Since these experiments were conducted simultaneously, a comparison of Ca-Alt and AP-Alt of each genotype was graphed and is presented in Figure 6.10.

On the left ventricle epicardial layer, NCX Flox hearts present Ca-Alts and AP-Alt simultaneously (Figure 6.10 A). Ca-Alt became more prominent as the frequency increases, being significantly different at 10 Hz (p-value < 0.05), 11 Hz (p-value < 0.05) and 14 Hz (p-value < 0.01; N = 2). This is also translated across the ventricular wall inducing TW-Alts (Figure 6.8, black lines). However, NCX KO hearts significantly augment Ca-Alt without executing AP-Alt (Figure 6.10 B), therefore there is a lack of TW-Alts (Figure 6.8 blue lines).

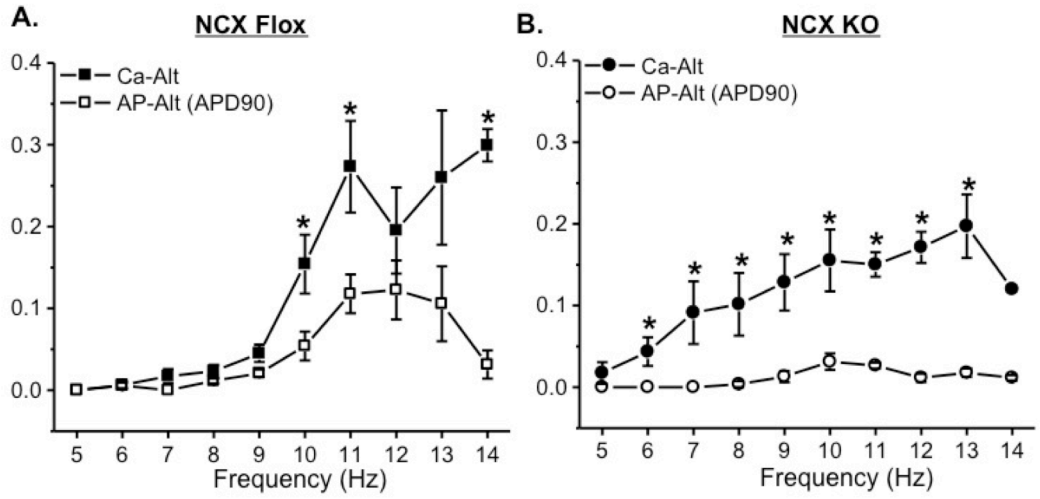

Figure 6.10 Heart rate dependency of AP-Alt at APD90 (open symbols) and Ca-Alt (filled symbols) of NCX Flox (A) and NCX KO (B). Data obtained as the heart rate was increased from 5 Hz to 14 Hz. Data represents means ± SE (N=5, respectively) * p < 0.05 when comparing genotypes.

Experiments presented in this chapter, demonstrate that the ablation of NCX1 defines the Li^+ sensitivity of Ca^{2+} transients. Furthermore, in the absence of NCX1, Li^+ cannot induce Ca-Alt. Additionally, NCX KO do not present T-waves in the ECG recordings due to both a faster repolarization of AP and a lower transmural gradient of AP repolarization in these KO mice. Finally, in the absence of NCX, Ca-Alt cannot be transduced either in AP-Alt or TW-Alt.

CHAPTER 7 *: Discussion*

Role of NCX1 in Epicardial Intracellular Ca^{2+} Dynamics

One of the central aspects of this thesis work has been the evaluation of the role of the sarcolemma NCX1 in an intact mouse heart at body temperature (37°C). This was performed in hearts that were extra-corporeally preserved on a horizontal Langendorff perfusion set-up (i.e. PLFFM). The ability to perfuse the heart with ionic solutions that mimics blood, to keep the heart viable outside of its host environment, provided the opportunity to measure cellular and subcellular events occurring at the whole heart level. Perfusion with different fluorescent indicators, such as rhod-2 and mag-fluo4, allowed us to perform measurements of the intracellular Ca^{2+} dynamics at the epicardial layer of the left ventricle. The perfusion of Tyrode solutions containing the equimolar replacement of Na^+ by Li^+ has served throughout this dissertation as a way to evaluate the fractional contribution of the NCX1 exchanger.

Fractional replacement of Na^+ by Li^+ in the perfused Tyrode solution impaired the transport of cytosolic Ca^{2+} out of the cell via NCX1. Measurements of the cytosolic free Ca^{2+} levels via rhod-2 fluorescence when NCX1's turnover rate was reduced, clearly indicated augmentations in the resting diastolic levels (Figure 3.2), SR-Ca^{2+} release (Figure 3.5), and promoted kinetic differences in the recovery of Ca^{2+} by the SR (Figure 3.6 B). However intracellular Ca^{2+} dynamics does not rely solely on the extrusion of cytosolic Ca^{2+} from the cell, but also on other intracellular organelles that are essential for Ca^{2+} regulation (i.e. SR). Thus, a complementary way to evaluate the role of NCX1 in intracellular Ca^{2+} dynamics was to evaluate the impairment of NCX1 when other known Ca^{2+} transport proteins were pharmacologically blocked.

7.1 NCX1 regulates intracellular Ca^{2+} dynamics even in absence of SR Ca^{2+} release

The sarcolemma NCX1 protein becomes highly active when there is an increase if free Ca^{2+} concentration in the cytosol of the Cell. During the cardiac cycle this situation is mostly achieved during the CICR process to extrude cytosolic Ca^{2+} from the cell. As Ca^{2+} is released from the SR, it will bind to the intracellular binding domain of NCX1 activating the translocation of 3 extracellular Na^+ for 1 intracellular Ca^{2+}.

Interestingly, although Li^+ is electrochemically equivalent to Na^+, it cannot be translocated through the exchanger due to smaller ionic radii (Mahler and Persson, 2012). When Li^+ was used to impair NCX1, cytoplasmic Ca^{2+} levels were increased and produced augmentation of the release of Ca^{2+} from the SR (Figure 3.2 and Figure 3.5, respectively). These results are similar to those obtained by Baker et al (1969) when they first observed that LiCl perfusion increased intracellular Ca^{2+} levels (Baker, Blaustein et al. 1969). More recent studies using rabbit cardiomyocytes also observed increases in the SR-Ca^{2+} release upon Na-Li Tyrode replacement solutions (Litwin, Li et al. 1998).

With the aim of differentiate if the effect of Li^+ effect was on the Ca^{2+} influx through the plasma membrane or by increasing the SR Ca^{2+} release, we performed experiments to block Ca^{2+} release from the SR. This was accomplished by the use of a pharmacological strategy to block Ca^{2+} release and Ca^{2+} uptake with a combination of Ry and Tg.

Ry, a plant alkaloid, is commonly used in Ca^{2+} signaling experiments to lock the RyR2 in a sub-conductance state (Mitchell, Powell et al. 1984) and at concentrations

higher than 10 time the dissociation constant, to block RyR2. Tg is a plant-derived sesquiterpene lactone with an extremely high affinity and specificity for SERCA2a (Lytton, Westlin et al. 1991; Young, Xu et al. 2001; Toyoshima and Nomura 2002). Small concentrations of this particular drug were needed to efficiently inhibit the conformational change of the enzyme, preventing Ca^{2+} re-entry into the SR (Toyoshima and Nomura 2002). The concentrations used throughout this dissertation were designed specifically to reduce the SR-Ca^{2+} release and prevent further uptake from the SERCA2a pump. Once the hearts were perfused with a combination of these drugs, the rhod-2 Ca^{2+} transient signal decreased (Figure 4.7B). This is concurrent with previously published literature using these drugs (Litwin, Li et al. 1998; Nemec, Kim et al. 2010; Kornyeyev, Petrosky et al. 2011; Escobar, Perez et al. 2012; Ferreiro, Petrosky et al. 2012).

The elimination of SR Ca^{2+}-release, via Ry+Tg, produced a decrease in the systolic Ca^{2+} that will finally lead to a reduction in the NCX forward mode activity. However the impairment of NCX1, even in the absence of SR Ca^{2+}-release, produced significant changes in the intracellular Ca^{2+} levels and amplitude of cytosolic Ca^{2+} transients (Figure 3.3 and Figure 3.7, respectively).

This decrease in Ca^{2+} transient amplitude suggests that the SR-Ca^{2+} signaling was eliminated and the application of 70 mM Na-Li Tyrode could be implemented to evaluate the contribution of NCX1 to extrude cytosolic Ca^{2+}. Upon the perfusion of 70 mM Na-Li Tyrode there not only was a significant increase in the resting diastolic levels (Figure 3.3), but also a reduction the Ca^{2+} transient amplitudes (Figure 3.7). The fact that the cytosolic Ca^{2+} diastolic levels previously increased when Na-Li Tyrode solutions were used under normal conditions (Figure 3.2) and when SR-Ca^{2+} release was eliminated (Figure 3.3), indicates that NCX1 impairment was responsible for these changes and functions independent from SR-Ca^{2+} release. A similar proposal was introduced by Janiak et al (1996) when they perfused cardiomyocytes with Ni^{2+} to block NCX1 reverse-mode after depletion of the SR via Ry+Tg (Janiak, Lewartowski et al. 1996). Collectively, these results suggest that NCX1 was acting in the forward-mode prior to impairment. On the other hand, the reduced Ca^{2+} transient amplitude produced when Ry+Tg was applied is a representation of the Ca^{2+}-influx through the LTCC (Figure 3.7A, navy blue trace). Some studies have shown that additional Ca^{2+}-entry through the LTCC can assist in the increase SR load that finally will promote an increase in the SR Ca^{2+} release (Linz and Meyer 1998; Piacentino, Gaughan et al. 2002). However Figure 3.7 clearly indicates that no additional Ca^{2+}-entry occurred in the presence of 70 mM LiCl, but a reduction in the Ca^{2+} released from the SR. This data eliminates the possibility that previously shown increases in the cytosolic Ca^{2+} amplitude (Figure 3.5A) were due to an additional Ca^{2+}-influx through the LTCC.

On the other hand, NCX1 is reversible in the sense that it can induce a Ca^{2+} influx when the cytosolic Na^{+} levels are increased. This electro-difusive behavior is thought to occur immediately after Na^{+}-channels open at the initiation (phase 0) of an AP (Larbig, Torres et al. 2010) or induced by pharmacological application of Digitoxin (i.e. Ouabain) to block the Na^{+}/K^{+}-ATPase and induce CICR (Bolck, Munch et al. 2004). Experiments conducted using equimolar replacements of Na^{+} by Li^{+} will impair the exchanger but not the influx through voltage dependent Na^{+} channels (NaV 1.5). The absence of selectivity, between Na^{+} and Li^{+}, in the Na + channel reflect the inability of Aspartic, Glutamic, Lysine and Alanine motive in the channel selectivity to discriminate between this monovalent caions. the As a consequence, Na^{+}-influx through Na-channels when an AP is elicited is also accompanied by a Li^{+}-influx that can potentially accumulate in the cytosol when Na-Li Tyrode is perfused in the heart. Li^{+} cannot

permeate through the NCX1 or be pumped out through the Na/K-ATPase; however since only 50% of extracellular Na^+ was replaced by Li^+, the accumulation of Li^+ in the cytosol can permit the extrusion of cytosolic Na^+ and consequently introduce a Ca^{2+}-influx in the unimpaired NCX1. This concept was evaluated in several experiments throughout this dissertation to verify that forward-mode was the favored conformation of NCX1. For instance, when perfused with Na-Li Tyrode to impair NCX1 after SR-Ca^{2+} release was eliminated produced a decrease in Ca^{2+} transient amplitude (Figure 3.7). The fact that there was a decrease in amplitude and not an increase favors the idea that NCX1 was not functioning in the reverse-mode to increase previous Ca^{2+} transient amplitudes when SR proteins were intact (Figure 3.4-3.5A). This is consistent with analysis of NCX reverse-mode activity in single guinea pig ventricular myocytes, where they found that Ca-entry was four-times less likely to come from NCX1 than LTCC for CICR and that the amplitude of release is primarily from the SR (Sipido, Maes et al. 1997)

7.2 Intra-SR Ca^{2+} dynamics is modified when NCX1 is impaired

Unfortunately the use of fluorescent dyes in the whole-heart does not provide information on the exact concentration or the source of the Ca^{2+} fluxes. In contrast, what can be derived from Ca^{2+}-fluorescence is the degree of change and kinetic variations of the cytosolic Ca^{2+} transients. However, cytosolic Ca^{2+} recordings are indirect recordings of the intra-SR Ca^{2+} dynamics. Direct recordings of intra-SR Ca^{2+} dynamics were obtained using the fluorescent indicator mag-fluo4. Simple replacement of 70 mM Na-Li Tyrode in hearts loaded with mag-fluo4 revealed similar increases in resting free Ca^{2+} and magnitude of release from within the SR (Figure 3.8-3.9) as illustrated in rhod-2 recordings from the cytosol (Figure 3.2-3.5A). Interestingly, the Ca^{2+}-transient kinetics differed between cytosolic and intra-SR recordings. Previously published data from our laboratory showed that kinetic differences in cytosolic and intra-SR Ca^{2+}-transients were highly dependent on the luminal Ca^{2+} levels and can be influenced by cytosolic buffering (Kornyeyev, Reyes et al. 2010). The downward slope of cytosolic transients indicates the removal of Ca^{2+} by SERCA2a and NCX1 (i.e. relaxation phase). When NCX1 was impaired, there were discrepancies between the different concentrations of Na-Li Tyrode. We speculated that the increases in Ca^{2+} diastolic levels could initiate for the SERCA2a to pump faster, however this was only represented with 35 mM Na-Li was applied and was not significant (Figure 3.6C). Only when 105 mM LiCl was perfused the decay time was significant, but these results showed a slowing of the pump activity, not an acceleration (Figure 3.6C insert). The controversy between these results indicated a possible luminal regulation on the SERCA2a. Once intra-SR Ca^{2+} levels were elevated (Figure 3.8) there is an inhibitory regulatory mechanism on the luminal side of SERCA2a to halt Ca^{2+}-entry thereby slowing the up-take of cytosolic Ca^{2+}. Evaluation of the intra-SR Ca^{2+} kinetics revealed no significant differences in the ability to replenish the SR-Ca^{2+} although these results did suggest a small acceleration (Figure 3.10). Within the SR there are many luminal proteins associated with the RyR2 channel such as calsequestrin (CSQ2), triadin and junctin (Zhang, Kelley et al. 1997). CSQ2 is a low affinity-high capacity Ca^{2+} binding protein that sequesters intra-SR Ca^{2+} (Ca^{2+}-bound) to allow room for additional free Ca^{2+} (Gyorke and Carnes 2008) (Gyorke and Terentyev 2008) (Terentyev, Viatchenko-Karpinski et al. 2002; Szentesi, Pignier et al. 2004; Qin, Porta et al. 2005; Knollmann, Chopra et al. 2006; Kornyeyev, Petrosky et al. 2011). As Ca^{2+} is pumped into the SR, it binds to CSQ2. Only the free (un-bound) Ca^{2+} is released from

the SR into the cytosol when RyR2s open. The luminal regulation of CSQ2 on the RyR2 is widely studied in its correlation with the human pathology CPVT.

7.3 NCX1 and Excitation-Contraction Coupling

When CSQ2 is knocked-out (KO), large amounts of free Ca^{2+} ions are readily available to be released out of the RyR2 (Knollmann, Chopra et al. 2006). However the duration of cytosolic Ca^{2+}-release and reuptake appears to be similar when compared to their WT hearts (Petrosky, Zepeda et al. 2012) (Knollmann, Chopra et al. 2006; Kornyeyev, Petrosky et al. 2011). Recently we investigated the regulatory properties of RyR2 activation in this transgenic mouse model and revealed that CSQ2 is not only a buffering protein, but also participates as a luminal sensor for the RyR2 (Kornyeyev, Petrosky et al. 2011). This was prominent in restitution curves of CSQ2 KO hearts when compared to WT hearts. The lack of CSQ2 in the SR allowed for more Ca^{2+} free ions to be readily available to be expelled by RyR2 when a second pulse is introduced (Kornyeyev, Petrosky et al. 2011).

The time intervals between Ca^{2+}- releases were also evaluated in terms of the fractional recovery of Ca^{2+}-release, to determine SR-Ca^{2+} regulation when NCX1 was impaired (Figure 3.15). The SR can store large amounts of Ca^{2+} so that when triggered, the RyR2s can spew a large quantity of Ca^{2+} ions to activate the myofilaments resulting in a mechanical response, contraction (Fabiato 1992). The refractoriness of Ca^{2+} release determines the efficiency of the SR to release free Ca^{2+} into the cytosol. In order for free Ca^{2+} to be available; the SERCA2a has to be efficient in restoring the Ca^{2+} reservoir. The fractional recovery of Ca^{2+}-release was slower when NCX1 was impaired (Figure 3.15). This is expected since the duration of cytosolic Ca^{2+} transients at 50% recovery was longer when extracellular Li^{+} was increased (Figure 3.6B). The longer duration to reach 50% recovery is directly correlated to the time to peak of the Ca^{2+} transients being longer when Na-Li Tyrode was perfused (Figure 3.5B). The longer time to peak indicates a longer time for the RyR2 channels to be open thus, if as extra-systolic pulses were introduced, the ability to release additional free Ca^{2+} from the SR lessens the closer the second pulse (S2) is to the initial pulse (S1; Figure 3.15A). In CSQ KO hearts, intra-SR Ca^{2+} recordings (mag-fluo4) revealed that the time to reach 50% recovery was accelerated when compared to CSQ WT hearts (Kornyeyev, Petrosky et al. 2011). This acceleration in SERCA2a could suggest the lack of luminal regulation of CSQ2 on SERCA2a. On the other hand, restitution curves illustrated larger releases of Ca^{2+} when a second pulse was initiated suggesting a faster depletion of intra-SR Ca^{2+} stores (Kornyeyev, Petrosky et al. 2011), which can also be related to the enhanced rate of uptake and luminal regulation of CSQ2 on the RyR2. Since the mice used in this dissertation retained normal levels of CSQ2 in their SR (WT), then it is possible that luminal regulation of RyR2 to expel Ca^{2+} is limited by the dissociate rate of Ca^{2+} binding and unbinding from CSQ2 as Ca^{2+} is taken up by SERCA2a and readily available for when RyR2s open. A more likely scenario is that the impairment of NCX1 augments luminal free Ca^{2+} levels, which increases both the Ca^{2+} driving force and the opening time of RyR2. Therefore, a larger initial release of Ca^{2+} from the SR would deplete the free Ca^{2+} levels with the first pulse and limit the readily available free Ca^{2+} during the second elicited release. Intra-SR Ca^{2+} kinetics obtained when 70 mM Na-Li Tyrode was applied in WT hearts revealed no significant differences in the rate to 50% recovery or decay time, suggesting that the SERCA2a was efficient at pumping Ca^{2+} into the SR (Figure 3.10). If SERCA2a is not responsible for these kinetic changes observed in the

cytosolic Ca^{2+} transients when NCX1 was impaired, then the cytosolic and luminal regulation of the RyR2 channel may impose constraints on the regulation of intracellular Ca^{2+} dynamics.

At a lower heart rate (bradycardia), we were able to demonstrate that the inotropic consequences of fractional impairment of NCX1. The role of NCX1 to extrude cytosolic Ca^{2+} has revealed drier importance due to the direct consequences on the SR Ca^{2+} load that resulted in prominent increases in the Ca^{2+} release from this organelle when extracellular Li^{+} was fractionally substituted for Na^{+}. The cytosolic and luminal regulation of the RyR2 has also shown to be altered as a result of fractional NCX1 impairment; therefore when the heart rate was increased, the limitations on intracellular Ca^{2+} dynamics were amplified (Figure 3.11-3.14; normocardic and tachycardic conditions, respectively). Although under bradycardic conditions the reduction in NCX1's extrusion rate induced Ca^{2+} overload, the biphasic behavior of Ca-Alts was not inducible. As previously illustrated, the lack of cytosolic Ca^{2+} extrusion by NCX1 not only increased resting Ca^{2+} levels but also increased the timing of the RyR2 to be open during the first SR-Ca^{2+} release during restitution (S1; Figure 3.15A). Thus the ability for SERCA2a to sufficiently uptake cytosolic Ca^{2+} and have free Ca^{2+} ions available prior to the extra-systolic pulse, led to smaller Ca^{2+} transient amplitude during the second release (S2; Figure 3.15A). With less time between pulses, resulted in a prolonged refractoriness of Ca^{2+}-release (Figure 3.15B). Now, under normocardic (10 Hz) and tachycardic (14 Hz) conditions where the time between pulses is enviably shorter in duration, there is still an increase in initial Ca^{2+} transient amplitude (Amax) when Li^{+} impaired NCX1 (Figure 3.12A and 3.14A). Needless to say, the reduction in NCX1's rate to extrude cytosolic Ca^{2+}, in combination with increases in diastolic and intra-SR Ca^{2+} levels, lead to even less free Ca^{2+} ions available prior to the next stimulus (Amin; Figure 3.12B and 3.14B). Especially under tachycardic conditions, where fluctuations in Ca^{2+} transient amplitudes between pulses were already apparent (see Figure 3.13, far left traces), the augmentation of Ca-Alts was further induced when NCX1 was fractionally impaired by different extracellular Na-Li Tyrode solutions (Figure 3.14B). The fact that NCX1 impairment disrupts intracellular Ca^{2+} dynamics, it is then presumed that the membrane potential would also be disrupted. In other words, each time Ca^{2+} is released from the SR it was first prompted by the initiation of an AP, which consequently elicits the CICR process.

Role of NCX1 in Epicardial Electrical Signaling

As previously mentioned, APs were not always recorded with a predominant dome in mouse cardiomyocytes and with recent technological developments we now have the ability to record APs with the four distinct phases in both isolated cardiomyocytes and in Langendorff-perfused whole-hearts (Ferreiro, Petrosky et al. 2012). Currently the ability to record a clear spike-n-dome morphology in live mice are not yet made available; this could be partly due to their natural accelerated heart rate. In Langendorff-perfused mouse hearts, the separation of the organ from the host would detach the natural neuronal innervations that normally play a part in the regulation of the pacemaker activity. Once the Tyrode bath surrounding the heart reached 36-37°C, the heart will spontaneously beat at a higher rate (6-8 Hz). Ablations of SA and AV nodal cells at this time, assisted in the reduction of the heart's natural pacemaker activity that enabled us to pace the heart externally, as needed (see Chapter 2, section 2.4).

Because ablation only reduced the electrical conduction, the electrical coupling of the myocytes are still intact, thus, epicardial APs were recorded with clearly defined phases at lower frequencies (see Figure 1.4).

At a low pacing frequency (4 Hz), hearts perfused with the potentiometric dye (Di-8-ANEPPS) were recorded before and after perfusion with Na-Li Tyrode solutions; just as previously shown Ca^{2+}-dye perfused hearts. The time course of each ventricular AP is a representation of the exchange of ions across the plasma membrane. The initiation of an AP is primarily to elicit Ca^{2+} release from intracellular Ca^{2+}-stores (CICR) for myocardial contraction. In other words, each electrical stimulus will elicit myocardial contraction; thus the phenomena Excitation-Contraction Coupling (ECC). The additional perfusion of BBS minimizes the myocardial contraction, without disruption of the intracellular Ca^{2+} dynamics (Valverde, Kornyeyev et al., 2010), for clearer recordings with little to no movement artifact; therefore, changes in the intracellular Ca^{2+} dynamics as Na-Li Tyrode perfusion fractionally impaired NCX1 was anticipated to correspond to changes in the membrane potential.

7.4 NCX1 alters AP repolarization by modifying the late-depolarization phase

Under control conditions (0 mM LiCl), the morphology of the epicardial AP resembled a clear spike-n-dome behavior (Figure 4.1, black). Upon perfusion of any of the fractional Na^+ by Li^+ equimolar Tyrode solutions, the spike-n-dome characteristics attenuated (Figure 4.1). Despite the increases in the intracellular Ca^{2+} dynamics (Figure 3.2 and 3.8), the late-depolarization phase of the epicardial APs were less positive. Evaluation of the fractional contribution of NCX1 on the morphology of epicardial APs was accomplished by calculating the area under phase 0-1 (A1) and phase 2-3 (A2; Figure 4.2A). Bar graphs representing the contribution of phase 2 established that equimolar replacement of Na^+ by Li^+ significantly reduced the dome characteristic of the epicardial APs when more than half of the extracellular Na^+ was replaced with Li^+ (Figure 4.2B). These results are similar to those collected in guinea pig ventricular myocytes measuring a shortening in the APD and increases in SR-Ca^{2+} load during Li^+-perfusion (Spencer and Sham 2003). Hence the translocation of 1 Ca^{2+} out and 3 Na^+ into the cell would reduce the cationic influx across the plasma membrane, which in turn would result in a less depolarized plasma membrane during the plateau phase (phase 2) when CICR occurs.

Once again this electrogenic behavior of NCX1 is driven by an electrochemical gradient, not ATP-hydrolysis. With different intracellular binding sites for both Na^+ and Ca^{2+}, changes in the cytosolic concentration of either ion can drive the translocation of 3 Na^+ : 1 Ca^{2+}. In other words, NCX1 is a low-affinity-high-capacity protein that is sensitive to small changes in intracellular [Na^+] and [Ca^{2+}], therefore it can function in the forward and reverse-mode. In order to maintain Ca^{2+}-homeostasis during the CICR phenomena when large amounts of Ca^{2+} are spewed out of the SR and into the cytosol, NCX1 will favor the forward-mode to extrude excess intracellular Ca^{2+}. Whereas, the reverse-mode is thought to occur prior to the CICR process to extrude the intracellular Na^+ that entered the cell through the Na^+-channels during phase 0 of an AP. If in fact the reverse-mode does occur first, then there is an initial Ca^{2+} influx that could contribute to the beginning of the late-depolarization of the membrane. Incidentally, a Ca^{2+} influx would generate a cationic efflux that would repolarize the membrane not maintain depolarization.

The use of Li^+ to replace extracellular Na^+ was favored to fractionally impair NCX1 due to its ionic similarity to Na^+ allows Li^+ to bind to NCX1. Fractional Na-Li

Tyrode replacement suggests that when hearts were perfused with various equimolar Na-Li Tyrode solutions, some NCX1s will not be impaired and will function in either forward or reverse-mode. As a secondary active transporter, NCX1 is highly selective within its translocation pores, thereby prevents the translocation of Li^+. On the other hand, Li^+ can travel with extracellular Na^+ through Na^+-channels during phase 0. Since the intracellular binding sites to activate NCX1 differs from the translocation site for both Na^+ and Ca^{2+} ions, it is possible that increases in the intracellular [Li^+] could activate the reverse-mode of NCX1 to translocate intracellular Na^+ for extracellular Ca^{2+}. In this case, it is possible to have increases in intracellular Ca^{2+} levels and a faster repolarization that would correspond to a decrease in phase 2 of the AP. On the contrary, analysis of the APD at 50% repolarization in these Li^+-perfused hearts (Figure 4.3A) revealed that the reduced dome-like characteristic did not speed up the repolarization of the AP. In fact, when 75% of the extracellular Na^+ was replaced with equimolar Li^+, there was a significant increase in the duration of the AP (Figure 4.3A). Although the normalized rates of phase 0 significantly slowed down with increasing concentrations of Li^+, the relationship of NCX1 contribution in the late-repolarization phase remained in question. One possibility for a slower repolarization is the coupled activity of NCX1 and Na/K-ATPase in phase 3 of the epicardial AP. The inability of Na^+/K^+-ATPase to pump Li^+ out of the cell as the cytosolic [Li^+] : [Na^+] increased, suggests a decrease in the pump activity to pump K^+ into the cell consequently slowing the rate of repolarization. These discrepancies created by the use of Li^+ as a tool to impair NCX1 lead to two pharmacological experimental approaches to verify NCX1 mode of operation during the repolarization phase of epicardial APs.

7.5 Pharmacological treatment reveals that NCX1 functions in the forward-mode during the late-depolarization phase of epicardial APs

One experimental approach involves the use of pharmacological blockers specific for NCX1. If an accumulation of Li^+ in the cytosol (Li^+ entry via Na^+-channels) resulted either in NCX1 activation in the reverse-mode in the unimpaired NCX1 and/or a decrease in its coupled Na^+/K^+-ATPase activity, then perfusion with either the forward-mode or the reverse-mode NCX1 inhibitors (SEA0400 and KB-R7943, respectively) would significantly alter the repolarization of epicardial AP. As anticipated the perfusion of KB-R7943 and SEA0400 (in separate hearts) not only decreased the contribution of phase 2, but also decreased the duration of the epicardial AP at 50% repolarization that resulted in a faster AP repolarization (Figure 4.4). Studies revealed a lack of specificity when employing these NCX inhibitors in isolated tissue (Blaustein and Lederer 1999). Of particular interest was the LTCC that is found to be impaired when perfusion of KB-R7943 is applied to block NCX1 reverse-mode (Tanaka, Nishimaru et al. 2002; Tanaka, Namekata et al. 2005). Although SEA0400 has been reported to impair other channels as well, studies revealed that lower concentrations minimizes this contamination and therefore is more efficiently used to block NCX1 than KB-R7943 (Tanaka, Nishimaru et al. 2002; Tanaka, Namekata et al. 2005). Due to these allegations, experiments conducted in hearts loaded with rhod-2 were acquired to evaluate the effects of these drugs on the cytosolic Ca^{2+} transients (Figure 4.5 A-B).

Now upon perfusion with Na-Li Tyrode, increases in the intracellular Ca^{2+} diastolic levels and Ca^{2+} transient amplitude (Figure 3.2 and Figure 3.5A, respectively) were not translated to an increase in the late-depolarization phase (phase 2) of the epicardial APs (Figure 4.1). In fact the opposite occurred (Figure 4.2C), which supports

the hypothesis that NCX1 impairment would reduce the cationic influx across the plasma membrane that would normally maintain the dome-like characteristic of phase 2. This was verified by perfusion of NCX inhibitors that revealed a decrease in the contribution of phase 2 (Figure 4.4B). It was anticipated that a reduction in the late-depolarization phase, would shorten the duration of the AP. However in the Na-Li perfused hearts, the decrease in phase 2 did not induce a faster repolarization (Figure 4.3A). On the other hand, perfusion of either NCX1 inhibitor successfully shortened the APD at 50% repolarization as a result of a reduction in phase 2 (Figure 4.4C,B respectively). Moreover, hearts loaded with rhod-2 showed a significant increase in the Ca^{2+} transient amplitude upon perfusion of SEA0400 (Figure 4.5B), which also parallels to Li^{+}-treated hearts (Figure 3.5A). These results further support the idea that reduction of the NCX1 forward-mode activity is responsible for the increases the Ca^{2+} transient amplitude that correspond to the significant decrease in phase 2. In hearts perfused with the reverse-mode inhibitor (KB-R7943; Figure 4.5A), the lack in significant changes in the Ca^{2+} transient amplitude suggests that contamination to the LTCC is negligible (Figure 4.5C). However, this does not eliminate the possibility that NCX1 functions in the reverse-mode earlier in the CICR process.

Normally the upstroke of cytosolic Ca^{2+} transient indicates Ca^{2+} influx and the downward deflection resembles the Ca^{2+} efflux. Elongations in the Ca^{2+} transient kinetics (Figure 3.5B and Figure 3.6) suggested a longer opening of the RyR2 and a reduction in the extrusion rate of cytosolic Ca^{2+}, which could contribute to the slower repolarization measured at APD_{50} in Li^{+}-treated hearts. The use of NCX1 inhibitors revealed dissimilar results that imply that changes in the morphology of the AP repolarization were due to NCX1 reduced forward-mode activity and partially responsible for the changes in the intracellular Ca^{2+} dynamics. However these drugs do not fractionally impair the exchanger, instead they immobilize all exchanger activity. Thus the proposed explanation of the elongations in APD_{50} as a consequence of $[Li^{+}]$ accumulation to induce the activation of the NCX1 reverse-mode or impair the Na^{+}/K^{+}-ATPase activity during phase 2-3 could not be verified. Therefore an alternative pharmacological approach was investigated which included the perfusion of 50% equimolar Na-Li Tyrode.

Microelectrode recordings collected in hearts simultaneously recorded with rhod-2 and treated with Ry+Tg were analyzed in terms of the contribution of phase 2. Figure 4.7 illustrated simultaneous recordings of epicardial AP and Ca^{2+} transients before and after perfusion of Ry+Tg. As SR Ca^{2+}-release and reuptake was blocked, there was a decrease in the Ca^{2+} transient amplitude corresponding to a decrease in the contribution of phase 2 (Figure 4.7B and C, respectively); as previously seen (Mitchell, Powell et al. 1984; Ferreiro, Petrosky et al. 2012). If Li^{+} initially impairs and then activates the reverse-mode of NCX1, hearts pre-treated with Ry+Tg were expected to display an increase in Ca^{2+} transient amplitude and a faster repolarization upon Li^{+}-perfusion. Incidentally, perfusion of 50% Na-Li Tyrode significantly reduced the Ca^{2+} transient amplitude and increased the Ca^{2+} diastolic levels (Figure 3.7 and Figure 3.3, respectively), with no significant changes in the contribution of phase 2 (Figure 4.6). These results suggest that there is no additional Ca^{2+} influx through the LTCC in response to NCX1 reverse-mode activation even though there could be an accumulation of intracellular Li^{+}. It is then presumed that a reduction in NCX1 forward-mode activity will attenuate the repolarization phase by a reduced cationic influx (during phase 2) and consequently a shorter APD (during phase 3) of epicardial APs.

7.6 NCX1 impairment not only changes the APD but also the excitability of the heart

Structurally, mice have a higher density of t-tubules than other mammalian hearts, correlating to their natural heart rate of 500-600 beats per minute (Brette and Orchard 2003; Brette and Orchard 2007). The innate structure of mouse hearts, which contain a vast amount of transverse tubules (t-tubule), is primarily for the ion exchange required for their hearts to efficiently function; compared to larger animals (i.e. guinea pigs, canine, sheep, etc.) that have a slower heart rate and less t-tubular systems (Brette and Orchard 2003; Brette and Orchard 2007).

Therefore, although shorter than larger mammals, epicardial APs in mice have a longer refractory period at a lower frequency (4 Hz). The refractory period of an AP is determined by the time it takes for Na^+-channels to recover from inactivation. During the relative refractory period, elicited APs will be smaller and less pronounced (see Figure 1.12). To demonstrate the relative refractory period, the duration between systolic and extra-systolic pulses (S1 and S2, respectively) in terms of their maximum amplitude (A_{S2}/A_{S1}) was illustrated in the restitution curves generated before and after Li^+-perfusion (Figure 4.8).

Within the t-tubular systems of cardiomyocytes is a collection of transmembrane proteins specific for proper conduction of an AP and various secondary signaling pathways. The quantity and types of channels vary throughout the cardiac tissue and between species. Variations in t-tubular structure and channel location will modify the morphology of ventricular APs, not only between species but also between various cardiac pathophysiological conditions (i.e. heart failure). In any case, it has been shown that a slower heart rate results in a longer APD. The duration of an epicardial AP of a animal model is determined by several factors; the initial repolarization at phase 1, the second depolarization during phase 2, and the late-repolarization that occur during phase 3. The time course of an AP always starts with the influx of Na^+ (or Li^+) through Na^+-channels that will then lead to the activation of K^+-channels to open to start the membrane repolarization. Changes in the membrane potential produced by the inactivation of Na^+-channels will activate the opening of voltage-dependent LTCC. The co-localization of the plasma membrane LTCCs and the SR membrane RyR2s, allows for Ca^{2+} influx through the LTCCs to trigger Ca^{2+}-release from the intracellular stores (i.e. CICR). The critical part of the CICR process in cardiac myocytes is to further depolarize the membrane to extend the duration of the APs, so that the refractory period is long enough to maintain the contractile process. Ca^{2+} expelled from the SR for myocardial contraction will need to be replenished, thus cytosolic Ca^{2+} is pumped back into the SR by SERCA2a and any excess Ca^{2+} is extruded out of the cell by NCX1.

Impairment of NCX1 decreased the late-depolarization phase of the epicardial APs (Figure 4.2B), thus when an extra-systolic pulse was introduced in Li^+-perfused hearts, the refractory period was anticipated to shorten. A shorter refractory period would indicate that Na^+-channels are recovered from inactivation sooner in response to a faster repolarization. However, the ability to elicit a second AP in Li-perfused hearts was more difficult and less pronounced than in untreated hearts (Figure 4.8B). When compared to restitution curves generated with Ca^{2+}-loaded hearts, at 70 mM Na-Li Tyrode both Ca^{2+} and AP represent a slower refractoriness (Figure 4.8B). Although AP restitution was based on the excitability of the heart (via measurements of phase 0) and not during phase 2 when CICR occurs, it served a purpose in establishing a relationship between intracellular Ca^{2+} regulation and the electrical activity of the membrane via NCX1.

Moreover, Figure 4.8B illustrated that the AP restitution is faster than Ca^{2+} restitution under normal conditions (in black). This is expected since the opening of Na^{+}-channels are extremely rapid and occur prior to the opening of LTCC to trigger SR-Ca^{2+} release. As 70 mM LiCl was perfused in these hearts, both elements were affected by a reduction in the second amplitude when an extra-systolic pulse was introduced (S2). Earlier we mentioned that changes in the Ca^{2+} transient morphology participated in the altered refractoriness of Li^{+}-perfusion hearts. We also reported changes in the morphology of epicardial APs during fractional impairment of NCX1 by Li^{+} (Figure 4.1). One of these morphological changes was the APD at 50% repolarization and its possible correlation to the elongation of the Ca^{2+} transients measured at 50% recovery (Figure 4.3A and Figure 3.6B, respectively). However, only the changes in the intracellular Ca^{2+} transients revealed significance at 50% recovery when perfused with all Na-Li Tyrode solutions, with the exception of the analysis of APD_{50} with 105 mM Na-Li Tyrode. When NCX1 was highly impaired by 105 mM LiCl, the significant increase in APD_{50} somewhat correlated with the significant decrease in the dV/dt of the epicardial AP (Figure 4.3). Although there were significant decreases in the dV/dt in all Li^{+}-perfused hearts, the correlation between changes in APD_{50} and the refractoriness was not clearly established. It was then assumed that as a result of the molar ratio replacement of 105 mM Na^{+} by Li^{+}, the significant changes in APD_{50} were attributed to extreme Ca^{2+}-overload therefore an unreliable concentration. The extent of Ca^{2+}-overload in these cardiomyocytes was determined based on evaluation of the dramatic increases the cytosolic Ca^{2+} levels (Figure 3.2) and a significantly longer decay time in the Ca^{2+} transients (Figure 3.6C insert) that were acquired in the absence of a significant increase in the Ca^{2+} transient amplitude (Figure 3.5A).

In any case when NCX1 was fractionally impaired with 70 mM Na-Li Tyrode, there was a reduction in the contribution of phase 2 of the epicardial AP and a corresponding increase in the Ca^{2+} transient amplitude (Figure 4.1 and Figure 3.4, respectively). An increase in Ca^{2+}-release from the SR (Figure 3.9B) was established to be responsible for the extended time it took for Ca^{2+} transients to reach maximum amplitude (time to peak; Figure 3.5C) and not NCX1 working in reverse-mode (Figure 3.7 and Figure 4.5C). The longer time the RyR2 are open, the larger the release of Ca^{2+} into the cytosol; with Ca^{2+}-extrusion via NCX1 reduced, the SERCA2a activity will increase to reestablish intra-SR Ca^{2+}-stores and remove excess cytosolic Ca^{2+}. These events led to Ca^{2+}-overload in both Ca^{2+} compartments (cytosolic and intra-SR; Figure 3.2 and Figure 3.8, respectively). The extent of this overload may reduce the ability for the excitation of an extra-systolic AP, therefore delaying the relative refractory period. Another attribute of an increase in cytosolic Ca^{2+} is the activation of cytosolic protein kinases as PKA and CAMKII. These kinases are responsible for the phosphorylation of various intracellular channels, including the LTCC and Na^{+}-channels (Lakatta 2004; Wagner, Dybkova et al. 2006; Ashpole, Herren et al. 2012). As intracellular Ca^{2+} levels increase, Na^{+}-channel inactivation is impaired by CAMKII (Wagner, Dybkova et al. 2006; Ashpole, Herren et al. 2012) thus the refractoriness of the AP when NCX1 was impaired was slower.

Disturbances in the Ca^{2+} homeostasis of ventricular cardiomyocytes have shown to induce beat-to-beat alterations in the CICR process (Ca-Alt; Figure 3.11-3.14). Beat-to-beat fluctuations in the intracellular Ca^{2+} are then expected to come from beat-to-beat alterations in the duration of APs. However in Figure 4.9C, at 14 Hz, Na-Li Tyrode application in hearts loaded with rhod-2 illustrated that Ca-Alts appear prior to AP-Alts recorded in hearts loaded with Di-8-ANEPPS. The fact that Ca^{2+}-overload at higher heart

rates augments Ca-Alt but not AP-Alt (measured at APD_{50}) suggests that the reduced electrogenic property of the membrane, via NCX1 impairment, would reduce the excitability of the heart without significantly altering the APD. Although puzzling, the lack of significant changes in the AP-Alt can be attributed to a decrease in phase 2 that normally attributes a shorter APD in response to an accelerated heart rate. The additional reduction in the late-depolarization by NCX1 impairment at 14 Hz could shorten the APD in the sequential APs. This would result in a reduction in the alternating behavior that normally establishes the degree of alternans (Figure 4.9B). However the only other way to further evaluate the relationship between intracellular Ca^{2+} dynamics and the electrical signaling without overwhelming the heart was to use mice where NCX1 was ablated.

Epicardial Electrical Signaling and Intracellular Ca^{2+} Dynamics in NCX1 KO Hearts

The link between intracellular Ca^{2+}-handling and the appearance of TW-Alts have yet been established, however extensively studied (Verrier, Kumar et al. 2009; Cutler, Jeyaraj et al. 2011). What is known is the association between AP-Alts and the appearance of TW-Alt (Wilson and Rosenbaum 2007; Verrier, Kumar et al. 2009). AP-Alts appear as a consequence of various cardiac arrhythmogenic conditions, which include ventricular tachycardia (rapid stimulation), ischemia-reperfusion, and heart failure (Wilson and Rosenbaum 2007; Verrier, Kumar et al. 2009; Khananshvili 2013); conditions in which NCX1 has shown to be either down-regulated or up-regulated (Pogwizd, Qi et al. 1999; Hobai and O'Rourke 2000; Ranu, Terracciano et al. 2002; Matsumoto, Miura et al. 2003; Xu, Chen et al. 2011). Fluctuations in the APD are a result of alternating beat-to-beat lengths of the AP repolarization phase. The repolarization phase of ventricular APs defines the magnitude of the T-wave formation in the ECG. Shortening of this phase in endocardial APs or the elongation of this phase in epicardial cells could result in a negative deflection in the T-wave. Since NCX1 is an electrogenic sarcolemma transmembrane protein, it was then expected that ablation would modify the APD in addition to the excitability of the heart.

7.7 NCX1 Ablation Modifies AP Repolarization and Reduces the Appearance of TW-Alt at the Whole-Heart Level

Cardiac dysfunction and the appearance of alternans is not limited to a sudden increase in heart rate (tachycardia), but also prominently found under normocardic and bradycardic conditions when the APD is elongated. More specifically, the appearance of EADs and DADs occur as a result of heart failure or ischemia-reperfusion myocardial injury. One of the key features of heart failure is the overexpression of NCX1, which is thought to lead to the prolonged APD (Sipido, Volders et al. 2002). It is thought that manipulation of NCX1 expression or the use of pharmacological drugs to block NCX1 activity could treat heart failure; however due to the lack of adequate selective drugs for this exchanger, there is limited knowledge of NCX1's direct relationship to treatment of heart disease (Khananshvili 2013). It is then safe to assume that if overexpression of NCX1 would increase APD, then ablation of NCX1 would reduce the APD.

Once a mouse heart is cannulated to the PLFFM, removal of the right atrium and ablation of the SA and AV nodal cells are done to assist in the reduction of the heart's natural pacemaker activity. By implementing this maneuver, we are able to control the

heart rate externally (see Chapter 2, section 2.4) by reducing the electrical conduction pathway. Since the electrical coupling of myocytes are still intact, in epicardial AP traces with clearly defined phases are recorded (see Figure 2.8A). The morphology of an epicardial AP has been documented to change based on the temperature, the heart rate, and intracellular Ca^{2+} release mechanisms (Ferreiro, Petrosky et al. 2012). At room temperature, NCX KO and NCX Flox hearts exhibited similar morphology although the contribution of phase 2 in KO hearts was significantly smaller (Figure 5.5A,C). These results are similar to those recorded in NCX KO isolated cells (Pott, Philipson et al. 2005; Pott, Ren et al. 2007). This significant decrease in phase 2 contribution in NCX KO hearts was also seen once the surrounding Tyrode bath reached 37°C (Figure 5.5B,C). This was expected since NCX1 and other intracellular Ca^{2+} mechanisms are highly temperature dependent (Q10~2.6 (Petrosky, Mejia-Alvarez et al. 2013)) and NCX1 (Q10~3.9 (Bersohn, Vemuri et al. 1991)).

Microelectrode impalement at the epicardial layer of NCX KO hearts revealed AP recordings (4 Hz) with no significant changes to the contribution of phase 2 before and after treated with Na-Li Tyrode (Figure 5.6B). These results concur that ablation of NCX1 in these transgenic mice is efficiently reduced, resulting in an attenuated late-depolarization phase in the epicardial ventricular APs. However, simultaneous recordings of Ca^{2+}-transients revealed the possibility of NCX1 activity in neighboring cells that are not recorded by microelectrode impalement (Figures 6.2 and 5.6, respectively). Microelectrode impalement records the membrane potential from the PM, whereas a fluorescent recording of the membrane potential (via Di-8-ANEPPS) includes the PM and t-tubular systems (Ferreiro, Petrosky et al. 2012). Therefore, fiber-optic fluorescent recordings of Ca^{2+}-transients recording from the cytosolic compartment is able to detect NCX1 activity junctional to the SR as well as neighboring cells with normal expression of NCX1 in the conditional KO hearts

The lack of the late-depolarization phase in these NCX KO mice results in a faster repolarization, which reduces the APD. Normally a reduction in the APD occurs in response to an accelerated heart rate (Figure 6.9A). As seen in Li^{+}-perfusion experiments at 14 Hz, a decrease in phase 2 may have resulted in a decrease in AP-Alts measured at APD_{50} (Figure 4.9C). Microelectrode impalement recordings of the epicardial APs of both NCX Flox and KO hearts illustrated that at 50% repolarization, from the peak amplitude of phase 0, resulted in measurements of APD_{50} in phase 1 (Figure 6.9A). APD at 70% repolarization would constitute appropriate for analyzes of APD during phase 2; however due to the lack of phase 2 in NCX KO hearts, evaluation of the onset of AP-Alt would be more difficult (Figure 6.9B). Thus APD measurements at 90% repolarization were analyzed and compared between genotypes as the heart rate was increased from 5 to 14 Hz (Figure 6.9C). The appearance of AP-Alt in NCX KO hearts was not significant as the heart rate increased, whereas NCX Flox hearts revealed a large degree of alternans at higher frequencies (11-13 Hz; p-value < 0.01). On the other hand, at 14 Hz, the degree of AP-Alt was reduced in NCX Flox hearts (Figure 6.9C). These results attribute to the fact that at higher frequencies, not only does the duration of epicardial APs naturally become shorter but also the subsequent APs will shorten. Eventually the degree of shortening will be similar in concurrent APs, just as in NCX KO hearts and in Li^{+}-perfused hearts (Figure 6.9C and Figure 4.9C, respectively).

The duration of cardiac APs, from the endocardium to the epicardium, defines the morphology of ECG recordings. Since there is a shortening of the APD in NCX KO hearts, then the appearance of a T-wave would be eliminated. In vivo ECG recordings of NCX Flox and KO mice, conducted by Pott et al. (2007), revealed shorter QT intervals in

NCX KO mice (Pott, Ren et al. 2007). However these recordings were evaluated when the mouse was alive and alert, thus the natural accelerated heart rate of the mouse (~600bpm) would modify morphological attributes. Furthermore, these ECG recordings were derived from the collective electrical activity of the whole organ in 30sec intervals (Pott, Ren et al. 2007). Therefore, the Q-T segment evaluation included a J-wave between the S-T segment and what they considered a negative T-wave. The experiments conducted in Chapter 6 (Figure 6.7-6.8), measure the transmural electrical gradient (via ECG) of the left ventricle and were done simultaneously with epicardial AP microelectrode impalement of both NCX Flox and NCX KO mouse hearts (Figure 6.9). In this way we were able to evaluate the ECG waveforms respective of the repolarization of the epicardial AP of the left ventricle alone as the heart rate was increased (Figure 6.8 and Figure 6.9, respectively). Left ventricular transmural ECG recordings of NCX Flox and KO hearts, paced at 5 Hz, displayed a distinctive Q-R-S waveform (Figure 6.7). NCX Flox hearts present a positive T-wave, whereas NCX KO hearts presented a distinctive J-wave and little to no T-wave. In fact, NCX KO hearts presented no T-waves as the pacing frequency increased instead a more established J-wave presented itself (Figure 6.9). The presence of a J-wave is due to the fast repolarization of phase 1 in the epicardial APs. This explains why in NCX Flox hearts, the presence of a J-wave is minimal and NCX KO hearts have a faster AP repolarization (and no late-depolarization phase) present a more elaborate J-wave formation. The T-wave presented in Pott et al. (2007) for both genotypes showed an inverted (“negative”) T-wave, whereas transmural ECG recordings of the left ventricle of NCX KO hearts (Figure 6.8, light blue trace) revealed no T-wave formation. Nevertheless, their evidence of a shorter Q-T segment and the lack of a T-wave in the transmural ECG recordings presented in this dissertation are consistent with the idea that a decrease in NCX1 function would result in a reduced APD and as a consequence decrease the appearance of AP-Alt and induction of TW-Alt. Furthermore, when NCX1 is overexpressed in mice, Pott et al (2012) found a prolongation of the Q-T interval and a corresponding increase in their APD at 90% repolarization (Pott, Muszynski et al. 2012).

In addition to the ECG and microelectrode impalement, Ca^{2+}-transients were recorded via rhod-2 fluorescence. The fiber optic (200 μm diameter, ~40 cells) was placed within the same proximity as the microelectrode impalement, to ensure that the induction of AP-Alt and Ca-Alt are recorded from the same region of the left ventricle as the heart rate is increased.

7.8 Ca^{2+} Alternans appear first in NCX KO hearts at the Epicardial layer.

There are many ways to disrupt the Ca^{2+}-cycling in cardiomyocytes. Common targets are the major Ca^{2+}-release channels (LTCC, RyR2) and/or Ca^{2+}-dependent proteins (SERCA2a). However in this dissertation, the disruption of the Ca^{2+}-cycle was primarily accomplished by a reduction in NCX1 turnover rate in an intact mouse heart at 37°C. Since NCX1 is the major extruder of Ca^{2+} out of the cell, it is reasonable to assume that ablation would also modify the intracellular Ca^{2+} dynamics.

Echocardiographic recordings were conducted on these NCX KO mice when Henderson et al first introduced them in 2004. They revealed a modest decrease in cardiac function by evaluating the ejection fraction, velocity of fiber shortening and the fractional shortening of the left ventricles of NCX KO hearts (Henderson, Goldhaber et al. 2004). These attributes derived from the echocardiographic recording not only reveal the contractility of the heart, but also represent the rises and falls of Ca^{2+} levels of the

ventricular myocytes via pressure-volume loop. The higher the preload, the larger the pressure during ventricular filling (end-diastolic volume) would result in an increase Ca^{2+} sensitivity of troponin C as the sarcomeres stretched, thereby increases myocardial force contraction and the stroke volume. However, NCX KO hearts revealed a decrease in the stroke volume due to a decrease in the ejection fraction and an increase in the end-systolic volumes. These results suggest either intracellular Ca^{2+} levels are somewhat reduced or are less sensitive to troponin C in NCX KO hearts. The evaluation of the cardiac-ECC was then conducted in isolated cardiomyocytes of both NCX Flox and KO mice. They found that Ca^{2+}-efflux in the presence of caffeine was diminished in NCX KO hearts, however the SR-Ca^{2+} load appeared unchanged as well as the responses to increased stimulation and isoproterenol application (Henderson, Goldhaber et al. 2004). They concluded that the lack of NCX1 did not alter the intracellular Ca^{2+} dynamics but modified the initial Ca^{2+}-influx that would allow for downstream compensatory mechanisms to maintain Ca^{2+} homeostasis (Henderson, Goldhaber et al. 2004).

By examining the kinetics of NCX Flox and NCX KO Ca^{2+} transients (Figure 6.3), at the epicardial layer of the whole heart (37°C), we were able to verify that the Ca^{2+} transient kinetics are unchanged just as seen by Henderson et al in isolated myocytes (RT). On the other hand, Ca^{2+} current (I_{Ca}) recordings in these single-cell experiments notated significant differences in the amplitude of release and decay rate of I_{Ca} in NCX KO myocytes compared to NCX Flox myocytes (Henderson, Goldhaber et al. 2004; Pott, Philipson et al. 2005; Pott, Yip et al. 2007). Unfortunately, currents through NCX1 or LTCC are not detectable at the whole-heart level. Nevertheless the accelerated decay rate they found in KO myocytes retains valuable information when treated with Ry+Tg to eliminate any additional Ca^{2+} that would alter I_{Ca} recorded (Pott, Yip et al. 2007). The persistent accelerated decay rate remained until Ca^{2+}-dependent inactivation of I_{Ca} was removed by Ba^{2+} perfusion (Pott, Yip et al. 2007). These findings provide evidence that changes in the kinetics rely on subsarcolemmal Ca^{2+} levels in NCX KO mice (Pott, Yip et al. 2007).

As the heart rate was increased, both genotypes presented the typical negative-staircase phenomena in the whole-heart (Figure 6.6A-B) similar to that found in isolated NCX KO cardiomyocytes recorded at lower frequencies (i.e. 0.2 - 2 Hz (Henderson, Goldhaber et al. 2004)). Additionally, the evaluation of the Ca-Alts, under normal conditions (no Li-perfusion) when the frequency was increased from 5-14 Hz, was apparent in both genotypes (Figure 6.6, C). However, Ca-Alt presented earlier in NCX KO hearts representing only significant changes at 9 Hz (Figure 6.6 C p-value < 0.05). The lack of significance after 9 Hz was attributed to the decrease in Ca^{2+} transient amplitude of the first release (Amax) and possible Ca^{2+}-overload generated within the SR due to the Ca^{2+} dependent RyR2-CSQ2 interaction (Kornyeyev, Petrosky et al. 2011), resulting in a decrease in the degree of Ca-Alt as the heart rate surpassed the normal heart rate (10 Hz).

Simultaneous AP recordings of the left ventricle revealed that Ca-Alts and AP-Alts are more prominent in NCX Flox hearts as the heart rate surpassed 10 Hz (Figure 6.10A). The augmentation of alternans was shown to transduce across the ventricular wall in the form of TW-Alt (Figure 6.8, black lines). On the other hand, NCX KO hearts revealed an early induction of Ca-Alts without executing AP-Alts (Figure 6.10B), which resulted in the reduced appearance of TW-Alts (Figure 6.8, light blue lines). One possibility is the SR-Ca^{2+} load is challenged in NCX KO hearts as the time intervals between the beat-to-beat Ca^{2+}-release and re-uptake becomes shorter. Interestingly, in

overexpressed NCX1 transgenic mice tend to have a higher occurrence of spontaneous SR-Ca^{2+} release constituting to the generation of DADs (Pott, Muszynski et al. 2012).

7.9 Calcium Overload is apparent in NCX KO hearts at the Epicardial layer.

Ca^{2+}-overload in the dyadic cleft is commonly found in cardiomyocytes upon reperfusion after a myocardial infarction (i.e. ischemia-reperfusion). In ischemic hearts, the appearance of spatially discordant AP-Alts that perpetuates from myocardial infarctions have been shown to produce beat-to-beat fluctuations in the T-wave formation. Now, ischemia occurs when there is lack of blood flow to a portion of the cardiac tissue, thus a lack of nutrients and ions that can result in tissue damage. Upon reperfusion to the myocardial infarction, there are massive ionic imbalances within and around the ischemic cells. More specifically there is a rise in intracellular Ca^{2+} levels, resulting in Ca^{2+}-overload and abnormal Ca^{2+}-cycling. The sudden rise in intracellular Ca^{2+} has been shown to provoke mechanical and electrical cardiac dysfunction (Khananshvili 2013).

Experiments conducted by Valverde et al. (2010) revealed for the first time simultaneous recordings of intra-SR and cytosolic Ca^{2+} in the intact whole-heart during ischemia-reperfusion (Kornyeyev, Reyes et al. 2010). In this paper, they provided substantial evidence of Ca^{2+}-overload in the SR during ischemia induced cytosolic increases upon reperfusion. Depletion of the intra-SR Ca^{2+} stores later resulted in decreased Ca^{2+} transient amplitude and a decrease in the contribution of phase 2. A decrease in Ca^{2+}-release could explain the shortening in phase 2 although it does not entail if NCX1 contributes to the increases in intracellular Ca^{2+} levels. One possibility is the slowing of NCX1 to extrude cytosolic Ca^{2+} due to a decrease in SR-Ca^{2+} release. Another perspective is the increase in NCX1 reverse-mode activity for Ca^{2+}-entry. Either way it is apparent that NCX1 participates in the disruptive behavior of intracellular Ca^{2+} during ischemia-reperfusion.

In addition to Ca^{2+}-overload upon reperfusion there is also a notable increase in intracellular Na prior to the onset of increases in intracellular Ca^{2+} levels (Kusuoka, Porterfield et al. 1987; Hartmann and Decking 1999; Khananshvili 2013). The originations of the increased Na levels are attributed to the increased activity of the Na/H-exchanger (NHE) that results in cardiac acidosis (Said, Becerra et al. 2008; Khananshvili 2013). Inhibitors of the NHE have shown to decrease the augmentation of both intracellular Na^+ and Ca^{2+} levels, thereby reduces myocardial injury in a cardioprotective manner (Imahashi, Pott et al. 2005; Khananshvili 2013). Now NCX1 reverse-mode activity suggests not only Ca^{2+}-entry but also Na^+ extrusion. In NCX KO mice, ischemia-reperfusion resulted in a decrease in Na overload with no increases in intracellular Ca^{2+} (Imahashi, Pott et al. 2005). In fact NCX KO hearts were shown to be cardioprotective when subjected to global ischemia. Imahashi et al suggested that this cardioprotective nature was due to the lack of Ca^{2+}-entry via NCX1 that would result in ATP preservation, thus facilitates the Na/K-ATPase activity to decrease intracellular Na^+ levels (Imahashi, Pott et al. 2005). This suggests that NCX1 in the reverse-mode plays an important role in ischemia-reperfusion injury (Imahashi, Pott et al. 2005). However, the Na^+ influx that would normally occur in response to increases in cytosolic Ca^{2+} levels via NCX1 forward-mode, could also explain the decrease in Na^+ overload found in NCX KO hearts. On the other hand, the lack of increases in intracellular Ca^{2+} levels in these hearts could be attributed to the decrease in LTCC trigger activity to release SR-Ca^{2+}. The increases in intracellular Ca^{2+} levels in ischemic hearts do not present an increase

in SR-Ca^{2+} release, as is seen in NCX1 impairment experiments (Kornyeyev, Petrosky et al. 2011). It is then reasonable to assume that a decrease in SR release could be further reduced during ischemia-reperfusion in response to a decrease in LTCC triggered release.

Figure 6.5 illustrates a degree of Ca^{2+}-overload by challenging SR-Ca^{2+} load via perfusion of 70 mM LiCl. At 10 Hz, Ca^{2+} transients of NCX Flox hearts increased the amplitude of release, whereas NCX KO hearts presented no significant changes in Ca^{2+}-transient amplitude (Figure 6.5A). Interestingly when Li^{+} was washed out of the extracellular solution, NCX KO Ca^{2+}-transient amplitude significantly decreased when compared to initial Ca^{2+} transient amplitude (control). Surprisingly at 4 Hz, the Ca^{2+} transient amplitude upon Li^{+}-perfusion significantly increased in both genotypes, although the degree of increase was more prominent in NCX Flox hearts and was reduced significantly in upon Li^{+}-washout (Figure 6.2). On the other hand, Li^{+}-perfusion induced Ca-Alt (at 10 Hz) in both genotypes, and Li^{+}-removal decreased the degree of alternans in NCX Flox hearts whereas NCX KO hearts retained a similar degree of alternans (Figure 6.5B). Attenuation of Ca-Alt and Ca^{2+}-transient amplitude in NCX Flox hearts, as Li^{+} was washed from the extracellular solutions, relieves NCX1 impairment resulting in an accelerated extrusion of intracellular Ca^{2+}. Whereas the lack of normal expression levels of NCX in KO hearts, diminishes the extrusion of intracellular Ca^{2+} once Li^{+} was washed out. Thereby inducing Ca^{2+}-overload in the dyadic cleft of these cardiomyocytes without inducing larger SR-Ca^{2+} release (Figure 6.5B and A, respectively).

Although fluorescent measurements of the resting diastolic Ca^{2+} levels were elevated upon Li^{+}-perfusion at 10 Hz (Figure 6.5C) and 4 Hz (Figure 6.1C) in both genotypes, these increases were attributed to NCX impairment in the ventricular cardiomyocytes (Figure 3.2). However fiber optic recordings at the epicardial layer of an intact heart will collect emission from multiple cell types (e.g. endothelial cells and ventricular cells) (Escobar, Perez et al. 2012). Nevertheless, ventricular cardiomyocytes are excitable cells and therefore fluorescent Ca^{2+}-transient signals elicited by an electrical stimulus (i.e. AP) are recorded from the ventricular myocytes and not other tissue. These findings on the functional effects of NCX1 impairment on cardiomyocyte Ca^{2+} diastolic levels are consistent with studies recorded on isolated cells where cytosolic levels are either controlled or accessible (Hilgemann 1990; Nicoll, Longoni et al. 1990; Hobai and O'Rourke 2000).

7.10 Conditional KO of NCX1 provides supporting evidence of crosstalk between NCX1, RyR2 mediated Ca^{2+} release and the late-depolarization phase of Epicardial APs.

The co-localization of NCX1 and LTCC within the t-tubules and their junctional proximity to the RyR2 for CICR sets up a platform for a dynamic environment that is tightly coupled to the regulation of intracellular Ca^{2+} homeostasis. The conditional KO of NCX1 has been documented to compensate for the lack of extrusion of intracellular Ca^{2+} out of the cell by early inactivation of the LTCC (Henderson, Goldhaber et al. 2004; Pott, Philipson et al. 2005; Pott, Yip et al. 2007). Whereas in mice that overexpress NCX1 there are no changes to the functionality of these proteins (Yao, Su et al. 1998), with the exception of increased SR-Ca^{2+} release and faster myocardial relaxation (i.e. increase in Ca^{2+}-efflux) (Terracciano, Souza et al. 1998). Altogether these transgenic mouse models where NCX1 is either up-regulated or down-regulated present Ca^{2+}-compensatory

mechanisms that are reflected in the electrical activity of ventricular myocytes. AP recordings of NCX KO cardiomyocytes presented in this dissertation (Figures 5.5 and 5.6) and published by other researchers to have a decrease in APD (Pott, Philipson et al. 2005; Pott, Ren et al. 2007). Contrary to ablation of NCX1, literature on NCX1 overexpression cardiomyocytes observed a prolongation in the APD (Yao, Su et al. 1998; Pott, Muszynski et al. 2012).

Modifications to the late-depolarization phase of mouse APs have been demonstrated throughout this dissertation to be related to the lack of the monovalent cationic influx of Na through the NCX1 as it extrudes excess cytosolic Ca^{2+}. Previously published, in WT mice, have also demonstrated that SR-Ca^{2+} release can result in morphological changes to the AP (Ferreiro, Petrosky et al. 2012). These experiments include the use of Nifedipine to block the LTCC (Bayer, Rodenkirchen et al. 1977; Bridge, Smolley et al. 1990; Lopez-Lopez, Shacklock et al. 1995; Litwin, Li et al. 1998) and the application of Ry+Tg to diminish the SR-Ca^{2+} release and reuptake mechanisms (Mitchell, Powell et al. 1984; Ferreiro, Petrosky et al. 2012). The functionality of the sarcolemma NCX1 protein is to assist in the regulation of intracellular ion levels (i.e. Ca^{2+} and Na^{+}) powered by the electrochemical gradient. When intracellular Ca^{2+} levels are increased, Ca^{2+} will bind to a region of the cytoplasmic loop (i.e. CBD1 and CBD2) of NCX1 to activate the forward-mode (see Figure 1.7). As intracellular Na levels increase, Na will bind to the XIP region of the intracellular loop (see Figure 1.7) disabling the forward-mode and active the reverse-mode (see also Figure 1.8). As seen in cardiomyocytes treated with Nifedipine (Ferreiro, Petrosky et al. 2012), a decrease in Ca^{2+}-influx via the LTCC would result in a diminished Ca^{2+}-transient amplitude in addition to a decrease in the phase 2 contribution of the epicardial AP. In NCX KO hearts, it is established that 50% of the LTCC inactivate earlier to lessen the triggered SR-Ca^{2+} release, even though the SR-Ca^{2+} content appears to be normal (Henderson, Goldhaber et al. 2004).

The myocardial relaxation phase occurs during the late-repolarization phase of a ventricular cardiomyocyte. During this time is when Ca^{2+} is either reuptaken by SERCA2a or extruded from the cell either by NCX1 (major contributor) or the PM Ca^{2+}-ATPase (minor contributor). In transgenic rats that overexpress the PM Ca^{2+}-ATPase, an accelerated decline time of Ca^{2+}-transients occurs only in the absence of intra-SR Ca^{2+} release (He, Giordano et al. 1997). It is therefore notated that the PM Ca^{2+}-ATPase is miniscule in intracellular Ca^{2+} regulation. Thus, even though NCX KO hearts express normal levels of the PM Ca^{2+}-ATPase (Henderson, Goldhaber et al. 2004), this is the only extrusion mechanism available when treated with Ry+Tg. Hence fluorescent recordings of Ca^{2+}-transients in NCX KO hearts were unattainable at the whole-heart level after perfusion of Ry+Tg. Nevertheless, AP recordings were acquired in NCX Flox and KO hearts during Ry+Tg treatment and, before and after Li-treatment (Figure 5.7) to establish whether or not intra-SR Ca^{2+} release and reuptake were attributed to the decline in the contribution of phase 2. The contribution of phase 2 was calculated individually for each genotype and compared in Figure 5.8. Clearly NCX KO epicardial APs resemble no significant changes in the late-depolarization phase after the SR was depleted (Figure 5.8D; Ry+Tg), whereas NCX Flox hearts show a significant decrease in the contribution of phase 2 (Figure 5.8C). These results are consistent with the idea that NCX1 activity defines the late-repolarization phase of epicardial APs. An increase in SR-Ca^{2+} release in NCX overexpressed cardiomyocytes resulted in an increase in NCX1 activity and a prolonged APD (Terracciano, Souza et al. 1998; Yao, Su et al. 1998; Pott, Muszynski et al. 2012). Early inactivation of the LTCCs in NCX KO cardiomyocytes

consequently decreases the trigger of SR Ca^{2+} release due to lack of NCX1 activity and therefore has a shortening of the APD (Henderson, Goldhaber et al. 2004; Pott, Henderson et al. 2007; Pott, Yip et al. 2007). However, Na^+ and Ca^{2+} are not the only ions that define the AP morphology. In fact, K^+ is the crucial ion for re-establishing the resting membrane potential during phase 1 (KITO), phases 2 and 3 (K^+ delayed-rectifiers) and phase 4 (Kir). K^+-efflux is primarily to counter the cationic influx of Na^+ ions through the Na^+-channels ($Na^+_{V1.5}$; phase 0) and forward-mode of NCX1 (phase 2).

In order to evaluate K^+ conductance at the whole-heart level in NCX KO mice, experiments were conducted with perfusion of [200 μM] $BaCl_2$, to block the Kir during the late-depolarization phase of epicardial APs (Figures 5.9 and 5.10). Surprisingly in the absence of K^+-efflux via the Kir, there was a substantial increase in the APD at 70% and 90% repolarization in both genotypes (Figure 5.10C,D). In 2007, a group of researchers using these conditional NCX KO mice found an increase in expression of the slow K_{ITO} channels (Pott, Henderson et al. 2007; Pott, Ren et al. 2007). The up-regulation of these slow K^+-channels (i.e. $K_{v4.2}$) indicated a faster repolarization (Pott, Ren et al. 2007), however the fast K_{ITO} channels (i.e. $K_{v4.3}$) and other K^+-channels (i.e. $K_{v2.1}$, $K_{v1.4}$, and $K_{v1.5}$) were found to be unchanged. Thus, when Kir channels were blocked by Ba2+ treatment, an increase in phase 2 morphology of both genotypes led to inquiry if residual NCX1 is responsible for the increase in NCX KO hearts. Since these transgenic NCX KO hearts are conditionally ablated, they retain a percentage of functional NCX1. After all at the whole-heart level it is difficult to know the proximity of the residual functional NCX1 proteins when recording at the epicardial layer via microelectrode impalement. Figure 5.6 illustrated that upon Li^+-perfusion, the contribution of phase 2 was left unchanged in NCX KO hearts, however simultaneously Ca^{2+}-transient recordings revealed some NCX1 activity within the same region of the heart (Figure 6.2). Therefore shortly after perfusion of BaCl2, 70 mM Na-Li Tyrode was perfused to impair any residual NCX1 in NCX KO hearts (Figure 5.9, mid-right). At APD70, it is clear that removal of the K^+ counter current revealed Na^+-influx via residual NCX1 activity in the conditional KO hearts (Figure 5.10D).

Disadvantages and Limitations:

Fluorescent recordings of Ca transients at a whole heart level have provided several limitations. One limitation is the multiple cell types at the epicardial layer of the heart that are also perfused with the fluorescent dyes. Emissions from these cell types are shown to primarily affect cytosolic diastolic levels and not the Ca-transients (Escobar, Perez et al. 2012). In addition to this, fluorescent loading of the whole heart limits the dye content in the ventricular cardiomyocytes. This can lead to saturation of the signal, which could lead to morphological changes in the Ca-transient amplitude and decay kinetics (i.e. 105 mM LiCl; Figure 3.5 and 3.6). Depending on the diameter of the optical fiber used, the depth and number of cells that are collected can vary kinetic features of the AP (Ferreiro, Petrosky et al. 2012), as seen in Chapter 4 when measuring APD at 50% repolarization (Figure 4.3).

In Chapter 2, a part of the recording protocol on the PLFFM was to maintain the heart rate at 4 Hz. Thus, SA nodal cells were ablated and the addition of [7.5-10 μM] blebbistatin is normally perfused to immobilize the hearts recorded at 37ºC. Under most experimental conditions this is idea for recording at the whole-heart level to reduce movement artifact, however in experiments that use of mag-fluo4 to measure the intra-

SR free Ca^{2+} perfusion of BBS was not possible. This is due to the fact that mag-fluo4 requires the excitation of a blue laser (473 nM; via PLFFM), which has been determine to photoinactivate BBS (Sakamoto, Limouze et al. 2005). Photoinactivation of BBS not only removes the inhibitory effect but also creates free radicals that can damage the tissue. In this case, experiments conducted in the Sarcoplasmic Reticulum section of Chapter 3 were achieved by carefully restricting the proximal area around the heart to constrain mobility. In addition to the floating flexibility of the fiber optic, the angle in which it was placed also assisted in the reduction of possible tissue damage as the heart beat. Ca^{2+}-transients were corrected in the analysis program for the baseline and collective traces were averaged for analysis of Ca^{2+} transient amplitude and kinetics.

Chapters 5 and 6 focus on experiments conducted on the transgenic mouse model where NCX1 is conditionally knocked out. Typically the removal of a cardiac-specific protein in the development of a transgenic mouse model depends on the critical nature of that protein for the survival to adulthood. More often the generation of a cardiac-specific KO mouse decreases the contractility of the heart or are shared key proteins in the brain development of the mouse. This led to the development of Cre-loxp technology where a key protein can be conditionally ablated either by oral consumption of the cre enzyme prior to experimentation of the expression of this enzyme under the mlc-2 promoter. The ablation of NCX1 was designed as the latter due to the lethality of the global KO of NCX1 at embryonic day 9.5 (Henderson, Goldhaber et al. 2004; Pott, Philipson et al. 2005). We were kindly provided with the adult conditional NCX1 knock-out (KO) mice by K.Phillipson. These KO mice have 80% of its cardiomyocytes missing the protein whereas the other 20% of the cells retain normal expressions of NCX1 (Henderson, Goldhaber et al. 2004). When isolating these KO cardiomyocytes, a caffeine pulse can be applied to each cell to test for NCX1 activity. Those cells that show a diminished decay time of the Ca^{2+}-transients or lack I_{NCX} are selected for further experimentation. However, when using an intact heart with no ability to select purely ablated cardiomyocytes, microelectrode impalement for AP recordings are the only experimental way to assist in identifying degree of ablation within a specific region of the epicardial layer. After experimentation however, hearts can be collected and processed for rt-PCR analysis. Selectivity of hearts with higher degree of ablation would be used for data comparison. Unfortunately this procedure was implemented later and not all hearts could be processed for verification of the degree of ablation. Nevertheless, the use of NCX Flox hearts from the NCX KO germ-line were determined to be somewhat unreliable as control WT hearts. Additionally, evaluation of rt-PCR analysis of the expression of functional NCX1 (retains exon 11 sequence) would not entail the location of NCX1 expression. It is possible that at the epicardial layer of the KO hearts used in this dissertation did not express functional NCX1, instead the endocardial and mid-myocardial layers are where the 20-40% NCX1 expression is retained. Nevertheless data collected in Chapters 5 and 6 have provided a substantial amount of information about the conditional ablation of NCX at the whole-heart level.

Conclusions:

All in all, the use of whole-heart preparation is an ideal way to study physiological events of cardiomyocytes, in comparison to single-cell recordings. Although isolated cell experiments are insightful to the basic foundation of how channels and organelles function, single-cell measurements are far from physiological conditions. Thus this dissertation was compiled solely with experiments conducted in intact mouse hearts using a modified version of the PLFFM. The primary focus was to evaluate the role of NCX1 in epicardial Ca^{2+} dynamics and electrical signaling. In doing this we were able to provide substantial evidence to support our central hypothesis: **NCX1 impairment will lead to an increase in the cytosolic Ca^{2+} and consequently an accumulation of Ca^{2+} in the SR. As a result of this accumulation, a larger Ca^{2+}-release produced from the SR will activate NCX1, modifying the action potential repolarization**.

Cardiomyocytes are dynamic excitable cells that rely on changes in intracellular Ca^{2+} levels for myocardial contraction and relaxation. Thus a specialized network of ionic channels, pumps and exchangers that lie within the PM and t-tubular system, are integrated in such a way that the junctional SR and SR-membrane proteins can work synergistically to regulate intracellular Ca^{2+} dynamics. Upon electrical stimulation, changes in the membrane potential will activate the opening of voltage-sensitive Na-channels. The Na^{+} current across the membrane will activate the opening of LTCC initiating the phenomena CICR. As Ca^{2+} is released from the SR (via RyR2), it will bind to myofilaments for myocardial contraction (systole). A representation of systole during CICR was acquired by evaluation of the upstroke of Ca^{2+}-transients (measured via rhod-2), whereas the downstroke entails Ca^{2+2+} extrusion. It is reasonable to assume that immediate extrusion of excess cytosolic Ca^{2+} would primarily be via NCX1, since the co-localization of NCX1 to LTCC (within the t-tubules) and their junctional proximity to RyR2; whereas the Ca^{2+} re-sequestered by SERCA2a would occur later (in the relaxation phase).

Ca^{2+}-transient kinetics assist in the determination of how long the RyR2 channels are open (time to peak) and the duration to 50% recovery entails the efficiency of cytosolic Ca^{2+} extrusion after myocardial contraction. An increase in myocardial contractility is another way of measuring changes in Ca^{2+} diastolic levels. Upon Na-Li Tyrode perfusion, we demonstrated that impairment of NCX1 not only modified cytosolic Ca^{2+} dynamics but also the intra-SR Ca^{2+} dynamics. Increases in the resting Ca^{2+} levels were recorded in both intracellular compartments (Figures 3.2 and 3.8). As an electrogenic transporter that exchanges three Na^{+} for one Ca^{2+}, NCX1 drives an influx of monovalent cations in order to extrude excess cytosolic Ca^{2+}. Thus, augmentation of intracellular Ca^{2+} diastolic levels were determined to be a resultant of reduction in the extrusion rate of Ca^{2+}, which would then lead to the accumulation of cytosolic Ca^{2+}. With SERCA2a as the only other competing extruder of cytosolic Ca^{2+}, will increase pump activity thereby increasing the intra-SR Ca^{2+} levels, producing a larger release of Ca^{2+} every beat (Figures 3.5 and 3.9). Hence, as a result of high luminal Ca^{2+} content when NCX1 was impaired by Li^{+}, modifications to the intracellular Ca^{2+} dynamics reduced Ca^{2+} refractoriness (Figure 3.15), which were amplified at higher heart rates (Figure 3.12 and 3.14). Altogether these results demonstrate that NCX1 plays a significant role in the maintenance of intracellular Ca^{2+} homeostasis.

The electrogenicity of this Ca^{2+}-mediated transporter (NCX1) can produce transient changes to the membrane potential and thereby modify the repolarization phase of cardiac APs. The loss of this electrogenicity imposed by NCX1 was found to

also modify the electrical excitability of the heart during the cardiac cycle (Figure 4.8). Modifications to the electrical excitability are defined by the duration of cardiac APs. This was clearly demonstrated in AP recordings from NCX1 transgenic mouse models. The reduction in transport of Na^+ through the NCX1, led to the reduction in the contribution of phase 2 of the epicardial APs in WT hearts (Figure 4.2, 4.4 and 5.6). A decrease in the late-depolarization phase of epicardial APs indicates a faster repolarization and therefore can promote early after-depolarizations and AP-Alts. However NCX KO hearts revealed shorter APD and little to no AP-Alt as the heart rate increased from 5 Hz-14 Hz (Figure 6.9). On the other hand, in the absence of NCX1, the onset of Ca-Alt is shifted to lower hearts rates (Figure 6.6). Interestingly this shift prevented the translation of intracellular Ca-Alt to TW-Alt (Figure 6.8) via NCX1. Hence, fluctuations in the SR Ca^{2+}-release cannot modify the repolarization phase of epicardial APs in NCX KO hearts.

In summary, modification to the activity of NCX1 would limit the access for normal regulation of intracellular Ca^{2+} levels as the cell prepares for myocardial contraction. Deviations in intracellular Ca^{2+} levels can perpetuate a chemical response that can modify the electrical activity of the cell via NCX1. Throughout this dissertation it has been demonstrated that NCX1 plays a key role in intracellular Ca^{2+} dynamics and participates in defining the electrical activity of the heart. Furthermore, by addressing the mechanisms around NCX1 that links the function of an intracellular organelle (SR) with the membrane potential, is essential for developing pharmacological strategies for treatment of various cardiac arrhythmias.

REFERENCES:

Allingham, J. S., R. Smith, et al. (2005). "The structural basis of blebbistatin inhibition and specificity for myosin II." Nature structural & molecular biology **12**(4): 378-379.

Altamirano, J., Y. Li, et al. (2006). "The inotropic effect of cardioactive glycosides in ventricular myocytes requires Na+-Ca2+ exchanger function." J Physiol **575**(Pt 3): 845-854.

Armoundas, A. A., I. A. Hobai, et al. (2003). "Role of sodium-calcium exchanger in modulating the action potential of ventricular myocytes from normal and failing hearts." Circulation research **93**(1): 46-53.

Ashpole, N. M., A. W. Herren, et al. (2012). "Ca2+/calmodulin-dependent protein kinase II (CaMKII) regulates cardiac sodium channel NaV1. 5 gating by multiple phosphorylation sites." Journal of Biological Chemistry **287**(24): 19856-19869.

Baker, P. F., M. P. Blaustein, et al. (1969). "The influence of calcium on sodium efflux in squid axons." J Physiol **200**(2): 431-458.

Barman, P., S. C. Choisy, et al. (2011). "beta-Adrenoceptor/PKA-stimulation, Na(+)-Ca(2+) exchange and PKA-activated Cl(-) currents in rabbit cardiomyocytes: a conundrum." Cell calcium **49**(4): 233-239.

Barrientos, G., D. D. Bose, et al. (2009). "The Na+/Ca2+ exchange inhibitor 2-(2-(4-(4-nitrobenzyloxy)phenyl)ethyl)isothiourea methanesulfonate (KB-R7943) also blocks ryanodine receptors type 1 (RyR1) and type 2 (RyR2) channels." Molecular Pharmacology **76**(3): 560-568.

Barry, W. H. (2000). "Na(+)-Ca(2+) exchange in failing myocardium: friend or foe?" Circ Res **87**(7): 529-531.

Bayer, R., R. Rodenkirchen, et al. (1977). "The effects of nifedipine on contraction and monophasic action potential of isolated cat myocardium." Naunyn-Schmiedeberg's archives of pharmacology **301**(1): 29-37.

Bayliss, W. M. (1902). "On the local reactions of the arterial wall to changes of internal pressure." Journal of Physiology-London **28**(3): 220-231.

Bers, D. M. (2002). "Cardiac excitation-contraction coupling." Nature **415**(6868): 198-205.

Bers, D. M. (2008). "Calcium cycling and signaling in cardiac myocytes." Annu Rev Physiol **70**: 23-49.

Bers, D. M. and J. H. Bridge (1989). "Relaxation of rabbit ventricular muscle by Na-Ca exchange and sarcoplasmic reticulum calcium pump. Ryanodine and voltage sensitivity." Circ Res **65**(2): 334-342.

Bersohn, M. M., R. Vemuri, et al. (1991). "Effect of temperature on sodium-calcium exchange in sarcolemma from mammalian and amphibian hearts." Biochimica et biophysica acta **1062**(1): 19-23.

Blaustein, M. P. and W. J. Lederer (1999). "Sodium/calcium exchange: its physiological implications." Physiological reviews **79**(3): 763-854.

Blaustein, M. P. and J. M. Russell (1975). "Sodium-Calcium Exchange and Calcium-Calcium Exchange in Internally Dialyzed Squid Giant-Axons." Journal of Membrane Biology **22**(3-4): 285-312.

Blaustein, M. P., J. M. Russell, et al. (1974). "Calcium efflux from internally dialyzed squid axons: the influence of external and internal cations." Journal of Supramolecular Structure **2**(5-6): 558-581.

Bogdanov, K. Y., T. M. Vinogradova, et al. (2001). "Sinoatrial nodal cell ryanodine receptor and Na(+)-Ca(2+) exchanger: molecular partners in pacemaker regulation." Circ Res **88**(12): 1254-1258.

Bolck, B., G. Munch, et al. (2004). "Na+/Ca2+ exchanger overexpression impairs frequency- and ouabain-dependent cell shortening in adult rat cardiomyocytes." American Journal of Physiology-Heart and Circulatory Physiology **287**(4): H1435-H1445.

Bolli, R. and E. Marban (1999). "Molecular and cellular mechanisms of myocardial stunning." Physiological reviews **79**(2): 609-634.

Bonazzola, P., P. Egido, et al. (2002). "Lithium and KB-R7943 effects on mechanics and energetics of rat heart muscle." Acta Physiol Scand **176**(1): 1-11.

Brette, F. and C. Orchard (2003). "T-tubule function in mammalian cardiac myocytes." Circ Res **92**(11): 1182-1192.

Brette, F. and C. Orchard (2007). "Resurgence of cardiac t-tubule research." Physiology **22**: 167-173.

Bridge, J. H., J. R. Smolley, et al. (1990). "The relationship between charge movements associated with ICa and INa-Ca in cardiac myocytes." Science **248**(4953): 376-378.

Cai, X. and J. Lytton (2004). "The cation/Ca2+ exchanger superfamily: phylogenetic analysis and structural implications." Molecular Biology and Evolution **21**(9): 1692-1703.

Carmeliet, E. (2004). "Intracellular Ca(2+) concentration and rate adaptation of the cardiac action potential." Cell calcium **35**(6): 557-573.

Choi, B. R. and G. Salama (2000). "Simultaneous maps of optical action potentials and calcium transients in guinea-pig hearts: mechanisms underlying concordant alternans." J Physiol **529 Pt 1**: 171-188.

Chudin, E., J. Goldhaber, et al. (1999). "Intracellular Ca(2+) dynamics and the stability of ventricular tachycardia." Biophys J **77**(6): 2930-2941.

Clusin, W. T. (2008). "Mechanisms of calcium transient and action potential alternans in cardiac cells and tissues." American journal of physiology. Heart and circulatory physiology **294**(1): H1-H10.

Cutler, M. J., D. Jeyaraj, et al. (2011). "Cardiac electrical remodeling in health and disease." Trends in pharmacological sciences **32**(3): 174-180.

Cyon, E. (1866). "Über den Einfluss der Temperaturänderungen auf Zahl, Dauer und Stärke der Herzschläge." Berichte über die Verhandlungen der Königlich Sächsischen Gesellschaft der Wissenschaften zu Leipzig. Mathematisch-Physische Classe **18**: 256-306.

de Burgh Daly, I. and A. J. Clark (1921). "The action of ions upon the frog's heart." Journal of Physiology-London **54**(5/6): 367-383.

Diaz, M. E., S. C. O'Neill, et al. (2004). "Sarcoplasmic reticulum calcium content fluctuation is the key to cardiac alternans." Circulation research **94**(5): 650-656.

DiFranco, M., J. Capote, et al. (2005). "Optical imaging and functional characterization of the transverse tubular system of mammalian muscle fibers using the potentiometric indicator di-8-ANEPPS." The Journal of membrane biology **208**(2): 141-153.

Döring, H. (1990). "The isolated perfused heart according to Langendorff technique--function--application." Physiologia Bohemoslovaca **39**(6): 481.

Dou, Y., P. Arlock, et al. (2007). "Blebbistatin specifically inhibits actin-myosin interaction in mouse cardiac muscle." Am J Physiol Cell Physiol **293**(3): C1148-1153.

Du, C., G. A. MacGowan, et al. (2001). "Calibration of the calcium dissociation constant of Rhod(2)in the perfused mouse heart using manganese quenching." Cell calcium **29**(4): 217-227.

Escobar, A. L., C. G. Perez, et al. (2012). "Role of inositol 1,4,5-trisphosphate in the regulation of ventricular Ca2+ signaling in intact mouse heart." Journal of molecular and cellular cardiology **53**(6): 768-779.

Fabiato, A. (1983). "Calcium-induced release of calcium from the cardiac sarcoplasmic reticulum." Am J Physiol **245**(1): C1-14.

Fabiato, A. (1992). "Two kinds of calcium-induced release of calcium from the sarcoplasmic reticulum of skinned cardiac cells." Adv Exp Med Biol **311**: 245-262.

Fabiato, A. and F. Fabiato (1975). "Contractions induced by a calcium-triggered release of calcium from the sarcoplasmic reticulum of single skinned cardiac cells." J Physiol **249**(3): 469-495.

Fan, J., Y. M. Shuba, et al. (1996). "Regulation of cardiac sodium-calcium exchanger by beta-adrenergic agonists." Proc Natl Acad Sci U S A **93**(11): 5527-5532.

Farman, G. P., K. Tachampa, et al. (2008). "Blebbistatin: use as inhibitor of muscle contraction." Pflugers Arch **455**(6): 995-1005.

Fedorov, V. V., I. T. Lozinsky, et al. (2007). "Application of blebbistatin as an excitation-contraction uncoupler for electrophysiologic study of rat and rabbit hearts." Heart Rhythm **4**(5): 619-626.

Ferreiro, M., A. D. Petrosky, et al. (2012). "Intracellular Ca2+ release underlies the development of phase 2 in mouse ventricular action potentials." American journal of physiology. Heart and circulatory physiology **302**(5): H1160-1172.

Gyorke, S. and C. Carnes (2008). "Dysregulated sarcoplasmic reticulum calcium release: potential pharmacological target in cardiac disease." Pharmacology & therapeutics **119**(3): 340-354.

Gyorke, S. and D. Terentyev (2008). "Modulation of ryanodine receptor by luminal calcium and accessory proteins in health and cardiac disease." Cardiovasc Res **77**(2): 245-255.

Harris, D. M., G. D. Mills, et al. (2005). "Alterations in early action potential repolarization causes localized failure of sarcoplasmic reticulum Ca2+ release." Circ Res **96**(5): 543-550.

Hartmann, M. and U. Decking (1999). "Blocking Na< sup>+</sup>,ÄìH< sup>+</sup> Exchange by Cariporide Reduces Na< sup>+</sup>-overload in Ischemia and is Cardioprotective." Journal of molecular and cellular cardiology **31**(11): 1985-1995.

He, H. P., F. J. Giordano, et al. (1997). "Overexpression of the rat sarcoplasmic reticulum Ca2+ ATPase gene in the heart of transgenic mice accelerates calcium transients and cardiac relaxation." Journal of Clinical Investigation **100**(2): 380-389.

Henderson, S. A., J. I. Goldhaber, et al. (2004). "Functional adult myocardium in the absence of Na+-Ca2+ exchange: cardiac-specific knockout of NCX1." Circ Res **95**(6): 604-611.

Hilge, M. (2012). "Ca2+ regulation of ion transport in the Na+/Ca2+ exchanger." J Biol Chem **287**(38): 31641-31649.

Hilgemann, D. W. (1989). "Giant Excised Cardiac Sarcolemmal Membrane Patches - Sodium and Sodium-Calcium Exchange Currents." Pflugers Archiv-European Journal of Physiology **415**(2): 247-249.

Hilgemann, D. W. (1990). "Regulation and Deregulation of Cardiac Na+-Ca2+ Exchange in Giant Excised Sarcolemmal Membrane Patches." Nature **344**(6263): 242-245.

Hilgemann, D. W. (1995). The giant membrane patch. Single-channel recording, Springer**:** 307-327.

Hilgemann, D. W. and A. Collins (1990). "Outward Na/Ca Exchange Current (Inaca) in Giant Excised Cardiac Sarcolemmal Membrane Patches." Biophys J **57**(2): A308-A308.

Hilgemann, D. W., D. A. Nicoll, et al. (1991). "Charge Movement during Na+ Translocation by Native and Cloned Cardiac Na+/Ca2+ Exchanger." Nature **352**(6337): 715-718.

Hobai, I. A. and B. O'Rourke (2000). "Enhanced Ca(2+)-activated Na(+)-Ca(2+) exchange activity in canine pacing-induced heart failure." Circ Res **87**(8): 690-698.

Hodgkin, A. L. and R. D. Keynes (1957). "Movements of Labelled Calcium in Squid Giant Axons." Journal of Physiology-London **138**(2): 253-281.

Huxley, A. F. and R. E. Taylor (1958). "Local activation of striated muscle fibres." J Physiol **144**(3): 426-441.

Imahashi, K., C. Pott, et al. (2005). "Cardiac-specific ablation of the Na+-Ca2+ exchanger confers protection against ischemia/reperfusion injury." Circ Res **97**(9): 916-921.

Iwamoto, T., S. Kita, et al. (2004). "Molecular determinants of Na+/Ca2+ exchange (NCX1) inhibition by SEA0400." J Biol Chem **279**(9): 7544-7553.

Iwamoto, T., S. Kita, et al. (2001). "Structural domains influencing sensitivity to isothiourea derivative inhibitor KB-R7943 in cardiac Nna(+)/Ca(2+) exchanger." Molecular Pharmacology **59**(3): 524-531.

Janiak, R., B. Lewartowski, et al. (1996). "Functional coupling between sarcoplasmic reticulum and Na/Ca exchange in single myocytes of guinea-pig and rat heart." Journal of molecular and cellular cardiology **28**(2): 253-264.

Katz, M. G., J. D. Swain, et al. (2010). "Cardiac gene therapy: optimization of gene delivery techniques in vivo." Human gene therapy **21**(4): 371-380.

Khananshvili, D. (2013). "The SLC8 gene family of sodium-calcium exchangers (NCX) - structure, function, and regulation in health and disease." Molecular aspects of medicine **34**(2-3): 220-235.

Kimura, J., S. Miyamae, et al. (1987). "Identification of sodium-calcium exchange current in single ventricular cells of guinea-pig." J Physiol **384**: 199-222.

Knollmann, B. C., N. Chopra, et al. (2006). "Casq2 deletion causes sarcoplasmic reticulum volume increase, premature Ca2+ release, and catecholaminergic polymorphic ventricular tachycardia." The Journal of clinical investigation **116**(9): 2510-2520.

Kornyeyev, D., A. D. Petrosky, et al. (2011). "Mechanisms Regulating the Organellar Ca2+ Dynamics in Intact Hearts During Ischemia-Reperfusion." Biophys J **100**(3, Supplement 1): 292a.

Kornyeyev, D., A. D. Petrosky, et al. (2011). "Calsequestrin 2 deletion shortens the refractoriness of Ca(2+) release and reduces rate-dependent Ca(2+)-alternans in intact mouse hearts." Journal of molecular and cellular cardiology.

Kornyeyev, D., M. Reyes, et al. (2010). "Luminal Ca2+ content regulates intracellular Ca2+ release in subepicardial myocytes of intact beating mouse hearts: effect of exogenous buffers." American Journal of Physiology-Heart and Circulatory Physiology **298**(6): H2138-H2153.

Kornyeyev, D., M. Reyes, et al. (2010). "Luminal Ca(2+) content regulates intracellular Ca(2+) release in subepicardial myocytes of intact beating mouse hearts: effect of exogenous buffers." American journal of physiology. Heart and circulatory physiology **298**(6): H2138-2153.

Kos, C. H. (2004). "Cre/loxP system for generating tissue-specific knockout mouse models." Nutrition Reviews **62**(6): 243-246.

Kusuoka, H., J. K. Porterfield, et al. (1987). "Pathophysiology and pathogenesis of stunned myocardium. Depressed Ca2+ activation of contraction as a consequence of reperfusion-induced cellular calcium overload in ferret hearts." The Journal of clinical investigation **79**(3): 950-961.

Lakatta, E. G. (2004). "Beyond Bowditch: the convergence of cardiac chronotropy and inotropy." Cell calcium **35**(6): 629-642.

Langendorff, O. (1898). "Untersuchungen am überlebenden säugethierherzen." Pflügers Archiv European Journal of Physiology **61**(9): 291−332.

Langer, G. A. (1964). "Kinetic Studies of Calcium Distribution in Ventricular Muscle of Dog." Circ Res **15**(5): 393-&.

Larbig, R., N. Torres, et al. (2010). "Activation of reverse Na(+)-Ca(2+) exchange by the Na(+) current augments the cardiac Ca(2+) transient: evidence from NCX knockout mice." Journal of Physiology-London **588**(17): 3266-3276.

Laurita, K. R., R. Katra, et al. (2003). "Transmural heterogeneity of calcium handling in canine." Circ Res **92**(6): 668-675.

Leblanc, N. and J. R. Hume (1990). "Sodium current-induced release of calcium from cardiac sarcoplasmic reticulum." Science **248**(4953): 372-376.

Linz, K. W. and R. Meyer (1998). "The late component of L-type calcium current during guinea-pig cardiac action potentials and its contribution to contraction." Pflugers Archiv : European journal of physiology **436**(5): 679-688.

Litwin, S. E., J. Li, et al. (1998). "Na-Ca exchange and the trigger for sarcoplasmic reticulum Ca release: studies in adult rabbit ventricular myocytes." Biophys J **75**(1): 359-371.

Lopez-Lopez, J. R., P. S. Shacklock, et al. (1995). "Local calcium transients triggered by single L-type calcium channel currents in cardiac cells." Science **268**(5213): 1042-1045.

Luttgau, H. C. and R. Niedergerke (1958). "The Antagonism between Ca and Na Ions on the Frogs Heart." Journal of Physiology-London **143**(3): 486-505.

Lytton, J. (2007). "Na+/Ca2+ exchangers: three mammalian gene families control Ca2+ transport." Biochem. J **406**: 365-382.

Lytton, J., M. Westlin, et al. (1991). "Thapsigargin inhibits the sarcoplasmic or endoplasmic reticulum Ca-ATPase family of calcium pumps." J Biol Chem **266**(26): 17067-17071.

Johan Mähler and Ingmar Persson(2012). A Study of the Hydration of the Alkali Metal Ions in Aqueous Solution. Inorg Chem; 51(1): 425–438.

Matsuda, T., Y. Koyama, et al. (2005). "Functional proteins involved in regulation of intracellular Ca(2+) for drug development: pharmacology of SEA0400, a specific inhibitor of the Na(+)-Ca(2+) exchanger." J Pharmacol Sci **97**(3): 339-343.

Matsumoto, T., T. Miura, et al. (2003). "Does enhanced expression of the Na+-Ca2+ exchanger increase myocardial vulnerability to ischemia/reperfusion injury in rabbit hearts?" Mol Cell Biochem **248**(1-2): 141-147.

Matsuoka, S., D. A. Nicoll, et al. (1993). "Initial Localization of Regulatory Regions of the Cardiac Sarcolemmal Na+-Ca2+ Exchanger." Proc Natl Acad Sci U S A **90**(9): 3870-3874.

Mazzanti, M. and L. J. DeFelice (1990). "Ca channel gating during cardiac action potentials." Biophys J **58**(4): 1059-1065.

Mejia-Alvarez, R., C. Manno, et al. (2003). "Pulsed local-field fluorescence microscopy: a new approach for measuring cellular signals in the beating heart." Pflugers Arch **445**(6): 747-758.

Mitchell, M. R., T. Powell, et al. (1984). "The effects of ryanodine, EGTA and low-sodium on action potentials in rat and guinea-pig ventricular myocytes: evidence for two inward currents during the plateau." Br J Pharmacol **81**(3): 543-550.

Montana, V., D. L. Farkas, et al. (1989). "Dual-wavelength ratiometric fluorescence measurements of membrane potential." Biochemistry **28**(11): 4536-4539.

Mullins, L. J. and F. J. Brinley (1975). "Sensitivity of Calcium Efflux from Squid Axons to Changes in Membrane-Potential." Journal of General Physiology **65**(2): 135-152.

Neely, J. R., Lieberme.H, et al. (1967). "Effect of Pressure Development on Oxygen Consumption by Isolated Rat Heart." Am J Physiol Cell Physiol **212**(4): 804-&.

Nemec, J., J. J. Kim, et al. (2010). "Calcium oscillations and T-wave lability precede ventricular arrhythmias in acquired long QT type 2." Heart rhythm : the official journal of the Heart Rhythm Society **7**(11): 1686-1694.

Nicoll, D. A., S. Longoni, et al. (1990). "Molecular cloning and functional expression of the cardiac sarcolemmal Na(+)-Ca2+ exchanger." Science **250**(4980): 562-565.

Niederge.R and R. K. Orkand (1966). "Dependence of Action Potential of Frogs Heart on External and Intracellular Sodium Concentration." Journal of Physiology-London **184**(2): 312-&.

Niederge.R and R. K. Orkand (1966). "Dual Effect of Calcium on Action Potential of Frogs Heart." Journal of Physiology-London **184**(2): 291-&.

Niedergerke, R. (1963). "Movements of Ca in Beating Ventricles of Frog Heart." Journal of Physiology-London **167**(3): 551-&.

Niedergerke, R. (1963). "Movements of Ca in Frog Heart Ventricles at Rest and during Contractures." Journal of Physiology-London **167**(3): 515-&.

Oehlke, J., M. Beyermann, et al. (1997). "Evidence for extensive and non-specific translocation of oligopeptides across plasma membranes of mammalian cells." Biochimica Et Biophysica Acta-Biomembranes **1330**(1): 50-60.

Opie, L. H. (2004). Heart physiology: from cell to circulation, Wolters Kluwer Health.

Ottolia, M. and K. D. Philipson (2013). NCX1: Mechanism of Transport. Sodium Calcium Exchange: A Growing Spectrum of Pathophysiological Implications, Springer**:** 49-54.

Petrosky, A. D., R. Mejia-Alvarez, et al. (2013). "Impact of SR Ca2+ Release on the Cardiac Action Potential Repolarization during Postnatal Development." Biophys J **104**: 290.

Petrosky, A. D., B. Zepeda, et al. (2012). "Relationship Between Ca2+ Alternans and T-Wave Alternans: Role of Calsequestrin and Sorcin." Biophys J **102**: 553.

Pfaffl, M. W. (2001). "A new mathematical model for relative quantification in real-time RT-PCR." Nucleic Acids Research **29**(9).

Pham, Q., K. J. Quan, et al. (2003). "T-wave alternans: marker, mechanism, and methodology for predicting sudden cardiac death." Journal of electrocardiology **36 Suppl**: 75-81.

Philipson, K. D. and D. A. Nicoll (2000). "Sodium-calcium exchange: a molecular perspective." Annu Rev Physiol **62**: 111-133.

Piacentino, V., 3rd, J. P. Gaughan, et al. (2002). "L-type Ca(2+) currents overlapping threshold Na(+) currents: could they be responsible for the "slip-mode" phenomenon in cardiac myocytes?" Circ Res **90**(4): 435-442.

Pogwizd, S. M. (2000). "Increased Na(+)-Ca(2+) exchanger in the failing heart." Circ Res **87**(8): 641-643.

Pogwizd, S. M., M. Qi, et al. (1999). "Upregulation of Na(+)/Ca(2+) exchanger expression and function in an arrhythmogenic rabbit model of heart failure." Circ Res **85**(11): 1009-1019.

Pogwizd, S. M., K. Schlotthauer, et al. (2001). "Arrhythmogenesis and contractile dysfunction in heart failure: Roles of sodium-calcium exchange, inward rectifier potassium current, and residual beta-adrenergic responsiveness." Circ Res **88**(11): 1159-1167.

Pott, C., S. A. Henderson, et al. (2007). "Na+/Ca2+ exchanger knockout mice: plasticity of cardiac excitation-contraction coupling." Ann N Y Acad Sci **1099**: 270-275.

Pott, C., A. Muszynski, et al. (2012). "Proarrhythmia in a non-failing murine model of cardiac-specific Na+/Ca 2+ exchanger overexpression: whole heart and cellular mechanisms." Basic Res Cardiol **107**(2): 247.

Pott, C., K. D. Philipson, et al. (2005). "Excitation-contraction coupling in Na+-Ca2+ exchanger knockout mice: reduced transsarcolemmal Ca2+ flux." Circ Res **97**(12): 1288-1295.

Pott, C., X. Ren, et al. (2007). "Mechanism of shortened action potential duration in Na+-Ca2+ exchanger knockout mice." Am J Physiol Cell Physiol **292**(2): C968-973.

Pott, C., M. Yip, et al. (2007). "Regulation of cardiac L-type Ca2+ current in Na+-Ca2+ exchanger knockout mice: functional coupling of the Ca2+ channel and the Na+-Ca2+ exchanger." Biophys J **92**(4): 1431-1437.

Qin, J., M. Porta, et al. (2005). "Lumlumenal calcium regulation of single ryanodine receptor channels (RyRs)." Biophys J **88**(1): 486A-486A.

Quednau, B. D., D. A. Nicoll, et al. (2004). "The sodium/calcium exchanger family-SLC8." Pflugers Archiv : European journal of physiology **447**(5): 543-548.

Ranu, H. K., C. M. Terracciano, et al. (2002). "Effects of Na(+)/Ca(2+)-exchanger overexpression on excitation-contraction coupling in adult rabbit ventricular myocytes." Journal of molecular and cellular cardiology **34**(4): 389-400.

Reeves, J. P. and C. C. Hale (1984). "The Stoichiometry of the Cardiac Sodium-Calcium Exchange System." Journal of Biological Chemistry **259**(12): 7733-7739.

Reuter, H. and N. Seitz (1968). "Dependence of Calcium Efflux from Cardiac Muscle on Temperature and External Ion Composition." Journal of Physiology-London **195**(2): 451-&.

Ringer, S. (1883). "A further contribution regarding the influence of the different constituents of the blood on the contraction of the heart." J Physiol **4**(1): 29-42.

Rosenbaum, D. S. (2008). "T-wave alternans in the sudden cardiac death in heart failure trial population: signal or noise?" Circulation **118**(20): 2015-2018.

Rosenbaum, D. S., L. E. Jackson, et al. (1994). "Electrical alternans and vulnerability to ventricular arrhythmias." New England Journal of Medicine **330**(4): 235-241.

Said, M., R. Becerra, et al. (2008). "Increased intracellular Ca2+ and SR Ca2+ load contribute to arrhythmias after acidosis in rat heart. Role of Ca2+/calmodulin-dependent protein kinase II." American journal of physiology. Heart and circulatory physiology **295**(4): H1669-1683.

Sakamoto, T., J. Limouze, et al. (2005). "Blebbistatin, a myosin II inhibitor, is photoinactivated by blue light." Biochemistry **44**(2): 584-588.

Sasse, P., J. Zhang, et al. (2007). "Intracellular Ca2+ oscillations, a potential pacemaking mechanism in early embryonic heart cells." J Gen Physiol **130**(2): 133-144.

Satoh, H., K. S. Ginsburg, et al. (2000). "KB-R7943 block of Ca(2+) influx via Na(+)/Ca(2+) exchange does not alter twitches or glycoside inotropy but prevents Ca(2+) overload in rat ventricular myocytes." Circulation **101**(12): 1441-1446.

Schouten, V. J. A. and H. E. D. J. Terkeurs (1985). "The Slow Repolarization Phase of the Action-Potential in Rat-Heart." Journal of Physiology-London **360**(Mar): 13-25.

Schram, G., M. Pourrier, et al. (2002). "Differential distribution of cardiac ion channel expression as a basis for regional specialization in electrical function." Circ Res **90**(9): 939-950.

Sham, J. S., L. Cleemann, et al. (1992). "Gating of the cardiac Ca2+ release channel: the role of Na+ current and Na(+)-Ca2+ exchange." Science **255**(5046): 850-853.

Shimizu, W. and C. Antzelevitch (1999). "Cellular and ionic basis for T-wave alternans under long-QT conditions." Circulation **99**(11): 1499-1507.

Shinada, T., Y. Hirayama, et al. (2005). "Inhibition of the reverse mode of the Na+/Ca2+ exchange by KB-R7943 augments arrhythmogenicity in the canine heart during rapid heart rates." Journal of electrocardiology **38**(3): 218-225.

Shmigol, A. V., D. A. Eisner, et al. (2001). "Simultaneous measurements of changes in sarcoplasmic reticulum and cytosolic [Ca2+] in rat uterine smooth muscle cells." Journal of Physiology-London **531**(3): 707-713.

Sipido, K. R., M. Maes, et al. (1997). "Low efficiency of Ca2+ entry through the Na(+)-Ca2+ exchanger as trigger for Ca2+ release from the sarcoplasmic reticulum. A comparison between L-type Ca2+ current and reverse-mode Na(+)-Ca2+ exchange." Circ Res **81**(6): 1034-1044.

Sipido, K. R., P. G. Volders, et al. (2002). "Altered Na/Ca exchange activity in cardiac hypertrophy and heart failure: a new target for therapy?" Cardiovasc Res **53**(4): 782-805.

Skrzypiec-Spring, M., B. Grotthus, et al. (2007). "Isolated heart perfusion according to Langendorff‚Äîstill viable in the new millennium." Journal of pharmacological and toxicological methods **55**(2): 113-126.

Spencer, C. I. and J. S. Sham (2003). "Effects of Na+/Ca2+ exchange induced by SR Ca2+ release on action potentials and afterdepolarizations in guinea pig ventricular myocytes." American journal of physiology. Heart and circulatory physiology **285**(6): H2552-2562.

Szentesi, P., C. Pignier, et al. (2004). "Sarcoplasmic reticulum Ca2+ refilling controls recovery from Ca2+-induced Ca2+ release refractoriness in heart muscle." Circ Res **95**(8): 807-813.

Tanaka, H., I. Namekata, et al. (2005). "Unique excitation-contraction characteristics of mouse myocardium as revealed by SEA0400, a specific inhibitor of Na+-Ca2+ exchanger." Naunyn-Schmiedeberg's archives of pharmacology **371**(6): 526-534.

Tanaka, H., K. Nishimaru, et al. (2002). "Effect of SEA0400, a novel inhibitor of sodium-calcium exchanger, on myocardial ionic currents." Br J Pharmacol **135**(5): 1096-1100.

Ter Keurs, H. E. and P. A. Boyden (2007). "Calcium and arrhythmogenesis." Physiological reviews **87**(2): 457-506.

Terentyev, D., S. Viatchenko-Karpinski, et al. (2002). "Luminal Ca2+ controls termination and refractory behavior of Ca2+-induced Ca2+ release in cardiac myocytes." Circ Res **91**(5): 414-420.

Terracciano, C. M., A. I. Souza, et al. (1998). "Na+-Ca2+ exchange and sarcoplasmic reticular Ca2+ regulation in ventricular myocytes from transgenic mice overexpressing the Na+-Ca2+ exchanger." J Physiol **512 (Pt 3)**: 651-667.

Toyoshima, C. and H. Nomura (2002). "Structural changes in the calcium pump accompanying the dissociation of calcium." Nature **418**(6898): 605-611.

Ussing, H. H. (1947). "Interpretation of the Exchange of Radio-Sodium in Isolated Muscle." Nature **160**(4060): 262-263.

Valverde, C. A., D. Kornyeyev, et al. "Transient Ca2+ depletion of the sarcoplasmic reticulum at the onset of reperfusion." Cardiovasc Res **85**(4): 671-680.

Verrier, R. L., K. Kumar, et al. (2009). "Basis for sudden cardiac death prediction by T-wave alternans from an integrative physiology perspective." Heart rhythm : the official journal of the Heart Rhythm Society **6**(3): 416-422.

Vittone, L., C. Mundina-Weilenmann, et al. (2002). "Time course and mechanisms of phosphorylation of phospholamban residues in ischemia-reperfused rat hearts. Dissociation of phospholamban phosphorylation pathways." Journal of molecular and cellular cardiology **34**(1): 39-50.

Volders, P. G., M. A. Vos, et al. (2000). "Progress in the understanding of cardiac early afterdepolarizations and torsades de pointes: time to revise current concepts." Cardiovasc Res **46**(3): 376-392.

Wagner, S., N. Dybkova, et al. (2006). "Ca2+/calmodulin-dependent protein kinase II regulates cardiac Na+ channels." Journal of Clinical Investigation **116**(12): 3127-3138.

Wan, X., K. R. Laurita, et al. (2005). "Molecular correlates of repolarization alternans in cardiac myocytes." J Mol Cell Cardiol **39**(3): 419-428.

Wilson, L. D. and D. S. Rosenbaum (2007). "Mechanisms of arrythmogenic cardiac alternans." Europace : European pacing, arrhythmias, and cardiac electrophysiology : journal of the working groups on cardiac pacing, arrhythmias, and cardiac cellular electrophysiology of the European Society of Cardiology **9 Suppl 6**: vi77-82.

Xie, L. H., D. Sato, et al. (2008). "Intracellular Ca alternans: coordinated regulation by sarcoplasmic reticulum release, uptake, and leak." Biophys J **95**(6): 3100-3110.

Xu, L., J. Chen, et al. (2011). "Analysis of Na(+)/Ca (2+) exchanger (NCX) function and current in murine cardiac myocytes during heart failure." Molecular biology reports.

Yao, A., Z. Su, et al. (1998). "Effects of overexpression of the Na+-Ca2+ exchanger on [Ca2+]i transients in murine ventricular myocytes." Circ Res **82**(6): 657-665.

Young, H. S., C. Xu, et al. (2001). "Locating the thapsigargin-binding site on Ca(2+)-ATPase by cryoelectron microscopy." Journal of molecular biology **308**(2): 231-240.

Zhang, L., J. Kelley, et al. (1997). "Complex formation between junctin, triadin, calsequestrin, and the ryanodine receptor. Proteins of the cardiac junctional sarcoplasmic reticulum membrane." J Biol Chem **272**(37): 23389-23397.

Zimmer, H. G. (1998). "The isolated perfused heart and its pioneers." News in Physiological Sciences **13**: 203-210.

Zipes, D. P., A. J. Camm, et al. (2006). "ACC/AHA/ESC 2006 Guidelines for Management of Patients With Ventricular Arrhythmias and the Prevention of

Sudden Cardiac Death: A Report of the American College of Cardiology/American Heart Association Task Force and the European Society of Cardiology Committee for Practice Guidelines (Writing Committee to Develop Guidelines for Management of Patients With Ventricular Arrhythmias and the Prevention of Sudden Cardiac Death)." Journal of the American College of Cardiology **48**(5): e247-e346.

Zoghbi, M. E., J. A. Copello, et al. (2004). "Differential Ca2+ and Sr2+ regulation of intracellular divalent cations release in ventricular myocytes." Cell calcium **36**(2): 119-134.

Zygmunt, A. C., R. J. Goodrow, et al. (2000). "I(NaCa) contributes to electrical heterogeneity within the canine ventricle." American journal of physiology. Heart and circulatory physiology **278**(5): H1671-1678.

Journal of Molecular and Cellular Cardiology 52 (2012) 21–31

Contents lists available at SciVerse ScienceDirect

Journal of Molecular and Cellular Cardiology

journal homepage: www.elsevier.com/locate/yjmcc

Original article

Calsequestrin 2 deletion shortens the refractoriness of Ca^{2+} release and reduces rate-dependent Ca^{2+}-alternans in intact mouse hearts

Dmytro Kornyeyev [a], Azade D. Petrosky [a], Bernardo Zepeda [a], Marcela Ferreiro [a], Bjorn Knollmann [b], Ariel L. Escobar [a,*]

[a] School of Engineering, University of California Merced, Merced, CA, USA
[b] Division of Clinical Pharmacology, School of Medicine, Vanderbilt University, Nashville, TN, USA

ARTICLE INFO

Article history:
Received 19 June 2011
Received in revised form 18 September 2011
Accepted 20 September 2011
Available online 29 September 2011

Keywords:
Whole heart
Calcium
Calsequestrin
Ventricular arrhythmias
Alternans

ABSTRACT

Calsequestrin (Casq2) is a low affinity Ca^{2+}-binding protein located in sarcoplasmic reticulum (SR) of cardiac myocytes. Casq2 acts as a Ca^{2+} buffer regulating free Ca^{2+} concentration in the SR lumen and plays a significant role in the regulation of Ca^{2+} release from this intracellular organelle. In addition, there is experimental evidence supporting the hypothesis that Casq2 also modulates the activity of the cardiac Ca^{2+} release channels, ryanodine receptors (RyR2). In this study, Casq2 knockout mice (Casq2−/−) were used as a model to evaluate the effects of the Casq2 on the cytosolic and intra-SR Ca^{2+} dynamics, and the electrical activity in the ventricular epicardial layer of intact beating hearts. Casq2−/− mice have accelerated intra-SR Ca^{2+} refilling kinetics (76 ± 22 *vs.* 136.5 ± 15 ms) and a reduced refractoriness of Ca^{2+} release (182 ± 32 ms Casq2+/+ and 111 ± 22 ms Casq2−/−). In addition, mice display reduced Ca^{2+} alternans (67% decline in the amplitude of Ca^{2+} alternans at 7 Hz, 21oC) and less T-wave alternans at the electrocardiographic level. The results presented in this paper support the idea of Casq2 acting both as a buffer and a direct regulator of the Ca^{2+} release process. Finally, we propose that alterations in Ca^{2+} release refractoriness shown here could explain the relationship between Casq2 function and an increase in the risk for ventricular arrhythmias.

1. Introduction

Calsequestrin 2 (Casq2) is the major Ca^{2+}-binding protein located in sarcoplasmic reticulum (SR) of cardiomyocytes [1]. Casq2, together with the cardiac ryanodine receptor (RyR2), triadin, and junctin, forms the so-called junctional complex of Ca^{2+} release units (CRU) [2]. These CRU play a key role in regulating the phenomenon known as Ca^{2+}-induced Ca^{2+} release (CICR). CICR controls the massive Ca^{2+} efflux from the SR in response to the activation of RyR2 by Ca^{2+} ions entering the cell through voltage-dependent L-type Ca^{2+} channels during action potential (AP) [3,4].

As a low-affinity, high-capacity Ca^{2+}-binding protein [5], Casq2 was initially thought to be a Ca^{2+}-storage protein (for review see Ref. [6]). Nevertheless, more recent studies suggested that Casq2 can also be involved in controlling CICR by regulating sites at the luminal side of the RyR2 complex [7–10]. The pathophysiological importance of Casq2 has been revealed by the identification of mutations in Casq2 gene that have been associated with catecholaminergic polymorphic ventricular tachycardia (CPVT) in humans [11–13].

Interestingly, cardiac contractile function is not affected in mice lacking Casq2 or in humans displaying changes in Casq2 properties [13,14]. Moreover, Ca^{2+} storage and release measured in isolated cardiac myocytes have been shown to be largely unaltered [14,15].

In order to consider Casq2 as a potential target for clinical treatment, it is important to identify the role of Casq2 in the regulation of the cardiac function. Although the role of Casq2 has been studied in cardiac ventricular myocytes [10,16,17], a further assessment of subcellular Ca^{2+} dynamics in intact hearts of transgenic mice lacking this protein [14] will help us to understand its physiological role during the cardiac cycle. The goal of our experimental approach was to evaluate the role of Casq2 in the regulation of Ca^{2+} release in intact hearts. Specifically, we tested the following idea: if Casq2 directly regulates RyR2, the ablation of this protein should change the time-dependency of recovery of Ca^{2+} release (restitution) and consequently the dependency of Ca^{2+} transients on heart rate. Additionally, as intracellular Ca^{2+} release modifies the repolarization of the AP, transmural changes of the AP repolarization across the ventricular free wall could lead to proarrhythmic electrical events detectable on an electrocardiographic recording. This concept of an intra-organelle protein controlling the electrical activity of the plasma membrane will enlighten novel possible regulatory mechanisms of the cardiac function.

* Corresponding author at: School of Engineering, University of California, Merced, P.O. Box 2039, Merced, CA, 95344, USA. Tel.: +1 209 281 4618; fax: +1 209 228 4047.
E-mail address: aescobar4@ucmerced.edu (A.L. Escobar).

0022-2828/$ – see front matter © 2011 Elsevier Ltd. All rights reserved.
doi:10.1016/j.yjmcc.2011.09.020

To evaluate this mechanism, we conducted experiments on intact hearts under conditions similar to *in vivo* to preserve the integrity of the cardiac tissue. Alterations in the Ca^{2+} transients' restitution, the time course of the SR Ca^{2+} replenishment, heart rate dependency of the Ca^{2+} transients and modification of the electrocardiographic profile were observed. Thus, we conclude that the ablation of Casq2 not only defines the refractoriness of contractility but also alters the electrocardiographic activity under tachycardic conditions.

2. Materials and methods

2.1. Transgenic KO animals

Transgenic mice lacking Casq2 (Casq2−/−) and wild-type (Casq2+/+) animals [14] were used for all studies. All animal studies were approved by the UC Merced Institutional Animal Care and Use Committee (IACUC) and performed in accordance with NIH guidelines.

2.2. Heart preparation

Hearts were obtained from young (3–7 week-old) animals. The aorta was cannulated on a horizontal Langendorff apparatus and perfused with Tyrode solution (2 mM $CaCl_2$, 140 mM NaCl, 5.4 mM KCl, 1 mM $MgCl_2$, 0.33 mM Na_2HPO_4, 10 mM HEPES, 10 mM glucose, pH = 7.4). All reagents and chemicals were purchased from Sigma-Aldrich Chemical Company unless otherwise indicated. Temperature of extracellular solutions was controlled with a Peltier unit. All solutions were equilibrated with 100% oxygen.

2.3. Fluorophores loading

Mag-fluo-4 AM was used to measure the intra-SR free [Ca^{2+}]. The dye was dissolved in 45 μl of DMSO/pluronic acid and 1 ml of normal Tyrode (final concentration 61.2 μM). The loading was performed as described before (see Ref. [18,19] for additional information on this technique). Previously results published by our laboratory demonstrated that, despite relatively high concentration of Ca^{2+} in SR, mag-fluo-4 inside the SR does not become saturated under our experimental conditions and can be effectively used to monitor intra-SR Ca^{2+} dynamics [19]. Moreover, there was no evidence of the effect of the dye saturation on the amplitude or the kinetics of the fluorescence signals recorded with mag-fluo-4 in the hearts of the transgenic mice lacking Casq2.

Rhod-2 AM (final concentration of 44.5 μM) and the potentiometric dye di-8-ANEPPS (final concentration of 1.6 μM) were used to measure cytosolic Ca^{2+} signals and membrane potential respectively. These dyes were prepared in a similar way as mag-fluo-4 AM. For measurements with di-8-ANEPPS intact hearts were immobilized by adding blebbistatin (7.5 μM) into Tyrode solution. A number of studies have shown that, at this concentration, blebbistatin has no significant side effects on either Ca^{2+} transients or AP [20–23]. All dyes were purchased from Invitrogen, USA.

2.4. Optical setup

A modified version of our custom-made setup for Pulsed Local-Field Fluorescence microscopy [24] was employed to measure fluorescent signals from the intact heart. Two solid-state Nd-YAG lasers, blue (473 nm) and green (532 nm), were used as illuminating sources (Enlight Technologies, USA). Both lasers were optically multiplexed by ferroelectric modulators (Newport, USA).

The excitation light was focused into a multimode optical fiber and the emitted light was carried back through the same fiber, filtered to eliminate the reflected excitation component, and focused on an avalanche diode connected to an integrating I–V converter controlled by Digital Signal Processor (DSP 320, Texas Instruments). Fluorescence signals were digitized at 5 MHz and filtered to 500 kHz.

One end of the optic fiber was gently placed on the tissue to attenuate the motion artifacts. After electrically ablating the pacemaker cells with an ophthalmic bipolar pencil (Mentor Ophthalmics, USA), the hearts were paced at various rates by means of an electrical stimulator ISOSTIM A320R (WPI, USA) controlled by a PC. A set of bipolar pacing platinum electrodes was positioned at the base of the left ventricle.

2.5. Whole heart electrophysiological measurements

APs were recorded from the epicardial layer of the left ventricle. The signals were recorded using glass microelectrode filled with 3 M KCl (10–20 MΩ resistance) and an electrometric amplifier Duo 773 (WPI, USA). The electrical signals were digitized at frequency of 500 kHz.

Electrocardiographic recordings were performed by placing one Ag–AgCl micropellet inside the left ventricle and a second pellet outside the left ventricle. Signals were amplified by a custom-made DC-coupled instrumentation amplifier and were digitally sampled identically to the AP recordings.

2.6. Restitution protocols

Restitution curves were obtained by applying an additional stimulation pulse (S2) at different times (described as S1–S2 coupling intervals) with respect to the regular pacing pulses (S1). By changing the time interval between electrical stimulations (S1–S2), we were able to analyze the kinetics of the recovery of different variables such as Ca^{2+}-transients, intra-SR Ca^{2+} signals and AP triggering. Fractional recovery ratios (A2/A1) were calculated from the amplitudes of the variables at the S2 (extrasystolic) and S1 (regular baseline pacing) stimulations. Restitution curves were built using data from several independent experiments (hearts) and presented as semilog plots to better illustrate the exponential nature of the recovery process.

2.7. Statistical analysis

Data are presented as means ± standard deviations (SD). The total number of animals used in this study was 87 (44 Casq2−/− and 43 Casq2+/+). Normality test (Shapiro–Wilk) was performed prior to application of one-way ANOVA. Differences were considered to be significant if the value of p was less than 0.05.

3. Results

3.1. Cytosolic Ca^{2+}-transients from the epicardial layer of Casq2 KO mice

Casq2 ablation is expected to modify intracellular Ca^{2+} dynamics. We evaluated this hypothesis by measuring cytosolic Ca^{2+} transients in hearts from Casq2+/+ and Casq2−/− mice loaded with rhod-2 AM. Unexpectedly, the Ca^{2+} transients recorded from both genotypes did not reveal significant differences between them (Fig. 1 A). The time to peak and the decay time constants were similar at 2 mM extracellular [Ca^{2+}] (Table 1) most likely due to morphological factors, namely changes in the SR volume [14] or homeostatic conditions such as a divalent saturation of Casq2.

This latter possibility was tested by reducing the intra-SR [Ca^{2+}]. For example, when extracellular Ca^{2+} was reduced from 2 mM to 0.5 mM, mag-fluo-4 diastolic fluorescence level decreased by 16 ± 11% (n = 8, $p = 0.001$, 37 °C, 4 Hz).

As expected, the amplitude of Ca^{2+}-transients for both genotypes declined as a result of a reduction in the extracellular [Ca^{2+}] (Figs. 1B and C). A summary of the effect of extracellular Ca^{2+} on the

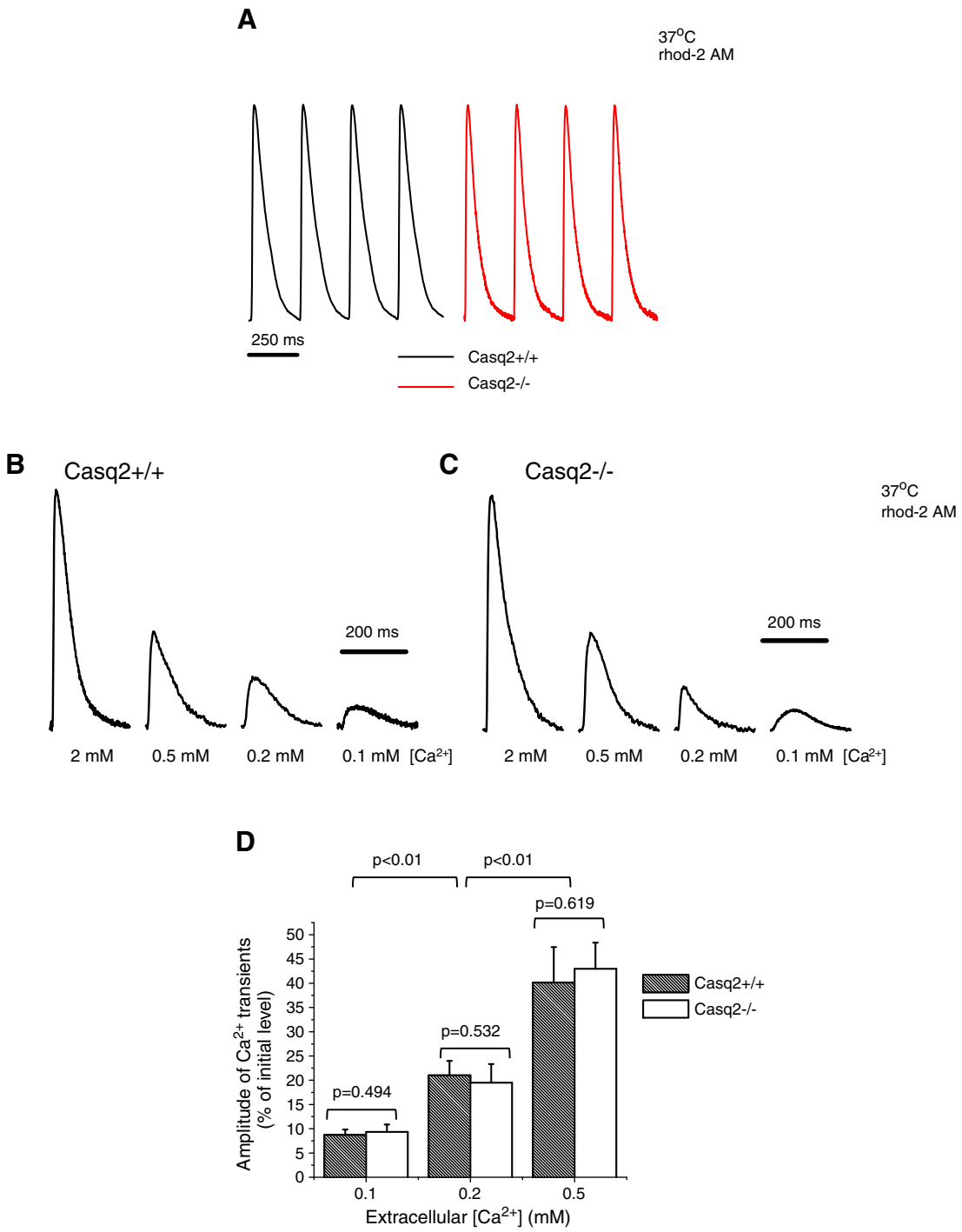

Fig. 1. Typical Ca^{2+}-transients recorded with the cytosolic Ca^{2+} indicator (rhod-2 AM) in the intact hearts of Casq2+/+ (black line) and Casq2−/− (red line) mice at 37 °C and at a stimulation frequency of 4 Hz (A). Cytosolic Ca^{2+} transients (rhod-2 AM) recorded from the intact hearts of Casq2+/+ (B) and Casq2−/− (C) at different concentrations of $CaCl_2$ in Tyrode solution (37 °C and 4 Hz). Panel D shows the effect of low extracellular Ca^{2+} on the amplitude of Ca^{2+} release in control (empty columns) and knockout (filled columns) animals. Data is expressed as percentage of the initial amplitude determined at 2 mM $CaCl_2$. Data are means ± standard deviations (n = 3–5). *p* values located above the pairs of columns represent the results of the comparison Casq2+/+ *versus* Casq2−/− for that particular pair of columns.

amplitude of the Ca^{2+} transients is presented in Fig. 1D. The differences are significant for different extracellular [Ca^{2+}] but not between both genotypes at the same extracellular [Ca^{2+}].

Additionally, the rise time of the Ca^{2+} transients increased as extracellular Ca^{2+} decreased. This effect was more prominent in Casq2−/− than in the control animals. Lower extracellular Ca^{2+} (0.1 mM) significantly increased the time to peak and the rise time of Ca^{2+} transients, in 1.6-fold and 2-fold respectively for Casq2−/− animals in comparison to Casq2+/+ (Table 1). Summarizing, the experiments presented in this section showed that, at physiological extracellular Ca^{2+}, the absence of Casq2 did not affect the kinetics of cytosolic Ca^{2+} transients of beating hearts stimulated with low (bradycardic) frequency.

Table 1
Effect of extracellular Ca^{2+} on Ca^{2+} dynamics in the hearts of control animals (Casq2+/+) and transgenic mice lacking Casq2 (Casq2−/−). The experiments were conducted at 37 °C and 4 Hz. The decay time constant was determined as the time between 10% and 90% of the relaxation divided by 2.2. Rise time is the time between 10% and 90% of increase in the signal during Ca^{2+} release. Data are means ± SD.

Parameter	Concentration of [Ca^{2+}] in Tyrode solution					
	2 mM			0.1 mM		
	Casq2+/+	Casq2−/−	*p* value	Casq2+/+	Casq2−/−	*p* value
Number of experiments (hearts)	9	7		8	7	
Time to peak (ms)	16 ± 2	16 ± 1	0.998	31 ± 7	51 ± 8	0.001
Rise time (ms)	7 ± 1	8 ± 1	0.908	15 ± 2	30 ± 6	0.001
Decay time constant (ms)	59 ± 4	53 ± 9	0.093	64 ± 5	60 ± 5	0.131

3.2. Refractoriness of Ca^{2+} release from the epicardial layer of Casq2 KO mice

The refractoriness of Ca^{2+} release is defined as the time-dependent recovery (restitution) of Ca^{2+} release. This strongly depends on how fast the SR can be reloaded and become ready to release Ca^{2+} in addition to the refractoriness of the trigger (I_{Ca}). A significant change in the SR Ca^{2+} buffer capacity should introduce a modification in the refractoriness of Ca^{2+} release [19]. Thus, we generated restitution curves by applying an additional extrasystolic stimulation pulse (see Section 2.6) (Figs. 2A and B). The fractional recovery of Ca^{2+} release was calculated as the ratio between the amplitude of the Ca^{2+} transient after an extrasystolic stimulation (A2 on Fig. 2C) and the amplitude of the Ca^{2+} transient during regular pacing

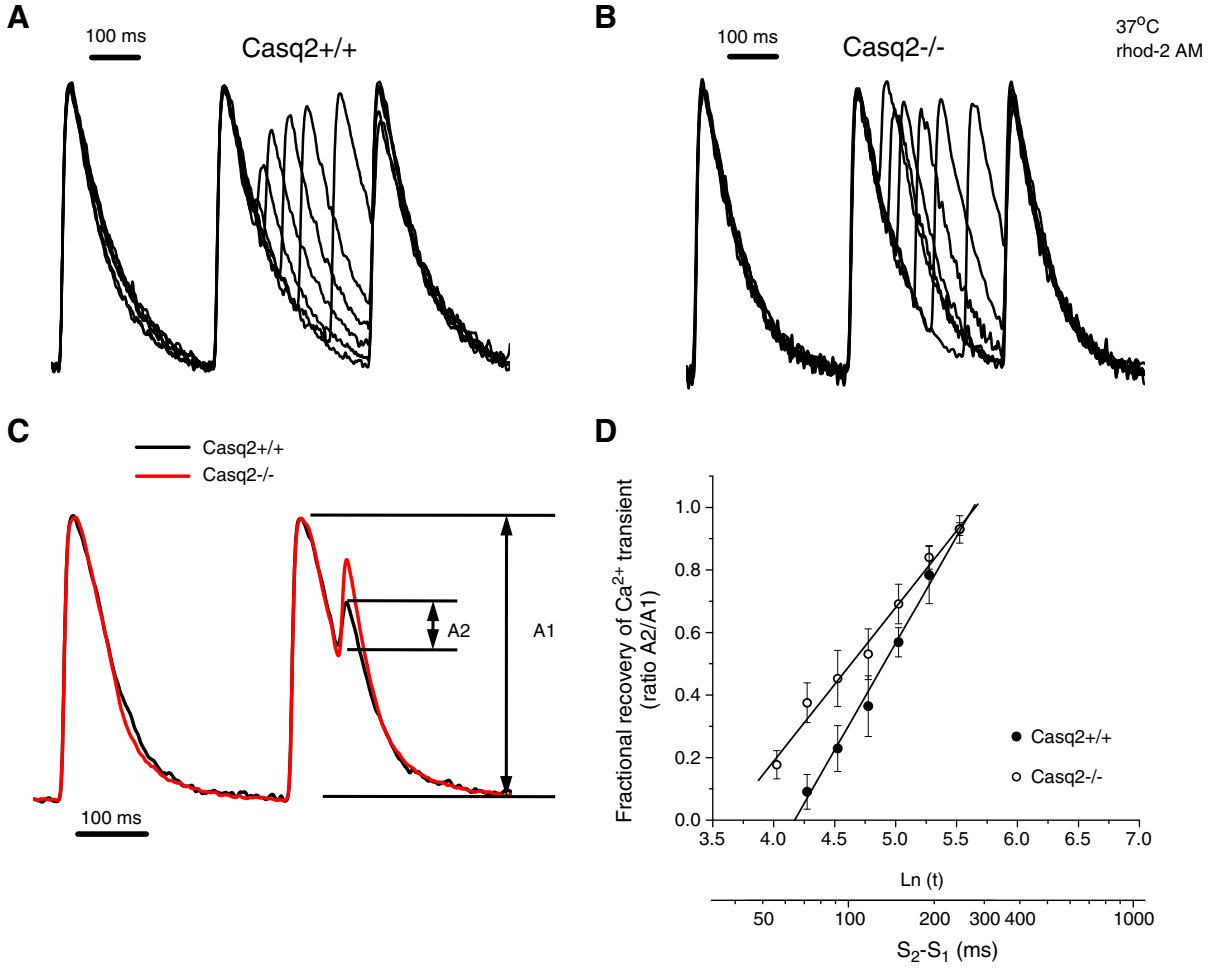

Fig. 2. Typical Ca^{2+}-transients recorded with a cytosolic Ca^{2+} indicator (rhod-2 AM) from epicardial layers of intact hearts of Casq2+/+ (A) and Casq2−/− (B) mice. The levels of rhod-2 fluorescence were normalized to the amplitude of the first peak and the normalized traces were superimposed. Panel C compares typical traces recorded when the S1–S2 coupling intervals were similar for Casq2+/+ and Casq2−/−. Restitution of Ca^{2+} release (D) was analyzed using the ratio A2/A1, where A1 is the amplitude of Ca^{2+} release during regular pacing (S1 stimulus) and A2 is the amplitude of the Ca^{2+} release in response to a premature (S2) stimulation. The recordings were obtained at 37 °C and at stimulation frequency of 3 Hz (n = 3–4). Semilogarithmic plots in panel D, contain the averaged values of the A2/A1 ratio calculated by combining the data from the selected time periods (bins) corresponding to S1–S2 coupling intervals. The time constants for the exponential restitution process were 182 ± 32 ms for the Casq2+/+ and 111 ± 22 ms for the Casq2−/−. See Results section for more details.

(A1). The largest differences between genotypes were observed at shorter S1–S2 coupling intervals (Fig. 2D). Our experiments revealed noticeably reduced refractoriness of Ca^{2+} release in Casq2−/− mice.

3.3. Effect of reducing intraluminal free Ca^{2+} content on Ca^{2+} dynamics in Casq2 KO mice

We have already shown that the perfusion of hearts with EGTA–AM diminished the level of free Ca^{2+} in the SR by impairing the activity of the SR Ca^{2+} ATPase (SERCa2a) [19]. The idea tested here was to evaluate the intracellular Ca^{2+} dynamics when the SR Ca^{2+} content was modified without changing the extracellular [Ca^{2+}].

The comparison of the normalized Ca^{2+} transients recorded with rhod-2 in presence of EGTA–AM for the two genotypes is shown in Fig. 3A. The exogenous buffer modified the relaxation kinetics of the cytosolic Ca^{2+} transients [19,25] revealing a fast (τ_1) and slow (τ_2) component (Fig. 3A). The kinetics of the cytosolic Ca^{2+}-transients was similar for Casq2+/+ and Casq2−/− mice for the first 150 ms after the peak (Fig. 3A). No significant differences between Casq2+/+ and Casq2−/− were found in τ_1 (20 ± 2 ms and 23 ± 4 ms, respectively, at 37 °C; n = 6, $p = 0.075$), or in the time to 50% relaxation (Fig. 3B). This effect can be explained by the presence of EGTA–AM, which accelerates the initial phase of the relaxation of Ca^{2+} transients by competing with the Ca^{2+} dye. On the contrary, the second component of the relaxation kinetics (τ_2) was significantly faster for Casq2−/− than for Casq2+/+ (Fig. 3B).

In addition, the recovery of Ca^{2+} release (Fig. 3D, typical recording during a double-pulse experiment is shown in Fig. 3C) was also faster for Casq2−/− in the presence of EGTA–AM. Time to 50% peak recovery was determined at room temperature (21 °C, 1 Hz pacing) and showed a faster recovery for Casq2−/− than for Casq2+/+ mice (285 ± 27 ms and 150 ± 20 ms, respectively, n = 6, p < 0.001).

3.4. How does the presence of Casq2 modify the intra-SR Ca^{2+} dynamics?

We hypothesized that the ablation of Casq2 will induce profound changes in the intra-SR Ca^{2+} dynamics. To evaluate this hypothesis we used an experimental approach described in our previous publications [19, 23]. The hearts were loaded with mag-fluo-4, which was used as a low affinity Ca^{2+} indicator to provide us with direct measurements of Ca^{2+} dynamics inside the SR in intact whole-heart preparations [19].

The relaxation kinetics of the intra-SR signal was found to be slightly faster for the hearts of Casq2−/− mice (Fig. 4A). The cytosolic Ca^{2+} and intra-SR Ca^{2+}-transients were fitted with a double exponential function. The time constant of the fast component and the time to 50%

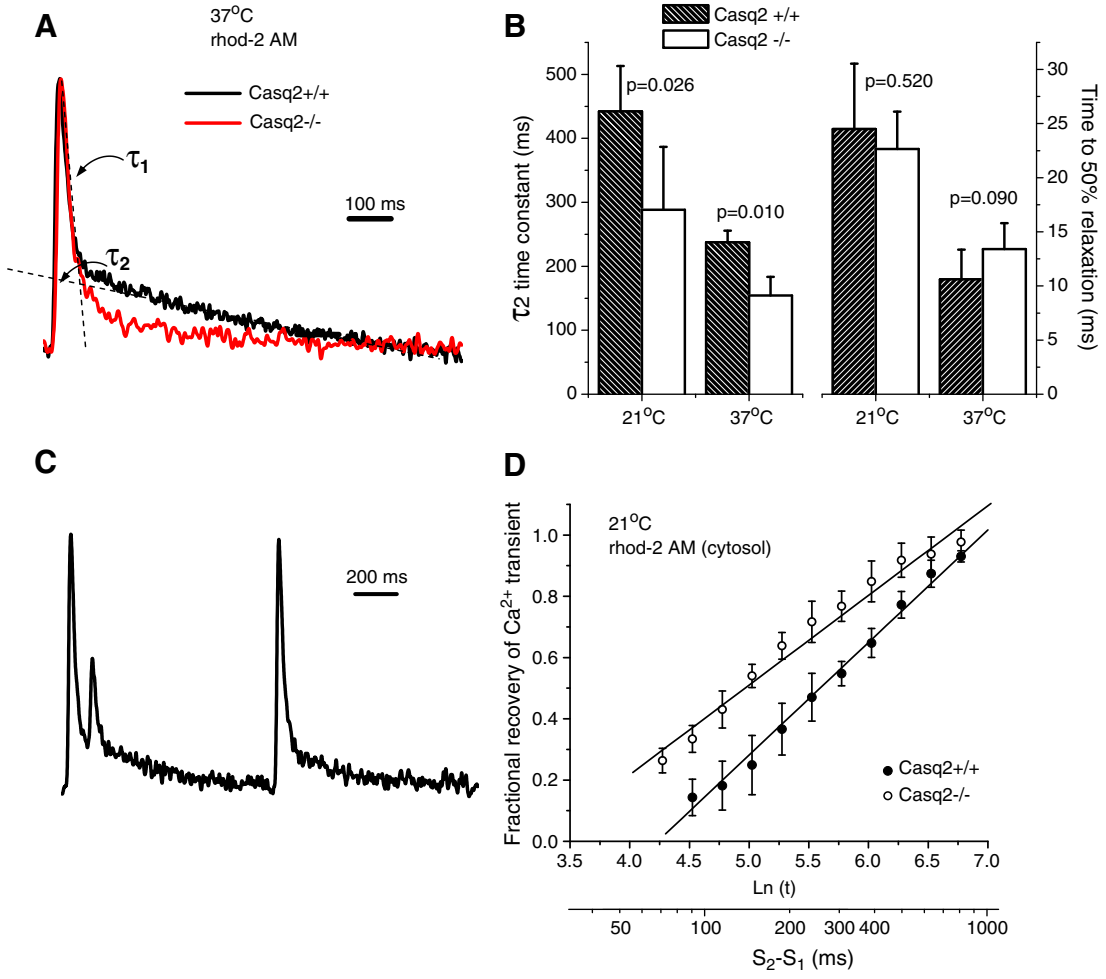

Fig. 3. Cytosolic Ca^{2+}-transients recorded from hearts of Casq2+/+ (black line) and Casq2−/− (red line) mice using rhod-2 AM (A, C). Measurements were conducted at 21 °C and at stimulation frequency of 1 Hz (71 μM EGTA–AM) was present in the loading solution). The rate constant of the slow component (τ2) for rhod-2 signal as well as time to 50% relaxation of cytosolic Ca^{2+} transients are shown in panel B. *p*-values are given for each pair of the columns (Casq2+/+ *versus* Casq2−/−, n = 6). Panel C represents typical traces obtained with double-pulse protocol used for estimation of the restitution of Ca^{2+} release. The restitution was analyzed using the ratio between the amplitudes of normal (regular pacing) and premature (in response to S2 stimulation) Ca^{2+} releases. Semilogarithmic plots in panel D contain the averaged values of the ratio calculated using the data from certain time periods (S1–S2 coupling intervals), n = 5–6.

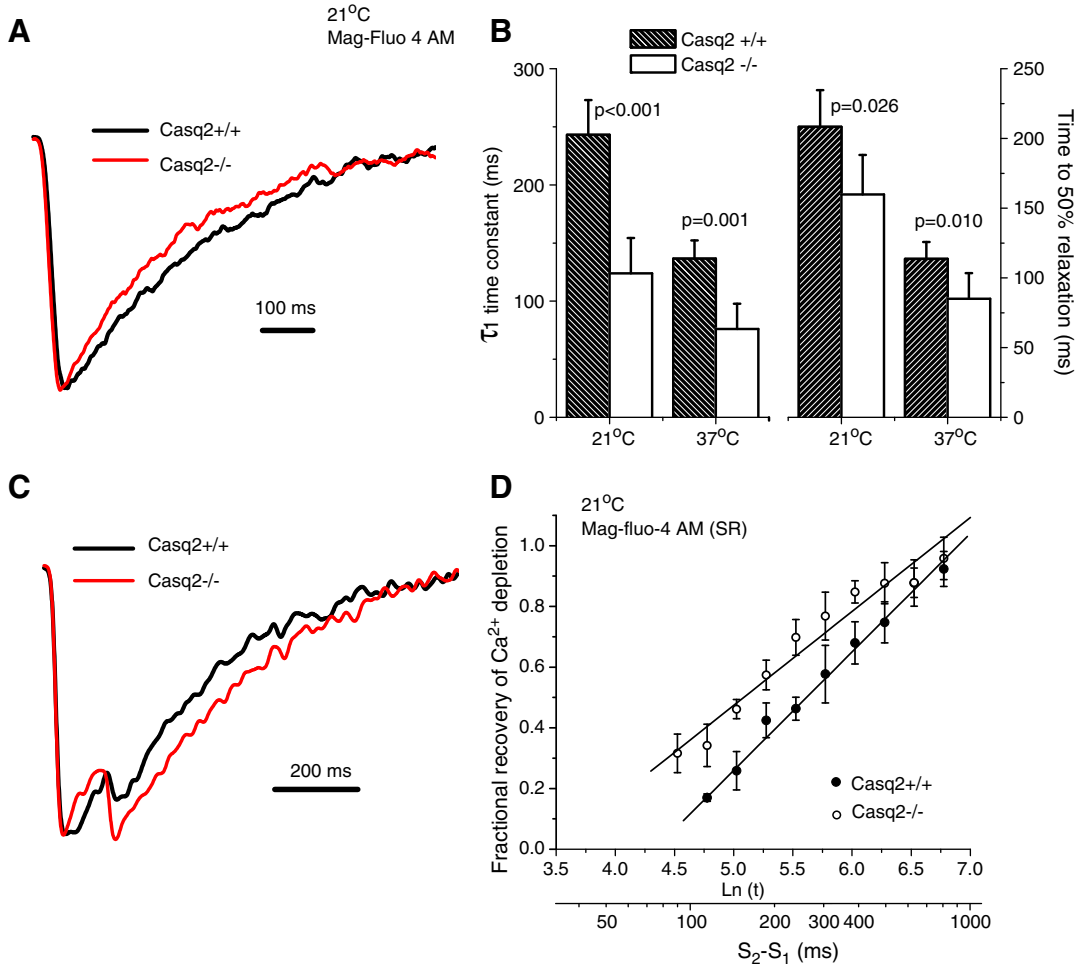

Fig. 4. Intra-SR Ca^{2+} transients recorded from hearts of Casq2+/+ (black line) and Casq2−/− (red line) mice using mag-fluo-4 AM (A, C). Measurements were conducted at 21 °C and at a stimulation frequency of 1 Hz (71 μM EGTA–AM was added into the loading solution). The rate constant of the fast component of the signal relaxation (τ1) for mag-fluo-4 signal as well as time to 50% relaxation of the intra-SR Ca^{2+}-transients are shown in panel B. *p*-values are given for each pair of the columns (Casq2+/+ *versus* Casq2−/−, n = 6). Panel C represents typical traces obtained with double-pulse protocol used for estimation of the restitution of Ca^{2+} release. The recordings were selected to compare Ca^{2+} releases starting from the same normalized level of depletion. Transients were normalized to the amplitude of nadir. Restitution was analyzed using the ratio between the amplitudes of normal (regular pacing) and premature (in response to S2 stimulation) Ca^{2+} releases/depletions. Semilogarithmic plots in panel D contain the averaged values of the ratio A2/A1 calculated using the data from certain time periods (S1–S2 coupling intervals), n = 5–6.

relaxation were statistically different between genotypes (Fig. 4B). The data presented in Figs. 3 and 4 indicate that both cytosolic and intra-SR Ca^{2+}-transients had faster relaxation kinetics for the Casq2−/− than for Casq2+/+ mice during the time period between 150 and 300 ms. Thus, the removal of Casq2 leads to a faster reload of the Ca^{2+} stores. Such an effect can be attributed to the action of Casq2 as a Ca^{2+} buffer.

As shown in Fig. 4D, the restitution of Ca^{2+} depletion was faster for Casq2−/− mice. Furthermore, this effect was also observed for time to 50% of the fractional recovery of intra-SR Ca^{2+}-transients measured under the same conditions (243 ± 3 ms and 172 ± 10 ms for Casq2+/+ and Casq2−/−, respectively, n = 5–6, p = 0.001). Interestingly, Fig. 4C illustrates that, when the second stimulation occurred at the same level of intra-SR [Ca^{2+}], Casq2−/− hearts displayed a larger Ca^{2+} depletion than the Casq2+/+. Although Casq2 as a buffer can potentially influence the restitution of Ca^{2+} release by changing the free Ca^{2+} dynamics in the SR, the fact that the amplitude of Ca^{2+} release (depletion) in absence of Casq2 was larger for the same free intra-SR [Ca^{2+}] favors the idea that Casq2 acts also as a local regulator that modifies the SR Ca^{2+} release.

3.5. Frequency dependency of Ca^{2+}-transients: effect of Casq2 on Ca^{2+}-alternans

The dependence of cardiac contractility on heart rate is a key factor governing the mechanical functionality of the heart. Additionally, the differences in Ca^{2+}-transient restitution could influence the frequency dependency of Ca^{2+} transients. Thus, it is reasonable to expect that both genotypes could display differences in the amplitude of the Ca^{2+} transients as function of the heart rate. Indeed, this is the case for the Casq−/− as shown in Supplemental material Fig. 1 where the KO animals were able to maintain the amplitude of Ca^{2+}-transients at higher heart rates (n = 5).

Not only the mechanical behavior of the heart is regulated by heart rate but also instabilities of the electrical activity can be triggered during tachycardia. Previously, we have shown that an acceleration of Ca^{2+} transients restitution can shift the appearance of Ca^{2+}-alternans toward higher frequencies suggesting a close relationship between these two phenomena [19]. To test this idea we recorded cytosolic Ca^{2+} transients in Casq2+/+ and Casq2−/− mouse hearts at different heart rates. Typical cytosolic Ca^{2+} transients recorded at

6 Hz (21 °C) with rhod-2 are shown in Fig. 5A (no EGTA was added into loading solution). The comparison of two genotypes reveals dramatic difference in the amplitude of Ca^{2+} alternans calculated as the ratio $(A_{max}-A_{min})/A_{max}$, where A_{max} and A_{min} are the maximal and the minimal amplitudes of Ca^{2+} transients during regular pacing at a given frequency. This ratio was plotted as function of the basic cycle length (Fig. 5 B). Compared to wild-type, Casq2−/− exhibited delayed onset of Ca^{2+}-alternans with significantly smaller amplitudes. For instance, at the basic cycle length of 143 ms, which corresponds to the stimulation frequency of 7 Hz, the amplitude of alternans was 0.72 ± 0.08 for control animals and 0.24 ± 0.07 for knockouts ($p = 0.01$, n = 3). This result is consistent with the idea that the onset and amplitude of cardiac alternans depend on the refractoriness of Ca^{2+} release.

3.6. Effects of Casq2 on epicardial electrical activity

The amplitude of Ca^{2+} release does not merely depend on the free SR Ca^{2+} and the functional properties of RyR2. It also depends on the electrical activity of cardiomyocytes, namely, the time-course of the AP, which determines Ca^{2+} influx via voltage-dependent Ca^{2+} channels that triggers CICR. Thus, the refractoriness of Ca^{2+} release could be tightly controlled by the restitution of the AP (AP triggering recovery) and the voltage-dependent Ca^{2+} channels. In order to rule out this possibility, we conducted AP measurements for Casq2+/+ and Casq2−/− animals using di-8-ANEPPS, a dye sensitive to membrane potential. Typical optically recorded AP traces are shown in Fig. 6A. The time-course of AP, absolute and relative refractory periods for the different genotypes were not significantly different. The duration of the absolute refractory period was 61 ± 5 ms and 55 ± 11 ms for Casq2+/+ and Casq2−/− animals, respectively ($p = 0.477$, n = 3–6). The duration of the relative refractory period was 102 ± 15 ms and 103 ± 26 ms for Casq2−/– and Casq2+/+, respectively ($p = 0.910$, n = 3–6). The AP triggering recovery was analyzed by plotting the ratio of the amplitude of premature S2 AP to the amplitude of the S1 AP appearing as a result of regular pacing. This result suggests that the modification in the restitution of the Ca^{2+} release in Casq2 knockouts was not caused by an altered AP triggering recovery.

The AP triggering recovery is a reasonable way to distinguish if the absence of Ca^{2+} release during the extrasysolic stimulus was due to the absence of an AP. However, it is not a robust test to evaluate the restitution of the Ca^{2+} influx across the plasmalemma. To identify the rate limiting step that defines the refractoriness of Ca^{2+} release we performed experiments in which SR Ca^{2+} release was impaired by a combination of pharmacological tools. Ryanodine (15 μM) and thapsigargin (4 μM) were used to lock the RyR2 in a subconductance state and inhibit the transport mediated by the SERCa2 pump. Under these conditions, there were no significant differences (Figs. 6 C and D) in the Ca^{2+} transient restitutions between both genotypes. This indicates that the rate-limiting step defining the restitution differences between both genotypes is the Ca^{2+} release from the SR.

3.7. Effects of Casq2 on T-wave alternans

We already stated that during tachycardia the heart can develop electrical instabilities like T-wave alternans (TW-Alt). TW-Alt is

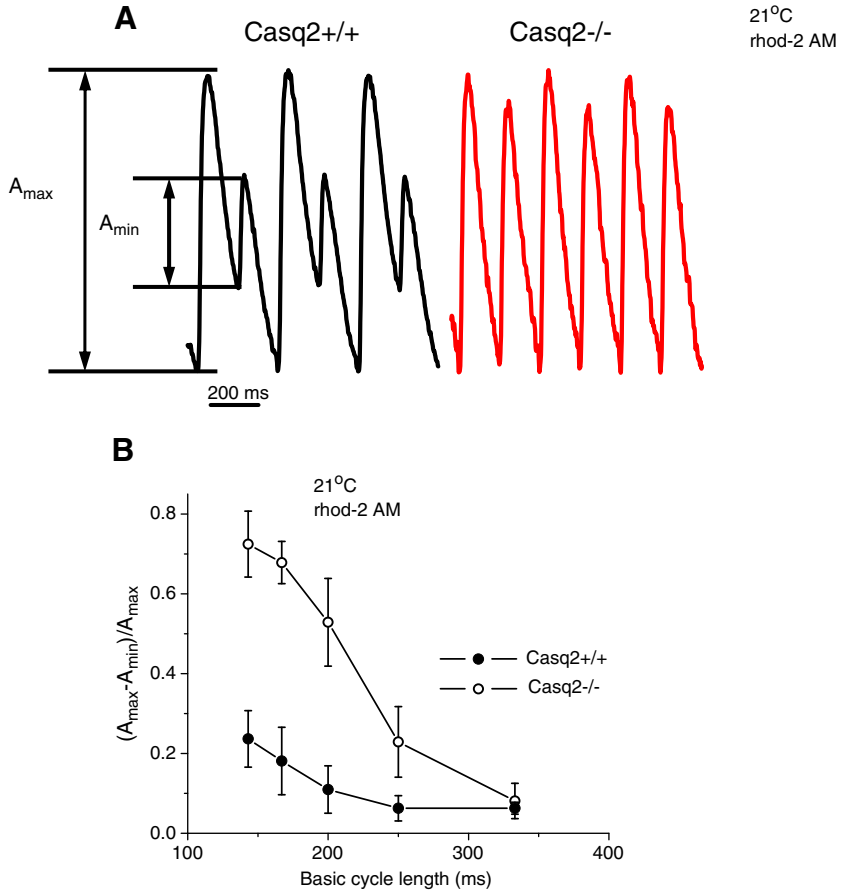

Fig. 5. (A) Typical cytosolic Ca^{2+} transients (rhod-2 fluorescence, 21 °C, 6 Hz) showing alternans, which is more pronounced in Casq2+/+ (red line). (B) Dependence of the Ca^{2+}-alternans on basic cycle length during regular pacing of intact hearts from Casq2+/+ and Casq2−/− mice at 21 °C. The cytosolic Ca^{2+} transients were recorded using rhod-2 AM. No EGTA was added into the loading solution. The data are means ± standard deviations (n = 3).

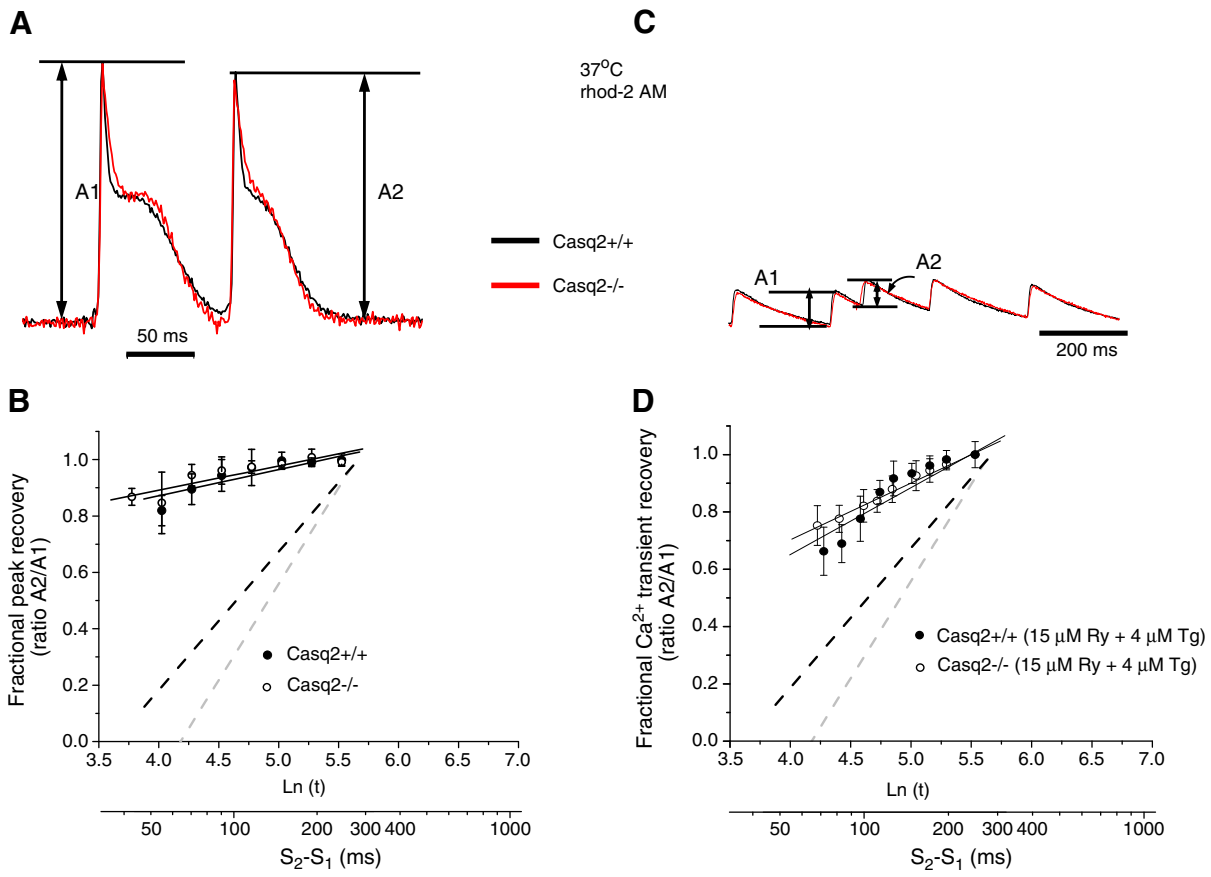

Fig. 6. AP triggering recovery of AP recorded in the presence of blebbistatin using potentiometric dye di-8-ANEPPS at 37 °C and at a stimulation frequency of 4 Hz. The typical traces are shown in panel A. The ratio of the peaks of APs in response to the additional (A2) and normal (A1) stimulation pulse was used to estimate the recovery of the AP's peak. The values of A2/A1 ratio were grouped according to the time periods (bins). Then averaged values were plotted against ln (t), where t is the time between regular and extrasystolic stimulations. The data were collected from n = 3–5 independent experiments (B). Restitution of Ca^{2+} transients in the cytosol during the AP stimulation in the presence of 15 μM ryanodine and 4 μM thapsigargin (C). Semilogarithmic plots in panel D contain the averaged values of the ratio calculated using the data from certain time periods (S1–S2 coupling intervals), n = 5. The dotted lines in plots B and D correspond to the Ca^{2+} transients restitution plots shown in Fig. 2D. All the experiments were performed at 37 °C.

usually observed as alternating beat-to-beat changes in the amplitude of the T-wave of the electrocardiogram (ECG) and constitutes an important arrhythmogenic mechanism that can lead to sudden cardiac death [26]. The likelihood of developing TW-Alt increases with tachycardia. This phenomenon is thought to be associated with abnormalities in intracellular Ca^{2+} handling and/or cellular metabolism [27–29]. Actually, Ca^{2+}-alternans can trigger alternans in the repolarization of the AP. Data supporting this idea is presented in Fig. 2 of Supplemental material where alternations in Ca^{2+} transients amplitude and in the duration of the AP are shown. Furthermore, Casq−/− hearts present a shift in the frequency at which Ca^{2+} transients alternate and a very similar shift in the frequency at which the repolarization of the AP alternates. These experiments demonstrate the relationship between Ca^{2+}-alternans and AP alternans. Additionally, they illustrate that the Casq−/− animals are less prone to display alternans in the AP repolarization.

Transmural differences in the alternations in the duration of the AP can not only lead to electrical instabilities but also can generate TW-Alt. To illustrate this idea we performed transmural electrocardiographic recordings in both genotypes and evaluated the frequency dependency of the T-wave amplitude. At a heart rate of 4 Hz, there are no significant differences between wild type and KO animals (Figs. 7A and B). At higher heart rates (9 Hz), TW-Alt occurs in both models. However, the Casq−/− mice display a smaller TW-Alt than wild type animals (Figs. 7C and D). Furthermore, when a complete frequency scan was performed, the KO hearts displayed a smaller TW-Alt appearing at a higher heart rate (Fig. 7E). These results clearly demonstrate that the ablation of an intra-organelle protein not only modifies the organellar Ca^{2+} dynamics but also change the whole electrical activity of the heart.

4. Discussion

4.1. Epicardial Ca^{2+}-transients in Casq2 KO mice

In this paper, we evaluate for the first time the role of Casq2, the major SR Ca^{2+} buffering protein, in the intracellular Ca^{2+} dynamics in the intact heart, under physiological conditions (*i.e.* body temperature and physiological heart rate). Interestingly, no significant differences between Casq2+/+ and Casq2−/− mice were found in the kinetics and the amplitude of Ca^{2+}-transients recorded at the epicardial layer (Fig. 1A). These experimental findings are in agreement with Ca^{2+}-transients recorded on enzymatically isolated ventricular cardiac myocytes from animals having the same genotypes [14]. A possible interpretation of these results is that the increase in the SR volume in myocytes lacking Casq2 [14] compensates the decrease in the buffer capacity caused by the ablation of Casq2. However, when decreased levels of Casq2 in cardiac myocytes were achieved by means of the injection of recombinant adenoviruses with coding regions of canine Casq2 in antisense orientation [30,31], an approach that prevents the adaptive changes in the SR volume, myocytes depleted of Casq2 displayed cytosolic Ca^{2+}-transients with smaller amplitudes than control ones. The effect was attributed to the duration of CICR rather than the modification of the trigger (L-type Ca^{2+} current, I_{Ca}).

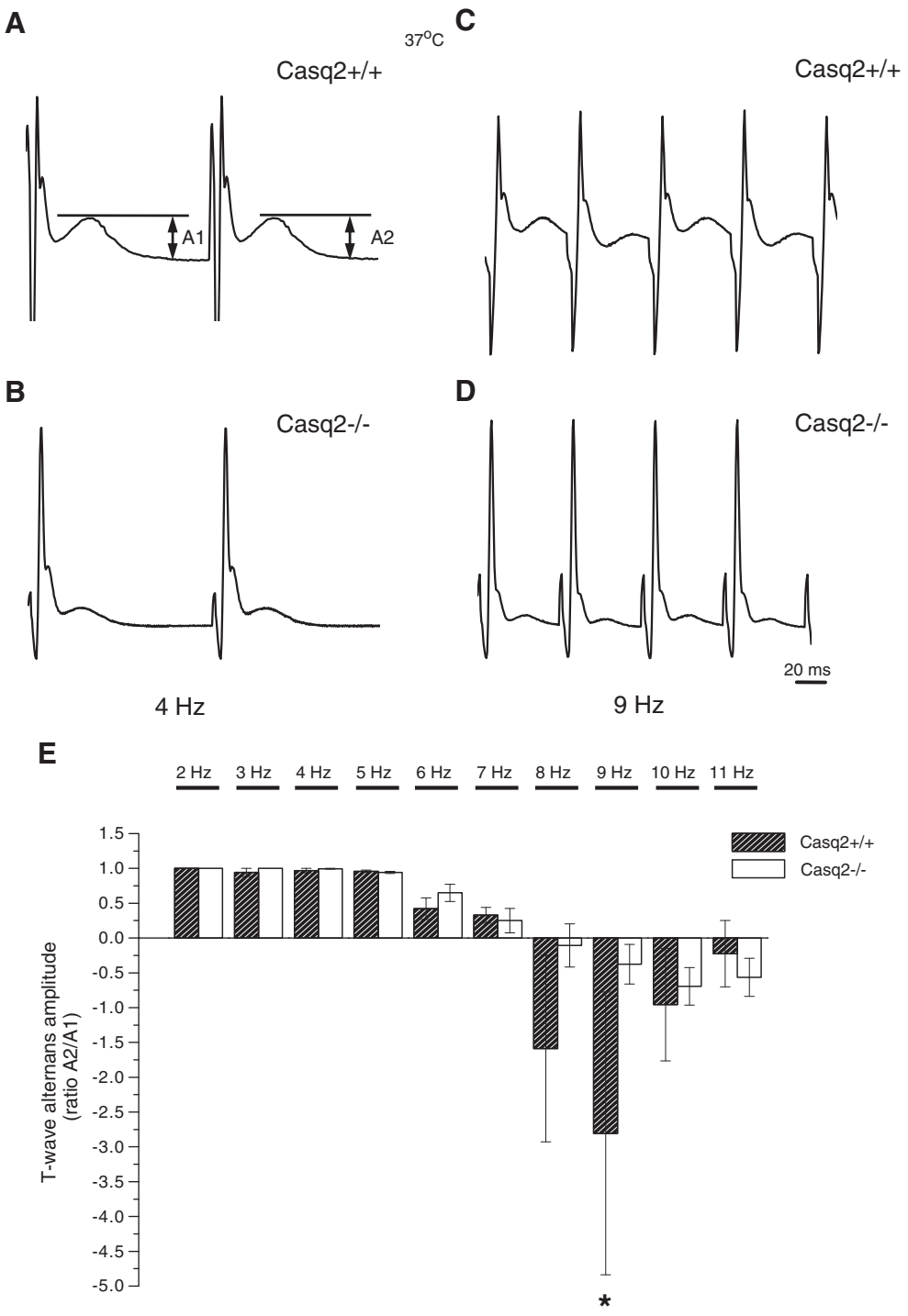

Fig. 7. Effect of Casq2 ablation on TW-Alt. Panels A and B show a comparison of electocardiographic recordings obtained from Casq2+/+ and Casq2−/− when the hearts were paced at 4 Hz. QRS complex and T-wave can clearly be observed, none of the T-waves for each genotype shows a TW-Alt. Upon increase in the heart rate to 9 Hz it is possible to observe alternans in the T-wave, however the amplitude of the TW-Alt is smaller in the KO hearts (C and D). A complete frequency scan for both genotypes is presented in Panel E. The amplitude of the TW-Alt is significantly larger for the wild type animals n = 4 for Casq2+/+ and n = 9 for Casq2−/−. The isoelectric line is used as a reference to measure the TW-amplitudes. All the experiments were done at 37 °C. Asterisk marks the data columns with statistically significant difference ($p<0.05$) between genotypes.

Alternatively, it is possible that under physiological conditions the free SR [Ca^{2+}] of an intact heart was high enough to saturate all the Ca^{2+} biding sites on Casq2, thereby reducing the dynamic buffer capacity of this protein. In order to test this latter possibility, we performed experiments at different extracellular [Ca^{2+}] (Fig. 1 D). Although this should set the free SR Ca^{2+} to different values, no differences were found between Casq2+/+ and Casq2−/− mice indicating that even under conditions where Casq2 should not be fully saturated with Ca^{2+} the amplitude of Ca^{2+} transients remained the same. However, when extracellular [Ca^{2+}] was reduced to 0.1 mM (Table 1), the time to peak of Ca^{2+} transients measured in Casq2−/− animals was significantly slower than in the control ones. This suggests that

under these experimental conditions the Ca^{2+} release process was activated for a longer time or that the recruitment of local Ca^{2+} release sites (*i.e.* Ca^{2+} sparks) was less efficient in Casq2−/− animals.

4.2. Casq2 regulates refractoriness of SR Ca^{2+} release during the cardiac cycle

Exogenous Ca^{2+} buffers can alter the properties of Ca^{2+} sparks by increasing the intra-SR Ca^{2+} buffer capacity [33]. Additionally, myocytes virally deprived of Casq2 display changes in the rhythmicity of Ca^{2+}-transients and restitution behavior of Ca^{2+}-release sites [30,31]. In our present work, we demonstrate that a premature AP can induce a higher release of Ca^{2+} from the SR when Casq2 is not present (Fig. 2). This effect can have important consequences on the refractoriness of cardiac contractility but also may be responsible for premature spontaneous Ca^{2+} release events that lead to afterdepolarizations.

Ca^{2+} termination and recovery has been extensively studied by others [32–37]. Differences between those experiments and the ones presented in this paper might be due to differences in the experimental conditions. For example, in previous studies, the cells were maintained at room temperature where the rate of Ca^{2+} transport by the SERCa2a pump is highly impaired leading to possible changes in intra-SR [Ca^{2+}] [31]. Additionally, in most of these papers the cells were not continuously stimulated to mimic the complex Ca^{2+} dynamics in myocytes during a regular cardiac cycle.

The acceleration of the Ca^{2+}-transient restitution process in Casq2−/− (Fig. 2B) can be controlled by several factors like a faster rise in free SR [Ca^{2+}] and/or a direct regulation of RyR2 kinetic activity. The faster SR Ca^{2+} replenishment, mediated by the SERCa2a pump activity, could be attributed to a decrease in the total SR Ca^{2+} buffer capacity. Furthermore, in the absence of Casq2, the diffusion of Ca^{2+} from the "uptaking" sites (longitudinal SR) to the "releasing" sites (terminal cistern) could be speeded up by the absence of immobile binding sites along the Ca^{2+} diffusional path. On the other hand, if the refilling time is the main factor setting the differences in refractoriness between Casq2+/+ and Casq2−/−, the larger the degree of SR depletion the larger the Casq2 effect will be. Moreover, under conditions where the SR Ca^{2+} load (free SR Ca^{2+}) was modified by adding EGTA–AM as an exogenous buffer the differences in the Ca^{2+} restitution were still present. This indicates that in a wider range of intra SR Ca^{2+} the presence of Casq2 still exerts a control of the Ca^{2+} transient restitution (Fig. 3D). Finally, as shown in Fig. 6 the differences in the restitution of Ca^{2+}-transients between genotypes are not due to differences in AP triggering recovery or the Ca^{2+} influx through the plasma membrane.

4.3. Ablation of Casq2 modifies intra-SR Ca^{2+} dynamics

Although the kinetics of cytosolic Ca^{2+} transients is tightly coupled to the intra-SR Ca^{2+}, the only direct way to discriminate between the different hypotheses related to the role of Casq2 in the regulation of the ventricular SR Ca^{2+} signaling is by directly assessing the intra-SR Ca^{2+} dynamics. Figs. 4A and B show that the rate of rise of the free intra-SR [Ca^{2+}] is significantly faster in hearts from animals lacking Casq2. This faster rise in free intra-SR [Ca^{2+}], both at room and at physiological temperatures, is consistent with the idea that there is a decrease in the luminal Ca^{2+} buffer capacity in absence of Casq2. This result is also in agreement with the outcome of the restitution experiments (Figs. 2 and 3) where the restitution of the Ca^{2+}-transients is faster in Casq2−/−.

Additionally, restitution of SR Ca^{2+} depletion is also much faster in hearts from KO animals (Fig. 4D). These intra-SR Ca^{2+} restitution experiments show that for the same fractional free [Ca^{2+}] within the SR the amplitude of Ca^{2+} depletion during a second pulse is considerably larger in KO animals (Fig. 4C). This result suggests that in absence of Casq2 the Ca^{2+} release process is less inhibited than in the presence of Casq2. This demonstrates for the first time that under physiological conditions Casq2 is not only buffering Ca^{2+} but, perhaps more important, it also regulates the release machinery as well. Moreover, a decrease in Casq2 content is also known to be associated with an acceleration of the relaxation kinetics of intra-SR Ca^{2+} waves in isolated canine cardiac myocytes [38]. Furthermore, the faster Ca^{2+} replenishment of the SR has been suggested to be involved in the genesis of ventricular tachycardia, which is caused by mutations that either decrease the level of Casq2 expression or impair the Ca^{2+} binding ability of the protein [6].

4.4. Role of Casq2 in arrhythmogenesis

Tachycardia, an increase in heart rate, is known to induce several pathophysiological syndromes. The increase in the heart rate can trigger TW-Alt which is detected as alternating beat-to-beat changes in the T-wave and represents an important arrhythmogenic mechanism that can trigger transmural reentry arrhythmias. In general, tachycardia will limit the time for SR Ca^{2+} refilling. This will reduce SR Ca^{2+} load resulting in less Ca^{2+}-bound Casq2 and causing less Ca^{2+} release from the SR. Smaller release will leave a higher residual intra-SR Ca^{2+} level and a subsequent SR refilling (on top of residual) will result in higher SR load and Ca–Casq2 levels. This will promote a larger release leaving a lower intra-SR residual level and the cycle starts again. This alternating Ca^{2+} dynamics (Ca^{2+}-alternans) is shown in Fig. 5A. Finally, Ca^{2+}-alternans will induce differences in Na^{+}–Ca^{2+} exchanger activity leading to differences in AP repolarization (see Fig. 2 Supplemental material) and this will be manifested in the ECG waveform as TW-Alt (Fig. 7). In the present work, we show that the amplitude of Ca^{2+}-alternans was significantly reduced in the absence of Casq2 (Fig. 5B). The shift in the frequency dependency of alternans in Casq2 knockouts was most likely the result of acceleration of the restitution of Ca^{2+} release, which was consistently faster in the animals lacking Casq2 when measured at several stimulation frequencies. In other words, it appears that the fast recovery of Ca^{2+} release allows the intact hearts of Casq2−/− mice to function without Ca^{2+} alternans at higher frequencies in comparison to Casq2+/+ animals. This supports the idea that Casq2 is a key element in the genesis of Ca^{2+} alternans and TW-Alt. Our results also suggest that reduction or loss of Casq2 will diminish TW-Alt as shown in Fig. 7E. At the same time, the accelerated restitution and loss of Ca^{2+} release refractoriness due to loss of Casq2 will increase the likelihood of spontaneous premature Ca^{2+} release events that will lead to delayed afterdepolarizations and triggered arrhythmias. Clinically, the loss of Ca^{2+} release refractoriness results in a phenotype of catecholaminergic polymorphic ventricular tachycardia caused by focal triggered activity originated in the ventricle [39].

5. Conclusion

In conclusion, our experiments revealed that Casq2 ablation modified the Ca^{2+} dynamics in the cardiac myocytes of the intact mouse hearts. The faster rise in SR [Ca^{2+}] in Casq2−/− hearts during Ca^{2+} reuptake led to an acceleration of the restitution of Ca^{2+} release. As a result, the Casq2−/− hearts were less sensitive to frequency-induced alternans. This defines the role of Casq2 in the genesis of TW-Alt. The data are in accordance with the hypothesis that Casq2 plays an important and dual role in the regulation of CICR acting as a Ca^{2+} chelator and as a Ca^{2+}-sensing factor modulating the Ca^{2+} release process.

Supplementary materials related to this article can be found online at doi: 10.1016/j.yjmcc.2011.09.020.

Disclosures statement

None.

Acknowledgments

We thank Heather Orrell, Dr. Julio Copello, Dr. Alicia Mattiazzi, Dr. Guillermo Perez. Dr. Fabiana Scornik and Dr. Cecilia Mundina-Weilenmann for critically reviewing the manuscript. This work was supported by the National Institute of Health (R01HL57832 grant to A.E. and R01HL88635 to B.K.).

References

[1] Campbell KP, MacLennan DH, Jorgensen AO, Mintzer MC. Purification and characterization of calsequestrin from canine cardiac sarcoplasmic reticulum and identification of the 53,000 dalton glycoprotein. J Biol Chem 1983;258:1197–204.
[2] Flucher BE, Franzini-Armstrong C. Formation of junctions involved in excitation–contraction coupling in skeletal and cardiac muscle. Proc Natl Acad Sci USA 1996;93:8101–6.
[3] Endo M, Tanaka M, Ogawa Y. Calcium induced release of calcium from the sarcoplasmic reticulum of skinned skeletal muscle fibers. Nature 1970;228:34–6.
[4] Fabiato A, Fabiato F. Contractions induced by a calcium-triggered release of calcium from the sarcoplasmic reticulum of single skinned cardiac cells. J Physiol 1975;49:469–95.
[5] Mitchell RD, Simmerman HK. Jones LR Ca^{2+} binding effects on protein conformation and protein interactions of canine cardiac calsequestrin. J Biol Chem 1988;263:1376–81.
[6] Györke S, Terentyev D. Modulation of ryanodine receptor by luminal calcium and accessory proteins in health and cardiac disease. Cardiovasc Res 2008;77:245–55.
[7] Sato Y, Ferguson DG, Sako H, Dorn II GW, Kadambi VJ, Yatani A, et al. Cardiac-specific overexpression of mouse cardiac calsequestrin is associated with depressed cardiovascular function and hypertrophy in transgenic mice. J Biol Chem 1998;273:28470–7.
[8] Knollmann BC, Knollmann-Ritschel BE, Weissman NJ, Jones LR, Morad M. Remodeling of ionic currents in hypertrophied and failing hearts of transgenic mice overexpressing calsequestrin. J Physiol (Lond) 2000;525:483–98.
[9] Györke I, Hester N, Jones LR, Györke S. The role of calsequestrin, triadin, and junctin in conferring cardiac ryanodine receptor responsiveness to lumenal calcium. Biophys J 2004;86:2121–8.
[10] Terentyev D, Viatchenko-Karpinski S, Vedamoorthyrao S, Oduru S, Györke I, Williams SC, et al. Protein–protein interactions between triadin and calsequestrin are involved in modulation of sarcoplasmic reticulum calcium release in cardiac myocytes. J Physiol 2007;583:71–80.
[11] Lahat H, Pras E, Olender T, Avidan N, Ben-Asher E, Man O, et al. A missense mutation in a highly conserved region of CASQ2 is associated with autosomal recessive catecholamine-induced polymorphic ventricular tachycardia in Bedouin families from Israel. Am J Hum Genet 2001;69:1378–84.
[12] Postma AV, Denjoy I, Hoorntje TM, Lupoglazoff J-M, Da Costa A, Sebillon P, et al. Absence of calsequestrin 2 causes severe forms of catecholaminergic polymorphic ventricular tachycardia. Circ Res 2002;91:e21–6.
[13] Liu N, Priori SG. Disruption of calcium homeostasis and arrhythmogenesis induced by mutations in the cardiac ryanodine receptor and calsequestrin. Cardiovasc Res 2008;77:293–301.
[14] Knollmann BC, Chopra N, Hlaing T, Akin B, Yang T, Ettensohn K, et al. Casq2 deletion causes sarcoplasmic reticulum volume increase, premature Ca^{2+} release, and catecholaminergic polymorphic ventricular tachycardia. J Clin Invest 2006;116:2510–20.
[15] Chopra N, Kannankeril PJ, Yang T, Hlaing T, Holinstat I, Ettensohn K, et al. Modest reductions of cardiac calsequestrin increase sarcoplasmic reticulum Ca^{2+} leak independent of luminal Ca^{2+} and trigger ventricular arrhythmias in mice. Circ Res 2007;101:617–26.
[16] Stevens SC, Terentyev D, Kalyanasundaram A, Periasamy M, Györke S. Intra-sarcoplasmic reticulum Ca^{2+} oscillations are driven by dynamic regulation of ryanodine receptor function by luminal Ca^{2+} in cardiomyocytes. J Physiol 2009;587:5003–4.
[17] Alcalai R, Wakimoto H, Arad M, Planer D, Konno T, Wang L, et al. Prevention of ventricular arrhythmia and calcium dysregulation in a catecholaminergic polymorphic ventricular tachycardia mouse model carrying calsequestrin-2 mutation. J Cardiovasc Electrophysiol 2011;22:316–24.
[18] Shannon TR, Guo T, Bers DM. Ca^{2+} scraps. Local depletions of free $[Ca^{2+}]$ in cardiac sarcoplasmic reticulum during contractions leave substantial Ca^{2+} reserve. Circ Res 2003;93:40–5.
[19] Kornyeyev D, Reyes M, Escobar AL. Luminal Ca^{2+} content regulates intracellular Ca^{2+} release in subepicardial myocytes of intact beating mouse hearts: effect of exogenous buffers. Am J Physiol Heart Circ Physiol 2010;298:H2138–53.
[20] Dou Y, Arlock P, Arner A. Blebbistatin specifically inhibits actin–myosin interaction in mouse cardiac muscle. Am J Cell Physiol 2007;293:1148–53.
[21] Fedorov VV, Lozinsky IT, Sosunov EA, Anyukhovsky EP, Rosen MR, Balke CW, et al. Application of blebbistatin as an excitation–contraction uncoupler for electrophysiologic study of rat and rabbit hearts. Heart Rhythm 2007;4:619–26.
[22] Farman G, Tachampa K, Mateja R, Carzorla O, Lacampagne A, de Tombe PP. Blebbistatin: use as inhibitor of muscle contraction. Pflugers Arch — Eur J Physiol 2008;455:995–1005.
[23] Valverde CA, Kornyeyev D, Ferreiro M, Petrosky AD, Mattiazzi A, Escobar AL. Transient Ca^{2+} depletion of the sarcoplasmic reticulum at the onset of reperfusion. Cardiovasc Res 2010;85:671–80.
[24] Mejía-Alvarez R, Manno C, Villalba-Galea CA, del Valle Fernández L, Costa R, Fill M, et al. Pulsed local-field fluorescence microscopy: a new approach for measuring cellular signals in the beating heart. Pflugers Arch 2003;445:747–58.
[25] Diaz ME, Trafford AW, Eisner DA. The effect of exogenous calcium buffers on the systolic calcium transient in rat ventricular myocytes. Biophys J 2001;20:1915–25.
[26] Pham Q, Quan KJ, Rosenbaum DS. T-wave alternans: marker, mechanism, and methodology for predicting sudden cardiac death. J Electrocardiol 2003;36:75–81.
[27] Huser J, Blatter LA, Lipsius SL. Intracellular Ca^{2+} release contributes to automaticity in cat atrial pacemaker cells. J Physiol 2000;524:415–22.
[28] Kockskamper J, Blatter LA. Subcellular Ca^{2+} alternans represents a novel mechanism for the generation of arrhythmogenic Ca^{2+} waves in cat atrial myocytes. J Physiol 2002;545:65–79.
[29] Blatter LA, Kockskamper J, Sheehan KA, Zima AV, Huser J, Lipsius SL. Local calcium gradients during excitation–contraction coupling and alternans in atrial myocytes. J Physiol 2003;546:19–31.
[30] Terentyev D, Viatchenko-Karpinski S, Györke I, Volpe P, Williams SC, Györke S. Calsequestrin determines the functional size and stability of cardiac intracellular calcium stores: mechanism for hereditary arrhythmia. Proc Natl Acad Sci USA 2003;100:11759–64.
[31] Viatchenko-Karpinski S, Terentyev D, Györke I, Terentyeva R, Volpe P, Priori SG, et al. Abnormal calcium signaling and sudden cardiac death associated with mutation of calsequestrin. Circ Res 2004;94:471–7.
[32] Terentyev D, Viatchenko-Karpinski S, Valdivia HH, Escobar AL, Györke S. Luminal Ca^{2+} controls termination and refractory behavior of Ca^{2+}-induced Ca^{2+} release in cardiac myocytes. Circ Res 2002;91:414–20.
[33] Del Principe F, Egger M, Niggli E. Calcium signalling in cardiac muscle: refractoriness revealed by coherent activation. Nat Cell Biol 1999;1:323–9.
[34] Szentesi P, Pignier, Egger M, Kranias EG, Niggli E. Sarcoplasmic reticulum Ca2+ refilling controls recovery from Ca^{2+}-induced Ca^{2+} release refractoriness in heart muscle. Circ Res 2004;95:807–13.
[35] Brochet DX, Yang D, Di Maio A, Lederer WJ, Franzini-Armstrong C, Cheng H. Ca^{2+} blinks: rapid nanoscopic store calcium signaling. Proc Natl Acad Sci USA 2005;102:3099–104.
[36] Cheng H, Lederer MR, Lederer WJ, Cannell MB. Calcium sparks and $[Ca^{2+}]_i$ waves in cardiac myocytes. Am J Physiol 1996;270:C148–59.
[37] Sobie EA, Song LS, Lederer WJ. Local recovery of Ca^{2+} release in rat ventricular myocytes. J Physiol 2005;565:441–7.
[38] Terentyev D, Kubalova Z, Valle G, Nori A, Vedamoorthyaro S, Terentyeva R, et al. Modulation of SR Ca release by luminal Ca and calsequestrin in cardiac myocytes: effects of CASQ2 mutations linked to sudden cardiac death. Biophys J 2008;95:2037–48.
[39] Györke S. Molecular basis of catecholaminergic polymorphic ventricular tachycardia. Heart Rhythm 2009;6:123–9.

Intracellular Ca^{2+} release underlies the development of phase 2 in mouse ventricular action potentials

Marcela Ferreiro, Azadé D. Petrosky and Ariel L. Escobar

Am J Physiol Heart Circ Physiol 302:H1160-H1172, 2012. First published 23 December 2011; doi:10.1152/ajpheart.00524.2011

Am J Physiol Heart Circ Physiol 302: H1160–H1172, 2012.
First published December 23, 2011; doi:10.1152/ajpheart.00524.2011.

Intracellular Ca^{2+} release underlies the development of phase 2 in mouse ventricular action potentials

Marcela Ferreiro, Azadé D. Petrosky, and Ariel L. Escobar

Biological Engineering and Small Scale Technologies Program, School of Engineering, University of California, Merced, California

Submitted 24 May 2011; accepted in final form 15 December 2011

Ferreiro M, Petrosky AD, Escobar AL. Intracellular Ca^{2+} release underlies the development of phase 2 in mouse ventricular action potentials. *Am J Physiol Heart Circ Physiol* 302: H1160–H1172, 2012. First published December 23, 2011; doi:10.1152/ajpheart.00524.2011.—The ventricular action potential (AP) is characterized by a fast depolarizing phase followed by a repolarization that displays a second upstroke known as phase 2. This phase is generally not present in mouse ventricular myocytes. Thus we performed colocalized electrophysiological and optical recordings of APs in Langendorff-perfused mouse hearts founding a noticeable phase 2. Ryanodine as well as nifedipine reduced phase 2. Our hypothesis is that a depolarizing current activated by Ca^{2+} released from the sarcoplasmic reticulum (SR) rather than the "electrogenicity" of the L-type Ca^{2+} current is crucial in the generation of mouse ventricular phase 2. When Na^+ was partially replaced by Li^+ in the extracellular perfusate or the organ was cooled down, phase 2 was reduced. These results suggest that the Na^+/Ca^{2+} exchanger functioning in the forward mode is driving the depolarizing current that defines phase 2. Phase 2 appears to be an intrinsic characteristic of single isolated myocytes and not an emergent property of the tissue. As in whole heart experiments, ventricular myocytes impaled with microelectrodes displayed a large phase 2 that significantly increases when temperature was raised from 22 to 37°C. We conclude that mouse ventricular APs display a phase 2; however, changes in Ca^{2+} dynamics and thermodynamic parameters also diminish phase 2, mostly by impairing the Na^+/Ca^{2+} exchanger. In summary, these results provide important insights about the role of Ca^{2+} release in AP ventricular repolarization under physiological and pathological conditions.

potentiometric dyes; ventricular action potential; mouse heart; ventricular arrhythmias; Na^+/Ca^{2+} exchanger; cardiac repolarization

VENTRICULAR REPOLARIZATION is a key event in understanding cardiac electrical activity, both under normal or pathophysiological conditions (51). Although ventricular action potentials (APs) usually present a late depolarizing phase (phase 2) before the final repolarization (8), electrical signals recorded from different ventricular layers (i.e., epicardium, mid-myocardium, and endocardium; Ref. 33) display different kinetic features of this repolarization process. These kinetic differences are responsible for a transmural repolarization gradient throughout the ventricular wall (34). Moreover, this functional sequence of events sheds light on a variety of clinical electrocardiographic problems related to cardiac arrhythmias (10, 20). Furthermore, epicardial APs display a complex morphology named "spike and dome" behavior (33). Changes in the time course of this process are commonly observed in several pathological conditions such as the appearance of the J wave during hypothermia (55) and the Brugada syndrome (54). In both conditions, these alterations can serve as a substrate for the genesis of arrhythmias.

Several experimental animal models, showing human-like electrophysiological characteristics (i.e., canine or feline), have been used to mimic in vitro and in vivo alterations in the electrical behavior of the epicardium (19). However, those animal models do not have the genetic advantage of mouse models where cardiac transgenesis has been well established (18). Unfortunately, mouse cardiac electrophysiological properties have been considered to be different from those of other mammals. For example, durations reported for mouse APs are on average up to 10 times shorter than human ones (23, 40). Furthermore, compelling evidence from experiments performed on isolated mouse ventricular cardiac myocytes shows that the repolarization of the AP is highly monotonic lacking of a distinguishable phase 2 (1, 9, 22, 25, 29, 30, 35, 40, 50, 52). This specific characteristic has set some limitations on the use of mice as a model for the study of syndromes where alterations of the repolarization of the ventricle are central in the genesis of the disease.

In the present study, we evaluated the controversial subject of the presence of phase 2 in mouse hearts and the mechanisms involved in the genesis of phase 2. We tested the hypothesis that a depolarizing current activated by Ca^{2+} released from the sarcoplasmic reticulum (SR) rather than the "electrogenicity" of the L-type Ca^{2+} current is crucial in the generation of mouse ventricular phase 2. This mechanism has been suggested to be involved in the development of a slow phase of repolarization in a different experimental model (rat), the cardiac structure (trabeculae), and experimental conditions (temperature of 26°C) rather than the ones presented in the present study (46).

To test our hypothesis, we first performed several experimental series to resolve the controversy between patch-clamp measurements in isolated myocytes and our optically recorded epicardial APs. We also took into account the effect of the regional localization of the epicardial recordings, the experimental approach (optical vs. electrical), the temperature, the dependency on intracellular Ca^{2+} release, the role of the Ca^{2+} conductances in the plasma membrane, the transport of Na^+ ions through the Na^+/Ca^{2+} exchanger, and the emergent properties of the tissue.

We conclude that APs recorded from ventricular myocytes show phase 2 both at the whole heart and at the isolated cell levels. This phenomenon is highly dependent on temperature and intracellular Ca^{2+} dynamics. Finally, we postulate that phase 2 appears as a consequence of the activation of ionic conductance/transport (i.e., Na^+/Ca^{2+} exchanger) driven by Ca^{2+} release from the SR.

Address for reprint requests and other correspondence: A. L. Escobar, School of Engineering, Univ. of California, Merced, 5200 North Lake Road, Merced, CA 95343 (e-mail: aescobar4@ucmerced.edu).

METHODS

Whole heart preparation. Hearts were dissected from young C57BL/6 mice (3 to 7 wk old). Briefly, each animal was euthanized by cervical dislocation and the heart was rapidly removed. The heart was placed in the recording chamber, where the aorta was cannulated and placed into a horizontal Langendorff apparatus (48). The heart was constantly perfused with normal Tyrode solution containing the following (in mM): 2 $CaCl_2$, 140 NaCl, 5.4 KCl, 1 $MgCl_2$, 0.33 Na_2HPO_4, 10 HEPES, and 10 glucose, pH 7.4 at 37°C. In Li^+ replacement experiments, NaCl was equimolarly replaced with LiCl. The temperature of the solution outside the heart was controlled with a Peltier unit. Pacemaker cells of the sinoatrial and atrioventricular nodes were electrically ablated with the aid of an ophthalmic bipolar pencil (Mentor Ophthalmics, Santa Barbara, CA) to gain external control of the heart rate. During the experiments, each heart was continuously paced at 4 or 5 Hz through a silver bipolar electrode placed at the base of the left ventricle. The stimulus electrodes were wired to an electrical stimulator ISOSTIM A320 (World Precision Instruments, Sarasota, FL) controlled by a PC. All solutions were equilibrated with 100% oxygen. This protocol was approved by the University of California Merced Institutional Animal Care and Use Committee.

Ventricular myocyte dissociation. Mouse ventricular myocytes were enzymatically isolated using the Langendorff coronary retroperfusion technique (38). Briefly, each heart was placed on a Petri dish containing a Tyrode solution at 37°C. The aorta was cannulated, and the coronary arteries were washed with Tyrode solution for 6 min, followed by 6 min with a Ca^{2+}-free Tyrode solution containing the following (in mM): 140 NaCl, 5.4 KCl, 1 $MgCl_2$, 0.33 Na_2HPO_4, 10 HEPES, and 10 glucose, pH 7.4 at 32°C. The heart was then perfused for 7 min with Ca^{2+}-free Tyrode solution containing 1 mg/ml type 2 collagenase (322 U/mg) (Worthington Biochemical). Subsequently, hearts were perfused with a Ca^{2+}-free Tyrode solution and the cells were dissociated by the aid of a fire-polished glass Pasteur pipette in the presence of 1 mg/ml of BSA. Finally, the cells were filtered with a nylon mesh and maintained in Tyrode solutions containing 0.2 and then 2 mM $CaCl_2$. Only rod-shaped and Ca^{2+}-tolerant cells were used in the experiments.

Ca^{2+} and potentiometric dye loading. Rhod-2 AM (Invitrogen, Carlsbad, CA) was used to measure Ca^{2+} signals in the cytosol. An aliquot of 50 μg of the dye was dissolved in 45 μl of DMSO with 2.5% pluronic and added to 1 ml of normal Tyrode. Perfusion with the dye began after the spontaneous heart rate became regular (within 10 min after cannulation). The time of loading was 25–35 min.

Membrane potential was optically measured with the potentiometric dye di-8-anneps (Invitrogen). The dye (10 μg) was dissolved in pluronic/DMSO, as indicated for rhod-2 AM, and 10 ml of Tyrode were added to achieve a final concentration of 1.6 μM. Di-8-anneps was perfused in the same way as rhod-2 AM. The loading procedure was carried out at room temperature for 30 min, then the perfusate was switched to Tyrode solution, and the temperature was increased to 37°C. Downward fluorescence signals reflecting plasma membrane depolarization were used as an indication of dye loading. After di-8-anneps was removed from the perfusate, the amount of dye that remained in the plasma membrane and the tubular system was enough to generate a detectable signal for ≥3 h. Optical recordings of the membrane potential were calibrated against intracellular microelectrode measurements for each experiment.

Optical setup. A modified version of our custom-made pulsed local field fluorescence (PLFF) microscopy setup (14, 37) was employed to measure APs from intact hearts. Solid-state neodymium-doped yttrium aluminum garnet (Nd-YAG) lasers were used as an illuminating source. Green light (532 nm) was obtained from a MGL-50B-1 CW Ng-YAG laser (Enlight Technologies, Branchburg, NJ).

The pulses of light used for excitation were focused with an aspheric lens (Thorlabs; NA 0.47) into multimode optical fibers for the transmission of the exciting light to the epicardial layer (32, 47). The light emitted by the dye was carried back through the same fiber, filtered with a 590-nm emission barrier filter to eliminate the reflected excitation component, and focused on an avalanche diode. The photocurrent was finally amplified by a resistive current-to-voltage converter controlled by a Digital Signal Processor (DSP 320; Texas Instruments). The head-stage unit and their corresponding high-voltage power supply were custom built. The electrical signals produced by the measurements of fluorescence were filtered to a bandwidth of 500 kHz and sampled at a frequency of 5 MHz. The acquisition system was controlled by a PC running a custom-designed G-based software program (LabVIEW; National Instruments).

Finally, one end of the optical fiber was gently placed a few hundreds of micrometers from the tissue surface. The motion of the heart was noticeably decreased upon addition of 10 μM blebbistatin to the perfusing Tyrode solution. A number of studies (11, 16, 17, 47) have shown that, at this concentration, blebbistatin has no significant side effects on either Ca^{2+} transients or APs.

Whole heart electrophysiological measurements. Transmembrane APs were recorded from the left atrium and epicardial layer of the right and left ventricles over the anterior wall. The signals were recorded using glass microelectrode filled with 3 M KCl (10–20 MΩ resistance) connected to a high input impedance amplifier (World Precision Instruments-Duo 773 Electrometer). The electrical signals were filtered to a bandwidth of 500 kHz, digitally sampled at a frequency of 5 MHz, and then digitally resampled to 2 kHz. The acquisition system was controlled by a PC running a custom-designed G-based software program (LabVIEW; National Instruments).

AP refractoriness was obtained by applying an additional stimulation pulse at different times with respect to the regular pacing pulses. By changing the time interval between electrical stimulations, we were able to obtain the values for the refractory period.

Single myocytes electrophysiological measurements. Ventricular myocyte APs were measured under current-clamp conditions (Axopatch 200B; Molecular Devices) using intracellular sharp microelectrodes filled with 3 M KCl (40–60 MΩ resistance). Pipette resistance and capacitance was analogically compensated to improve the recording bandwidth. Data were filtered at 10 kHz and digitized through a Digidata 1440A acquisition system (Molecular Devices) with pClamp 10 software at a sampling rate of 100 kHz. Ventricular myocytes were placed in a chamber on the stage of an inverted microscope (Olympus IX70). Myocytes were continuously perfused with oxygenated Tyrode solution at 37°C.

Analysis of the recordings. An integration-subtraction procedure was utilized to measure the contribution of phase 2 to the total area under the AP. First, phases 0 and 1 of the AP were fitted with an exponential function of the form:

$$ph_{01} = V_m + V_{amp} \cdot \left(1 - e^{-\frac{t-t_1}{\tau_{on}}}\right) \cdot e^{\frac{t-t_1}{\tau_{off}}}$$

where V_m is the resting membrane potential, V_{amp} is the amplitude of the AP, τ_{on} is the time constant for phase 0, τ_{off} is the time constant for phase 1, and t_1 is the delay time with respect to the electrical stimulus. Note that first, all the amplitudes were measured as a difference between the actual membrane potential and the resting membrane potential.

Second, the area under this function ph_{01} was calculated using a numerical integration procedure (A_{ap01}).

Third, the area under the whole AP was calculated by numerically integrating the AP trace (A_{ap}). Finally, the contribution of the phase 2 to the total AP was calculated using the following expression

$$\%ph_2 = \frac{A_{ap} - A_{ap01}}{A_{ap}} \cdot 100 = \frac{A_{ap2}}{A_{ap}} \cdot 100 \quad \text{where } A_{ap2} = A_{ap} - A_{ap01}$$

Statistical analysis. Data are expressed as means ± SE; *n* indicates the number of independent experiments. The total number of animals used in this study was 52. Statistical significance was tested using

ANOVA. The difference was considered to be significant if the value of P was <0.05.

Drugs and chemicals. All reagents and chemicals were purchased from Sigma Chemical (St. Louis, MO) unless indicated.

RESULTS

Presence of phase 2 in epicardial AP. Mouse epicardial electrical activity has usually been measured using monophasic AP recordings (29). Although this approach is very useful to detect the presence of local APs, it only provides a qualitative description of the epicardial electrical activity. In this study, we performed PLFF microscopy measurements on mouse hearts previously loaded with the potentiometric dye di-8-anneps. Figure 1*A* shows both an optically and electrically recorded AP from the left ventricle using a 200-μm optical fiber and a intracellular sharp microelectrode, respectively. The four phases of a ventricular AP can be clearly observed. Two very distinguishable features are a very deep phase 1 and a prominent phase 2. In Fig. 1*C*, the contribution of phase 2 to the AP is shown in a bar graph for the electrical and optical recordings. There are no significant differences in the AP kinetic parameters ($n = 15$ animals) using either method. Figure 1*C*, *inset*, shows a graphical scheme that illustrates how the contribution of phase 2 to the AP was evaluated. A detailed description of the mathematical procedure has been described in METHODS. This method for evaluating the contribution of phase 2 to the AP provided us with a parameter that has less scattering than the usual report of AP durations (APDs) at different levels of repolarization. However, the contribution of phase 2 to the atrial AP was negligible (Fig. 1*B*). A comparison of the contribution of phase 2 to the repolarization of the AP between the left atrium and the left ventricle is shown in a bar graph presented in Fig. 1*D*. The observed differences (15 animals left ventricle and 5 animals left atrium) are statistically significant ($P < 0.05$). Additionally, APD at 50 and 90% of the repolarization (APD_{50} and APD_{90}) are also presented in Table 1.

Potentiometric dyes not only stain the surface membrane but the T system as well (49). On the other hand, electrical recordings are self-calibrated, and although the myocytes are electrically connected between them, the electrical signal measured with this technique is spatially confined by the space constant λ of the tissue. In Fig. 2*A*, we show simultaneous electrical and optical APs recordings measured from the epicardium of the left ventricle in a mouse heart perfused with a Langendorff apparatus. Similar kinetic features as the deep phase 1 and a prominent phase 2 are evident in both optical and

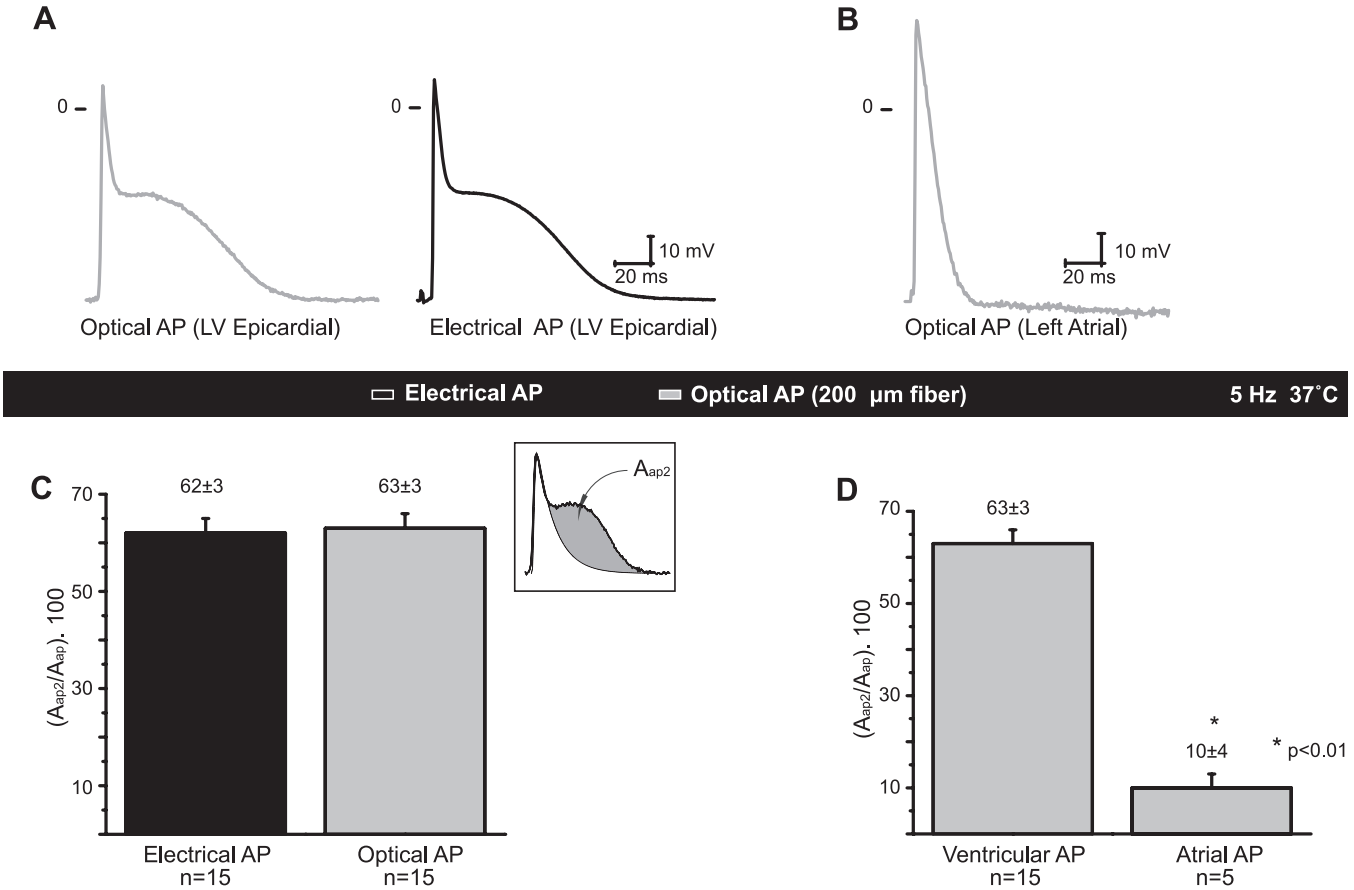

Fig. 1. Phase 2 in epicardial ventricular action potential (AP). *A*: typical optical recording of a left ventricle AP. Four phases of AP can be clearly observed. *B*: electrical AP recordings measured from the left ventricular (LV) epicardium of a perfused mouse heart. Both types of recordings (*A*) show identical kinetic features (*B*). Optical recordings of left atrium AP, the AP traces (A_{ap}) relaxed monotonically to the resting membrane potential. *C*: comparison between the contribution of phase 2 to left ventricle and left atrium AP ($n = 15$ animals left ventricle and 5 animal left atrium) is statistically significant ($P < 0.01$). *Inset*: graphical scheme that illustrates how the contribution of phase 2 to the AP was evaluated. *D*: bar graph of the percentage of phase 2 contributions to the epicardial AP. There are not significant differences between the AP kinetic measured with either of 2 techniques. Recordings were performed at 37°C and externally paced at 5 Hz. Electrical recordings were performed by impaling cells with a 20 MΩ microelectrode and optical recordings using a 200-μm optical fiber.

Table 1. *Intact heart AP parameters*

LV Epicardium (5 Hz/37°C)	Electrical AP (n = 15)	Optical AP (n = 15; 200-μm Ø fiber)	Electrical AP (n = 5)	Optical AP (n = 5; 1,000-μm Ø fiber)
Resting potential −mV	66.7 ± 1.3		73.2 ± 2.9	
Amplitude				
Phase 0, mV	76.2 ± 1.7		83.8 ± 3.5	63.1 ± 2.9
Phase 1, mV	40.1 ± 0.5	41.1 ± 0.9	42.7 ± 1.8	39.9 ± 3.3
Phase 2, mV	40.5 ± 0.6	41.7 ± 1.0	45.3 ± 1.2	42.0 ± 3.2
Magnitude				
Phase 1, mV	36.1 ± 1.6	35.1 ± 5.1	40.7 ± 4.3	23.7 ± 4.0
$APD_{90\%}$, ms	87.2 ± 3.2	87.7 ± 3.2	102.6 ± 5.8	100.3 ± 7.6
$APD_{50\%}$, ms	33.3 ± 5.4	37.6 ± 4.6	51.3 ± 12.8	54.9 ± 14.1
Time to peak, ms	2.6 ± 0.3	3.4 ± 0.3	1.9 ± 0.3	5.8 ± 0.9*

Values are means ± SE; n = 15 hearts. Action potential (AP) parameters of mouse ventricular epicardium recorded at 37°C and 5 Hz. $APD_{90\%}$, AP duration at 90% repolarization; APD_{50}%, AP duration at 50% repolarization. *$P < 0.05$.

electrical measurements, when a 200-μm multimode optical and a 20 MΩ microelectrode were used at the same location.

Usually, an important limitation of measuring intracellular signals from multicellular preparations in three dimensions is to know where the measured signals are coming from. For example: how different myocytes, located across and along the ventricular wall of an intact beating heart, will contribute to the measured intracellular AP? We have already shown that the PLFF microscopy provides the possibility to measure fluorescence signals from different tissue levels depending on the diameter of the optical fiber (37). Figure 2, *A* and *B*, compares electrical and optical traces recorded simultaneously at the same location using 200-μm and 1,000-μm optical fibers. Membrane potentials measured with the 200-μm fibers (Fig. 2*A*) were not significantly different than the ones measured with sharp microelectrodes. This indicates that, within a depth of field of ~215 μm (the axial optical resolution of a 200-μm fiber), the tissue was highly isopotential. On the other hand, when a 1,000-μm optical fiber was used (Fig. 2*B*), the time to peak of the AP was significantly modified. Moreover, for this latter condition the delay between the stimulus and the AP was shorter for the optical recording. This suggests that the larger fiber was able to detect cellular layers that depolarize sooner than the epicardial layer. Moreover, as the AP propagates faster along the epicardium than transmurally, thus it is more likely that the differences in the delay for the two different types of fiber are due to the contribution of APs from deeper layers.

Nonetheless, phase 2 was clearly present independently of the transmural depth of our recordings and the contribution of this phase to the AP was not significantly different for measurements obtained with optical fibers having different diameters (Fig. 2*C*). Table 1 summarizes the differences between AP kinetic parameters measured with the two types of optical fibers and the simultaneous electrical recordings.

In canine models, the distribution of the time courses of APs depends not only on the transmural dispersion but also present differences along the epicardial layer. To test whether these epicardial differences were also present in the mouse model, we performed experiments to map the epicardial AP waveforms. Regions like the base, middle, and apex of the left ventricle and the middle of the right ventricle were measured. Traces of all epicardial recordings are shown in Fig. 3*A*. We

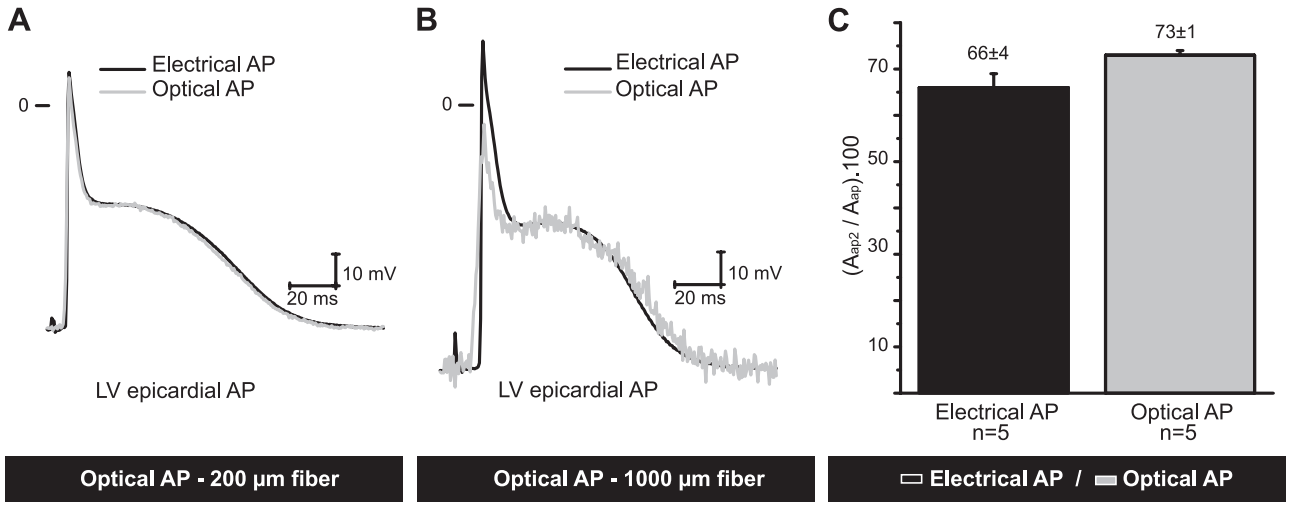

Fig. 2. Phase 2 in epicardial ventricular AP: effect of the fiber optic diameter. *A*: comparison of typical electric and optical recordings when a 200-μm optical fiber was used; traces are mostly identical. *B*: electrical and optical traces measured with a 1,000-μm optical fiber show significant differences in the delay time from the stimulus and the time to peak (see Table 1). *C*: bar graph that shows the contribution of phase 2 to the AP for simultaneous electrical and optical recordings using a 1,000-μm optical fiber. Although the phase 2 contribution seems to be larger for the optical recording, no statically differences were found between the 2 type of measurements (n = 5 animals). All the recordings were performed at 37°C, and the electrical recordings performed with a 20-MΩ microelectrode.

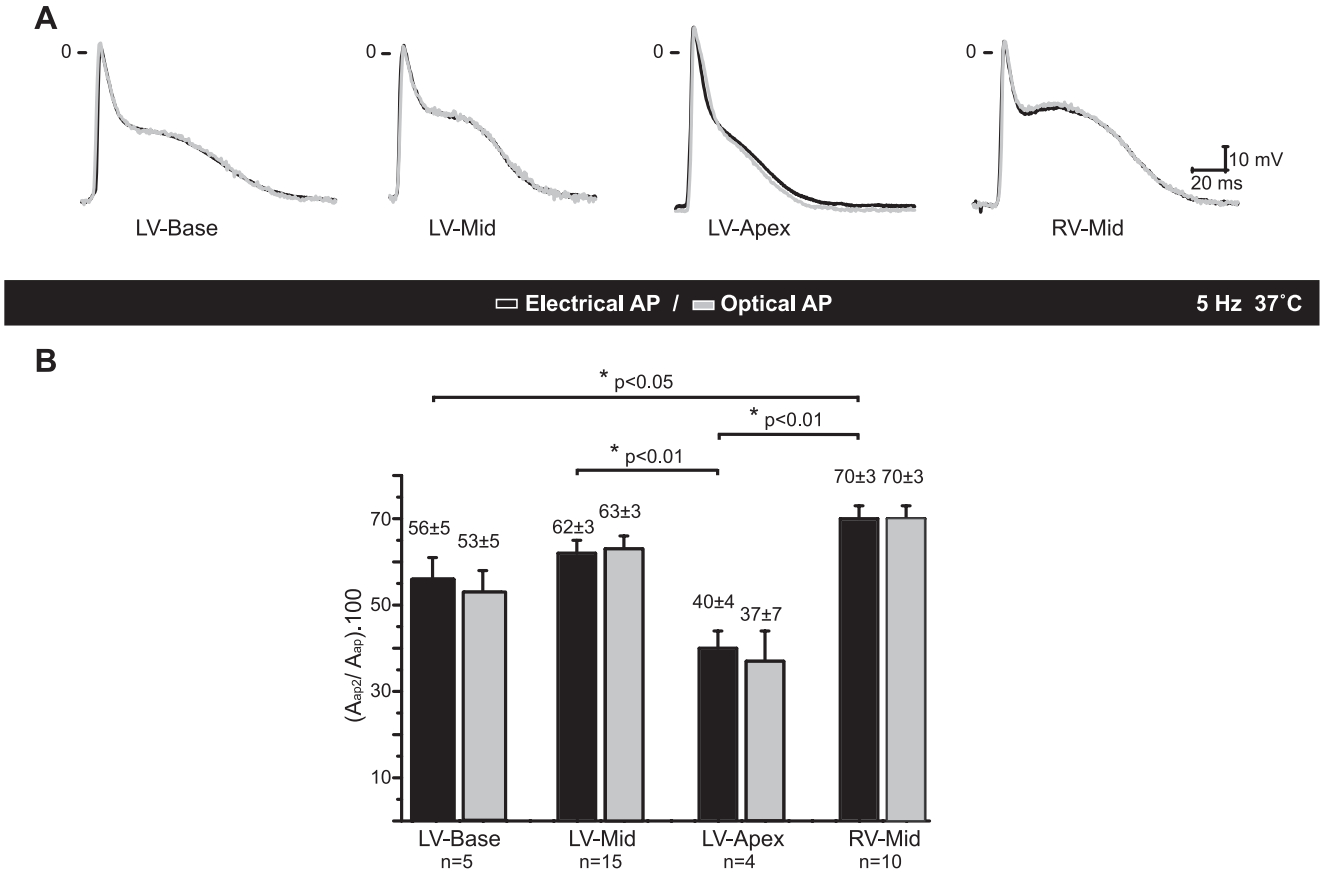

Fig. 3. Phase 2 in ventricular AP: epicardial distribution. *A*: simultaneous intracellular and 200-μm optical fiber recordings in different epicardial regions of a mouse heart. Although there are no differences between electrical and optical recordings for the same epicardial region, recordings from different places are dramatically dissimilar. *B*: percent contribution of phase 2 to the AP. Significant differences can be observed between the base of the left ventricle (LV-Base) and the central region of the right ventricle (RV-Mid). Additionally, there are significant differences between the apex of the left ventricle (LV-Apex) and central region of the right ventricle (RV-Mid) and the central region of the left ventricle (LV-Mid). All the recordings were performed at 37°C using a 200-μm optical fiber and the heart paced at 5 Hz.

can observe that the magnitude of phase 1 and the APD_{90} of the repolarization are different for the various recording areas. In addition, a plot of the relative contribution of phase 2 for the different regions is shown in Fig. 3*B*. This plot shows that although there are no significant differences between optical and electrical recordings for the same region, the differences between regions are highly statistically significant ($P < 0.05$; $n = 4$–15 hearts).

The fact that epicardial APs recorded from different regions of the heart displayed a significant phase 2 at a heart rate of 5 Hz opened the question of what will happen with the APD at a higher heart rate. Indeed, the resting heart rate of the mouse heart is close to 600 beats/min (10 Hz). To test if phase 2 in epicardial APs was compatible with a physiological heart rate, we performed experiments pacing the heart at different rates. Figure 4 shows the results from these experiments. Figure 4*A* illustrates the AP waveforms at heart rates from 5 to 10 Hz. It is possible to observe that phase 2 gets shorter with no changes in phase 1 duration. Both the APD_{90} (Fig. 4*B*) and the contribution of phase 2 to the AP (Fig. 4*C*) become significantly shorter and smaller as the heart rate increases. Note that the APs still show a significant contribution of phase 2.

Relationship between epicardial phase 2 and intracellular Ca^{2+} dynamics. Ventricular AP phase 2 has been largely associated with an influx of Ca^{2+} through the L-type voltage-activated Ca^{2+} channel (dihydropyridine receptor) (8, 44). To test if in mouse models phase 2 has the same pharmacological properties as in other mammalian species, we perfused hearts with 10 μM of nifedipine (a Ca^{2+} channel blocker). Figure 5*A* shows optical and electrical APs recordings from the left ventricle, where the application of nifedipine has a profound effect on the AP repolarization. This effect was completely removed after 15 min of washout of the drug. Figure 5*B* illustrates the statistical analysis of the contribution of phase 2 to the AP during the application and the washout of the drug. Nifedipine induced a significant reduction of the phase 2 ($n = 5$ animals; $P < 0.01$).

In other mammalian models, dihydropyridines not only reduce the Ca^{2+} current through L-type Ca^{2+} channels (26) but also reduce Ca^{2+} released from the SR in an indirect way. This mostly occurs by an impairment of the Ca^{2+} induced Ca^{2+} release (CICR) process due to a reduction in the size of the Ca^{2+} trigger. Figure 5*C* exemplifies the effect of nifedipine on epicardial Ca^{2+} transients measured by PLFF microscopy. Hearts loaded with the Ca^{2+} indicator rhod-2 were perfused with a Tyrode solution containing 10 μM of nifedipine. The drug produced a significant decrease in the amplitude of the Ca^{2+} transients ($n = 5$ animals); as shown in Fig. 5*C*, the decrease produced by nifedipine is statistically significant (Fig. 5*D*).

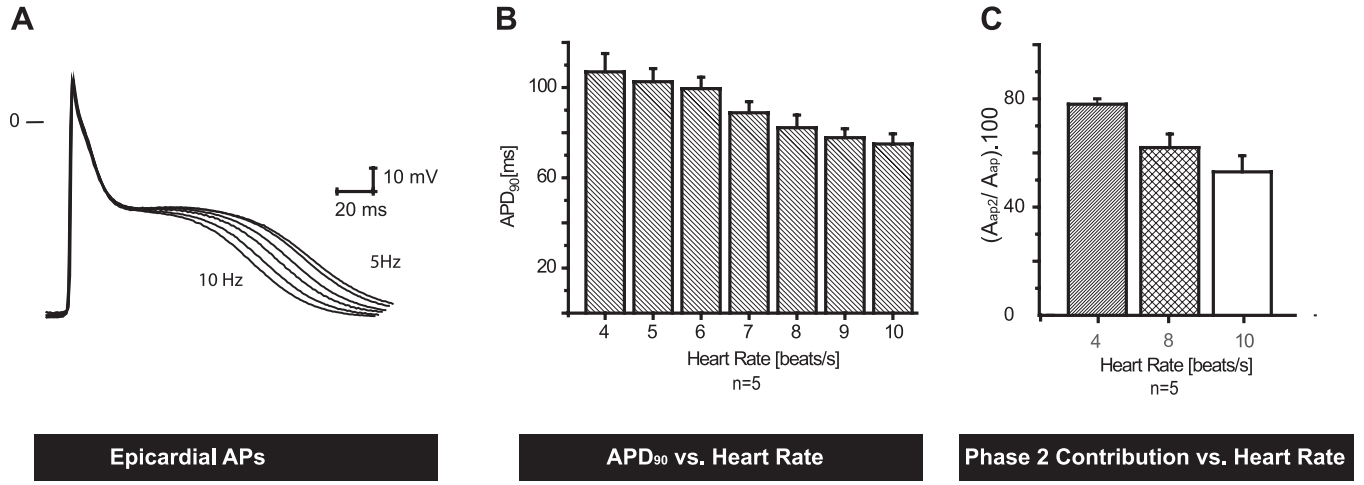

Fig. 4. Phase 2 in epicardial ventricular AP: heart rate dependency. *A*: traces of APs recorded with sharp microelectrodes at different heart rates from the LV epicardial layer. Recordings were obtained by pacing the heart from 5 to 10 Hz. *B*: bar graph of AP durations at 90% of the repolarization (ADP_{90}). It is possible to observe that the higher the heart rate the shorter the AP ($n = 5$ animals). *C*: contribution of phase 2 to the AP at different heart rates. Contribution of phase 2 is smaller at higher heart rates ($n = 5$ animals). All the recordings were performed at 37°C, and the electrical recordings were performed with a 20-MΩ microelectrode.

Although the current opinion on the role of L-type Ca^{2+} channels on the repolarization of the AP is that the Ca^{2+} current itself is mainly responsible for this long depolarizing effect during phase 2, it is possible that the Ca^{2+} released from the SR plays a key role in the genesis of the AP phase 2. Ryanodine, an alkaloid that binds to the SR Ca^{2+} release channel and locks the channels in a high open probability low subconductance state, and thapsigargin, a noncompetitive inhibitor of the sarco(endo)plasmic reticulum Ca^{2+}-ATPase pump, were used to impair SR Ca^{2+} release. Figure 5*G* illustrates the effect of 10 μM ryanodine and 2 μM thapsigargin on Ca^{2+} transients measured on the left ventricle epicardial layer. A dramatic and significant decrease in the amplitude of the Ca^{2+} transients was observed even though ryanodine does not have a direct effect on the dihydropyridine receptor (Fig. 5*H*). Figure 5*E* shows the effect of 10 μM ryanodine and 2 μM thapsigargin on the time course of epicardial AP. The elimination of SR Ca^{2+} release produces a very similar effect as nifedipine. Figure 5*F* shows the statistical analysis for the contribution of phase 2 to the repolarization of the AP.

On the mechanism that transduces intracellular Ca^{2+} dynamics into phase 2 of epicardial AP. Experiments illustrated in Fig. 5 show that contribution of phase 2 to the repolarization of the AP dramatically depends on SR Ca^{2+} release. Additionally, our laboratory has already reported that the kinetics of intracellular Ca^{2+} transients recorded from the left ventricle epicardial layer highly depends on temperature (32). Therefore, it is likely to expect that temperature will have a strong influence on the phase 2. We performed experiments to test this hypothesis, and the results are shown in Fig. 6. Temperature has an important effect in all the kinetic parameters of the AP. Specifically, if we increase the temperature from 23 ± 1°C (Fig. 6*B*) to 37 ± 1°C (Fig. 6*A*), it is possible to observe a decrease in the magnitude of phase 1 and an increase in the contribution of phase 2 to the AP repolarization. A statistical analysis of the phase 2 contribution is presented in Fig. 6*C*. Temperature has a significant effect on phase 2 in both optically and electrically recorded APs ($n = 5$ animals; $P < 0.01$). As temperature was increased from room temperature to 37°C the contribution of phase 2 increases by 119 ± 22%. This suggests that not only the kinetics of the Ca^{2+} transients but also that the mechanism that translates the changes in myoplasmic Ca^{2+} concentration into a depolarizing current during phase 2 are extremely temperature dependent (see DISCUSSION). The fact that an increase in temperature induces an increase in phase 2 is somehow counterintuitive. In fact, it is reasonable to expect that an increase in temperature will accelerate any kinetic process. However, the APD_{50} increased from 13.66 ± 0.3 to 43.27 ± 0.8 ms ($n = 5$ animals) when the temperature was increased from 23°C to 37°C. On the other hand, this same increment in the temperature did not produced a significant change in the APD_{90} (79.3 ± 6.8 ms to 92.7 ± 6.0 ms; $n = 5$ animals; $P > 0.05$). This is consistent with the idea that temperature mostly changes the morphology of the AP. Additionally, there were also no significant changes in the resting membrane potential when temperature was changed (−70.76 ± 2.9 to 72.47 ± 4.5 mV; $n = 5$ animals; $P > 0.05$).

To further explore if there were other AP kinetic properties modified by temperature in an anomalous way, we performed double-pulse experiments to evaluate the temperature dependency of the epicardial AP refractory period. Data presented in Fig. 6, *D–F*, show that an increase in the temperature produced a decrease in the refractory period. The reduction in the refractory period could be explained by a faster recovery from inactivation of Na^+ channels when temperature was increased (39) from 23°C to 37°C. Additionally, the enlargement in the rate of depolarization (phase 0) for the same temperature change could also contribute to the reduction of the refractory period at higher temperatures. Indeed under this condition, the time to peak of the AP was significantly reduced from 5.37 ± 0.95 to 2.24 ± 0.55 ms ($n = 5$ animals; $P < 0.05$).

The high temperature dependency of phase 2, in addition to the effect of intracellular Ca^{2+} dynamics on the repolarization of the AP, drove us to speculate that the depolarizing membrane current during phase 2 was carried through a Ca^{2+}

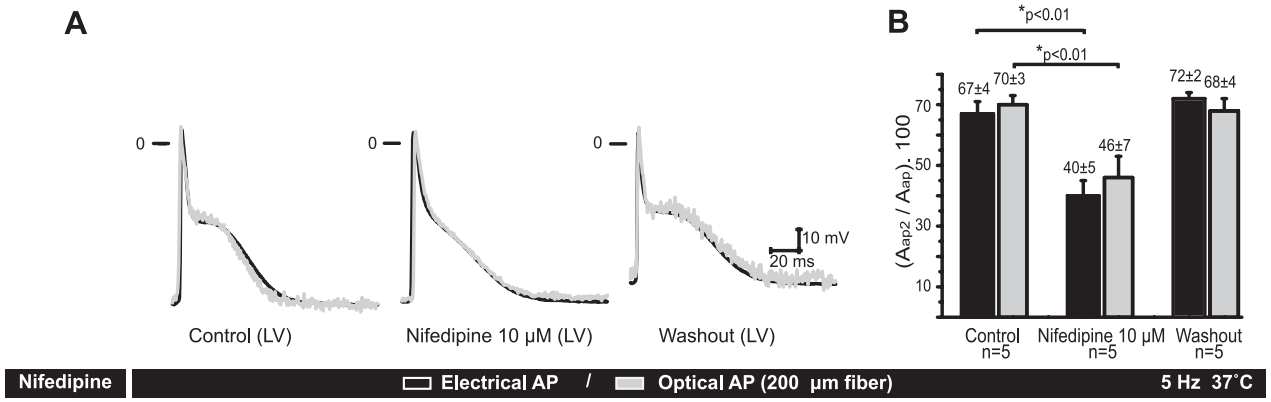

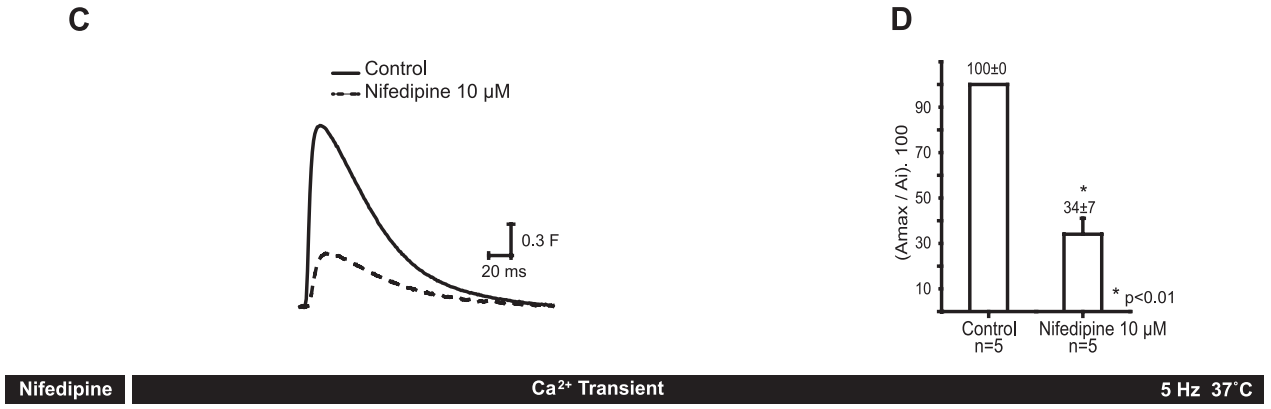

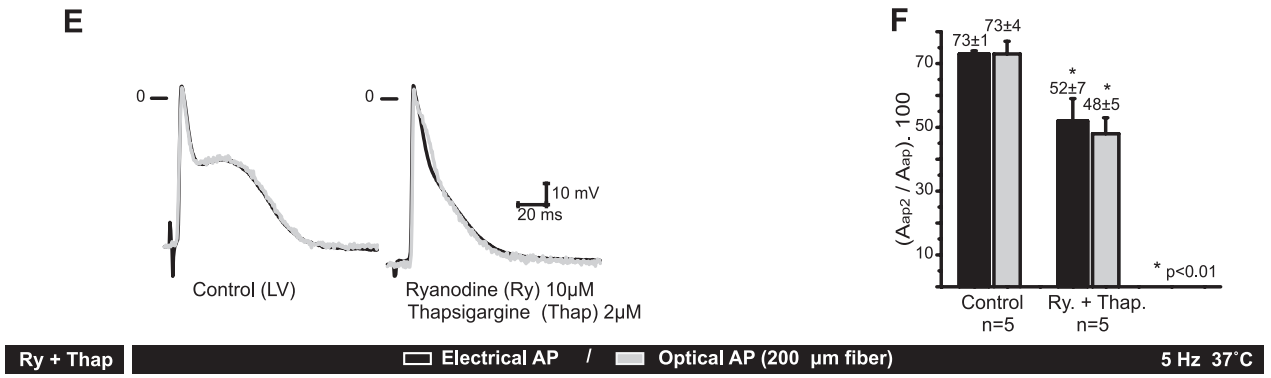

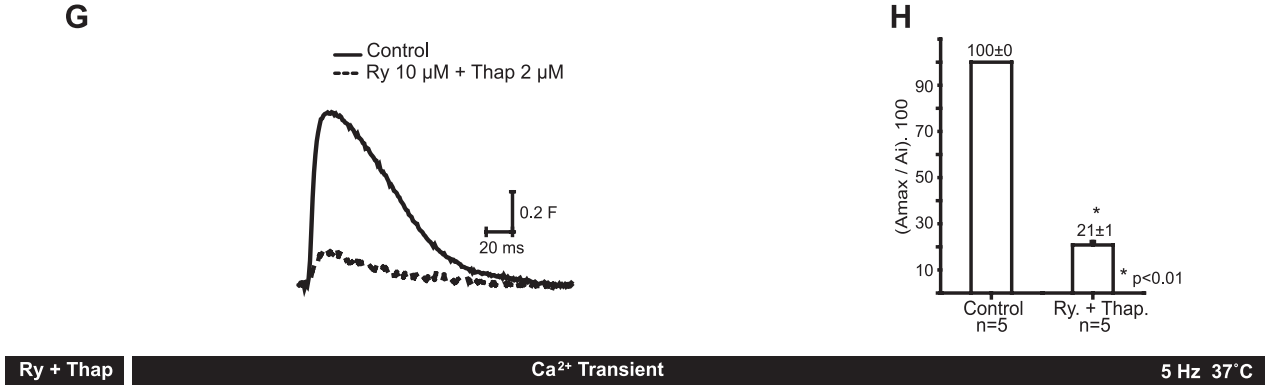

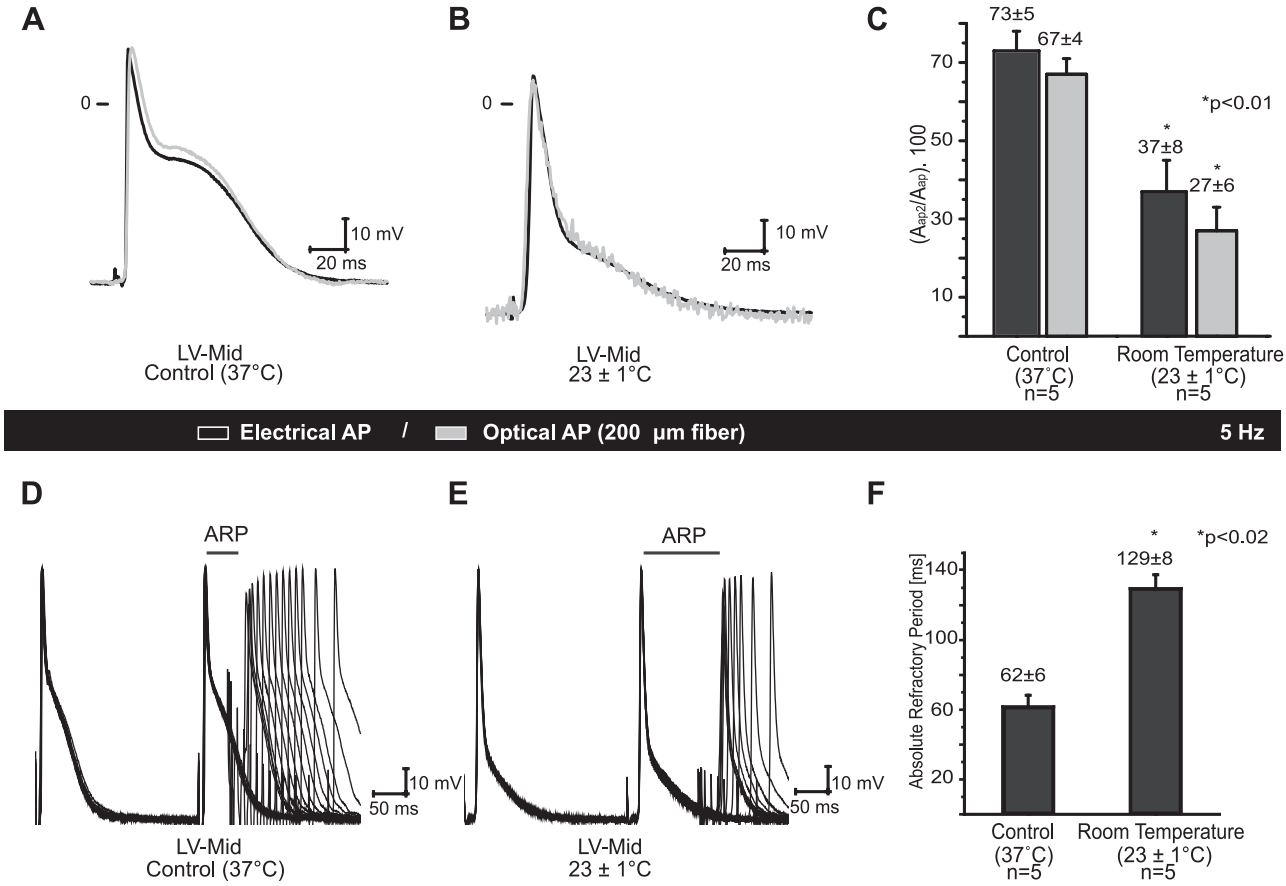

Fig. 6. Phase 2 in epicardial ventricular AP: temperature dependency. *A* and *B*: effect at 37°C (*A*) and room temperature (23 ± 1°C) (*B*) on AP recorded electrically and optically. Decrease in temperature accelerates the late repolarizing phase of APs. Graph bar presented in *C* shows that temperature has a significant effect on the phase 2 contribution to the AP ($n = 5$ animals; $P < 0.01$). *D* and *E*: typical double pulse experiments design to measure the absolute refractory period (ARP) at 37°C and at 23 ± 1°C, respectively. It is possible to observe that although the AP are longer at 37°C than at 23 ± 1°C the ARP is shorter (*F*; $n = 5$ animals; $P < 0.02$). Experiments were obtained by externally pacing the heart at 4 Hz and AP measurements were performed by means of glass microelectrodes or by using 200-µm optical fibers.

mediated transporter. The most likely transmembrane protein governing this kinetic process appears to be the Na^+/Ca^{2+} exchanger. Unfortunately, known pharmacological antagonists of this transporter also interact with other membrane proteins involved in the CICR process. On the other hand, it is well known that Li^+ cannot be transported through the Na^+/Ca^{2+} exchanger. Furthermore, Li^+ can permeate just as well as Na^+ through the voltage-dependent Na^+ channel allowing the upstroke of an AP. Thus the equimolar replacement of Na^+ by Li^+ in the external Tyrode solution can serve as a way to evaluate the fractional contribution of the Na^+/Ca^{2+} exchanger to the phase 2. Experiments testing this idea are shown in Fig. 7*A* where the effect of replacing half of the NaCl by LiCl in optically recorded APs is presented. This fractional equimolar substitution of Na^+ by Li^+ has a dramatic effect on the AP repolarization. However, the effect on the repolarization of the AP shown in Fig. 7*A* can be explained as a direct reduction of the transport turnover number of the Na^+/Ca^{2+} exchanger or by a direct effect of the Li^+ treatment on the amplitude of the Ca^{2+} transient. If indeed Li^+ reduces the Ca^{2+} released from the SR, then an acceleration of the repolarization process is also expected to be observed. To test this latter idea, we

Fig. 5. Phase 2 in epicardial ventricular AP: pharmacological sensitivity. *A*: typical AP traces show the effect produced by the application and washout of Tyrode solution containing 10 µM of nifedipine. Both the electrical and optical recordings show a dramatic effect of the drug on the AP time course and the recovery after 15 min of washout. *B*: bar graph of the percent phase 2 contributions to the epicardial AP, the differences between the AP kinetic measured with either technique were significant ($n = 5$ animals; $P < 0.01$). *C*: pharmacological effect on the epicardial Ca^{2+} transients when the heart was perfused with 10 µM of nifedipine. *D*: graph bar that shows the percentile effect of the nifedipine treatment on the amplitude of Ca^{2+} transients ($n = 5$ animals, $P < 0.01$). *E*: effect of ryanodine (10 µM) and thapsigargin (2 µM) on the time course of electrical and optical APs recorded from the epicardial layer of the left ventricle. Traces show a profound effect of sarcoplasmic reticulum Ca^{2+} release on the repolarization of the APs. Contribution of phase 2 to the AP repolarization has been significantly reduced by the application of ryanodine and thapsigargin ($n = 5$ animal; $P < 0.01$) as shown by a bar graph in *F*. *G*: application of 10 µM ryanodine and 2 µM thapsigargin dramatically reduced the amplitude of the epicardial Ca^{2+} transients. Solid trace represents the control condition and the dotted trace the remaining Ca^{2+} transient reflecting the influx of Ca^{2+} through the plasmamembrane in absence of Ca^{2+} release from the sarcoplasmic reticulum. *H*: graph bar that shows the effect of the nifedipine treatment on the amplitude of Ca^{2+} transients ($n = 5$ animals; $P < 0.01$) as a percentage of the pretreatment control amplitude. All the optical recordings were performed at 37°C using a 200-µm optical fiber, and the heart was externally paced at 5 Hz.

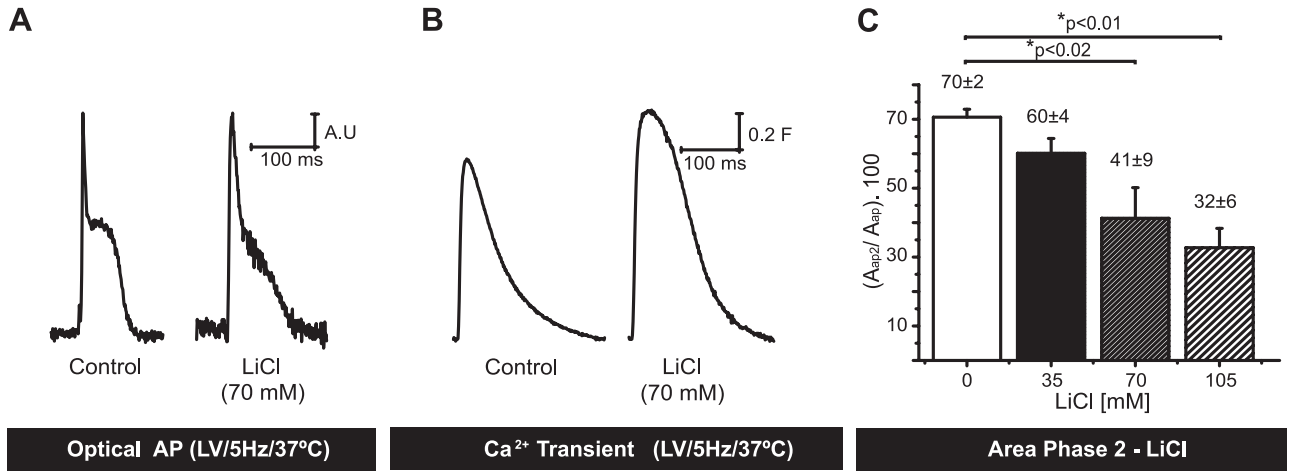

Fig. 7. Na^+/Ca^{2+} exchanger regulates phase 2 in ventricular AP. *A*: equimolar substitution of 70 mM of NaCl by 70 mM LiCl in the extracellular perfusate dramatically reduces the contribution of phase 2 to normalized optically recorded AP from the left ventricle of intact mouse hearts ($n = 5$ animals; $P < 0.02$). Traces are illustrated in arbitrary units (AU). *B*: Effect of replacing 70 mM Na^+ by 70 mM Li^+ on Ca^{2+} transients. Amplitude of the Ca^{2+} transients was increased by 20% ($n = 5$ animals; $P = 0.004$). Traces are presented as absolute fluorescence. *C*: bar graph demonstrating the incremental effect of Li^+ replacement on the phase 2 contribution to the AP ($n = 5$ animals). All experiments were performed at 37°C, and the hearts were paced a 4 Hz.

measured the amplitude of the epicardial Ca^{2+} transients measured under the same experimental conditions than the one described for Fig. 7*A* but using the indicator rhod-2 to track the intracellular Ca^{2+}. The results presented in Fig. 7*B* show that the Li^+ treatment does not diminish the amplitude of the Ca^{2+} transient; instead it induces an increment of this intracellular signal most likely due to an increase in intra SR Ca^{2+} load. A summary of the results obtained in AP recordings when Na^+ was equimolarly replaced by different fractions of Li^+ is presented in Fig. 7*C*. Phase 2 contribution to the AP was significantly decreased when 50 and 75% of Na^+ was replaced by Li^+. These results indicate that most of the membrane current that depolarizes the AP during phase 2 is carried through the Na^+/Ca^{2+} exchanger when this transporter is activated by Ca^{2+} released from the SR.

Phase 2 at the single cell level. Most of our actual knowledge on the kinetics of ventricular mouse APs comes from isolated ventricular myocyte experiments, where membrane potentials have been recorded using the whole cell patch-clamp recording under current-clamp conditions (3, 22, 36). Although this is a very powerful approach, it has the disadvantage that the myocytes are usually dialyzed through the recording pipette. Additionally, the internal solution usually contains a high concentration of the Ca^{2+} buffer EGTA to prevent cell contraction during an AP-induced Ca^{2+} release. Moreover, usually these experiments are generally performed at room temperature (22) to maintain the myocyte viability for a longer time. Experiments published under these conditions never display a phase 2 during the repolarization of the AP. To test if phase 2 is a single cell property that has been impaired by the factors described above, we performed experiments in enzymatically isolated ventricular myocytes impaled with high resistant sharp microelectrodes at 37°C. Figure 8*A* illustrates a chart of APs every 200 ms elicited by current pulses applied through the

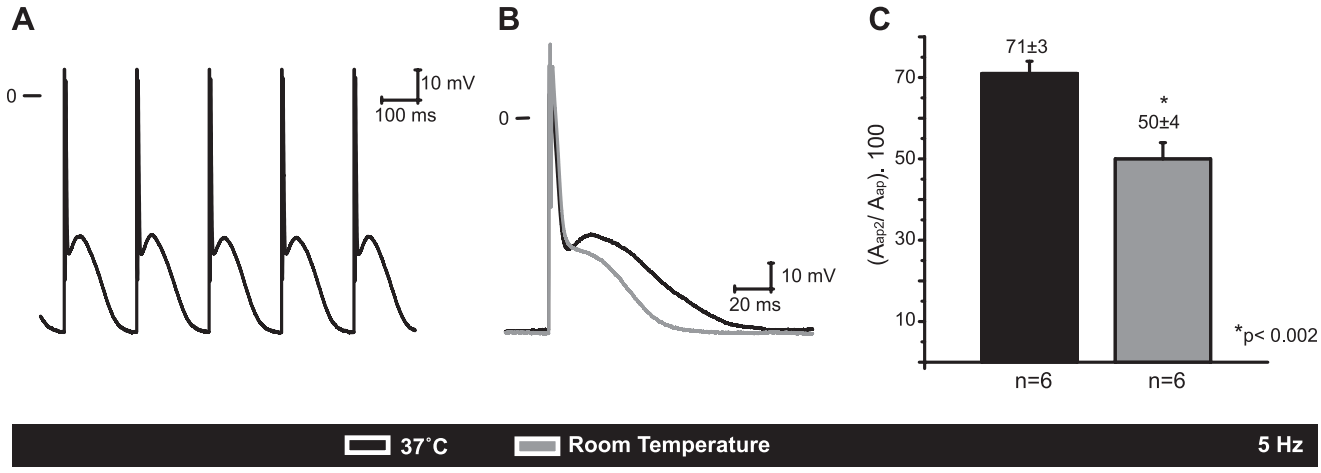

Fig. 8. Phase 2 in ventricular AP: isolated myocytes. *A*: isolated myocytes APs recorded under current clamp using 50-MΩ sharp microelectrodes. Cell was hyperpolarized to −79 mV and electrically stimulated by injecting short (0.2 ms) depolarizing current pulses through the recording microelectrode. All the phases of the AP (including phase 2) are present in the recording. *B*: effect of temperature on the repolarization of the AP. It can be observed that the reduction of the temperature accelerate the repolarization. This effect is further illustrated in *C*, where the temperature dependency of the phase 2 contribution to the AP has been plotted in a bar graph. At lower temperatures, a significant reduction can be observed in phase 2 ($n = 4–6$; $P < 0.002$).

microelectrode when the membrane potential was held at −79 mV. Under these experimental conditions, it is possible to clearly observe all the phases of the AP: a fast phase 0, a very deep phase 1, and a distinguishable phase 2. To evaluate if single cell phase 2 was also temperature dependent, we performed experiments at room temperature and 37°C. A typical recording of this type of experiment in the same cell is exemplified in Fig. 8*B*, and it shows a very similar phase 2 temperature trend as that recorded in the intact ventricle when the temperature was increased from room temperature to 37°C. Figure 8*C* shows a bar graph that represents the statistics on the contribution of phase 2 to the AP at two different temperatures ($n = 4$ to 6 animals; $P < 0.002$). Illustration of the kinetic parameters of single cell APs is shown in Table 2. These results indicate that mouse ventricular AP phase 2 is a characteristic of the single myocyte and not an emergent property of ventricular tissue.

DISCUSSION

Phase 2 on intact perfused mouse hearts. The presence of phase 2 during the repolarization of mouse ventricular AP has been a very controversial subject (40, 43). Indeed, this electrophysiological characteristic has challenged the utility of the mouse as a viable alternative to other larger mammalian models for the study of electrocardiological disorders. In this study, we evaluated the molecular and cellular mechanisms that delineate the kinetics of mouse ventricular AP repolarization. Using several different experimental approaches, we found that all of them show clear evidence of a strong contribution of phase 2 during the ventricular AP repolarization (Fig. 1). The fact that the small diameter optical fiber (200 μm) recordings and electrical recordings using sharp microelectrodes measurements are not significantly different suggests that cells beneath the tip of the optical fiber are sufficiently isopotential compared with the intracellular microelectrode recording (Fig. 2*A*). However, significant differences were found between the optical and the electrical recordings when a larger diameter optical fiber (1,000 μm) was used to optically measure the APs (Fig. 2*B*). The most important differences between a recording with a large diameter optical fiber and the intracellular microelectrode electrical measurement were the slower rise phase (phase 0) and the smaller magnitude of phase 1 of the optical recorded AP (1,000 μm). In addition, an early appearance of phase 0 was observed in optical recordings when compared with the electrical measurements. We have already shown that the fiber diameter does not only define the lateral optical spatial resolution but the optical axial resolution as well (37). For example, a fiber having a larger diameter not only delivers and collects photons from a wider area but also can detect signals from deeper layers within the tissue. The fact that the depolarizing phase 0 starts sooner in the optical recording than in the electrical one indicates that there are anatomical regions within the optical recording volume that depolarize earlier than the local intracellular measurement.

AP cannot only occur at different delay times in different regions of the epicardial layer (i.e., apex, base, left ventricle, right ventricle, etc.) but also can display disparity in morphology. This issue was explored in Fig. 3 where we showed that the middle of the left ventricle has a larger contribution of phase 2 than the apex and that the right ventricle displays a larger phase 2 than the left ventricle. These results indicate that there is a dispersion of the epicardial cellular repolarization properties from different regions of this outermost ventricular layer. Moreover, phase 2 is present during the repolarization of the epicardial AP at different heart rates (Fig. 4), indicating that at the intact heart level phase 2 is a physiological manifestation and not a mere consequence of a bradycardic heart rate.

Comparison of whole heart AP recordings with previous reports. There has been a common consensus in the field about the absence of phase 2 in mouse ventricular APs. With exception of our previous preliminary contributions (32, 47), there have been no reports using optical fiber techniques evaluating the kinetic features of ventricular AP repolarization in mouse models. However, several articles (2, 21, 36) have been published in Langendorff-perfused mouse hearts, using optical mapping techniques to measure ventricular APs. In the articles from Baker (2) and London (36), the authors conclude that there is no a plateau phase under control conditions. Glukhov (21) reported APDs that are longer than the ones reported by Baker (2) and London (36). Nevertheless, their recordings display a smaller distinguishable difference between phase 1 and phase 2 compared with the optical recordings presented in our current work. In general, differences between our data and optical mapping recordings could be interpreted as differences in optical resolution between both methods. Although optical mapping has differences with PLFF microscopy in spatial resolution, it is unlikely that these differences could explain alone the absence of phase 2. However, summarized scattering signals from the neighbor myocardium can introduce an important effect by making slower the rate of relaxation of phase 1. This could make the optical signal recorded by optical mapping to be more triangular in shape, masking phase 2 (36). Additionally, several authors (1, 25, 29) have reported intracellular electrical recordings using sharp microelectrodes in whole hearts or reduced mouse ventricular preparations at a mammalian physiological temperature (~37°C). The studies of Knollmann (30) and Hong (25) showed ventricular APs that relax fast and monotonically, not presenting a phase 2 plateau. Additionally, Anumonwo (1) showed a prominent phase 2 in fibers from the conduction system but recordings from endocardial and epicardial layers showed no indication of a plateau phase. The differences between our results and the ones presented by these authors could be due to the use of pharmacological agents to reduce contraction that also affect Ca^{2+} release from the SR (29) or the use of reduced ventricular preparations (1, 27).

Table 2. *Single cell AP parameters*

5 Hz	AP, 37°C ($n = 6$)	Room Temperature ($n = 4$)
Resting potential −mV	79.6 ± 1.7	80.8 ± 3.35
Amplitude		
Phase 0, mV	88.3 ± 4.2	86.6 ± 6.4
Phase 1, mV	31.7 ± 3.6	27.5 ± 3.3
Phase 2, mV	33.3 ± 3.2	27.5 ± 3.3
Magnitude		
Phase 1, mV	56.6 ± 2.7	59.5 ± 3.3
$APD_{90\%}$	84.9 ± 7.9	56.1 ± 9.10*

Values are means ± SE; $n = 6$-4 hearts. AP parameters of mouse ventricular isolated myocytes recorded using current-clamp technique (5 Hz) at 37°C and room temperature. *$P < 0.05$, room temperature vs. 37°C.

Finally, there are multiple published reports (9, 29, 30, 50) of electrical recordings using extracellular MAPs in mouse ventricles at ~37°C. These authors do not see any indication of a phase 2 in the repolarization of APs. However, there is one report (34) where the authors described the existence of a plateau phase in their extracellular recordings. They suggested that the differences between their recordings and the ones from others rely on the fact that Liu's (35) recordings were obtained in vivo.

Relationship between phase 2 and intracellular Ca^{2+} dynamics. A classical fingerprint of phase 2 in the repolarization of the AP is the role of the L-type Ca^{2+} current as the primary ionic current maintaining the plateau phase (4). Figure 5 shows that 10 μM nifedipine, a dihydropyridine that specifically blocks the voltage-dependent L-type Ca^{2+} channel, produces a significant change in the contribution of phase 2 to the repolarization of the mouse ventricular AP. This effect was completely washout after perfusing the coronary arteries with a drug-free Tyrode solution for 15 min. This result is consistent with the idea that the L-type Ca^{2+} channel is a key molecular entity in the pathway that controls the genesis of the phase 2 during the AP repolarization. In most mammalian species, activation of the L-type Ca^{2+} current in the ventricular tissues is not only involved in maintaining the depolarization during phase 2, but it also triggers the opening of RyR_2 located on the facing junction of the terminal cistern of the SR and activates the CICR process (15). In fact, blocking L-type Ca^{2+} currents with nifedipine will halt both processes as we show in Fig. 5, *A* and *C*. Traditionally, it has been accepted that the plateau phase is sustained by the depolarizing effect of the Ca^{2+} current and not as a consequence of the Ca^{2+} released by the SR. The results shown in Fig. 5*E* specifically challenge this concept. Our experiments were designed to evaluate if the Ca^{2+} released by the SR itself could have an impact in the genesis of phase 2. Without a reasonable doubt, this seems to be the case in hearts treated with a combination of ryanodine and thapsigargin. Neither of the drugs have a direct detectable effect on the L-type Ca^{2+} channels (14, 27) at the concentrations that were used in these experiments. This result suggests that the Ca^{2+} released from the SR can activate a Ca^{2+}-dependent depolarizing current that largely contributes to the phase 2 in APs measured in the ventricle of mouse models.

Even though the experiments shown in Fig. 5 revealed the role of intracellular Ca^{2+} dynamics in the repolarization of the AP, they are not sufficient to completely define the molecular entity of this plasmalemma Ca^{2+}-activated current involved in the genesis of phase 2. In principle, this depolarizing current can be carried by an efflux of anions or an influx of cations. Although Ca^{2+}-activated chloride channels have been identified in cardiac ventricular myocytes (53), an influx of cations is most likely to occur due to the larger electrochemical gradients for cations compared with the lower concentration gradients for chloride. Moreover, it has been shown that in Na^+/Ca^{2+} exchanger knockout animals APs repolarize faster than wild types at the single cell level (24, 41).

One typical difference between a membrane ionic flux carried through a voltage-activated channel and one mediated by a transporter is the temperature dependency of both processes. The amplitude of macroscopic L-type Ca^{2+} currents has only a very moderate temperature dependency with a Q_{10} of 1.56 (28), a single channel conductance with a Q_{10} of 1.63 (28), and a higher temperature dependency for the inactivation (Q_{10} 2.3) (31). In contrast, the activation of the Na^+/Ca^{2+} exchanger is extremely temperature dependent with a Q_{10} between 3 and 4 (5, 45; for a review, see Ref. 7). Following the same line of arguments, it is possible to expect that if the Na^+/Ca^{2+} exchanger activation is involved in the genesis of phase 2, the temperature will have a profound effect on this plateau phase of the ventricular AP repolarization. The results showed in Fig. 6 completely support this idea. At room temperature, the APs display a very moderate phase 2 that is significantly increased when the temperature was raised to 37°C. However, the lengthening of the APD_{50} produced by the appearance of phase 2 at 37°C did not increase the refractory period. In fact, the refractory period was significantly shorter at 37°C (Fig. 6, *D*-*F*). This decrease in the refractoriness at a longer APD can be explained mostly by a parallel increase in the recovery from inactivation rate and the activation rate of the Na^+ channels ($Na_V1.5$) without a significant change in the APD_{90} at higher temperatures. This idea is supported by the fact that the time to peak of the epicardial AP is significantly shorter at 37°C than at room temperature.

The temperature dependency of phase 2 is a compelling but not a conclusive evidence to demonstrate that the Na^+/Ca^{2+} exchanger is the transporting protein that defines the AP plateau. The classical way to deal with this paradigm is to use a pharmacological blocker/antagonist of the transporter. However, typical blockers of the Na^+/Ca^{2+} exchanger as KBR-7943 or SEA-0400 also block L-type Ca^{2+} channels in canine ventricular myocytes (6). As shown in Fig. 5 a blockade of the L-type Ca^{2+} channel will dramatically reduce the AP phase 2. On the other hand, Li^+ has traditionally been used as a way to discriminate between the transport through the Na^+/Ca^{2+} exchanger and other Na^+-dependent pathways (12, 45). Li^+ can permeate though the Na^+ channel but cannot be translocated through the active transport mechanisms such as the Na^+-K^+ ATPase or the Na^+/Ca^{2+} exchanger. Figure 7*A* illustrates that the partial replacement of Na^+ by Li^+ dramatically reduces the contribution of phase 2 to the repolarization of the AP. Moreover, the effect on the AP repolarization is not due to an attenuation of the intracellular Ca^{2+} release from the SR. In the presence of Li^+ (Fig. 7*B*), the amplitude of the Ca^{2+} was even larger than in control experiments. Furthermore, the larger the fraction of Na^+ that was replaced by Li^+ the larger the effect on phase 2 as seen in Fig. 7*C*.

To summarize, we propose that an influx of Na^+ through the forward mode of the Na^+/Ca^{2+} exchanger is at least partially responsible for phase 2. Consequently, the temperature dependency of phase 2 is mostly defined by the thermodynamics of the Na^+ influx driven through this transporter.

Phase 2 at the single cell level. The electrophysiological profile of isolated cells and cells forming part of an intact tissue can be dramatically different. Some of the factors that can contribute to these differences include electrical connectivity between cells, accumulation of ions in the extracellular space, and exposition to complex vectorial mechanical forces present in the tissue. These factors disappear when the cells are isolated in a dish and proteins of the extracellular matrix have been digested during the dissociation procedure. In particular, the question if phase 2 is a single cell characteristic or an emergent property of the tissue is central to our working hypothesis. Figure 8, *A* and *B*, shows that not only isolated

ventricular cardiac myocytes from mouse hearts present a phase 2 but also demonstrates that the kinetics of the AP repolarization displays a similar behavior as the one observed in the intact organ.

Therefore, why do our results show a predominant phase 2 that was not observed by other authors? Most of the published data dealing with the repolarization of single ventricular myocytes were done at room temperature and using the whole cell patch-clamp technique under current-clamp configuration (3, 22, 51). Under this experimental condition, it is very likely that the absence of phase 2 in those recordings is mostly due to the temperature effect on the genesis of the plateau. However, there is also an extensive set of published experimental work where experiments were performed under whole cell configuration but at temperatures between 32 and 37°C. Under these conditions, the repolarization of APs does not display phase 2 either (13, 36). One possible explanation is that the presence of high concentration of Ca^{2+} buffers like EGTA and/or the dialysis effect produced by the whole cell membrane rupture will impair the intracellular Ca^{2+} dynamics. Indeed, these factors can be critical in defining the amplitude and rate of Ca^{2+} release from the SR and the degree of activation of the Ca^{2+} dependent plasmalemma transport system. Interestingly, Remme et al. (42, 43) performed experiments using the perforated patch methodology at 37°C, a situation that highly resembles our sharp microelectrode recordings. Although in their work these authors did not comment on the detailed characteristics of the AP repolarization, it is possible to observe a phase 2 very similar to the one illustrated in our single cell experiments (Fig. 8*A*). This observation supports our hypothesis that phase 2 is an intrinsic property of mouse ventricular myocytes AP.

To conclude, we demonstrated for the first time the presence of the mouse ventricular APs phase 2. This phase 2 occurs at a more negative membrane potential compared with other mammalian species and is mediated by the activation of the Na^+/Ca^{2+} exchanger. The contribution of phase 2 to the repolarization of the APs is different for different epicardial regions and is also present at the isolated single myocyte level. Temperature and intracellular Ca^{2+} release from the SR regulate the repolarization process by modifying the ionic transport through the Na^+/Ca^{2+} exchanger. This mechanism present in the mouse model could be extrapolated to other mammalian species (46). Finally, we think that this work further validates the use of mouse models to study normal and pathophysiological phenomena related to cardiac arrhythmias.

ACKNOWLEDGMENTS

We are grateful to Drs. Guillermo J. Perez, Daniel J. Calvo, and Alicia R. Mattiazzi and Tania Silva for providing helpful comments and suggestions on the manuscript.

GRANTS

This study was supported by National Heart, Lung, and Blood Institute Grant R01-HL-084487 (to A. L. Escobar).

DISCLOSURES

No conflicts of interest, financial or otherwise, are declared by the author(s).

AUTHOR CONTRIBUTIONS

Author contributions: M.F. and A.L.E. conception and design of research; M.F., A.D.P., and A.L.E. performed experiments; M.F., A.D.P., and A.L.E. analyzed data; M.F., A.D.P., and A.L.E. interpreted results of experiments; M.F., A.D.P., and A.L.E. prepared figures; M.F. and A.L.E. drafted manuscript; M.F., A.D.P., and A.L.E. edited and revised manuscript; M.F., A.D.P., and A.L.E. approved final version of manuscript.

REFERENCES

1. **Anumonwo JM, Tallini YN, Vetter FJ, Jalife J.** Action potential characteristics and arrhythmogenic properties of the cardiac conduction system of the murine heart. *Circ Res* 89: 329–335, 2001.
2. **Baker LC, London B, Choi BR, Koren G, Salama G.** Enhanced dispersion of repolarization and refractoriness in transgenic mouse hearts promotes reentrant ventricular tachycardia. *Circ Res* 86: 396–407, 2000.
3. **Barry DM, Xu H, Schuessler RB, Nerbonne JM.** Functional knockout of the transient outward current, long-QT syndrome, and cardiac remodeling in mice expressing a dominant-negative Kv4 alpha subunit. *Circ Res* 83: 560–567, 1998.
4. **Beeler GW Jr, Reuter H.** Membrane calcium current in ventricular myocardial fibres. *J Physiol* 207: 191–209, 1970.
5. **Bersohn MM, Vemuri R, Schuil DW, Weiss RS, Philipson KD.** Effect of temperature on sodium-calcium exchange in sarcolemma from mammalian and amphibian hearts. *Biochim Biophys Acta* 1062: 19–23, 1991.
6. **Birinyi P, Acsai K, Banyasz T, Toth A, Horvath B, Virag L, Szentandrassy N, Magyar J, Varro A, Fulop F, Nanasi PP.** Effects of SEA0400 and KB-R7943 on Na^+/Ca^{2+} exchange current and L-type Ca2+ current in canine ventricular cardiomyocytes. *Naunyn Schmiedebergs Arch Pharmacol* 372: 63–70, 2005.
7. **Blaustein MP, Lederer WJ.** Sodium/calcium exchange: its physiological implications. *Physiol Rev* 79: 763–854, 1999.
8. **Cranefield PF, Hoffman BF.** Propagated repolarization in heart muscle. *J Gen Physiol* 41: 633–649, 1958.
9. **Danik S, Cabo C, Chiello C, Kang S, Wit AL, Coromilas J.** Correlation of repolarization of ventricular monophasic action potential with ECG in the murine heart. *Am J Physiol Heart Circ Physiol* 283: H372–H381, 2002.
10. **Di Diego JM, Antzelevitch C.** High $[Ca^{2+}]$o-induced electrical heterogeneity and extrasystolic activity in isolated canine ventricular epicardium. Phase 2 reentry. *Circulation* 89: 1839–1850, 1994.
11. **Dou Y, Arlock P, Arner A.** Blebbistatin specifically inhibits actin-myosin interaction in mouse cardiac muscle. *Am J Physiol Cell Physiol* 293: C1148–C1153, 2007.
12. **duBell WH, Boyett MR, Spurgeon HA, Talo A, Stern MD, Lakatta EG.** The cytosolic calcium transient modulates the action potential of rat ventricular myocytes. *J Physiol* 436: 347–369, 1991.
13. **DuBell WH, Lederer WJ, Rogers TB.** K(+) currents responsible for repolarization in mouse ventricle and their modulation by FK-506 and rapamycin. *Am J Physiol Heart Circ Physiol* 278: H886–H897, 2000.
14. **Escobar AL, Ribeiro-Costa R, Villalba-Galea C, Zoghbi ME, Perez CG, Mejia-Alvarez R.** Developmental changes of intracellular Ca^{2+} transients in beating rat hearts. *Am J Physiol Heart Circ Physiol* 286: H971–H978, 2004.
15. **Fabiato A, Fabiato F.** Excitation-contraction coupling of isolated cardiac fibers with disrupted or closed sarcolemmas. Calcium-dependent cyclic and tonic contractions. *Circ Res* 31: 293–307, 1972.
16. **Farman G, Tachampa K, Mateja R, Carzorla O, Lacampagne A, de Tombe PP.** Blebbistatin: use as inhibitor of muscle contraction. *Pflügers Arch* 455: 995–1005, 2008.
17. **Fedorov VV, Lozinsky IT, Sosunov EA, Anyukhovsky EP, Rosen MR, Balke CW, Efimov IR.** Application of blebbistatin as an excitation-contraction uncoupler for electrophysiologic study of rat and rabbit hearts. *Heart Rhythm* 4: 619–626, 2007.
18. **Field LJ.** Cardiovascular research in transgenic animals. *Trends Cardiovasc Med* 1: 141–146, 1991.
19. **Furukawa T, Myerburg RJ, Furukawa N, Bassett AL, Kimura S.** Differences in transient outward currents of feline endocardial and epicardial myocytes. *Circ Res* 67: 1287–1291, 1990.
20. **Glukhov AV, Fedorov VV, Lou Q, Ravikumar VK, Kalish PW, Schuessler RB, Moazami N, Efimov IR.** Transmural dispersion of repolarization in failing and nonfailing human ventricle. *Circ Res* 106: 981–991, 2010.
21. **Glukhov AV, Flagg TP, Fedorov VV, Efimov IR, Nichols CG.** Differential K(ATP) channel pharmacology in intact mouse heart. *J Mol Cell Cardiol* 48: 152–160, 2010.

22. **Guo W, Xu H, London B, Nerbonne JM.** Molecular basis of transient outward K^+ current diversity in mouse ventricular myocytes. *J Physiol* 521: 587–599, 1999.
23. **Gussak I, Chaitman BR, Kopecky SL, Nerbonne JM.** Rapid ventricular repolarization in rodents: electrocardiographic manifestations, molecular mechanisms, and clinical insights. *J Electrocardiol* 33: 159–170, 2000.
24. **Henderson SA, Goldhaber JI, So JM, Han T, Motter C, Ngo A, Chantawansri C, Ritter MR, Friedlander M, Nicoll DA, Frank JS, Jordan MC, Roos KP, Ross RS, Philipson KD.** Functional adult myocardium in the absence of Na^+-Ca^{2+} exchange: cardiac-specific knockout of NCX1. *Circ Res* 95: 604–611, 2004.
25. **Hong CS, Cho MC, Kwak YG, Song CH, Lee YH, Lim JS, Kwon YK, Chae SW, Kim DH.** Cardiac remodeling and atrial fibrillation in transgenic mice overexpressing junctin. *FASEB J* 16: 1310–1312, 2002.
26. **Kass RS.** Nisoldipine: a new, more selective calcium current blocker in cardiac Purkinje fibers. *J Pharmacol Exp Ther* 223: 446–456, 1982.
27. **Kirby MS, Sagara Y, Gaa S, Inesi G, Lederer WJ, Rogers TB.** Thapsigargin inhibits contraction and Ca^{2+} transient in cardiac cells by specific inhibition of the sarcoplasmic reticulum Ca^{2+} pump. *J Biol Chem* 267: 12545–12551, 1992.
28. **Klockner U, Schiefer A, Isenberg G.** L-type Ca-channels: similar Q10 of Ca-, Ba- and Na-conductance points to the importance of ion-channel interaction. *Pflügers Arch* 415: 638–641, 1990.
29. **Knollmann BC, Katchman AN, Franz MR.** Monophasic action potential recordings from intact mouse heart: validation, regional heterogeneity, and relation to refractoriness. *J Cardiovasc Electrophysiol* 12: 1286–1294, 2001.
30. **Knollmann BC, Schober T, Petersen AO, Sirenko SG, Franz MR.** Action potential characterization in intact mouse heart: steady-state cycle length dependence and electrical restitution. *Am J Physiol Heart Circ Physiol* 292: H614–H621, 2007.
31. **Kohlhardt M, Krause H, Kubler M, Herdey A.** Kinetics of inactivation and recovery of the slow inward current in the mammalian ventricular myocardium. *Pflügers Arch* 355: 1–17, 1975.
32. **Kornyeyev D, Reyes M, Escobar AL.** Luminal Ca^{2+} content regulates intracellular Ca^{2+} release in subepicardial myocytes of intact beating mouse hearts: effect of exogenous buffers. *Am J Physiol Heart Circ Physiol* 298: H2138–H2153, 2010.
33. **Litovsky SH, Antzelevitch C.** Transient outward current prominent in canine ventricular epicardium but not endocardium. *Circ Res* 62: 116–126, 1988.
34. **Liu DW, Gintant GA, Antzelevitch C.** Ionic bases for electrophysiological distinctions among epicardial, midmyocardial, and endocardial myocytes from the free wall of the canine left ventricle. *Circ Res* 72: 671–687, 1993.
35. **Liu G, Iden JB, Kovithavongs K, Gulamhusein R, Duff HJ, Kavanagh KM.** In vivo temporal and spatial distribution of depolarization and repolarization and the illusive murine T wave. *J Physiol* 555: 267–279, 2004.
36. **London B, Baker LC, Petkova-Kirova P, Nerbonne JM, Choi BR, Salama G.** Dispersion of repolarization and refractoriness are determinants of arrhythmia phenotype in transgenic mice with long QT. *J Physiol* 578: 115–129, 2007.
37. **Mejia-Alvarez R, Manno C, Villalba-Galea CA, del Valle Fernandez L, Costa RR, Fill M, Gharbi T, Escobar AL.** Pulsed local-field fluorescence microscopy: a new approach for measuring cellular signals in the beating heart. *Pflügers Arch* 445: 747–758, 2003.
38. **Mitra R, Morad M.** A uniform enzymatic method for dissociation of myocytes from hearts and stomachs of vertebrates. *Am J Physiol Heart Circ Physiol* 249: H1056–H1060, 1985.
39. **Nagatomo T, Fan Z, Ye B, Tonkovich GS, January CT, Kyle JW, Makielski JW.** Temperature dependence of early and late currents in human cardiac wild-type and long Q-T ΔKPQ Na^+ channels. *Am J Physiol Heart Circ Physiol* 275: H2016–H2024, 1998.
40. **Nerbonne JM, Nichols CG, Schwarz TL, Escande D.** Genetic manipulation of cardiac K(+) channel function in mice: what have we learned, and where do we go from here? *Circ Res* 89: 944–956, 2001.
41. **Pott C, Ren X, Tran DX, Yang MJ, Henderson S, Jordan MC, Roos KP, Garfinkel A, Philipson KD, Goldhaber JI.** Mechanism of shortened action potential duration in Na^+/Ca^{2+} exchanger knockout mice. *Am J Physiol Cell Physiol* 292: C968–C973, 2007.
42. **Remme CA, Scicluna BP, Verkerk AO, Amin AS, van Brunschot S, Beekman L, Deneer VH, Chevalier C, Oyama F, Miyazaki H, Nukina N, Wilders R, Escande D, Houlgatte R, Wilde AA, Tan HL, Veldkamp MW, de Bakker JM, Bezzina CR.** Genetically determined differences in sodium current characteristics modulate conduction disease severity in mice with cardiac sodium channelopathy. *Circ Res* 104: 1283–1292, 2009.
43. **Remme CA, Verkerk AO, Nuyens D, van Ginneken AC, van Brunschot S, Belterman CN, Wilders R, van Roon MA, Tan HL, Wilde AA, Carmeliet P, de Bakker JM, Veldkamp MW, Bezzina CR.** Overlap syndrome of cardiac sodium channel disease in mice carrying the equivalent mutation of human SCN5A-1795insD. *Circulation* 114: 2584–2594, 2006.
44. **Reuter H.** Slow inactivation of currents in cardiac Purkinje fibres. *J Physiol* 197: 233–253, 1968.
45. **Rojas H, Ramos M, Dipolo R.** A genistein-sensitive $Na^+/Ca2^+$ exchange is responsible for the resting $[Ca^{2+}]_i$ and most of the Ca^{2+} plasma membrane fluxes in stimulated rat cerebellar type 1 astrocytes. *Jpn J Physiol* 54: 249–262, 2004.
46. **Schouten VJ, ter Keurs HE.** The slow repolarization phase of the action potential in rat heart. *J Physiol* 360: 13–25, 1985.
47. **Valverde CA, Kornyeyev D, Ferreiro M, Petrosky AD, Mattiazzi A, Escobar AL.** Transient Ca^{2+} depletion of the sarcoplasmic reticulum at the onset of reperfusion. *Cardiovasc Res* 85: 671–680, 2010.
48. **Valverde CA, Mundina-Weilenmann C, Reyes M, Kranias EG, Escobar AL, Mattiazzi A.** Phospholamban phosphorylation sites enhance the recovery of intracellular Ca^{2+} after perfusion arrest in isolated, perfused mouse heart. *Cardiovasc Res* 70: 335–345, 2006.
49. **Vergara J, Delay M.** A transmission delay and the effect of temperature at the triadic junction of skeletal muscle. *Proc R Soc Lond B Biol Sci* 229: 97–110, 1986.
50. **Wickenden AD, Lee P, Sah R, Huang Q, Fishman GI, Backx PH.** Targeted expression of a dominant-negative K(v)4.2 K(+) channel subunit in the mouse heart. *Circ Res* 85: 1067–1076, 1999.
51. **Wilson FN, Macleod AG, Barker PS.** The distribution of the action currents produced by heart muscle and other excitable tissues immersed in extensive conducting media. *J Gen Physiol* 16: 423–456, 1933.
52. **Xu H, Barry DM, Li H, Brunet S, Guo W, Nerbonne JM.** Attenuation of the slow component of delayed rectification, action potential prolongation, and triggered activity in mice expressing a dominant-negative Kv2 alpha subunit. *Circ Res* 85: 623–633, 1999.
53. **Xu Y, Dong PH, Zhang Z, Ahmmed GU, Chiamvimonvat N.** Presence of a calcium-activated chloride current in mouse ventricular myocytes. *Am J Physiol Heart Circ Physiol* 283: H302–H314, 2002.
54. **Yan GX, Antzelevitch C.** Cellular basis for the Brugada syndrome and other mechanisms of arrhythmogenesis associated with ST-segment elevation. *Circulation* 100: 1660–1666, 1999.
55. **Yan GX, Antzelevitch C.** Cellular basis for the electrocardiographic J wave. *Circulation* 93: 372–379, 1996.

Cardiovascular Research (2010) **85**, 671–680
doi:10.1093/cvr/cvp371

Transient Ca^{2+} depletion of the sarcoplasmic reticulum at the onset of reperfusion

Carlos A. Valverde[1†], Dmytro Kornyeyev[2†], Marcela Ferreiro[2], Azadé D. Petrosky[2], Alicia Mattiazzi[1], and Ariel L. Escobar[2*]

[1]Facultad de Cs. Médicas, Centro de Investigaciones Cardiovasculares, UNLP, Conicet, La Plata, Argentina; and [2]Biological Engineering and Small Scale Technologies, School of Engineering, University of California, Merced, CA 95343, USA

Received 4 August 2009; revised 10 November 2009; accepted 11 November 2009; online publish-ahead-of-print 17 November 2009

Time for primary review: 20 days

Aims Myocardial stunning is a contractile dysfunction that occurs after a brief ischaemic insult. Substantial evidence supports that this dysfunction is triggered by Ca^{2+} overload during reperfusion. The aim of the present manuscript is to define the origin of this Ca^{2+} increase in the intact heart.

Methods and results To address this issue, Langendorff-perfused mouse hearts positioned on a pulsed local field fluorescence microscope and loaded with fluorescent dyes Rhod-2, Mag-fluo-4, and Di-8-ANEPPS, to assess cytosolic Ca^{2+}, sarcoplasmic reticulum (SR) Ca^{2+}, and transmembrane action potentials (AP), respectively, in the epicardial layer of the hearts, were submitted to 12 min of global ischaemia followed by reperfusion. Ischaemia increased cytosolic Ca^{2+} in association with a decrease in intracellular Ca^{2+} transients and a depression of Ca^{2+} transient kinetics, i.e. the rise time and decay time constant of Ca^{2+} transients were significantly prolonged. Reperfusion produced a transient increase in cytosolic Ca^{2+} (Ca^{2+} *bump*), which was temporally associated with a decrease in SR-Ca^{2+} content, as a mirror-like image. Caffeine pulses (20 mM) confirmed that SR-Ca^{2+} content was greatly diminished at the onset of reflow. The SR-Ca^{2+} decrease was associated with a decrease in Ca^{2+} transient amplitude and a shortening of AP duration mainly due to a decrease in phase 2.

Conclusion To the best of our knowledge, this is the first study in which SR-Ca^{2+} transients are recorded in the intact heart, revealing a previously unknown participation of SR on cytosolic Ca^{2+} overload upon reperfusion in the intact beating heart. Additionally, the associated shortening of phase 2 of the AP may provide a clue to explain early reperfusion arrhythmias.

Keywords Ischaemia/reperfusion • Sarcoplasmic reticulum • Calcium • Fluorescence

1. Introduction

Reperfusion after ischaemia causes a mechanical and electrical impairment of ventricular function.[1–5] The ischaemic insult may lead to an injury that could be reversible (stunning) or irreversible (infarction).[6] It is generally held that the two major triggers of myocardial stunning are Ca^{2+} overload and generation of reactive oxygen species.[6] Both take place at the onset or within seconds after the onset of reperfusion, supporting experimental evidence that suggests that myocardial dysfunction/injury occurred prior to reperfusion or developed extremely rapidly during reperfusion.[7] Abnormal intracellular Ca^{2+} cycling plays a key role in cardiac dysfunction and ventricular arrhythmias, particularly during the setting of transient cardiac ischaemia followed by reperfusion. Several reports describe an increase in cytosolic Ca^{2+} during ischaemia.[4,8,9] However, a detailed description of intracellular Ca^{2+} kinetics, necessary for complete understanding of the involvement of Ca^{2+} in the ischaemia/reperfusion damage in the intact beating heart, has not been yet provided. At the onset of reperfusion, Ca^{2+} overload is thought to be further exacerbated by

†The first two authors contributed equally to the study.

* Corresponding author. Tel: +1 209 228 4618, Fax: +1 209 228 4047, Email: aescobar4@ucmerced.edu

uncontrolled influx from the extracellular space.[7,10] In a previous work, in which we studied the time course of intracellular Ca^{2+} during reperfusion, a noticeable episode was consistently observed immediately after reperfusion. This event was a slight but consistent transient increase in diastolic Ca^{2+} (Ca^{2+} *bump*), which then decreased towards pre-ischaemic values.[5] This diastolic Ca^{2+} elevation occurred when the amplitude of Ca^{2+} transient was highly decreased. Although the increase in Ca^{2+} is brief, it might have important functional consequences because, at this time, intracellular Ca^{2+} attained the highest levels during reperfusion. However, its underlying mechanisms and physiological relevance have not been previously explored. Interestingly, a possible contribution of Ca^{2+} release from the sarcoplasmic reticulum (SR) in the genesis of Ca^{2+} overload at the onset of reperfusion has not been mechanistically evaluated before in intact hearts. This is particularly important in the light of new experiments revealing interactions between mitochondria and the endoplasmic/SR.[11,12]

The hypothesis underlying the present experiments is that the transient increase in diastolic Ca^{2+} at the beginning of reperfusion is due to Ca^{2+} release from the SR. The SR-Ca^{2+} depletion produced by this release of Ca^{2+} would diminish the amplitude of the following Ca^{2+} transients and shorten the action potential (AP), a condition that would in turn favour the appearance of arrhythmias. Interestingly, the epicardium, which is the outermost muscular layer of cardiac ventricle, is highly implicated in the genesis of several ventricular arrhythmias such as the Brugada syndrome and the short-QT syndrome.[13,14] The duration of the AP (in particular phase 2) is critically dependent on the intracellular Ca^{2+} dynamics.[15,16] Consequently, Ca^{2+} release from the SR is not only the key event triggering cardiac contraction but also could be a regulator of the electrical properties of the epicardial AP.

The effects of ischaemia/reperfusion on intracellular Ca^{2+} have been previously studied in cell suspensions or monolayers exposed to simulated ischaemia.[17,18] Moreover, intracellular Ca^{2+} measured in intact organs have been reported since the late 1980s, using the visible light-emitting protein aequorin or fluorescent indicators such as Indo-1, Fura-2, Fluo-3, or the more recently introduced Rhod-2.[5,9,19] To our knowledge, subcellular Ca^{2+} measurements in the intact heart, i.e. at the level of the organelles, have never been reported. In the present study, we used a novel technique, the pulsed local-field fluorescence (PLFF) microscopy,[20] which allows for the simultaneous detection of cytosolic Ca^{2+} transient and/or SR-Ca^{2+} transient and transmembrane AP, in the intact beating heart together with the assessment of left intra-ventricular pressure with an integrated silicon piezoresistive transducer system. Evidence will be presented demonstrating that SR-Ca^{2+} release contributes to the transient cytosolic increase of Ca^{2+} at the onset of reperfusion. It will be further shown that, by depleting the SR of Ca^{2+}, this release underlies the associated decrease in Ca^{2+} transient amplitude and may contribute to the shortening of AP during early reperfusion.

2. Methods

2.1 Heart preparation

The hearts were obtained from young Swiss Webster mice (3- to 7-week-old males). Animals used in this study were maintained in accordance with the National Institutes of Health Guide for the Care and Use of Laboratory Animals (NIH Publication No. 85–23, Revised 1996). The protocol was approved by the University of California Merced Institutional Animal Care and Use Committee (No. 2008–201). For details of this and the following methods sections, see Supplementary material online.

2.2 Electrocardiogram and ventricular pressure measurements

Transmural electrocardiogram (ECG) was recorded with a self-made DC coupled instrumentation amplifier (Burr Brown, TX, USA). Ventricular pressure was isovolumetrically measured with the aid of a plastic balloon and a differential pressure transducer (Motorola, USA).[5]

2.3 Fluorophores loading

Mag-fluo-4 AM, Rhod-2 AM, and Di-8-ANEPPS (Invitrogen, USA) were used to evaluate intra-SR, cytosolic Ca^{2+} concentrations, and transmembrane AP, respectively, in the epicardial layer of the mouse hearts.

2.4 Optical setup

A modified version of our custom-made setup for PLFF microscopy was employed to measure Ca^{2+} signals in the intact heart.[20]

2.5 Experimental protocol

After stabilization (pre-ischaemia), hearts were subjected to 12 min normothermic global ischaemia. Coronary perfusion was then restored for 30 min (reperfusion). This protocol was chosen based on the results of previous experiments which indicate that this ischaemic period produced a reversible altered Ca^{2+} handling and mechanical dysfunction, typical of the stunned heart.[5,8] Myocardial contractility and Ca^{2+} transients were not altered in control experiments ($n = 4$), in which all conditions of the ischaemia/reperfusion protocol (dye loading, shutter opening time for acquisition), except for the interruption of coronary flow, were reproduced.

2.6 Caffeine pulses

To evaluate intracellular SR-Ca^{2+} content, we measured the release of Ca^{2+} from the SR induced by a 20 mM caffeine pulse in Rhod-2 and Mag-fluo-loaded hearts. Caffeine pulses were applied along with the Tyrode solution. Normal Tyrode was changed to Tyrode plus caffeine 20 mM, while the heart was electrically paced. After 1 min, the perfusion solution was changed back to normal Tyrode without caffeine. The highest diastolic level achieved during caffeine pulse was used to evaluate SR-Ca^{2+} content. Application of caffeine might not be homogeneous in the whole heart. However, in these experiments, we performed the measurements of fluorescence in the same spot (where the optic fibre was positioned), during the whole protocol, which would assure homogenous fluorescence along the complete ischaemia/reperfusion protocol.

Two successive caffeine pulses were always performed. In control experiments, two successive pulses, separated by a 6 min interval, were applied in the pre-ischaemic period. In the ischaemia/reperfusion experiments, the second pulse was applied after 6 min of reperfusion and was compared with a first pulse evoked in the pre-ischaemic period.

2.7 Data analysis

Data are expressed as mean ± SEM. Statistical significance was determined by either Student's *t*-test for unpaired observations or ANOVA followed by Newman Keuls test, when more than two groups were

compared. The differences were considered statistically significant if *P*-value was less than 0.05.

3. Results

3.1 Cytosolic Ca^{2+} and Ca^{2+} kinetics during ischaemia

Several laboratories including ours have previously showed that ischaemia increased end-diastolic pressure (EDP), in association with a decrease in developed pressure (DP), to non-detectable levels.[3,5,21] EDP was further increased at the onset of reperfusion, whereas DP was greatly diminished with respect to pre-ischaemia (*Figure 1*). To gain further insights into the origin of these typical alterations of the ischaemic/reperfused heart, we explored the pattern of intracellular Ca^{2+} changes during ischaemia/reperfusion.

Figure 2A shows a typical example of cytosolic Ca^{2+} changes in a mouse heart at 3 min of global ischaemia. In agreement with the previous findings in several species and ischaemia/reperfusion models,[4,8,9] ischaemia produced a substantial increase in diastolic and systolic Ca^{2+} which was associated with a decrease in Ca^{2+} transient amplitude. The inset in *Figure 2A* indicates that blebbistatin, a mechanical uncoupler that prevents contractions by inhibiting actin–myosin interaction,[22] did not alter intracellular Ca^{2+} kinetics (Supplementary material online). *Figure 2B* and *C* shows overall results of the increase in diastolic and systolic Ca^{2+} and the associated decrease in Ca^{2+} transient amplitude, which reached 20% of pre-ischaemic values within the first 5 min of ischaemia. Insets show that the presence of blebbistatin did not modify the results observed in the absence of the uncoupler. Blebbistatin experiments provide evidence that no significant artifactual fluorescence changes were produced by contraction movements. *Figure 2D* and *E* shows that the kinetics of intracellular Ca^{2+} transients was slowed down during ischaemia. Both the rise time and decay time constant of Ca^{2+} transients were significantly prolonged, in agreement with the strong inhibition exerted by ischaemia/acidosis on SR-Ca^{2+} release and reuptake.[23–25]

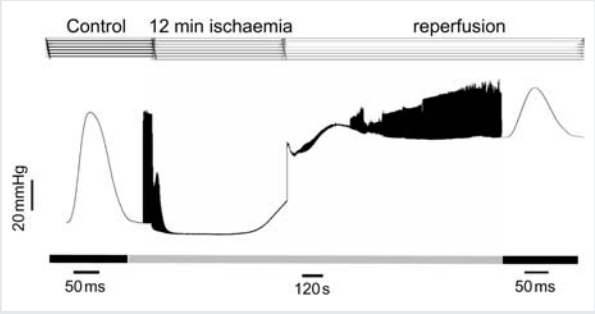

Figure 1 Time course of left ventricular pressure in a mouse heart submitted to ischaemia/reperfusion. Typical records of left ventricular DP showing that ischaemia increased EDP and reduced contractility to non-detectable levels. Reperfusion produced an immediate and long lasting increase in EDP. Contractility was depressed at the beginning of reflow and recovered during reperfusion. Similar results were obtained in six additional experiments of this type.

3.2 Cytosolic Ca^{2+} and Ca^{2+} kinetics during reperfusion

Figure 3A shows typical records of intracellular Ca^{2+} transients at different times during reperfusion. Intracellular Ca^{2+} transients were completely depressed at 1 min of reperfusion and slowly recovered towards pre-ischaemic levels during reperfusion. *Figure 3B* shows overall results of the time course of diastolic and systolic Ca^{2+} at the end of ischaemia and during the first minutes of reperfusion. Consistent with Ca^{2+} measurements during ischaemia, diastolic and systolic Ca^{2+} emerged from ischaemia at a high level with respect to pre-ischaemia. At the onset of reperfusion, there was a slight but consistent transient increase in cytosolic Ca^{2+} (Ca^{2+} *bump*) which was associated with diminished Ca^{2+} transient amplitude. *Figure 3C* shows that Ca^{2+} transient amplitude increased with reperfusion. Similar results were obtained in the presence of blebbistatin (Insets). *Figure 3D* and *E* shows overall results of Ca^{2+} transients kinetics during reperfusion. Whereas the decay time constant of Ca^{2+} transient fully recovered (*Figure 3E*), the time from 10 to 90% rise did not reach pre-ischaemic levels within the 30 min period of reperfusion (*Figure 3D*).

3.3 The increase in cytosolic Ca^{2+} at the onset of reperfusion is due to SR-Ca^{2+} release

Figure 4A shows a typical example of cytosolic Ca^{2+} increase at the beginning of reperfusion in an expanded time scale. Since the mechanism of this transient increase is not obvious, we explored the possibility that the SR was involved. To test this hypothesis, we evaluated the intra SR-Ca^{2+} content, by estimating the change in cytosolic Ca^{2+} produced when Ca^{2+} was released from the SR following an application of a 20 mM caffeine pulse through the coronary system in Rhod-2 loaded hearts. *Figure 4B* and *C* shows that two successive caffeine pulses separated by a 6 min interval induced a reproducible increase in diastolic Ca^{2+}. In contrast, a caffeine pulse applied at the beginning of reperfusion produced a smaller diastolic Ca^{2+} increase compared with that produced in pre-ischaemia (*Figure 4D*), suggesting that SR-Ca^{2+} content was lower at the beginning of post-ischaemic recovery than before ischaemia. Overall results are shown in *Figure 4E*. The decrease in SR-Ca^{2+} content observed might be explained by either one of the following possibilities: (i) the SR-Ca^{2+} content diminishes during ischaemia and is lower at the beginning of reperfusion than before ischaemia; (ii) the onset of reperfusion is associated with a release of Ca^{2+} from the SR, which causes SR-Ca^{2+} depletion, so that after 6 min of reperfusion, SR-Ca^{2+} content was lower than before ischaemia. To directly explore these possibilities, hearts loaded with Mag-fluo-4 were challenged with the ischaemia/reperfusion protocol, whereas the intraluminal SR-Ca^{2+} was continuously monitored. The procedure for dye loading and intra SR-Ca^{2+} measurement with Mag-fluo-4 is illustrated in *Figure 5A*. The dye was loaded at room temperature using coronary retroperfusion. After 30 min, temperature was increased to 37°C. As illustrated in *Figure 5A*, fluorescent transients recorded under these conditions show both a positive deflection due to

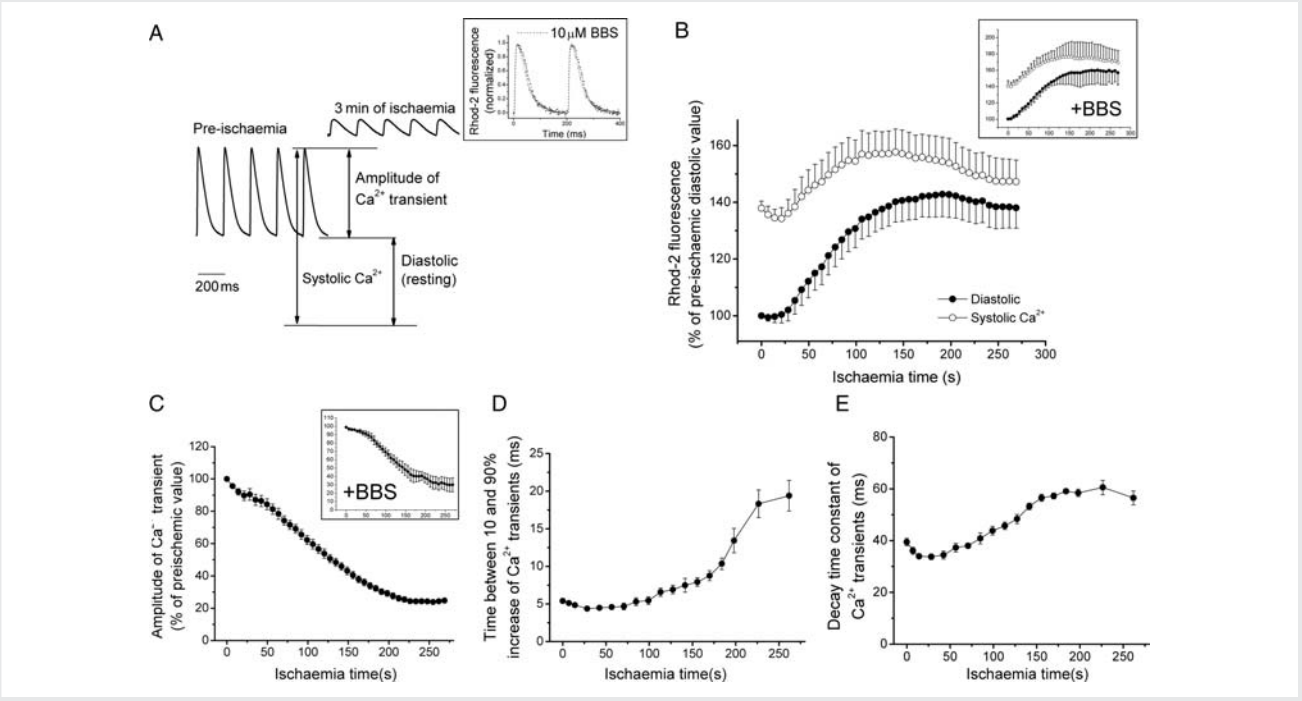

Figure 2 Time course of intracellular Ca^{2+} transient and kinetics during ischaemia. (*A*) Typical recordings of intracellular Ca^{2+} transients in an intact beating heart before and at 3 min of ischaemia. (*B–E*) Overall results showing that ischaemia increased diastolic and systolic Ca^{2+} (*B*), decreased the amplitude of Ca^{2+} transient (*C*), and slowed Ca^{2+} kinetics of Ca^{2+} transients (*D–E*), $n = 8$. Decay time constant was calculated as time between 10 and 90% decline divided by 2.2. Similar results were obtained in the presence of 10 μM of the mechanical uncoupler blebbistatin (BBS) (Insets in B–C. Axis legends in the insets are the same as the corresponding figure), $n = 3$.

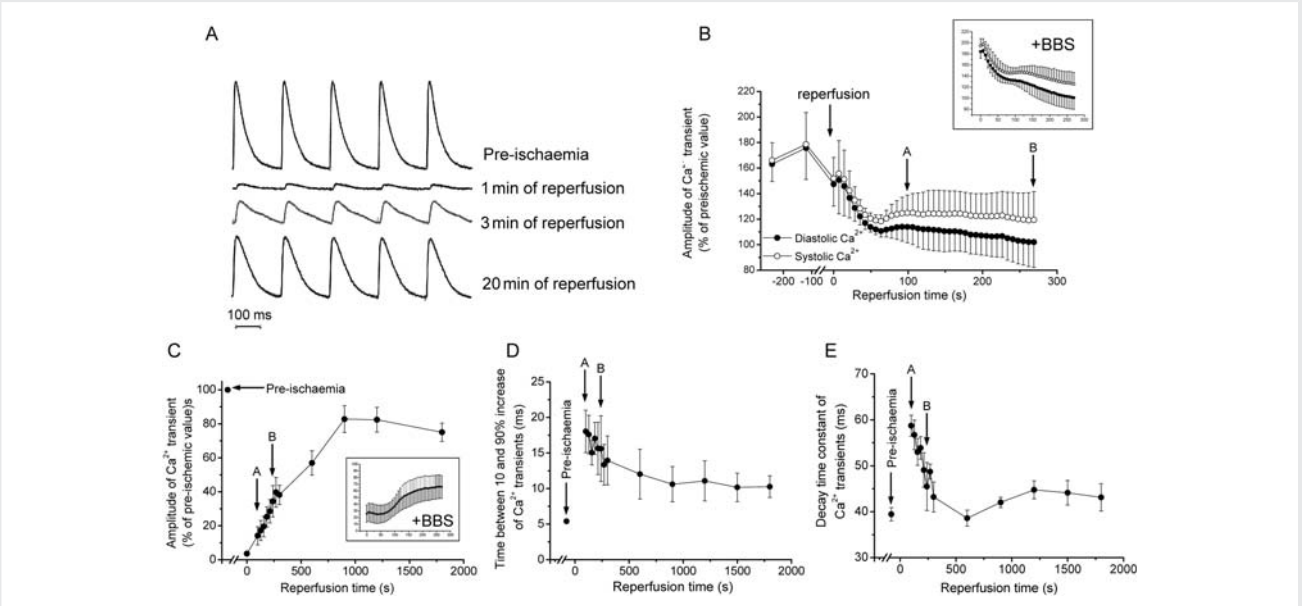

Figure 3 Time course of intracellular Ca^{2+} transient and dynamics during reperfusion. (*A*) Typical recordings of intracellular Ca^{2+} transients before ischaemia and during reperfusion. (*B*) Overall results of the time course of diastolic and systolic Ca^{2+} at two different times during ischaemia (8 and 10 min) and the first minutes of reperfusion. The increase in cytosolic Ca^{2+} at the beginning of ischaemia (*Figure 2*) still persisted at the end of ischaemia. Cytosolic Ca^{2+} transiently increased at the onset of reperfusion and then decreased towards pre-ischaemic values. (*C*) Amplitude of Ca^{2+} transients. (*D* and *E*) Rising time and decay time constant of Ca^{2+} transient, $n = 8$. Decay time constant was calculated as time between 10 and 90% decline divided by 2.2. (*B–D*) Arrows indicate pre-ischaemic values and the same time points during reperfusion. Insets indicate that similar changes in Rhod-2 fluorescence were obtained in the presence of 10 μM of blebbistatin (BBS) (Insets in *B* and *C*. Axis legends in the insets are the same as the corresponding figure), $n = 3$.

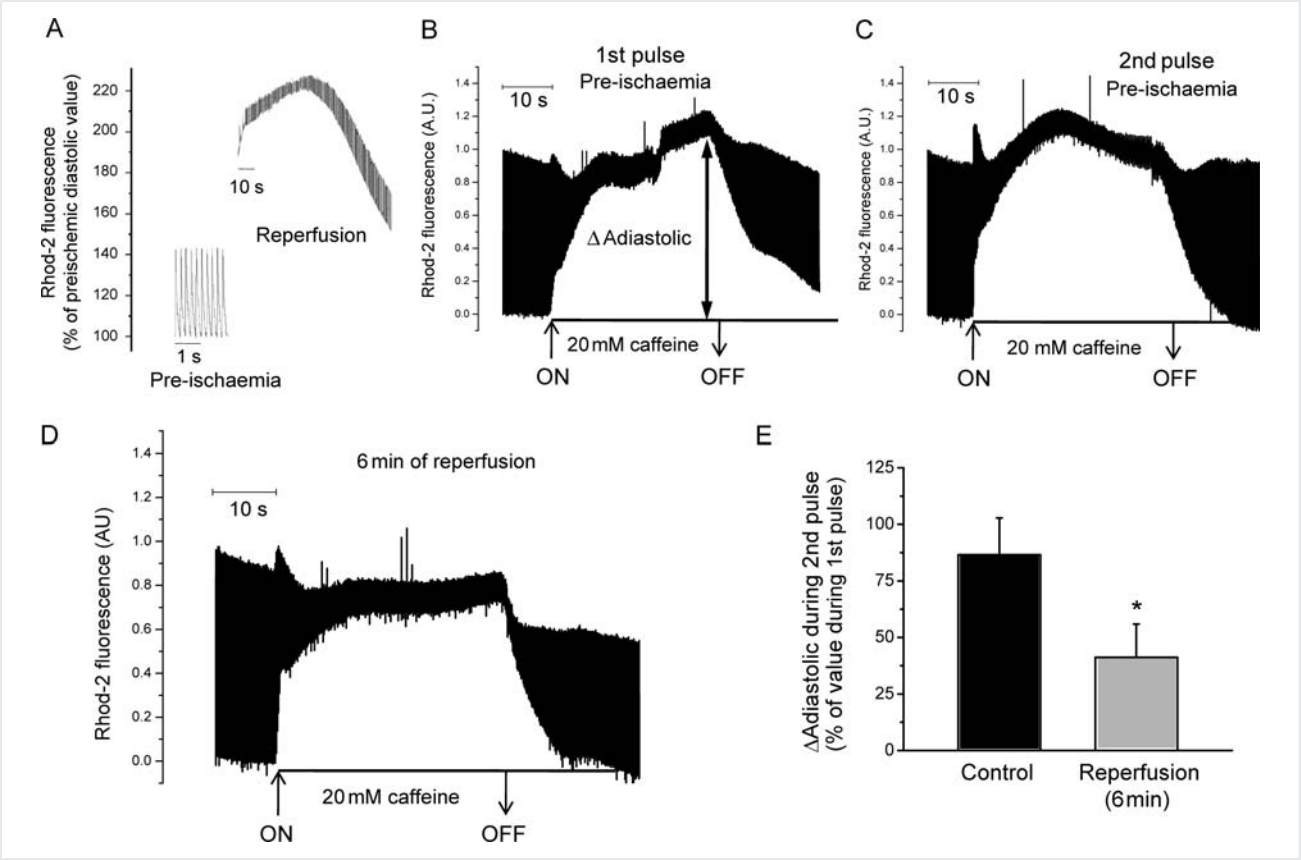

Figure 4 Changes in Rhod-2 fluorescence during reperfusion and in the response to caffeine pulses applied before ischaemia and during post-ischaemic recovery. (*A*) Typical recording of the time course of diastolic Ca^{2+} during the first 90 s of reperfusion, in an expanded time scale. As already shown (*Figure 3*), the onset of reperfusion produced a rapid and transient increase in diastolic Ca^{2+}. (*B* and *C*) Two successive caffeine pulses during pre-ischaemia induced a similar increase (amplitude) in diastolic Ca^{2+} (ΔAdiastolic). ΔAdiastolic: difference between the maximum diastolic fluorescence attained during the caffeine pulse and the diastolic fluorescence before caffeine. ON and OFF: moment of caffeine application and washout, respectively. (*D*) After 6 min of reperfusion, caffeine provoked a smaller increase in diastolic Ca^{2+} in the same heart. (*E*) Overall results of the experiments. Control indicates mean ΔAdiastolic values of the second of two successive pulses during pre-ischaemia, as shown in (B and C), expressed as % of the first one (*B*). Reperfusion (6 min) indicates mean ΔAdiastolic values of the caffeine pulse after 6 min of reperfusion expressed as % of the first caffeine pulse in pre-ischaemia [i.e. (D) as % of (B)]. $n = 6$. Asterisks (*) indicate statistically significant differences ($P < 0.05$) with respect to pre-ischaemic value.

Ca^{2+} binding to the dye in the myoplasm and a negative component due to the unbinding of Ca^{2+} from the dye in the SR. The increase in heart temperature induced the extrusion of the free dye from the cytosol.[26] The dye loaded into the SR stays trapped inside the organelle and reports the SR-Ca^{2+} transient movements. *Figure 5B* shows a typical recording of luminal SR-Ca^{2+} at 1 min of ischaemia. Whereas SR diastolic fluorescence increased, the amplitude of SR-Ca^{2+} transient decreased after 1 min of ischaemia compared with pre-ischaemic level. *Figure 5C* depicts overall results of diastolic and systolic Ca^{2+} and SR-Ca^{2+} transient amplitude during the first 5 min of ischaemia, where the increase in SR diastolic Ca^{2+} associated with a continuous decrease towards non-detectable values of SR-Ca^{2+} transients is evident.

Figure 5D shows typical recordings of luminal SR-Ca^{2+} transients in the pre-ischaemic period and at 2 and 5 min of reperfusion. As evident, reperfusion produced an abrupt decrease in luminal SR-Ca^{2+} content. These results clearly indicate that the transient increase in cytosolic Ca^{2+} during early reperfusion was primarily due to the release of Ca^{2+} from the SR. To further confirm this finding, caffeine pulses were applied to mice hearts loaded with Mag-fluo-4. *Figure 5E* represents a typical experiment ($n = 3$) in which the first caffeine pulse was fully reproduced by a second one applied 5 min later. At the onset of reperfusion (last trace to the right), caffeine evoked a small change in luminal diastolic SR-Ca^{2+} in the same heart, a result that should be expected from a reduced SR-Ca^{2+} content.

Figure 6 depicts overall results of the experiments in hearts loaded with Mag-fluo-4, showing the time course of intraluminal diastolic SR-Ca^{2+} during reperfusion. Noteworthy, resting diastolic Ca^{2+} level inside the SR just before reperfusion is significantly higher than that prior to ischaemia, as shown in *Figure 5B* and *C*. Results obtained with Rhod-2 in the ischaemia/reperfusion protocol are shown for comparison. The increase in diastolic Ca^{2+} in the cytosol (Rhod-2 fluorescence) is the mirror image of the decrease in diastolic SR-Ca^{2+}

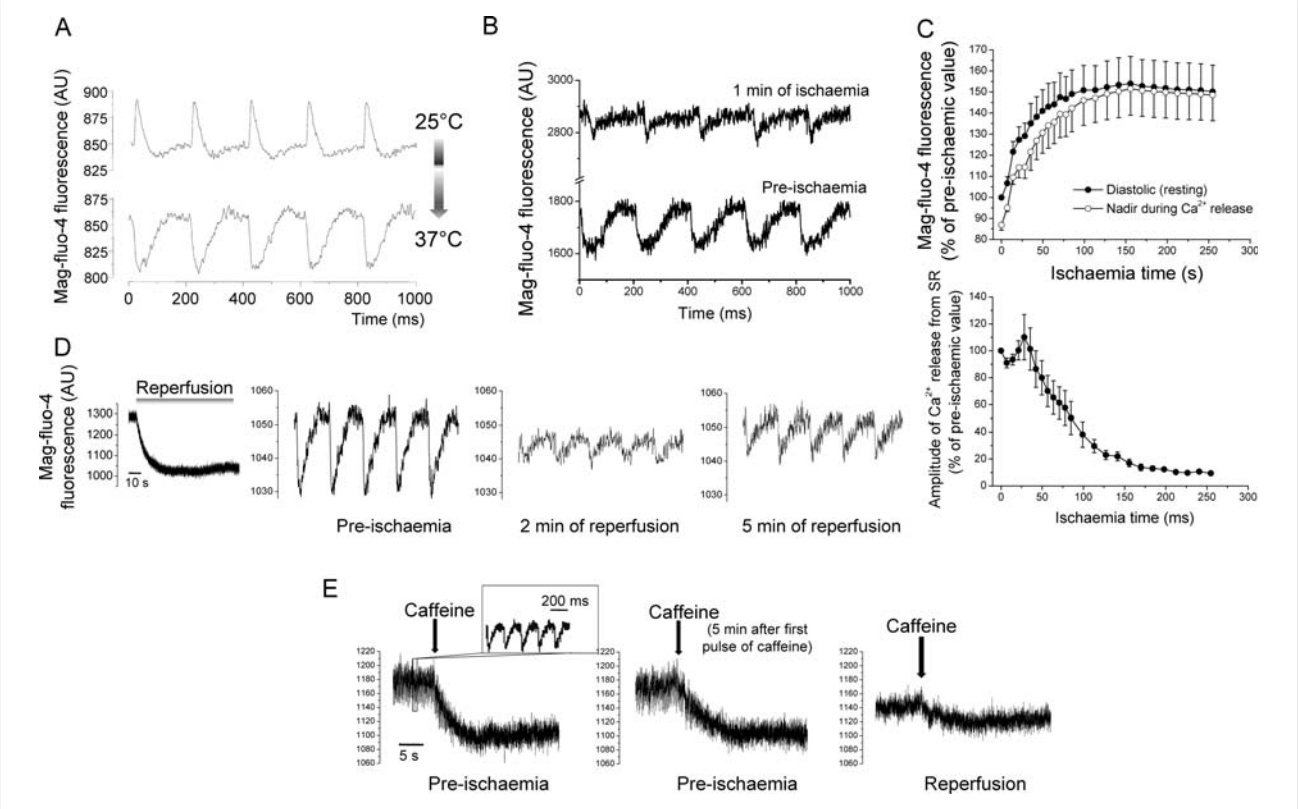

Figure 5 Reperfusion induces a rapid Ca^{2+} release from the SR. (*A*) Typical recordings showing the procedure for Mag-fluo-4 loading. (*B* and *C*) Typical recordings and overall results of intraluminal SR-Ca^{2+} during ischaemia. (*D*) Decrease in SR diastolic Ca^{2+} during the first minutes of reperfusion and typical recordings of SR-Ca^{2+} transients obtained in an intact beating heart before ischaemia and during reperfusion. There is an initial decrease in the amplitude of SR-Ca^{2+} transient compared with pre-ischaemia. The SR-Ca^{2+} gradually recovered with time of reperfusion. (*E*) Two successive caffeine pulses during pre-ischaemia induced a similar decrease in SR-Ca^{2+}. Inset: typical SR-Ca^{2+} transients in an expanded scale. Last record: after 6 min of reperfusion caffeine provoked a smaller decrease in intraluminal SR-Ca^{2+}.

(Mag-fluo-4 fluorescence). Insets in the figure depict typical records of Mag-Fluo-4 and Rhod-2 fluorescence in pre-ischaemia and during reperfusion. Taken together, the results imply that the beginning of reperfusion is associated with a release of Ca^{2+} from the SR.

3.4 Electrical changes occurring during ischaemia/reperfusion

Ischaemic insults followed by reperfusion may also induce alterations in cardiac excitability and dromotropism. To test whether mouse hearts displayed electrical alterations under our experimental conditions, we evaluated the electrophysiological function. *Figure 7A* illustrates that ischaemia produced dramatic alterations in the transmural ECG. The most notable features were an inversion of the T-wave and a decrease in excitability illustrated by the inability of the stimulus to elicit an AP. The excitability completely recovered after 15 min of reperfusion. Similar results were obtained in other five from six experiments of this type.

Experiments, in which we determined the epicardial transmembrane AP by optically measuring AP in hearts loaded with Di-8-ANEPPS, showed that another typical electrophysiological change during ischaemia is the shortening of the AP due to the dramatic reduction in phase 2. Typical recordings obtained at different times during the ischaemia/reperfusion are shown in *Figure 7B*. The AP shortening induced by ischaemia was maintained at the onset of reperfusion. Interestingly, pre-ischaemic AP waveshape was recovered after 15 min reperfusion. Furthermore, the decrease in AP duration, both in ischaemia and at the onset of reperfusion, was associated with a triangulation of the AP waveshape. These AP changes tightly correlate with the time course of transmural ECG recorded simultaneously (*Figure 7C*). Overall results of the contribution of the phase 2 to the AP at different times during ischaemia/reperfusion are presented in *Figure 7D*.

Since the AP shortening occurred simultaneously with a decrease in cytosolic Ca^{2+} transients, we hypothesized that both phenomena may be related: a decrease in Ca^{2+} release from the SR would slow the forward NCX mode and diminish the influx of Na^{+}, a major component of late repolarization (i.e. phase 2) of the AP in the mouse hearts.[27] *Figure 7E* shows that interventions that deplete the SR of Ca^{2+}, like ryanodine/thapsigargin or caffeine, were associated with a loss of phase 2 and triangulation of the AP. Taken together, these results suggest that the release of Ca^{2+} from SR at the onset of reperfusion may be responsible for two concomitant phenomena, namely, the decrease in Ca^{2+} transient amplitude and the disappearance of the plateau phase of the AP.

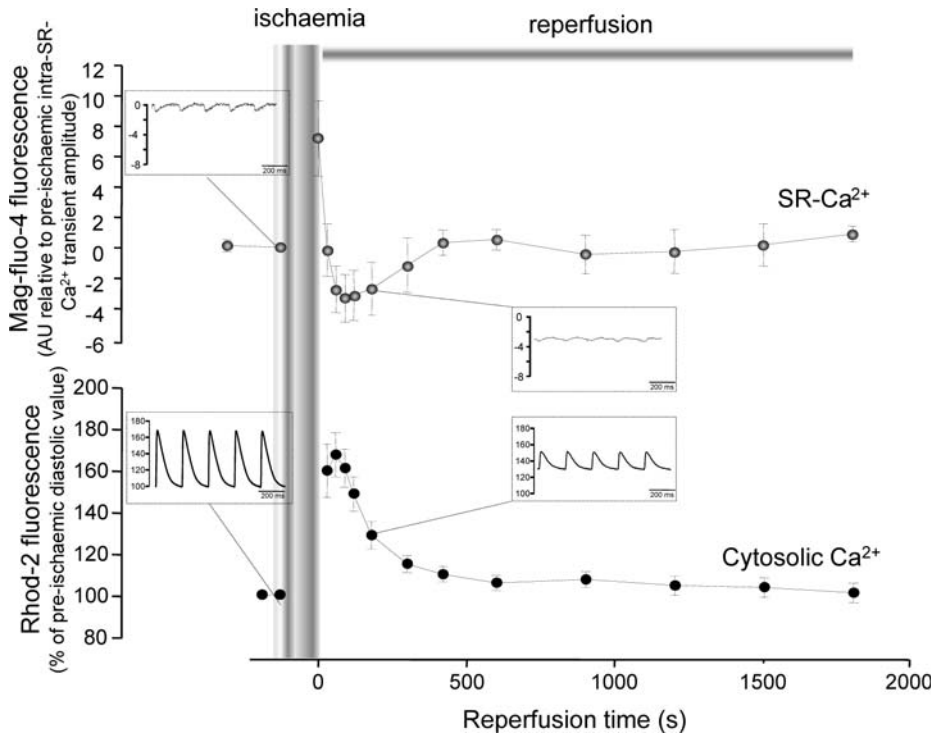

Figure 6 The increase in diastolic Ca^{2+} is the mirror-like image of the decrease in SR-Ca^{2+} content. Overall results of Mag-fluo-4 fluorescence (upper panel) in pre-ischaemia and reperfusion ($n = 9$). Changes in diastolic level of Mag-fluo-4 fluorescence during reperfusion are presented in arbitrary units and normalized to the amplitude of the intra-SR-Ca^{2+} transient before ischaemia. Each data point was calculated as the difference between current diastolic value during reperfusion and the pre-ischaemic diastolic value and then divided by the amplitude of the pre-ischaemic intra-SR-Ca^{2+} transient. Results of Rhod-2 obtained in experiments from the same group (lower panel) are shown for comparison ($n = 13$). Changes in diastolic level of Rhod-2 fluorescence are expressed as percentage of the pre-ischaemic diastolic value. As shown, the recovery profile of SR-Ca^{2+} (Mag-fluo-4) was a mirror-like image of cytosolic Ca^{2+} (Rhod-2). Insets depict typical records of Mag-fluo-4 and Rhod-2 fluorescence in pre-ischaemia and during reperfusion (*Y*-axis titles in the insets are the same as the figure).

4. Discussion

The main findings of the present experiments are: (i) the transient increase in cytosolic Ca^{2+} at the onset of reperfusion is due to SR-Ca^{2+} release; (ii) the SR-Ca^{2+} release produces a decrease in SR-Ca^{2+} content associated with a diminished Ca^{2+} transient amplitude and shortening of the phase 2 of AP. To the best of our knowledge, this is the first study in which SR-Ca^{2+} transients have been recorded in the intact heart. This approach clearly reveals the role of the SR in the increase in cytosolic Ca^{2+} at the beginning of reperfusion. The results further suggest that the decrease in SR-Ca^{2+} content produced by Ca^{2+} release from this compartment may contribute to maintaining the diminished duration of the AP at the onset of reflow. This would create a scenario particularly prone to arrhythmias.

4.1 Intracellular and subcellular Ca^{2+} measurements in the intact beating heart

Measurements of intracellular Ca^{2+} handling during whole organ ischaemia/reperfusion have been reported since the late 1980s using different fluorescent indicators or the visible light-emitting protein aequorin.[5,8,9] More recently, longer wavelength Ca^{2+} indicators, like Rhod-2, were introduced.[19] Rhod-2 has spectral properties that allow it to be used with optical mapping (OM) systems designed for potentiometric dyes.[28] In the present study, we used PLFF microscopy, a novel technique previously described by us,[20] that allows for simultaneous or alternative detection of intraventricular pressure and cytosolic Ca^{2+}, SR-Ca^{2+} transients, and transmembrane AP in the intact beating heart. This method improved the signal-to-noise ratio by combining the PLFF illumination with an integrating current-to-voltage conversion and with a digital evaluation of the integrated photocurrent. One limitation of our study is that myoplasmic Ca^{2+} was only assessed at the epicardium and differences in Ca^{2+} transients may arise from the ventricular transmural dispersion of the mechanisms underlying excitation–contraction coupling.[29] Moreover, since myoglobin (Mb) strongly absorbs light depending on tissue oxygenation, at 540 and 580 nm (oxy-Mb) and 550 nm (deoxy-Mb),[30] it could be argued that this may affect Ca^{2+} measurements with Rhod-2. However, this possibility seems unlikely because similar results were obtained in ischaemia/reperfusion experiments, in which hearts were simultaneously loaded with Rhod-2 and Fluo-4 (excited at 532 and 473 nm, respectively), supporting the idea that the changes of Rhod-2 signals observed reflect actual variations of Ca^{2+} during ischaemia/reperfusion.

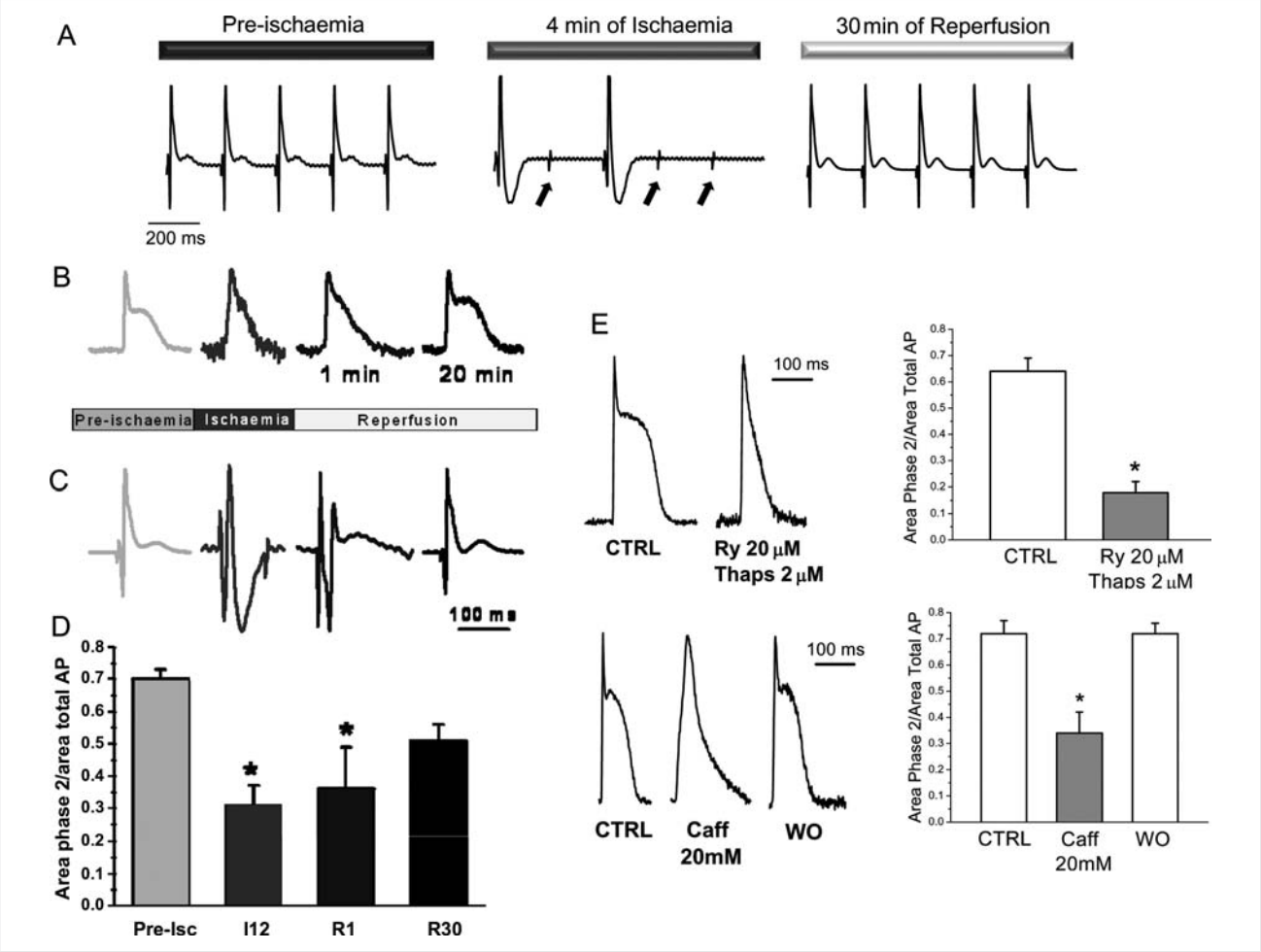

Figure 7 (*A–D*) Ischaemia impairs electrical excitability and shortens AP. (*A*) Typical recordings of transmural electrocardiograms during pre-ischaemia, ischaemia and reperfusion. Arrows indicate the moments when the electrical pacing was applied. (*B* and *C*) Typical recordings of intracellular AP and ECG measured simultaneously. Ischaemia significantly shortened phase 2 of AP. (*D*) Time course of the contribution of phase 2 to the AP, during ischaemia/reperfusion (Pre-Isc, I12, R1, and R30 indicate pre-ischaemia, 12 min of ischaemia, 1 and 30 min of reperfusion, respectively). Asterisk indicates the results with $P < 0.05$ when compared with pre-ischaemia, $n = 4–6$ experiments in each group. (*E*) Depletion of SR is associated with a loss of phase 2 of AP. Two interventions that deplete the SR of Ca^{2+}, like the combination of ryanodine/thapsigargin (Ry/Thaps) or caffeine (Caff), were associated with a loss of phase 2 of the AP, $n = 6$. *$P < 0.05$ with respect to control (without drug, CTRL) (WO indicates Washout).

The use of Mag-fluo-4 in the present study allowed us to assess, for the first time, SR-Ca^{2+} transients in the intact heart. This approach clearly shows a decrease in Ca^{2+} content at the onset of reperfusion that was further corroborated with the diminished caffeine-induced Ca^{2+} release. A major advantage of the PLFF microscopy is its much higher spatial resolution (up to 8 μm) than other standard OM methods (usually 950 μm). Moreover, avalanche photodiodes are 250 times more sensitive than PIN photodiodes generally used in OM.

4.2 Intracellular Ca^{2+} and Ca^{2+} dynamics during ischaemia/reperfusion

In agreement with the previous findings,[4,8,9] the experiments described in this paper confirmed that there is an increase in cytosolic Ca^{2+} during ischaemia. Several mechanisms have been considered to explain this cytosolic Ca^{2+} increase. Most of these mechanisms have been related to the acidosis associated with the ischaemic period like a decrease in Ca^{2+} myofilament responsiveness, a depression of SERCA2a activity and/or the mechanisms that extrude Ca^{2+}, and an inhibition of RyR2.[6,23,24] The dissociation between the decrease in DP and the increase in cytosolic Ca^{2+} during ischaemia would support a decrease in Ca^{2+} myofilament responsiveness as a main factor responsible for the increase in cytosolic Ca^{2+} during ischaemia. Moreover, the prolongation of both the rising and relaxation kinetics of the Ca^{2+} transients would suggest an inhibition of RyR2 and a depression of SERCA2a activity. Indeed, previous experiments clearly showed that acidosis reversibly inhibits RyR2.[24,25]

The data presented in *Figures 5C* and *6* imply that intra-SR-Ca^{2+} level was increased during ischaemia. This experimental observation supports our hypothesis that SR is one of the main sources of Ca^{2+} that is being released into cytosol during

reperfusion. Indeed, in order to return to pre-ischaemic Ca^{2+} concentrations, SR should extrude the extra Ca^{2+} ions accumulated during ischaemia.

4.3 The depletion of SR-Ca^{2+} content as the cause of the increase in diastolic Ca^{2+} at the beginning of reperfusion

The present results also confirmed an increase in cytosolic Ca^{2+} at the onset of reperfusion.[4,5] Although the mechanism of this increase in Ca^{2+} is not clear, it is generally accepted that it results from Ca^{2+} influx from the extracellular space.[6,7,10] Surprisingly, a possible role of the SR on cytosolic Ca^{2+} overload at the onset of reperfusion has not been directly evaluated in intact beating hearts. The present results clearly showed that the SR directly contributes to the cytosolic Ca^{2+} increase upon reperfusion. This contribution was confirmed by the measurements of cytosolic as well as intra-SR-Ca^{2+} after caffeine application. This manoeuvre revealed a decrease in SR-Ca^{2+} content at this time of reperfusion (*Figures 4* and *5*). More important, the decrease in SR-Ca^{2+} content was directly detected by the estimation of SR-Ca^{2+} with the fluorescent dye Mag-fluo-4 (*Figure 5D*). A small increase in cytosolic Ca^{2+} during ischaemia and a further increase upon reperfusion were observed in Rhod-loaded rabbit hearts.[4] It was found, however, that when the K_d for Rhod-2 and Ca^{2+} were corrected for the temperature and pH to calculate cytosolic Ca^{2+}, the increase in Ca^{2+} during ischaemia was greater than before correction and there was no further increase in Ca^{2+} upon reperfusion. The present experiments showed that ischaemia increased cytosolic Ca^{2+}, in agreement with these previous findings, and a transient but consistent increase in Ca^{2+} (Ca^{2+} *bump*) was still detected during early reperfusion. Since this increase was temporarily associated with a decrease in SR-Ca^{2+} content, assessed with a different dye, the possibility that it was an artefact seems unlikely. Moreover, control experiments demonstrated that a decrease in pH similar to that produced by acidosis, failed to affect diastolic fluorescence (data not shown). In any case, the main point of the present experiments is to show that SR depletion occurs at the onset of reperfusion. This Ca^{2+} release may be actually underestimated when measuring the bulk cytosolic Ca^{2+}, in which the Ca^{2+} contribution of a smaller compartment like the SR, may be diluted. Experimental evidence indicated that a fraction of the total SR was physically coupled and transferred Ca^{2+} locally to the mitochondria in cardiac muscle.[12] Moreover, de Brito and Scorrano[11] recently showed that mitofusin-2, a mitochondria dynamin-related protein, tethers ER to mitochondria, a juxtaposition required for efficient mitochondrial Ca^{2+} uptake. In this scenario, it cannot be excluded that mitofusin may be also involved in destiny of Ca^{2+} released by the SR. A mitofusin-mediated process leading to direct and rapid uptake by the mitochondria of the released SR-Ca^{2+} might be at least co-responsible for the fact that the relatively strong SR-Ca^{2+} depletion observed at the onset of reperfusion becomes hardly reflected in elevation of the basic concentration of free Ca^{2+} in the cell. In any case, the Ca^{2+} release from the SR described here is responsible for at least part of the cytosolic Ca^{2+} overload at the onset of reflow. Although the role of the SR at the onset of simulated reperfusion has been previously emphasized in isolated quiescent ventricular cardiomyocytes, the cytosolic Ca^{2+} pattern observed in these quiescent cells differed from the ones observed in the intact beating hearts.[18] The reason for these differences is not apparent to us. However, this may arise from the different ischaemia/reperfusion models and preparations described in the literature.

The trigger for SR-Ca^{2+} release at the beginning of reperfusion was not explored in the present experiments, but different mechanisms may contribute to this release. In the first place, the present results revealed that the SR emerged full of Ca^{2+} from ischaemia. Either the influx of Ca^{2+} from the extracellular space and/or the relief of RyR2 from the acidosis-induced RyR2 inhibition upon returning to normal pH may act independently or in combination to produce the release of Ca^{2+} from an overloaded SR. Indeed, recent experiments from our laboratory demonstrated that the return to normal pH after acidosis evoked a release of SR-Ca^{2+} produced by the rapid relief of the RyR2 from the previous acidosis-induced inhibition.[25]

4.4 The shortening of the AP at the beginning of reperfusion

Ischaemia evoked a shortening of the AP which still persists in early reperfusion and is mainly due to a decrease in phase 2 (*Figure 7*). The decrease in AP duration was associated with a triangulation of the AP waveshape. This AP shortening is also associated with a decrease in the amplitude of intracellular Ca^{2+} transients, which by slowing the direct NCX mode would decrease the Na^{+} influx, a main component of phase 2 of the AP in the mouse heart.[27] The fact that SR-Ca^{2+} depletion induced by different interventions like thapsigargin/ryanodine or caffeine was systematically associated with a decrease in phase 2 and AP triangulation is in agreement with this hypothesis. It is known that early reperfusion is prone to arrhythmias. The present results support the idea that the described shortening of the AP may be a main contributor in the genesis of early reperfusion arrhythmias. Interestingly, the presence of triangulation, independently of the length of AP, constitutes a proarrhythmic event.[31]

In summary, the present findings revealed for the first time that the increase in diastolic Ca^{2+} at the onset of reperfusion is associated with a release of Ca^{2+} from the SR. They also provided evidence indicating that the SR-Ca^{2+} depletion at the beginning of reperfusion underlies two related phenomena: a decrease in Ca^{2+} transient amplitude and in AP duration. This would provide an adequate scenario for the appearance of early reperfusion arrhythmias.

Supplementary material

Supplementary material is available at *Cardiovascular Research* online.

Conflict of interest: none declared.

Funding

This work was supported by the National Institute of Health (NIH R01-HL-084487 to A.L.E. and FIRCA # R03 TW007713-01 to A.M.); FONCYT & CONICET PICT # 05-26117; PIP # 5300 and 02139 to A.M.

References

1. Braunwald E, Kloner RA. The stunned myocardium: prolonged postischemic ventricular dysfunction. *Circulation* 1982;**66**:1146–1149.
2. Himori N, Walls AP, Burkman AM. Ischaemically induced alterations in electrical activity and mechanical performance of isolated blood perfused canine myocardial preparations. *Cardiovasc Res* 1990;**24**:786–792.
3. Vittone L, Mundiña-Weilenmann C, Said M, Ferrero P, Mattiazzi A. Time course and mechanisms of phosphorylation of phospholamban residues in ischemia-reperfused rat hearts. Dissociation of phospholamban phosphorylation pathways. *J Mol Cell Cardiol* 2002;**34**:39–50.
4. Stamm C, Friehs I, Choi YH, Zurakowski D, McGowan FX, del Nido PJ. Cytosolic calcium in the ischemic rabbit heart: assessment by pH- and temperature-adjusted rhod-2 spectrofluorometry. *Cardiovasc Res* 2003;**59**:695–704.
5. Valverde CA, Mundiña-Weilenmann C, Reyes M, Kranias EG, Escobar AL, Mattiazzi A. Phospholamban phosphorylation sites enhance the recovery of intracellular Ca^{2+} after perfusion arrest in isolated, perfused mouse heart. *Cardiovasc Res* 2006;**70**:335–345.
6. Bolli R, Marbán E. Molecular and cellular mechanism of myocardial stunning. *Physiol Rev* 1999;**79**:609–634.
7. Piper HM, Abdallah Y, Schäfer C. The first minutes of reperfusion: a window of opportunity for cardioprotection. *Cardiovasc Res* 2004;**61**:365–371.
8. Steenbergen C, Murphy E, Levy L, London RE. Elevation in cytosolic free calcium concentration early in myocardial ischemia in perfused rat heart. *Circ Res* 1987;**60**:700–707.
9. Kihara Y, Grossman W, Morgan JP. Direct measurement of changes in intracellular calcium transients during hypoxia, ischemia, and reperfusion of the intact mammalian heart. *Circ Res* 1989;**65**:1029–1044.
10. Kusuoka H, Porterfield JK, Weisman HF, Weisfeldt ML, Marban E. Pathophysiology and pathogenesis of stunned myocardium. Depressed Ca^{2+} activation of contraction as a consequence of reperfusion-induced cellular calcium overload in ferret hearts. *J Clin Invest* 1987;**90**:609–623.
11. de Brito OM, Scorrano L. Mitofusin 2 tethers endoplasmic reticulum to mitochondria. *Nature* 2008;**456**:605–610.
12. García-Pérez C, Hajnóczky G, Csordás G. Physical coupling supports the local Ca^{2+} transfer between sarcoplasmic reticulum subdomains and the mitochondria in heart muscle. *J Biol Chem* 2008;**283**:32771–32780.
13. Antzelevitch C. The Brugada syndrome: ionic basis and arrhythmia mechanisms. *J Cardiovasc Electrophysiol* 2001;**12**:268–272.
14. Antzelevich C. Heterogeneity and cardiac arrhythmias: an overview. *Heart Rhythm* 2007;**4**:964–972.
15. Litovsky SH, Antzelevitch C. Transient outward current prominent in canine ventricular epicardium but not endocardium. *Circ Res* 1988;**62**:116–126.
16. Guo D, Zhou J, Zhao X, Gupta P, Kowey PR, Martin J *et al.* L-type calcium current recovery versus ventricular repolarization: preserved membrane-stabilizing mechanism for different QT intervals across species. *Heart Rhythm* 2008;**5**:271–279.
17. Louch WE, Ferrier GR, Howlett SE. Changes in excitation–contraction coupling in an isolated ventricular myocyte model of cardiac stunning. *Am J Physiol Heart Circ Physiol* 2002;**283**:H800–H810.
18. Siegmund B, Ladilov YV, Piper HM. Importance of sodium for recovery of calcium control in reoxygenated cardiomyocytes. *Am J Physiol* 1994;**267**:H506–H513.
19. Qian YW, Clusin WT, Lin SF, Han J, Sung RJ. Spatial heterogeneity of calcium transient alternans during the early phase of myocardial ischemia in the blood-perfused rabbit heart. *Circulation* 2001;**104**:2082–2087.
20. Mejía-Alvarez R, Manno C, Villalba-Galea CA, del Valle Fernández L, Costa RR, Fill M *et al.* Pulsed local-field fluorescence microscopy: a new approach for measuring cellular signals in the beating heart. *Pflugers Arch* 2003;**445**:747–758.
21. Varma N, Morgan JP, Apstein CS. Mechanisms underlying ischemic diastolic dysfunction: relation between rigor, calcium homeostasis, and relaxation rate. *Am J Physiol* 2003;**284**:H758–H771.
22. Dou Y, Arlock P, Arner A. Blebbistatin specifically inhibits actin–myosin interaction in mouse cardiac muscle. *Am J Physiol* 2007;**293**:C1148–C1153.
23. Rapundalo ST, Briggs FN, Feher JJ. Effects of ischemia on the isolation and function of canine cardiac sarcoplasmic reticulum. *J Mol Cell Cardiol* 1986;**18**:837–851.
24. Xu L, Mann G, Meissner G. Regulation of cardiac Ca^{2+} release channel (ryanodine receptor) by Ca^{2+}, H^{+}, Mg^{2+}, and adenine nucleotides under normal and simulated ischemic conditions. *Circ Res* 1996;**79**:1100–1109.
25. Said M, Becerra R, Palomeque J, Rinaldi G, Kaetzel MA, Diaz-Sylvester PL *et al.* Increased intracellular Ca^{2+} and SR Ca^{2+} load contribute to arrhythmias after acidosis in rat heart. Role of Ca^{2+}/calmodulin-dependent protein kinase II. *Am J Physiol* 2008;**295**:H1669–H1683.
26. Valverde CA, Kornyeyev D, Escobar A, Mattiazzi A. Reperfusion causes cytosolic calcium overload due to rapid calcium release from the sarcoplasmic reticulum. *Circulation* 2008;**118**:5407. (Abstract).
27. Henderson SA, Goldhaber JI, So JM, Han T, Motter C, Ngo A *et al.* Functional adult myocardium in the absence of Na^{+}–Ca^{2+} exchange: cardiac-specific knockout of NCX1. *Circ Res* 2004;**95**:604–611.
28. Choi BR, Salama G. Simultaneous maps of optical action potentials and calcium transients in guinea-pig hearts: mechanisms underlying concordant alternans. *J Physiol* 2000;**529**:171–188.
29. Laurita KR, Katra R, Wible B, Wan X, Koo MH. Transmural heterogeneity of calcium handling in canine. *Circ Res* 2003;**92**:668–675.
30. Du C, MacGowan GA, Farkas DL, Koretsky AP. Calcium measurements in perfused mouse heart: quantitating fluorescence and absorbance of Rhod-2 by application of photon migration theory. *Biophys J* 2001;**80**:549–561.
31. Hondeghem LM, Carlsson L, Duker G. Instability and triangulation of the action potential serious proarrhythmia, but the action potential duration prolongation is antiarrhythmic. *Circulation* 2001;**103**:2004–2013.